

Limitations of Test
Methods for
PLASTICS

JAMES S. PERARO
EDITOR



STP 1369

STP 1369

Limitations of Test Methods for Plastics

James S. Peraro, editor

ASTM Stock Number: STP1369



ASTM
100 Barr Harbor Drive
West Conshohocken, PA 19428-2959

Printed in the U.S.A.

Library of Congress Cataloging-in-Publication Data

Limitations of test methods for plastics / James S. Peraro, editor.

p. cm.— (STP ;1369)

"ASTM stock number: STP 1369."

ISBN 0-8031-2850-9

1. Plastics—Testing. I. Peraro, James S., 1935— II. American Society for Testing and Materials.

TA455.P5 L56 2000

620.1'923'0287—dc21

99-057208

Copyright © 2000 AMERICAN SOCIETY FOR TESTING AND MATERIALS, West Conshohocken, PA. All rights reserved. This material may not be reproduced or copied, in whole or in part, in any printed, mechanical, electronic, film, or other distribution and storage media, without the written consent of the publisher.

Photocopy Rights

Authorization to photocopy items for internal, personal, or educational classroom use, or the internal, personal, or educational classroom use of specific clients, is granted by the American Society for Testing and Materials (ASTM) provided that the appropriate fee is paid to the Copyright Clearance Center, 222 Rosewood Drive, Danvers, MA 01923; Tel: 508-750-8400; on-line: <http://www.copyright.com/>.

Peer Review Policy

Each paper published in this volume was evaluated by two peer reviewers and the editor. The authors addressed all of the reviewers' comments to the satisfaction of both the technical editor(s) and the ASTM Committee on Publications.

To make technical information available as quickly as possible, the peer-reviewed papers in this publication were prepared "camera-ready" as submitted by the authors.

The quality of the papers in this publication reflects not only the obvious efforts of the authors and the technical editor(s), but also the work of the peer reviewers. In keeping with longstanding publication practices, ASTM maintains the anonymity of the peer reviewers. The ASTM Committee on Publications acknowledges with appreciation their dedication and contribution of time and effort on behalf of ASTM.

Foreword

This publication, *Limitations of Test Methods for Plastics*, contains papers presented at the symposium of the same name held in Norfolk, Virginia, on 1 November 1998. The symposium was sponsored by ASTM Committee D20 on Plastics. The symposium chairman was James S. Peraro, consultant, Newark, Delaware.

Contents

Overview	vii
GENERAL/DESIGN	
What Does a Property Data Sheet Really Tell You?—S. B. DRISCOLL AND C. M. SHAFFER	3
On the Variation of Compliance Measurements in Polymeric Solids—S. W. BRADLEY, W. L. BRADLEY, AND P. M. PUCKETT	10
Estimation of Lifetime Under Non-Isothermal Conditions—D. BLAESE AND E. SCHMACHENBERG	22
Discussion	30
Closure	31
MECHANICAL	
A Comparison of Tension Test Data Using ASTM D 638 and ISO 527—M. J. FRIDAY	35
Discussion	43
The Usefulness of HDT and a Better Alternative to Describe the Temperature Dependence of Modulus—M. P. SEPE	44
Interpretations of Tensile Properties of Polyamide 6 and PET Based Thermoplastics Using ASTM and ISO Procedures—N. JIA AND V. A. KAGAN	54
Tension Testing of Thin Bulk Adhesive Specimens—P. ALBRECHT, J. YOU, M. ALBRECHT, AND K. ELEY	72
A Study of Bond Strength Testing for Solvent Cement Joints in PVC Piping Systems—J. R. PASHAL	93
Discussion	106
IMPACT/FRACTURE	
Notched Impact Testing of Thermoplastics: A New Perspective—P. S. LEEVERS AND M. DOUGLAS	109
Instrumented Pendulum Impact Testing of Plastics—M. P. MANAHAN, SR., C. A. CRUZ, JR., AND H. E. YOHN	118

Development of a Standard for Determining KIC and GIC for Plastics at High Loading Rates: the ESIS Protocol for 1 m/s Testing —A. PAVAN AND J. G. WILLIAMS	130
PENT—Universal Test for Slow Crack Growth in Plastics —N. BROWN AND X. LU	146
CHEMICAL/RHEOLOGICAL	
Temperature Measurements in TGA —M. KELSEY AND J. FOREMAN	157
Pitfalls in Measurement of non-Newtonian Materials —P. WHITTINGSTALL	167
Factors Affecting the Accuracy of TMA Measurements —J. FOREMAN, M. KELSEY, AND G. WIDMANN	181
Acetone Immersion Testing per ASTM Test Method D2152 —J. HOULE	197
Reinforced Epoxy Resin Cure Assessment in Composite Materials: Measure and Effects —G. ZAFFARONI, C. CAPPELLETTI, S. GUERRA, AND S. RISETTI	206
Indexes	219

Overview

Testing is the means by which information (data) is developed on materials or products, and tests have been used for over 2000 years to provide a wide range of technical information describing a material's properties and characteristics. The first published test standard for plastics was written by ASTM Committee D20 in 1937. The early published test standards were simple in form and composition. Test methods were usually generic and written for the limited number of the then-known polymeric materials. They addressed all material types and were used for the determination of traditional properties such as tensile, flex, impact, and flammability. As polymers evolved into a vast array of polymer types, all different in structure and properties, so have test methods. ASTM standards are no longer those simple documents prepared when plastics were the new curious materials, but have continued to evolve as the technology of plastics has evolved. Test methods range from the very simple to very complex, such as those used to generate property data for engineering applications. Every ASTM committee attempts to provide standards that reflect the latest technology in testing of materials to meet the widening need of the global marketplace. The end result is that today's test methods not only generate more meaningful data but are used for a wide range of applications.

What started out to be simple generic test methods have necessarily become more complicated and difficult to comprehend. As test methods have become more sophisticated and complicated in scope and application, more knowledge about materials and their characteristics is needed by those using ASTM test methods to develop test data and by those who analyze and utilize the data. Generally, the result is a lack of understanding of the variables that contribute to and influence test results. It has been long understood by the testing community that every test method ever written, whether written for metals or non-metals, is composed of variables. There are many sources of variables and all have a direct influence on the accuracy of the generated test data. The sum total of all variables defines test limitations.

Test limitations are a compilation of the variables (1) present within a test method; (2) associated with the material under investigation; and (3) those external to but not related to the test method or material. Test and material variables are the primary source of variability. The external variables are primarily those influenced by an individual's knowledge of the characteristics of the material under investigation or the test method(s) to be used in its evaluation, and the ability to properly analyze the generated test results as related to the intended use or application. Misinterpretation, misuse, or misapplication of the test method or the use of the data generated all contribute to test limitations. Unfortunately these limitations are not fully understood, resulting in inappropriate claims or conclusions pertaining to materials or products made from plastics.

ASTM enjoys an excellent reputation as a leading organization in the development of test methods used worldwide. ASTM technical committees have developed over 10,000 test standards. Unfortunately, there is a general belief that the results obtained from these test standards are absolute, which is not the case since each has its limitations. ASTM standards are living documents and are continually being updated and revised to reflect the latest in testing technology. Limitations are not limited to the ASTM test standards. In the United States there are over 400 standards writing organizations, and when you add all the test standards worldwide (ISO, DIN, BSI etc.) there are an enormous number of test standards all with their own set of limitations.

It has been acknowledged for many years that there was a need for a symposium discussing the limitations inherent in all test methods. ASTM has always encouraged the use of symposia or other formal programs to educate those interested in the proper use and application of ASTM standards or

the principles by which they were developed. In order to promote and educate the business and technical communities about the limitations of test methods of plastics, ASTM D20 on Plastics decided to schedule a symposium on this very important and timely subject. In November 1998 a symposium entitled Limitations of Testing was held in Norfolk, Virginia.

In this symposium, 21 papers from both Europe and the United States were grouped into four major categories, namely General/Design, Mechanical, Impact/Fracture, and Chemical/Rheology. Some of the papers could have been placed in more than one category. It was a difficult task for the committee to make the final decision on the location of the paper and the order of presentation.

General/Design

In this section papers are presented covering issues facing engineers in the selection of the optimum material candidate and the development of test data for a specific performance criteria. There is a generally accepted protocol that is used by engineers in making a qualified decision based on available facts. The problem is knowing what is required of the product and what is the true functional behavior of the polymer. What is not often completely understood is the correlation of published data and the relevance to design. The various options and concerns are reviewed.

Creep tests can be conducted in either tensile or flexural modes. The time-dependent viscoelastic deformation of polymers and composites is compared and the differences in material compliance is analyzed. The constitutive relationship for creep compliance that takes into account the effect of dilatational stresses is determined. Estimation of lifetime under non-isothermal conditions is also presented. Not only are the thermal and mechanical loading of great importance to estimation of life expectancy, but also the influence of the chemical medium and immersion time. Two possible methods of obtaining this information are discussed: (1) time-temperature extrapolation of the measured aging process, and (2) a functional estimation of time-temperature collectives, the latter being more precise.

Mechanical

In this section, traditional tests such as tensile, and deflection under flexural load (DTUL) are covered. Papers discuss the development of testing procedures for materials and the influence of variables on the generated data. The implications of conversion from ASTM to ISO standards for material characterization for greater opportunity and to compete more effectively in the global market are reviewed. As global interaction increases, it is important that the concerns raised during conversion can be harmonized between the two sets of standards. Also, the comparison of tensile data generated by ASTM and ISO procedures and the results obtained from round-robin tests are discussed for a variety of polymers. Common errors made by laboratories were examined. Data are also presented showing the common variables that affect test results in both ASTM and ISO tensile tests.

Deflection temperature under load (DTUL) measures the temperature at which a specimen of a certain geometry deflects a fixed amount under a very specific set of conditions. However, it is often used in material selection as a measure of the maximum continuous use temperature for that material. The development of dynamic mechanical analysis (DMA) has shown that traditional DTUL test results often give a false measure of the thermal performance of polymeric materials. By measuring the elastic modulus versus temperature by DMA the thermal profile of any polymer can be obtained and a more realistic assessment of the elevated temperature performance can be obtained. New techniques were also presented for testing adhesive bond strength tests for piping systems. The technique developed utilized lap-shear plaques to predict performance in the pipe joint systems. Results indicate extreme sensitivity to minor variations in preparation.

Impact/Fracture

Papers in this section discuss the variables that have a significant effect on impact resistance. Impact tests measure the response of materials to dynamic loading. Pendulum impact tests such as IZOD and Charpy are used widely to quantify the impact performance of plastic materials. Both tests are used widely to develop impact data and are considered as a primary performance index for impact properties, but cannot be used for design considerations. In these tests there are a large number of variables associated with sample preparation, the test apparatus, and the test procedure. Data are presented comparing instrumented and non-instrumented IZOD and Charpy tests, the effects of the variables, and their influence on the test results. A new approach using fracture mechanics is presented for the determination of the impact fracture resistance G_c , or impact fracture toughness K_{Ic} . The fracture mechanics perspective is based on an explanation of impact speed and geometry based on the thermal decohesion model. Analysis leads to a prediction of an apparent impact fracture resistance G_{ca} . Also, a new standardized test procedure to measure K_{Ic} and G_{Ic} for plastics at a moderately high rate of loading, namely 1 m/s, has been proposed. The test procedure is based on previously developed fracture mechanics technology for the determination of K_c and G_c . Round robin test data developed over a period of five years are reviewed and show the consistency in the test data, validating the test protocol.

Chemical/Rheological

Papers on advanced testing techniques primarily in the area of rheological testing were presented. Thermomechanical analysis (TMA) is compared to the coefficient of linear thermal expansion (CLTE) and the measurement of the glass transition temperature (T_g). Variables are identified and the effect on temperature measurements is discussed for CLTE and T_g . In another presentation, capillary and rotational viscometry is compared. The flow curve of the apparent viscosity versus shear rate emphasizes the dangers of using a single viscosity value such as Melt Flow Index. Both orthodox and unorthodox measurements are discussed for viscosity measurements for controlled stress and controlled rate devices. A more direct volumetric method to measure volume swell ratio has been developed for cross-linked polyethylene and compared to the gravimetric method using the deswelling or solvent evaporation techniques. The results show that the direct volumetric technique is more accurate and not subject to the limitations of the other techniques.

This symposium reflects the current work being undertaken within the ASTM D20 subcommittees to insure that all test methods are written in such a way as to be understood and used properly.

Acknowledgments

The symposium committee gratefully acknowledges the efforts of the authors, the ASTM D20 technical committee that helped put this symposium in motion, and the 44 individuals who reviewed the presented papers prior to publication of this STP. Finally, for any symposium to be successful, the majority of the individuals involved work behind the scenes, especially Dorothy Fitzpatrick and her staff at ASTM who provided the administrative services. Without their effort this symposium would not have been so successful.

*James S. Peraro;
Symposium Chairman and Editor*

General/Design

Stephen Burke Driscoll¹ and Christopher M. Shaffer²

What Does a Property Data Sheet Really Tell You?

Reference: Driscoll, S.B., and Shaffer, C.M., "What Does a Property Data Sheet Really Tell You?," *Limitations of Test Methods for Plastics, ASTM STP 1369*, J. S. Peraro, Ed., American Society for Testing and Materials, West Conshohocken, PA, 2000.

Abstract: Today's engineer, whether a student in training or a practicing professional, is faced with a myriad of design considerations when selecting the optimum material candidate for a functional product. The normal protocol followed includes prioritizing performance credentials, selecting candidate polymeric material , reviewing the properties and processing characteristics of each, and then making a qualified decision based on the available facts.

The problems, however, are both knowing fully what will be required of the product, in a wide range of use/abuse environments, and understanding as thoroughly as possible the true functional behavior of the polymer. What often is not completely understood is the correlation between published data sheets and the relevance to design considerations. How meaningful is the information found in a typical data sheet? How easily, if at all, can the design engineer integrate this information in a series of design iterations, leading to an improved product?

How useful is the information most routinely published? Certainly a great deal of information is readily available in a number of formats, including proprietary databanks maintained and freely distributed by the various material suppliers. This information is equally available via the Internet, and much follows the CAMPUS template containing both single- and multi-point data (International Standards Organization-ISO 10350 and 11403 respectively).

Regardless of the quantity and ready availability of this information, how can published Izod impact behavior be successfully used to make a better, more durable product? How can the Distortion Temperature Under Load (DTUL) of a material translate into practical continuous use temperature? What published data are really useful? And what are meaningless?

Finally, what really is needed - and is usually missing - to help the design engineer predictably produce a safe, reliable, and durable product?

Keywords: Plastics, physical properties, impact and flow behavior.

¹ Professor, Department of Plastics Engineering, The University of Massachusetts-Lowell, 01854

² Student, Department of Plastics Engineering, The University of Massachusetts-Lowell, 01854

Introduction

The design engineer is faced with a myriad of problems when selecting material candidates for a product. As we become more sophisticated in our use of information resources, we expect our resin suppliers to equal or better our demands for performance data. Our history of being a "creature of habit", routinely using materials that have worked well for us in past product development programs, is no longer valid in contemporary design strategies.

Considerable work in our industry has led to the global recognition of ASTM D4000, Classification System for Specifying Plastics Materials. This protocol provides the necessary guidelines for developing line call-outs for polymeric materials, and reduces to consensus-balloted formats a range of tables/cells for specific properties. By prioritizing the requirements, and assigning minimum performance values, it is possible to generate a listing of material candidates which can be used for initial screening purposes.

A problem, woven throughout the fabric of this protocol, is the quality and utility of data generated and incorporated into these tables/cells. As stated in the abstract, how meaningful is the information found in a data sheet or product bulletin? It is important to recognize that the data sheet has very specific purposes, often sales and marketing related, and the technical content is not always intended for design and processing engineers. In fact, most date sheet do contain a caveat, warning the reader that the information supplied is general in nature, only approximate values, and intended to serve only as a guideline, and is not part of a material specification.

What Properties Should Be Reported?

Granted, there is a dichotomy existing with the data sheet. What physical properties should be published, as requested by the sales and marketing groups, versus what information is really useful to the materials, process, and design engineers?

This is not a new problem. We have been attempting to balance these two opposing requests for many years. In fact, you might be surprise to learn that many years ago, back in 1969, there was a special session at the Society of Plastics Engineers (SPE) Annual Technical Conference (ANTEC) devoted to this same question. (1)

In the December 1979 issue of Plastics Engineering an excellent article, "Get the MOST for Your Money from Your Resin Supplier", stated that fewer than half of the reviewed data sheet from international suppliers provided all of the information needed to enable you to make the best choices. (2) The article continued by contrasting the surveyed property data. The tabulation indicated three strong trends. The majority of the published data was aimed at the end product (materials engineer), considerably less information was for the mold design and processing engineers.

Noted below is an abbreviation of these published observations:

Table 1 - Published Data

Available data	Where needed		
	End Product	Mold Design	Processing
A) Properties included in more than 80 percent of product data sheets surveyed:			
Specific gravity	Y	Y	Y
Tensile strength	Y	N	N
Elongation	Y	Y	N
Izod impact	Y	N	N

Flexural modulus	Y	Y	N
Hardness	Y	Y	N

B) Properties included in 50 to 80 percent of product data sheets surveyed:

Mold shrinkage	N	Y	Y
Melting point	Y	N	N
Tensile modulus	Y	N	N
Flexural strength	Y	N	N
Coeff. of Linear Thermal Exp.	Y	Y	Y
Moisture absorption	Y	Y	Y
Thermal conductivity	Y	Y	Y

C) Properties included in fewer than 50 percent of product data sheets surveyed:

Flow temperature or normal processing			
temperature	N	Y	Y
Specific volume	Y	Y	Y
Specific heat	Y	Y	Y
Fatigue endurance	Y	N	N
Poisson's ratio	Y	N	N

The author, Paul E. Sample, the current chair of the D20 Committee on Plastics, derived very nicely a series of six check-points for selecting the appropriate family and grade of material. These are:

1. polymeric family
2. molecular weight
3. melt behavior
4. specific gravity
5. mold shrinkage
6. strength & impact behavior

This primer was complemented ten years later by another impressive article, "Interpreting Supplier Data Sheets".(3) In this encyclopedia chapter, the authors intended their article to delineate the limitations of data for engineering design. ASTM and other testing organizations were cited for their development of standards to ensure reproducibility of data for quality control purposes and purchase specifications, although not always for generating engineering data.

The authors included a caveat that in many of the testing procedures the data should not be used for design purposes unless the application conditions are similar to the test conditions in terms of size, shape, strain rate, and environmental conditions, including temperature and relative humidity. They also noted that the properties of plastics parts are seldom as high as data sheet values. This can be attributed, in part, to the fact that the reported values are obtained using specimens specifically designed and molded at conditions optimized for that test.

At the 1993 SPE ANTEC, a thought-provoking paper, "Heat Deflection Temperature (HDT) and Notched Izod: Two Key Measurements That Have Outlived Their Usefulness" addressed the use of short-term tests to design for rigidity and strength under load at elevated temperatures.(4) The author concluded that such simple tests as DTUL and Izod are meaningless in judging material suitability in applications in which exposure to elevated temperatures is more than momentary.

6 LIMITS OF TEST METHODS FOR PLASTICS

This same battle cry was voiced five years later, at the 1998 SPE ANTEC in Atlanta.(5) A special session focused on materials properties that are often misused. For example, two papers addressed again the usefulness of the DTUL test and Charpy/Izod impact behavior in relation to material toughness. (During this symposium and printed in this Special Technical Publication (STP) will be additional papers addressing these two topics.)

Consequently, for just shy of three decades, we have continued to discuss these limitations of test methods for plastics. Fortunately, we can report some progress in resolving these issues. Noted below are some abbreviated comments on typical physical properties, commonly published, and what is useful or meaningless about these tests.

Mechanical Properties:

Thanks to the considerable quantity of data published on these important physical properties, this does represent one of the few areas in which the design engineer can use published information to make a better product. Knowing the load bearing characteristics of a material, whether in tension, compression, or flexure, does translate in to very specific geometrical requirements for safely loading a product. Knowing the modulus, which is synonymous with stiffness and rigidity, allows the design engineer to select the appropriate material, minimize wall thickness, and save money.

Rather than publishing single-data point, the prevailing trend, welcomed by many in the global testing community is the generation of multi-point data. For example, the complete stress-strain curve v. line call-outs of data at isolated conditions, such as tensile yield stress or elongation at yield.

For the design engineer, what is even more important, is knowing the mechanical behavior as a function of temperature and other environmental conditions. Until recently, with the market introduction of new, high performance engineering thermoplastics, these data have been rarely published. It is very encouraging that the resin manufacturers are now recognizing that their customers are becoming technically more mature and sophisticated and, consequently, that these data are beginning to be published.

However, most often the data sheet does not indicate which specimen geometry was used, the length of the mandated extensometer, the strain rate, and, most critically, which modulus is being reported. Was it the initial tangent modulus or a chord modulus, now being discussed as the preferred property in some countries. Remember, the data sheet of an imported material might not indicate explicitly the preferred property, such as modulus.

Useful Information:

Analogous to melt index reporting of temperature and weight (e.g. 190/2.16), is it too much to ask the resin manufacturer to report automatically on the data sheet the ASTM D638 Tensile Properties of Plastics specimen type (I - V) and the strain rate along with the extensometer used? Also useful would be including the complete stress v. strain curve, which illustrates overall ductility, rather than a limited series of single data points, such as the elongation and stress at yield or at break.

Even though the D4000-based material specifications should include all of the above-stated information, there might be some missing guidelines in selected documents. Consequently, the various D20 materials Sub-committees are currently reviewing their standards in order to complete this necessary information.

It is very satisfying to report that the D790 Flexural Properties of Plastics protocol has recently undergone complete revision and has passed the consensus balloting process. The three point procedure has been streamlined, in an attempt to harmonize with its ISO

178 counterpart, and the four-point bending procedure is being issued separately under a new ASTM D20 Committee on Plastics jurisdiction number (D6286).

Certainly, this will minimize any confusion when reading future data sheets. No longer will one have to question how the material was tested, which span to depth ratio was used, nor guess the testing speed. However, the question of which modulus should be reported still lingers.

Other mechanical properties-Hardness, which often correlates with modulus, is not commonly reported. Although fixed for Rockwell studies, a major concern for other hardness tests is the time delay between penetrating the plastics material and recording the hardness value. This concern for stress relaxation is legitimate and warrants continued scrutiny.

Creep data are invaluable for predicting the long-term functional behavior of a material or product. However, the current body of data (seldom, if ever, reported on product data sheets) cannot be compared for a series of material candidates. Polymers must be tested exactly the same way (*test mode, initial stress level, time, and temperature) in order to have a valid comparison, without relying on mathematical adjustments. The concept of the use of creep modulus has been widely adopted. However, one must still adhere to the paradigms of linear viscoelasticity to allow valid comparisons of different polymeric materials.

Impact properties-Impact behavior, especially ASTM D256 Pendulum Impact Resistance) is one of the more commonly reported "primary" physical properties. The limited data generated poses serious problems. How was the material molded, which section of the test bar specimen was tested (gate, mid-, or dead end), how was it notched (and at what cutting wheel rpm and sled feed rate), and how many hours after notching was the specimen impacted? When was the last time you saw this information on a data sheet or in a product bulletin?

Unlike instrumented impact testing (D3763), the pendulum test (both D256 and D4812 un-notched specimen) generates a single, fixed data point. Again, knowing the complete, detailed force v. deformation response of the impact event, as generated using D3763, will provide the design engineer with a greater appreciation for the nature of the fracture: punched hole or tear fracture, brittle v. ductile, etc.

Coupling these data with an analysis of impact behavior as a function of temperature, thickness, and impact speed is truly invaluable information, and should lead, obviously, to enhanced product ruggedness and safety.

Electrical properties-Interestingly, much of the electrical data is obtained by varying the testing frequency, analogous to instrumented variable rate impact testing. Strangely, what is standard operating procedure for one grouping of physical properties is not automatically adopted when measuring other equally important properties.

Flow Behavior and Thermal Characteristics:

Time and space allow only abbreviated discussion of two other commonly reported data sheet line items: melt flow rate - melt index (flow behavior) and DTUL (functional performance of a solid). Similar to Izod impact, these are also single data point tests. While providing some information for quality control purposes, neither one is eligible for consideration as design-caliber data.

The shear regime encountered during an extrusion plastometer trial (Melt Index/Melt Flow Rate - MI/MFR) does not fairly represent actual processing conditions. This single data point, tested at a fixed temperature, certainly does not reflect the actual processability of a polymer, most often at quite different melt temperatures. The advent

8 LIMITS OF TEST METHODS FOR PLASTICS

of capillary rheometry enhances the value of viscosity v. shear rate. When performed at several temperatures, these data provide more meaningful information to the processing engineer. When, however, did you read capillary data in a typical data sheet?

An extension of this upgraded strategy was the important introduction of dynamic mechanical techniques for measuring the complex melt viscosity (both elastic and viscous components) as a function of temperature, shear rate, and time...all within the linear viscoelastic region. While ASTM D4440 Complex Melt Viscosity using Dynamic Mechanical Rheological Techniques (DMRT) has been globally adopted since the early 1980s, and most routinely used by resin manufacturers in their own R&D efforts, these data still are a rarity on a product bulletin. Why?

The ASTM D648 DTUL "...covers the determination of the temperature at which an arbitrary deformation occurs when specimens are subjected to an arbitrary set of testing conditions." As stated in the Significance and Use section, "...this test is particularly suited to control and development work...and data obtained (by this test method) may not be used to predict the behavior of plastics materials at elevated temperatures...unless under similar conditions..."

If we truly practice what we preach, working smart and not hard, we really should question why the DTUL is routinely reported. It does not have any immediate value to either the processing or the design engineer. Knowing that poly "X" has a DTUL of 80 C tells them nothing about the behavior of the material 5- or 10 degrees either side of the single data point. How often will the design engineer encounter a product environment that mimics the 264 psi outer fiber stress level cited in D648? How can a student engineer in training, use successfully one material boasting a DTUL 80 C to replace a second polymer exhibiting a DTUL of 90 C, or only 60 C?

Again, it is truly gratifying to state, as a teacher, that the new generation of product brochures, bulletins, and data sheets now include multi-point thermal characteristics. Publishing the tensile strength v. temperature and the more commonly used modulus v. temperature (Clash-Berg, ASTM D1043) and more recently, the fully instrumented ASTM D4065 series dynamic mechanical properties in tension (D5026) compression (D5024), and three point bending (D5023) as well as in torsion (D5279) and dual cantilever beam geometries (D5418) has significantly expanded our body of knowledge.

Knowing the change in stiffness v. temperature, especially when contrasting an amorphous v. semi-crystalline polymer, is critical to the design engineer when selecting the appropriate material candidate(s) for a product which will be used a wide range of environmental conditions. The decreasing slope of modulus with increasing temperature does provide the necessary information about the maximum continuous use temperature over a wide range of stiffness values. Work published by Michael Takemori of GE Corporate Research, in the late 1970s, has illustrated very convincingly this approach. (6)

Conclusion:

In conclusion, as we review our usual collection of data sheets, we should question the quality and relevance of these published data. With an eye towards learning more about how a polymer can be processed (melting temperature, T_m, viscosity v. shear rate, shrinkage characteristics, thermal conductivity, as well as thermal stability and degradation and the ability to be recycled, etc.), we must question the disadvantage of not having these data.

And certainly, we must recognize that the design engineer needs to know more meaningful information about how the polymer will perform under intended conventional use and abnormal abuse conditions (modulus v. temperature, creep behavior, impact toughness, and fatigue endurance, etc.).

Do we continue our reluctance , either through omission or commission, to upgrade our data sheets with information that is more useful to the materials, design, and

processing engineers, or do we become more pro-active in surveying what these professionals really want and need? (Remember, if we place the blame on sales and marketing, we can also re-educate them towards thinking the obvious public relations bonus of being the first to publish a new generation of truly useful data sheets.

Or, perhaps, do we make a ten-year advance reservation now for still another meeting on this topic? Time will tell...but I suspect the opinions of our customers will be deafening.

References:

- (1.) Society of Plastics Engineers (SPE) Annual Technical Conference (ANTEC), 1969, Volume 15
- (2.) Sample, Paul E., "Get the Most for your Money from your Resin Supplier", *Plastics Engineering*, December 1979 pp. 26-28
- (3.) Lavengood, Richard and Frank Silver, "Interpreting Supplier Data Sheets", *ASM Engineered Materials Handbook*, Vol. 2 (1988), pp. 638-645
- (4.) Nunnery, L. E., "Heat Deflection Temperature (HDT) and Notched Izod: Two Key Measurements that Have Outlived Their Usefulness", *SPE ANTEC*, 1993, Volume 39, pp. 268-269
- (5.) Shastri, Ranganath and Hans Breuer, "PD3 Session on Material Properties that Are Too Often Misused", *SPE ANTEC*, 1998, Volume 44
- (6.) Takemori, Michael, "Towards an Understanding of the Heat Distortion Temperature", *SPE ANTEC*, 1978, Volume 24, pp. 216- 220

S. W. Bradley,¹ W. L. Bradley,² and P. M. Puckett³

On the Variation of Compliance Measurements in Polymeric Solids

Reference: Bradley, S. W., Bradley, W. L., and Puckett, P. M., “**On the Variation of Compliance Measurements in Polymeric Solids**,” *Limitations of Test Methods for Plastics, ASTM STP 1369*, J. S. Peraro, Ed., American Society for Testing and Materials, West Conshohocken, PA, 2000.

Abstract: Polymeric solids have tensile creep compliance, compression creep compliance, flexural creep compliance, and tangential or incremental tensile and compressive compliance. While these compliance values would all be numerically the same in a given metal, they will all be numerically distinct in polymeric solids. This paper investigates why these compliance values vary in polymeric solids and presents experimental data to indicate the magnitude of this variation between several of these compliance values in iso-polyesters and vinyl esters. The tensile creep compliance is found to be ~15% greater than the flexural creep compliance in vinyl esters while the incremental compliance at 3700 hours in a creep test is found to be approximately 25% less than the initial compliance on loading for iso-polyesters. The measured tensile and flexural creep compliances may be used to calculate the compressive creep compliance.

Keywords: tensile creep compliance, flexural creep compliance, tangential or incremental compliance, compressive creep compliance, vinyl esters, polyesters

Introduction

The use of solid polymers for long-term structural applications that are stiffness limited in design requires the determination of the modulus of elasticity or the compliance for loading in tension (or compression). For metals, this is a simple matter since the value determined from a tension test, a compression test or a flexural test will be the same. However, for solid polymers, the tensile and compressive compliance are not the same, and thus, the flexural compliance will be different from both[1], combining as it does tensile and compression in a single test. To further complicate matters, all three compliance values are time-dependent, for polymeric solids[2]. The creep compliance is the time-dependent creep strain divided by the constant applied stress that caused the creep, but the inverse is not the same as the relaxation

¹ Materials Performance, Inc., 1501 FM 2818, Suite, 208, College Station, TX, 77840

² Texas A&M University, Department of Mechanical Engineering, College Station, TX 77843

³Dow Chemical, 2301 N. Brazosport Blvd., B-1603, Freeport, TX 77541

modulus, except for very short or very long times [1]. The relaxation modulus is determined for constant strain with a monotonically decreasing stress, whereas the creep test is performed using constant stress [2].

For some engineering applications of solid polymers, resistance to buckling is the critical design consideration. Does one use the creep compliance (or its inverse, the so-called creep modulus), the stress relaxation modulus, or some other modulus value? The authors believe that the short time, or incremental modulus or compliance is more correct since compressive failures are instabilities. The purpose of this paper is to investigate these issues concerning the various compliance values of polymeric solids and to suggest which compliance is suitable for several specific applications. Experimental measurements of flexural creep compliance (or modulus) and tensile creep compliance (or modulus) for vinylesters will be presented and compared. The measurement of the incremental, or tangent compliance modulus late in a creep test will be presented and compared to the initial compliance, or instantaneous compliance measured during initial loading of the specimen for the creep test to see whether this incremental or tangential compliance value remains constant during creep testing, or during long-term service.

Theoretical Background

In this section the relationships between the various compliance values will be presented.

Creep and Relaxation Moduli

Using a standard linear model, as shown in Figure 1, the following differential equation can be used to describe the idealized, time-dependent behavior of polymeric solids [1]:

$$\frac{d\varepsilon}{dt} + \frac{E_2 \varepsilon}{\mu} = \frac{E_1 + E_2}{\mu} \frac{1}{E_1} P + \frac{1}{E_1} \frac{dP}{dt} \quad (1)$$

The mechanical analog in Figure 1 represents real deformation in polymers. The spring element represents time independent modes of deformation, primarily stretching of secondary bonds. Few primary bonds are stretched since the polymer chains are highly kinked or coiled. Furthermore, the glassy modulus would be much greater than the usual values of 3.5 GPa if the time independent strain was associated with stretching of primary bonds. “ E_1 ” then is associated with the stiffness of the secondary bonds in polymers.

The spring-dashpot element represents the time-dependent, or viscoelastic deformation in the polymeric solid. This deformation is the result of local rotations of the molecule, which allow it to unkink (or uncoil). “ E_2 ” is the restoring force, or natural tendency of the molecule to recoil, or rekink. This is sometimes referred to as an entropy spring, since the change in Gibbs free energy on strain recovery is due primarily to an increase in the entropy associated with a molecule as it goes from a unique, chain extended configuration to a fully recoiled configuration which can be realized with many different conformations. This energy change per unit strain (or local displacement) is relatively small, which means E_2 behaves like a very soft spring compared to E_1 , or $E_2 \ll E_1$. The local resistance to these molecular rotations which

12 LIMITS OF TEST METHODS FOR PLASTICS

gives rise to chain extension and viscoelastic deformation may be thought of as a viscosity, and thus, is represented by a dashpot of viscosity “ μ ”.

This standard linear solid can be used to model the behavior of amorphous polymers. Semi-crystalline polymers probably would require a more complex model to distinguish the deformation of the crystalline material from the amorphous. The primary limitation of the standard linear solid to model amorphous polymers is the assumption of a single viscosity “ μ ”, whereas the local viscosity of a real polymer would be quite heterogeneous.

The viscosity is a sensitive function of the local free volume, which varies significantly with temperature and can also vary with hydrostatic pressure through the change in the free volume that tensile or compressive stresses may affect. The authors propose that at temperatures where viscoelastic deformation via molecule unkinking and chain extension occurs, an increase in local free volume that results from tensile loading or a decrease in free volume for compressive loads should give rise to different rates viscoelastic deformation in tension and compression, and thus, different creep compliances. The authors have found no data which directly compared flexure, tensile and compressive creep compliance. The desire to determine the magnitude of the differences in time-dependent tension, compression, and flexural modulus is the motivations for this study. Solutions to this differential equation (Equation 1) for constant stress boundary conditions (creep) and constant strain boundary conditions (stress relaxation) are found to be:

$$\frac{\varepsilon(t)}{\sigma_0} = D(t) = \frac{1}{E_1} + \frac{1}{E_2} [1 - \exp(-\frac{t}{\tau_2})] \quad (2a)$$

$$E(t) = \frac{\sigma(t)}{\varepsilon_0} = E_1 - \frac{E_1^2}{E_1 + E_2} [1 - \exp(-\frac{t}{\tau_1})] \quad (2b)$$

where $\tau_1 = \frac{\mu}{E_1 + E_2}$ and $\tau_2 = \mu / E_2$, σ is the applied stress and $E(t)$ and $D(t)$ are the relaxation modulus and compliance respectively.

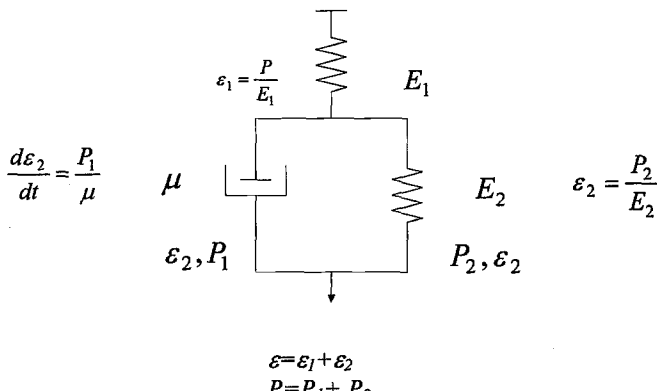


Figure 1- Standard Linear Solid Model for Viscoelastic Deformation of Polymers

Equation 2a for creep compliance can be inverted to give an effective "creep modulus" which may be more easily compared to the relaxation modulus, or

$$E_{\text{creep}} = \frac{\sigma_0}{\varepsilon(t)} = \frac{E_1 E_2}{E_1 + E_2} \left[1 - \frac{E_1}{E_1 + E_2} \exp \left(-\frac{t}{\tau_2} \right) \right]^{-1} = E_c \quad (3a)$$

To facilitate the comparison between creep and relaxation moduli, Equation 2b for relaxation modulus can be rearranged to give

$$E_{\text{relax}} = \frac{E_1 E_2}{E_1 + E_2} \left[1 + \frac{E_1}{E_2} \exp \left(-\frac{t}{\tau_1} \right) \right] = E_R \quad (3b)$$

Equations 3a and 3b can be easily shown to be identical for time equals zero and as time approaches infinity, but $E_R < E_c$ at all times in between. Likewise, the creep compliance $D_c(t)$ will always be less than the inverse of the relaxation modulus or the effective relaxation compliance " $D_R(t)$ ". This is easily understood by noting that in the stress relaxation test, the total viscoelastic strain at any time has occurred in response to stresses that are higher than the current stress, giving a larger total strain than one would have if one applied the current stress for the same period of time, as would occur in a creep test. This larger strain value at a given stress makes the effective relaxation compliance $[\varepsilon_0/\sigma(t)]$ greater than the creep compliance at any given time during their respective tests[6].

While the standard linear model does not precisely describe creep or stress relaxation behavior because of the assumption of a single relaxation time, the above arguments still apply to actual polymer behavior, where $D_c(t) < D_R(t)$. Thus, for constant load applications, the creep compliance or its inverse, the so-called effective creep modulus should be used, whereas for constant displacement (e.g., a plastic nut and bolt), the relaxation modulus should be used.

Tensile Creep Compliance versus Compressive Creep Compliance

As has been previously mentioned, creep deformation has two components, one resulting from stretching of the secondary chemical bonds between molecular chain segments, which gives elastic strain, and unkinking of molecules, which gives a viscoelastic component of strain. The first and second terms in Equation 2a are associated with bond stretching and molecular unkinking respectively. While bond stretching and bond compressing will give similar elastic strain contributions to the total creep strain, and creep compliance, the viscoelastic deformation in tension will be greater than the viscoelastic deformation in compression. This difference in viscoelastic deformation is due to the change in the free volume in response to the hydrostatic tension or hydrostatic compression[3], defined as

$$\mu = A \exp(B/f) \quad (4a)$$

$$\text{where } f = H + (\sigma_1 + \sigma_2 + \sigma_3)/F \quad (4b)$$

where σ_1 , σ_2 , and σ_3 are the principle normal stress, with $\sigma_1=\sigma$ for tensile creep tests and $\sigma_1=-\sigma$ for compressive creep tests, with the other two stresses equaling zero. The values A, B, H and F are material constants. The change in free volume (either increased in tension or decreased in compression) changes the intermolecular viscosity, and thus, the relaxation time for viscoelastic deformation, as can be seen in Equations 2 and 3. The greater the fraction of the total creep compliance associated with viscoelastic deformation, the greater will be the difference in the creep compliance (or creep modulus) in tension and compression.

For polymers reinforced with continuous fibers, the situation can be reversed. Long, thin fibers support tensile loading much more effectively than they support compressive loading. Tensile stresses straighten and stiffen the fibers, whereas fibers loaded in compression buckle, with a concurrent loss of stiffness. Thus, the tensile compliance in the direction of the fiber reinforcement should be less than the compressive compliance in the fiber direction. In the transverse direction, the compliance for tension and compression should behave more like pure resin, which has a higher compressive modulus.

In summary, unreinforced polymers will have a creep modulus in tension that is less than the creep modulus in compression or a creep compliance in tension that is larger than the creep compliance in compression. For continuous fiber polymeric composites, the situation is reversed.

Flexural Creep Compliance versus Tensile Creep Compliance

Flexural creep occurs with half the specimen in tension and half in compression. Thus, the compliance for flexural creep for polymeric solids (no reinforcement) should be less than that for tension, since the polymer creeps more slowly in compression than in tension, as previously discussed.

Williams [1] has shown using a simple analysis for three-point bending in a beam which behaves with a different modulus in tension than in compression that the flexural modulus is given by :

$$E_F = E_T \left(\frac{2\sqrt{E_c / E_T}}{1 + \sqrt{E_c / E_T}} \right)^2 \quad (5)$$

where $E_F(t)$, $E_C(t)$, and $E_T(t)$ are the creep moduli for polymeric solids in flexural, compressive, and tensile creep respectively. If one measures the flexural and tensile creep moduli, then the compressive creep modulus can be calculated by solving Equation 5 for the compressive creep modulus, which gives:

$$E_c = E_T \left(\frac{2 - \sqrt{E_c/E_T}}{\sqrt{E_c/E_T}} \right)^{-2} \quad (6)$$

There are at least three reasons why it is much easier to measure the flexural creep modulus than to measure the tensile creep modulus. First, the load required to give the same maximum stress (or strain) in flexure that one has in tension is given by

$$\frac{W_F}{W_T} = \frac{2d}{3L} \quad (7)$$

where "d" and "L" are the beam thickness and span length respectively. If one uses the d/L ratio recommended in ASTM D790 [4], which is between 16 and 40, then the required load in flexure is 1%–4% of the required load in tension, making the test apparatus simpler and less expensive.

Second, the displacements to be measured are much larger in flexural tests than in tensile tests, again making the test much simpler to set up and run, with

$$\frac{\delta_F}{\delta_T} = \frac{L}{6d} \quad (8)$$

where δ_F and δ_T are the displacements in flexure and in tension to give the same maximum strain values. Obviously, the d/L ratios recommended for flexural testing indicate the displacements to be measured will be much larger for flexural testing.

A third advantage of the flexural creep test compared to the tensile creep test is that the results are not directly affected by absorbed moisture and the swelling induced length change it produces in polymers that absorb significant moisture (7.5 wt%). Such swelling (or shrinking when the moisture is lost) is registered as additional creep strain in a tensile creep test. While absorbed moisture will increase the thickness of the specimen and be registered as a change in the load-line displacement, the thickness change will be small compared to the total load-line displacement in flexure. To the extent that the absorbed moisture plasticizes the polymer, the creep modulus will be effected in both flexure and tension in the same way, but this effect appears to be small except for temperatures that are near the glass transition temperature.

The determination of the creep compliance or creep modulus from the load-line displacement measurement is made using the standard relationship from beam theory for a simply supported beam that is loaded at the midpoint, with the result being

$$\delta(t) = \frac{WL^3}{48IE(t)} \quad (9)$$

where W is the load, L is the length between supports (or the span length), E is the creep modulus, and I is the moment of inertia, which is $(1/12)bd^3$, with "b" and "d" being the specimen width and thickness respectively. Rearranging the terms in Equation 9 gives the

16 LIMITS OF TEST METHODS FOR PLASTICS

calculated creep modulus (or compliance) as a function of the measured load-line displacement, or

$$E(t) = \frac{WL^3}{48I\delta(t)} \quad (10)$$

Equations 9 and 10 neglect shear deformation, which could give a small additional load-line displacement, causing one to underestimate the flexural creep modulus. A more exact solution by Williams[1] which includes shear deformation gives the following result:

$$E(t) = \frac{WL^3}{48\delta(t)I} [1 + 3(1 + \frac{\nu}{2}) \frac{d^2}{L^2}] \quad (11)$$

where all terms are as previously defined, and “ ν ” is Poisson’s ratio. As long as d/L assumes an appropriately small value (ASTM D790 [4] requires $d/L < 1/16$), the correction term included in Equation 11 in the brackets, but not included in Equation 10, is seen to be unnecessary.

Incremental or Tangential Modulus

In ASTM F-1216 [5], the buckling instability is calculated using the long-term creep modulus. As instability is inherently a short-term phenomenon, it would seem to make more sense to use the incremental modulus or tangent modulus for a short increase in load. Furthermore, the compression modulus or the flexural modulus would be more appropriate than the tensile modulus, which as we have already noted, should have a different value.

If the initial modulus and the incremental modulus at any time later in the creep test are the result of secondary bond stretching alone, then one would expect the incremental compliance (or modulus) to be the same as the initial modulus. However, the initial strain and compliance almost certainly include viscoelastic deformation for very short relaxation times. Once the sample has been in creep for 3700 hours, one would expect all of the short relaxation time processes to have taken place. Thus, the incremental compliance might include only bond stretching, giving a smaller value for the incremental compliance than the initial compliance and a larger incremental or tangent modulus than initial modulus (i.e. at $t = 0$, but just after loading).

Materials and Experimental Procedures

The polymers studied in this program were untoughened fabric filled, toughened iso-polyesters and vinyl esters. All materials were neat resins without any reinforcement. The ultimate tensile strengths and glass transition temperatures of the polymers used in this study are summarized in Table 1.

Table 1- *Material Properties of Esters Tested*

	Tensile Strength MPa	Heat Distortion Temp. °C
Iso-polyester A	40	97.8
Iso-polyester B	49.9	126.7
Iso-polyester C	-	-
Toughened Iso-polyester A	62	107
Toughened Iso-polyester B	49.6	107
Vinyl ester A, B	84	99-104

Flexural specimens were 10 cm long by 1.25 cm wide and 0.31 cm thick. The span width was 7.5 cm. The tensile specimens were 12.5 cm long, 1.25 cm wide, and 0.31 cm thick. Then tensile specimens were tabbed for gripping rather than being cut into a dogbone shape. The tensile specimens were tabbed using tapered aluminum tabs and a 0.6cm diameter hole was drilled through the tabs on each end of the specimen to allow pin loading for the creep test. The pin housing in the test fixture was a bearing to minimize any frictional stresses due to pin rotation during load transfer from the loading lever to the test specimen. Load was applied through a lever with a mechanical advantage of 8x using lead weights.

All tests were performed at room temperature, which was maintained at $23\text{ }^{\circ}\text{C} \pm 1\text{ }^{\circ}\text{C}$, but without any humidity control, which was seen to have given some scatter in the tensile creep results but not in the flexural creep results.

Strain gages were used to monitor the tensile creep strain, with computerized data acquisition. The resolution (of the strain gauge system) was 0.0001 cm/cm. The load-line displacement measurement was made using a dial gage with a resolution of 0.0006 cm.

A 12% load increment was added to some of the flexural creep specimens after they had crept for 3700 hours. The load increment, which took the maximum stresses from 25% of yield to 28% of yield, was held for 10s and then removed, with the strain increment on loading and unloading being measured. The stress and strain increments were then used to calculate the incremental or tangent compliance (or modulus). These values were compared to the initial values of compliance when the loading was first placed on the specimens at the beginning of the flexural creep tests.

Experimental Results and Discussion

Tensile versus Flexural Creep Compliance

The results of a long-time flexural creep test and a long-time tensile creep test on vinyl ester are presented in Figure 2 as creep compliance. The results support the expected greater creep compliance for tensile creep than flexural creep with $C_T(t) / C_F(t) = 1.15$ at $t \approx 3500$ hrs. This corresponds to $E_T / E_F = 0.865$. When substituted in Equation 6, this ratio

implies a compressive modulus which is $1.3 E_T$. Similar short-term results are seen in Figure 3 for a second vinyl ester, again with the expected larger tensile creep than flexural creep compliance. The ratio of $C_T(t)/C_F(t)$ will increase slightly as the fraction of total strain that is viscoelastic increases.

Moisture Effects in Tensile Creep—It should be noted that there appears to be much more scatter in the tensile creep than in the flexural creep in Figure 2, but not in Figure 3. The observed variations in tensile creep are associated with absorption and desorption of moisture as the relative humidity in the laboratory experiences seasonal fluctuations. These fluctuations are not observed in the short-time tests because the diffusion kinetics are too slow. The observed fluctuations in compliance correspond to strain fluctuations of 5×10^{-4} , which is consistent with moisture absorption of 0.22 wt%, epoxies can be used for vinyl esters.

Since extrapolation to a 50 year creep compliance or creep modulus depends critically on the short-term behavior, the moisture effects can potentially give significant errors, particularly if there is a one-time absorption of moisture into initially dry specimens. In tensile creep tests conducted over a two-year time period [7], the moisture fluctuations in the

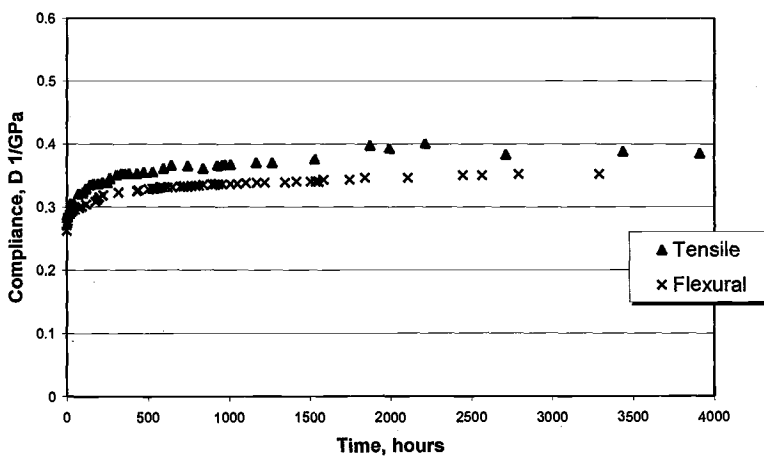


Figure 2- Comparison Of Creep Compliance For Tensile And Flexure Tests On Vinyl ester A for 3900 Hrs. at 23°C

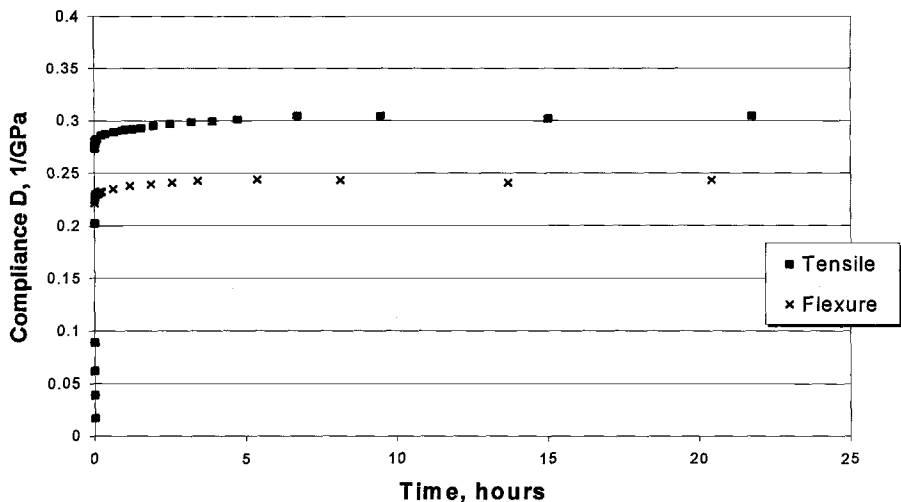


Figure 3—Comparison of Creep Compliance for Tensile and Flexural Tests on Vinyl ester B for 20 hours at 23°C.

vinylesters being tested introduced significant uncertainty into the long-term extrapolations. It should also be noted that vinylesters absorb much less moisture than most other engineering thermosets and many engineering plastics. The solution to this problem is to run pre-dried specimens in a dry atmosphere or water saturated specimens in a high humidity environment, which would include any acceleration due to the plasticizing effect of the moisture but not the erroneous, moisture-induced swelling strain.

Moisture Effects in Flexural Creep—There was no apparent effect of absorbed moisture on the flexural creep test results, as seen in Figure 2. Any change in the test specimen length due to absorbed moisture induced swelling will have no effect on the flexural creep, since the results depend only on the span width and not the specimen length. Any swelling induced increase in the specimen thickness will result in an error in the measured load-line displacement, but this error is small compared to the total load-line displacement in a flexural creep test. This is why the flexural creep test results in Figure 2 do not have the significant scatter that the tensile creep specimens have and is one reason to prefer flexural creep compliance measurements in preference to tensile creep measurements.

Initial Modulus versus Incremental (or Tangent) Modulus

Flexural creep compliance measurements on untoughened and toughened iso-polyester specimens are presented in Figure 4. At 3700 hours in these flexural creep tests, the load was increased by 12% for 10s before being removed with the incremental increase and subsequent decrease (which was the same as the increase) in the load-line displacement being noted. The load increment and load-line displacement increment may be used to calculate the incremental compliance (or tangent modulus), with the results presented in Table 2. The initial creep

compliance for initial load up of the specimens is also included in Table 2 and can be seen in Figure 4 as well. The measured incremental creep compliance was found to be ~23% less than the initial creep compliance for the untoughened iso-polyester and ~27% less than the initial creep compliance for the toughened iso-polyester.

Ideally, the initial modulus and the incremental modulus should be the result of secondary bond stretching alone, and therefore, should give identical values for their respective flexural compliances. However, the initial compliance (or modulus) includes some viscoelastic deformation for deformation increments with very short relaxation times. After creeping for 3700 hours, all such short-time relaxations should have occurred such that the incremental flexural compliance will be due to bond stretching alone. The corresponding incremental modulus (calculated as the inverse of the compliance) will be greater than the initial modulus determined on load up at the beginning of the creep test.

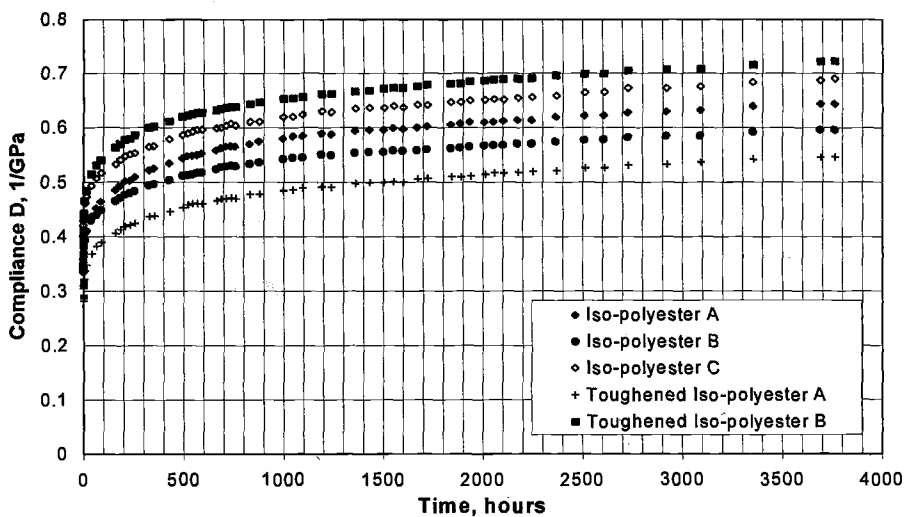


Figure 4- Flexural Creep Compliance for Iso-polyester Polymers

Table 2- *Comparison of Initial and Incremental Compliance Measurements*

Material ID	Initial Compliance 1/GPa	Incremental Compliance At 3700 hours, 1/GPa	Percent Difference
Iso-polyester A	0.33	0.25	23.3
Iso-polyester B	0.34	0.26	22.7
Iso-polyester C	0.37	0.28	24.4
Toughened Iso-polyester A	0.42	0.31	27.2
Toughened Iso-polyester B	0.30	0.18	29.7

Summary

The tensile creep compliance has been found to be ~15% greater than the flexural creep compliance for two vinyl esters tested in creep at ambient temperature. The incremental creep compliance measured at 3700 hours in a creep test was ~25% less than the initial compliance at the beginning of the creep test. The compression creep compliance was calculated from the measured tensile creep compliance and the flexural creep compliance, for a vinyl ester predicting a compression creep compliance that is 0.75 times the tensile creep compliance or a compression creep modulus that is 30% greater than the tensile creep modulus for a vinyl ester at ambient temperature. The effect of moisture on the creep compliance measurements was far greater in tensile creep tests than flexural creep tests in the vinyl esters that were studied. The observed variations in the compliance values for tension versus flexure tests were rationalized. The various compliance values were rationalized as being the result of viscoelastic deformation in the polymers, with the creep rates being influenced by the hydrostatic stress state.

References

1. Williams, J.G., *Stress Analysis of Polymers*, (New York: Halsted Press) 1980.
2. Kinlock, A.J. and Young, R.J., *Fracture Behavior of Polymers*, New York: Elsevier, 1983, pp. 26.
3. Doolittle, A.K., *J. Applied Physics*, 22, 1956, pp. 1471.
4. ASTM D-790-90 *Flexural Properties of Unreinforced and Reinforced Plastic and Electrical Insulating Materials* and ASTM-2990-93a *Tensile, Compressive Flexural Creep and Creep Rupture of Plastics*
5. ASTM F1216-93 *Rehabilitation of Existing Pipelines and Conduits by the Inversion and Curing of a Resin Impregnation Tube*
6. Schutte, Carol, "Environmental durability of glass-fiber Composites," *Materials Science and Engineering*, R13, No. 7, November 15, 1994.
7. Bradley, S.W., Puckett, P.M., Bradley, W.L. and Sue, H.J., "Viscoelastic Creep Characteristics of Neat Resin Thermosets Reinforced with E-Glass," *Journal of Composite Technology and Research*, 1998, Vol. 20, No. 1, pp. 51-58.

Dirk Blaese¹ and Ernst Schmachtenberg²

Estimation of Lifetime Under Non-Isothermal Conditions

Reference: Blaese, D. and Schmachtenberg, E., "Estimation of Lifetime Under Non-Isothermal Conditions," *Limitations of Test Methods for Plastics, ASTM STP 1369*, J. S. Peraro, Ed., American Society for Testing and Materials, West Conshohocken, PA, 2000.

Abstract: One possibility for prediction of lifetime of polymer products is given by the estimation of the limits of application by time-temperature-extrapolation of measured damage processes. A time-lapsing method for describing aging is given by the extrapolation with the statement of Arrhenius. If the temperature is not constant over lifetime there are two possibilities to estimate lifetime by time-lapsing lifetime tests. When the maximum temperature is supposed for the whole lifetime, an overdimensioning of the product is the result. The other way is a functional estimation of time-temperature-collectives for a more precise prediction of lifetime, which is shown in this presentation.

Keywords: prediction of lifetime, aging, time-temperature-shifting-principle, time-lapsing lifetime test

Introduction

The development of innovative products by using plastic materials represents a great challenge in respect to the material selection for the new product. The selection of a suitable material for a given application is not only influenced by the construction of the product and the processing of the material, but also essentially by the operating conditions of the product.

One problem at the material selection is the large number of different obtainable plastic materials. Only for thermoplastic materials are more than 10,000 commercial products available. The prices for these materials differ between \$1/kg (e.g. PE) and \$100/kg (e.g. PAEK). Closely associated with these costs for the raw material the properties of these plastic materials are very different. One example of this connection between price and property of a material is illustrated in Figure 1 for the property of heat resistance.

This connection shows that the production costs of technical products of plastic materials are the main reasons for a systematic material selection. In an evaluation of the production costs of a typical injection molding product shows that the material amounts to

¹ Dipl.-Ing., scientific staff, Institute for Plastics in Mechanical Engineering, University of Essen, Altendorfer Str. 3, D-45127 Essen, Germany

² Professor, Institute for Plastics in Mechanical Engineering, University of Essen, Altendorfer Str. 3, D-45127 Essen, Germany

55% of the production costs (Figure 2). This percentage of the material costs depends on the material and also on the output of the product.

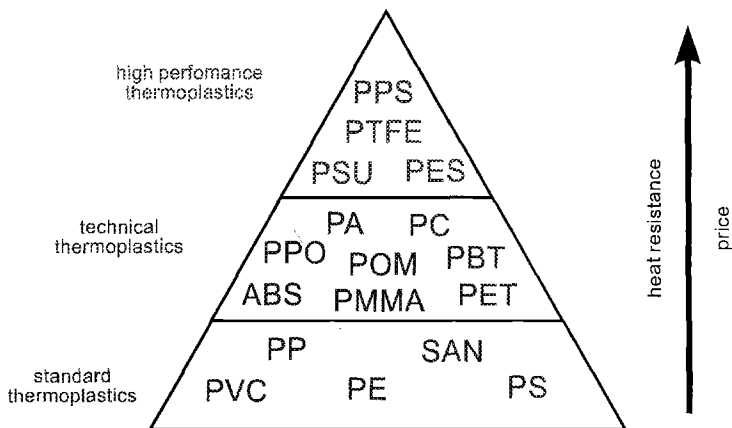


Figure 1 - *Classification of Thermoplastic Materials*

This points out that a systematic material selection is important for the economic production of plastic products as well as for the suitability for the application.

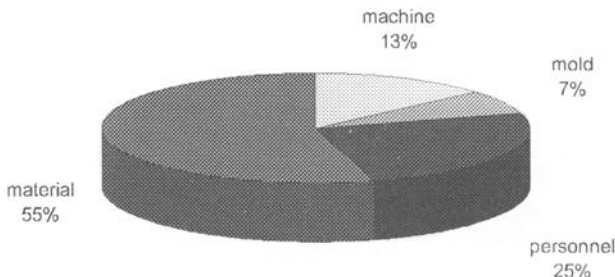


Figure 2 - *Production Costs (Example: injection molding, polyamide, weight 190 g, 180,000 pieces a year)*

Furthermore, plastic materials age under operating conditions. The lifetime of a product is influenced by its environment, temperature and mechanical loading. Figure 3 shows the decrease of strength of polyethylene-pipes with time. In this figure three different sections with three different gradients can be observed. The reason for these sections are the three different damaging processes of polyethylene by loading under temperature and an environment. [1,2]

This proves that the aging of a plastic material influences the lifetime of a product. Because of this it can be shown that the issue of aging and lifetime of a product is an essential factor in material selection which has to be taken into consideration.

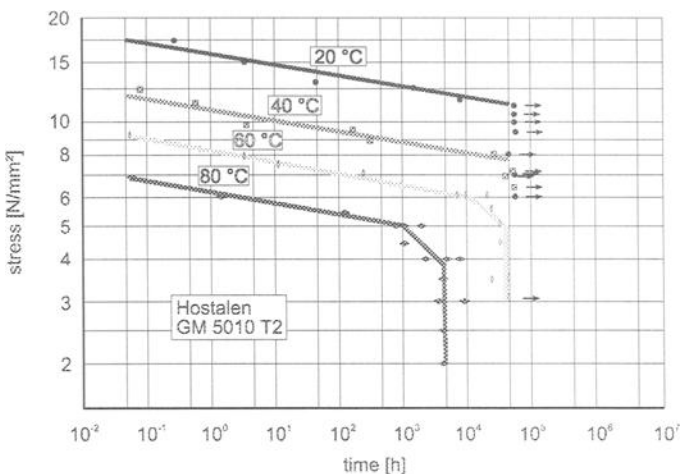


Figure 3 - Decrease of Strength by Time of a Polyethylene-Pipe [2]

Especially the influence of an environment can cause different interactions with the material. This can result in different failure mechanisms of the product.

It has to be taken into consideration that the different mechanisms cannot be analyzed separately. On the contrary, a superposition of these effects is the result because they influence each other.

We discuss below how is the lifetime of a product analyzed, as well as the suitability of the material for the given application after preselection of a plastic material.

Time-Temperature-Extrapolation with Arrhenius

Generally such an estimation of lifetime can be conducted by suitable and relevant product tests. It has to be guaranteed that the complexity of the application also can be reproduced in the product test. It is very important for the concept of these tests that a characteristic product value can be measured. This characteristic product value represents a measure for the damage of the product and depends on the loading of the product.

In practice a method is established which estimates the limits of application by time-temperature-extrapolation of the measured damage processes. So a lifetime prediction is possible by using the time-temperature-shifting-principle (Figure 4).

This time-temperature-shifting-principle says that the influence of a high temperature for a short time causes a comparable damage as a low temperature for a long time. One possibility to describe the time-temperature-shifting is given by the statement of Arrhenius. This is shown in equation 1:

$$\frac{t}{t_{\text{ref}}} = 10^{k \left(\frac{1}{T} - \frac{1}{T_{\text{ref}}} \right)} \quad (1)$$

where

t = required lifetime

t_{ref} = testing time

T = temperature

T_{ref} = testing temperature

k = shift factor

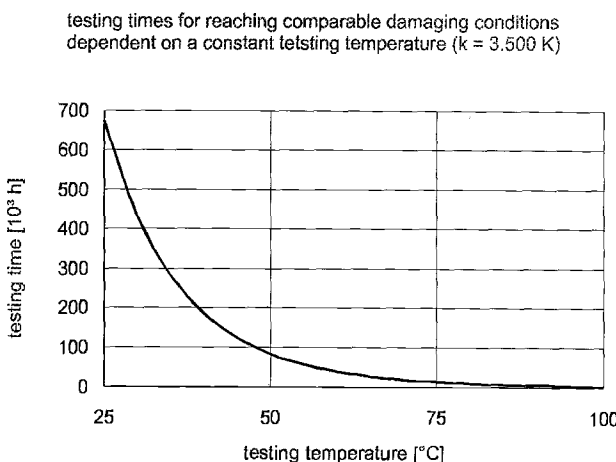


Figure 4 - Time-Temperature-Shifting-Principle

Thereby, k is the only unknown. This factor contains the influences of the used material, the given operating conditions like the environment and the loading as well as the influence of the design.

The shift factor k can be determined by the following product tests. For at least two different temperatures at different testing times the product must be taken from the test stand and the characteristic product value determined. The products are inspected to evaluate whether they suffer an identical damage according to the measured characteristic product value. This is equivalent for an identical damage of the product on account of the aging of the material.

With these two pairs of values, using the following equation 2, the shift factor k can be determined.

$$k = \frac{\log\left(\frac{t_1}{t_2}\right)}{\left(\frac{1}{T_1} - \frac{1}{T_2}\right)} \quad (2)$$

26 LIMITS OF TEST METHODS FOR PLASTICS

where

T_1 = temperature 1

T_2 = temperature 2

t_1 = damage time at the temperature 1

t_2 = damage time at the temperature 2

k = shift factor

With the determined shift factor k the time-temperature-shifting can be calibrated for the given application. This shift factor k is only valid for the given application, the material used and the evaluated product. An extension to other products is only limited possible because of these reasons.

By using the statement of Arrhenius for time-temperature-shifting it has to be noted that this statement is only valid in certain limits. These limits are the melting temperature or the glass transition temperature. An extrapolation should not be conducted over a too large temperature range. The insecurity of the results increases with increasing difference between testing temperature and operating temperature.

Estimation of Time-Temperature-Collectives

In practice a loading under a constant temperature for the whole lifetime is not realistic. On the contrary a complex time-temperature-profile is given (Figure 5).

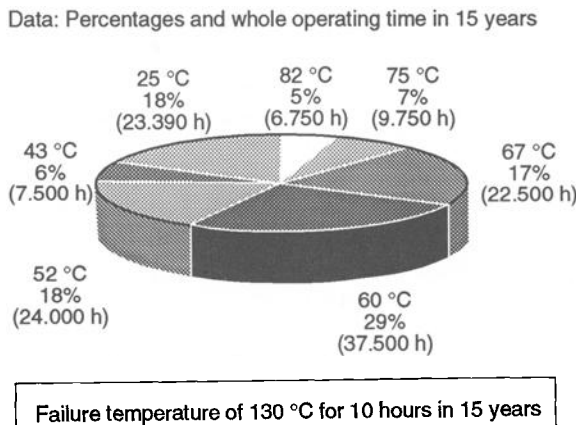


Figure 5 - Time-Temperature-Profile

In this case it is possible to suppose the highest temperature for the whole lifetime as the critical temperature for the strength of the product. This leads to a high demand on the properties of the material used. So this procedure leads to a large overdimensioning of the product and thus to a very uneconomic solution of the product idea.

A second way to consider such time-temperature-profiles is given by an estimation of the separate time-temperature-collectives with regard to their contribution of aging. For this the following procedure is imaginable:

1. An "influence" is defined as a specified time-interval during which a specified environment with a constant temperature and under a constant loading is influencing the product.
2. This influence affects an "aging" of the product. Different influences can be taken into consideration for the determination of aging of the product by addition of the different parts. So an "aging progress" is defined by several influences.
3. If the aging is advanced to a critical state the product changes its properties (e.g. decrease of strength, change of the molecular structure of the product or other).
4. The estimation of the different parts of aging caused by an influence is conducted with the help of the time-temperature-shifting-principle.

For each influence a reference-time would be calculated which causes a comparable aging progress at reference-temperature. By addition of the separate reference-times a total testing time for the product can be evaluated. This testing time at reference-temperature produces a comparable damaging of the product as it will be caused by the influence of the time-temperature-profile for the required lifetime.

The example described in the following explains this principle and shows at the same time the measurement of a suitable indicator-property for products loaded with an internal pressure.

For this product which is subjected to temperature, environment and internal pressure the time-temperature-profile is shown in Figure 5. With equation 1 it can be determined that with the assumed maximum temperature of 130°C for the total lifetime of 15 years a testing time of about 300,000 hours at a testing temperature of 120°C is required. With the principle of estimation of time-temperature-collectives as described above the testing time can be reduced to 107 hours at a testing temperature of 120°C.

Thus, the separate time-temperature-intervals are separately inspected. For each interval a testing time at testing temperature can be estimated with Arrhenius. With the described procedure the aging progress can be estimated. The addition of these aging progresses provides a measure of the real damage caused by the time-temperature-profile.

The percentages of time and aging evaluated with this principle are shown in Figure 6. By this it can be illustrated that the high temperature exposures are very critical and that they cause a high percentage of aging although they are in effect for only a short time. Because of this it is obvious that designing with this maximum temperature over the whole lifetime leads to a large overdimensioning of the product.

The characteristic product value to describe the damage of the product caused by the aging progress of the material is measured with a so-called "bursting test". This means that the parts are tested by a raising internal pressure up to failure. The bursting strength is used as the indicator for damage. A pressure-time-curve for this indicator is given in Figure 7 for the examined product. In Figure 7 there are shown three different curves for three different designs of the product. All products are made of a polyamide PA 66 with 30% glass fibre. A decrease of the strength caused by the aging of the material can be pointed out.

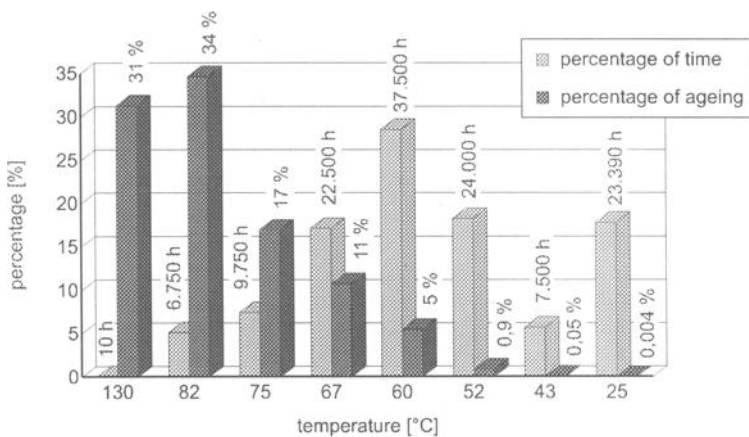


Figure 6 - Percentages of Time and Aging

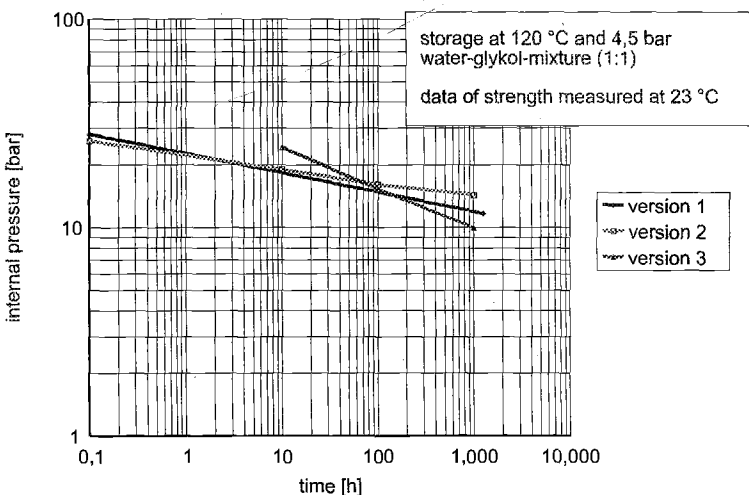


Figure 7 - Internal Pressure Strength for Describing the Damage [3]

To evaluate the above described theory such a pressure-time-curve was measured for a special product. A few parts of this product were also operated under real conditions for a determined time. The internal pressure strength of these parts can be compared with the measured values of testing (Figure 8). The operating time can be converted with the Arrhenius model and so these results can be compared with the results of the product tests.

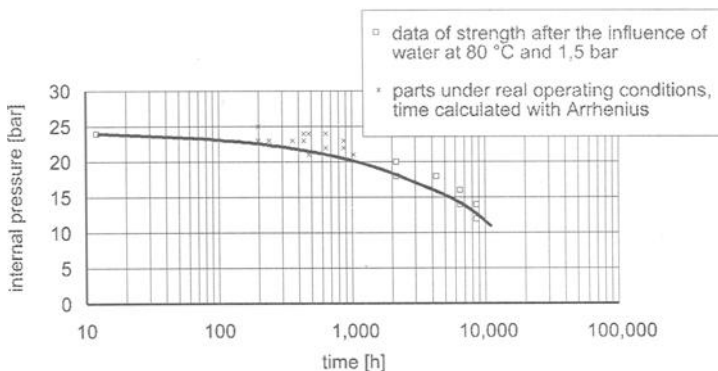


Figure 8 - *Comparison between Calculated and Measured Damage*

The results of this comparison illustrate that the parts under the real operating conditions show a higher internal pressure strength than those evaluated by the described theory. This shows that the estimation of time-temperature-collectives is an estimation on the safe side. With this theory overdimensioning can be avoided.

References

- [1] Menges, G., "Werkstoffkunde der Kunststoffe," 3. Auflage, Carl Hanser Verlag, München, Wien, 1990
- [2] Diedrich, G., Kempe, B. and Graf, K., "Zeitstandfestigkeit von Rohren aus Polyethylen (HDPE) und Polypropylen (PP) unter Chemikalieneinwirkung," Kunststoffe 69 (1979) 8, pp. 470-476
- [3] Schmachtenberg, E. and Blaese, D., "Werkstoffauswahl und Lebensdaueranalyse," internal report of the IKM, archive number IP 96085, 1987

DISCUSSION

Gary Runyan¹ (written discussion)—The paper addressed aging due to different times at different temperatures, basically an oxidative condition. There are also chemicals that will cause oxidative failures in plastics that appear to be identical to those caused by heat alone. The application I am thinking about is plastic pipe with chlorinated drinking water. In hot water plumbing applications, the pipe is subjected to thermal oxidation from the heat and chemical oxidation from the chlorine in the water. In tests, the failures induced by thermal oxidation appear to be identical to failures induced by chemical oxidation.

Do you have any ideas on how to combine these two aging processes into one accelerated conditioning program that would allow you to select a set of accelerated aging conditions that would simulate the thermal and chemical oxidative effects of a very long period of time? After conditioning, the product (in this case it would be pipe) could be tested to see if it still met the minimum performance requirements.

A test protocol based on this type of procedure would probably be much more economical and quicker than the current method of generating Arrhenius curves at multiple temperatures and chlorine levels by testing pipe samples to failure. Many of these tests take nearly two years to complete. Manufacturers, who are often interested in evaluating several different compounds, could use a faster, more economical method.

¹U.S. Brass, 901 10th Street, Plano, TX 75074.

CLOSURE

Blaese and E. Schmachtenberg (authors' closure)

Plastic products under real operating conditions are changing their properties because of different aging mechanisms. We can divide between aging because of mechanical loading (e.g. creeping), aging because of heat (e.g. oxidation, degradation) and aging because of a chemical (e.g. hydrolysis, environmental stress cracking, swelling). All these aging mechanisms result in different damage of the product. So it is very important to build up lifetime tests which integrate all these effects.

The main aim has to be that this test can predict lifetime of plastic products under complex conditions (e.g. heat, oxidation, chemicals and mechanical loading) within a short test time in the laboratory. We agree with the discusser that such a test will be a more economical and quicker method than the current method.

At this time we do not know enough about the different aging mechanisms to build up such a testing method. The interactions between the different processes are too complex that we do not know how to describe the different aging mechanisms and how to estimate which is the most important one.

The research work at the IKM deals with this theme of aging of plastic products under complex conditions with the aim to build up such a test. We hope that we can answer this question in a few years. At this time we only have the possibility to shorten the test time by the time-temperature-shifting-principle of Arrhenius.

How to do this if the operating temperature is not constant was shown in the presentation. But this is only valid if we do not have any change in the damage mechanism.

Mechanical

Matthew J. Friday¹

A Comparison of Tension Test Data Using ASTM D 638 and ISO 527

Reference: Friday, M. J., "A Comparison of Tension Test Data Using ASTM D 638 and ISO 527," *Limitations of Test Methods for Plastics, ASTM STP 1369*, J. S. Peraro, Ed., American Society for Testing and Materials, West Conshohocken, PA, 2000.

Abstract: Although several fundamental differences exist between ASTM D 638 Standard Test Method of Tensile Properties of Plastics and ISO 527 Plastics - Determination of Tensile Properties, the actual test results can be quite similar. Test data for both test methods have been gathered by an interlaboratory testing provider and the summary statistics of the two groups were compared. The thermoplastic resins tested in this study included polycarbonate (PC), polybutylene terephthalate (PBT), acrylonitrile-butadiene-styrene (ABS) and high impact polystyrene (HIPS). All resins were unfilled, unreinforced, and uncolored. The following properties were analyzed: Tensile Stress at Yield, Tensile Stress at Break, Elongation at Yield, and Modulus of Elasticity. After removing outliers, the data from the remaining labs were analyzed. The strength of agreement between ISO data and ASTM data varied depending on the property and material used. There were surprising similarities for modulus of elasticity since different speeds of testing and calculation methods were used.

Keywords: thermoplastics, tensile properties, interlaboratory testing, ASTM D 638, ISO 527, ABS, PBT, polycarbonate, polystyrene, tensile stress at yield, tensile stress at break, elongation at yield, modulus of elasticity

Introduction

The technical differences between ASTM Tensile Properties of Plastics D 638 and ISO 527-1&2 Plastics Determination of Tensile Properties include specimen dimensions (Table 1), speeds of testing, and modulus of elasticity calculations. Each of these conditions can affect the test results in different ways and to varying degrees. By measuring the tensile properties of ASTM and ISO specimens molded from the same thermoplastic resins, the relationship between the ASTM D 638 and ISO 527 test methods was studied. Since the ASTM D 638 and ISO 527 test methods are technically different the summary statistics from these test methods are viewed as two distinct populations. Therefore, descriptive statistics rather than inferential statistics were used in this comparison. No attempt was made to determine if the results from the two test

¹Program Manager, Collaborative Testing Services, Inc., 340 Herndon Parkway, Herndon, VA, 20170.

methods are statistically equivalent.

Test Design

The data for this comparison were gathered by an interlaboratory testing provider conducting an ongoing plastics testing program. Participants included domestic and international resin producers, users, and independent material testing labs. Interlaboratory testing assesses a laboratory's measurement capabilities by comparing their results with other laboratories testing the same materials and following the same test method. Many labs participate as part of their quality assurance system while others use the interlaboratory testing program to satisfy accreditation requirements. An additional benefit of such an industry-wide testing scheme is the analysis of overall testing results, such as this comparison of similar test methods.

Table 1 - *Specimen Dimensions*

	ASTM D 638 Type 1	ISO 527 Type 1A
Overall length, mm	≥ 165	≥ 150
Width at ends, mm	19 + 6.4	20.0 ± 0.2
Length of narrow parallel-sided section, mm	57 ± 0.5	80 ± 2
Gage length, mm	50 +0.25	50.0 ± 0.5
Distance between grips, mm	115 ± 5	115 ± 1
Radius of fillet, mm	76 ± 1	20 to 25
Thickness, mm	3.2 ± 0.4	4.0 ± 0.2
Width of narrow section, mm	13 ± 0.5	10.0 ± 0.2
Cross-sectional area of narrow section ¹ , mm ²	35.0 to 48.6	37.2 to 42.8
Perimeter of narrow section ¹ , mm	30.6 to 34.2	27.2 to 28.8

¹ Area and perimeter values are not specifications. These values were calculated from thickness and width specifications listed in the test methods for informational purposes only.

For the purposes of this comparison, certain testing protocols were followed. Each quarter, the participants received test specimens molded from two different grades of the same type of resin. In Tables 2 through 5, the different grades of resin are labeled with #1 and #2 following the resin type. The resins used in the testing program were unfilled, unreinforced, and uncolored thermoplastics. Only data from ASTM Type 1 and ISO Type 1A bars molded from the same lot of resin are compared. Both the ASTM and ISO test methods require a minimum of five specimens to be tested. Participants in the ISO 527 test report data for ten specimens per sample. For the ASTM D 638 test method, eight specimens are tested for each sample. The additional specimens were tested for greater precision of the Lab Means. Laboratories may enroll in the tests appropriate for their laboratory and test equipment; therefore, labs testing ASTM specimens are not the same

labs testing ISO specimens. The properties measured include Tensile Stress at Yield, Tensile Stress at Break, Elongation at Yield, and Modulus of Elasticity. The labs are asked to select the properties most appropriate for their equipment and lab. Therefore the number of labs reporting data will vary for each property.

The speeds of testing for stress and elongation measurements were the same for both ASTM and ISO specimens. The polycarbonate (PC), polybutylene terephthalate (PBT), and high impact polystyrene (HIPS) resins were tested at 50 mm/min. For the acrylonitrile-butadiene-styrene (ABS) resins a speed of testing of 5 mm/min was used. Modulus measurements for ASTM specimens were conducted at these same speeds. For the ISO specimens, a separate set of ten specimens were tested at 1 mm/min. In addition to the difference in speed of testing, tangent modulus was reported for ASTM specimens, and chord modulus at 0.05 and 0.25 percent strains was reported for ISO specimens.

The individual determinations reported by a lab for a sample are averaged to calculate a Lab Mean. The Lab Means are then analyzed through comparative statistics to remove outlying labs. The analysis procedure consists of a two-sample analysis that is essentially a T^2 bivariate control chart. The two sample approach detects both extreme data and inconsistency in testing between samples. With the outliers removed, a Grand Mean is then calculated by averaging the Lab Means of the remaining labs. The consensus values or Grand Means (Means) are presented in Tables 2 through 5 along with Between-Lab Standard Deviations (BL Std Dev) of the Grand Means. The Difference of the Means was calculated by subtracting the ISO mean from the ASTM mean. When comparing the data, differences can also be expressed as the number of standard deviations. For the sake of simplicity, the lesser of the two standard deviations was used in this comparison. Coefficient of Variances (COV) have also been calculated for this study to facilitate the comparison among the wide range of materials. The number of labs included in the Grand Means and the total number reporting data are listed in the tables as well (Labs (I/R)). Data in these tables are listed in numerical order of the mean values. Both ISO 527 and ASTM D 638 specify three significant figures for reporting stress and modulus measurements and two significant figures for elongation measurements. For the purpose of this comparison, one extra figure appears in the data tables.

Comparison of Test Data

The test specimens have obvious dimensional differences that may affect the test results. These differences are summarized in Table 1. Although the cross-sectional areas of the specimens are similar, the different geometries could affect the test results. During molding of these end-gated specimens, molecular alignment occurs to varying degrees in the outer layers of the specimen in the flow direction [1]. The ASTM Type 1 specimens have a slightly larger perimeter than the ISO Type 1A specimens, resulting in more material with molecular alignment in the cross-sectional area of the narrow section. Depending on the material and the degree of the anisotropy, the ASTM specimens may have higher strength and modulus values than the ISO specimens. The different surface area to volume ratio of the two specimen types could also affect the cooling stage of the specimens thereby influencing crystallization.

Tensile Stress at Yield (Table 2) is measured essentially the same way for both

Table 2 - Tensile Stress at Yield, MPa

Resin	ASTM D 638			ISO 527			Difference of Means	
	Mean	BL Std Dev	COV	Mean	BL Std Dev	COV	Labs (I/R)	% Diff
HIPS #1	20.95	0.83	3.96	89 / 100	19.65	0.61	3.10	30 / 34
HIPS #2	29.28	0.90	3.07	89 / 100	28.11	0.84	2.99	30 / 34
PBT #2	37.93	1.17	3.08	92 / 97	36.65	1.06	2.89	33 / 35
ABS #1	43.93	0.84	1.91	85 / 96	40.41	0.73	1.81	82 / 91
ABS #2	50.61	0.97	1.92	85 / 96	45.74	0.98	2.14	82 / 91
PBT #1	57.02	1.74	3.05	92 / 97	56.35	2.14	3.80	33 / 35
PC #1	60.51	1.19	1.97	77 / 93	59.28	1.27	2.14	21 / 27
PC #2	64.29	1.18	1.84	77 / 93	62.10	1.55	2.50	21 / 27
							2.19	3.41

Table 3 - Elongation at Yield, %

Resin	ASTM D 638			ISO 527			Difference of Means	
	Mean	BL Std Dev	COV	Mean	BL Std Dev	COV	Labs (I/R)	% Diff
HIPS #1	1.32	0.11	8.33	55 / 83	1.21	0.13	10.74	27 / 32
HIPS #2	1.74	0.14	8.05	55 / 83	1.67	0.11	6.59	27 / 32
ABS #1	2.55	0.12	4.71	62 / 83	2.40	0.12	5.00	54 / 78
ABS #2	2.70	0.15	5.56	62 / 83	2.35	0.12	5.11	54 / 78
PBT #1	3.80	0.36	9.47	62 / 80	3.64	0.25	6.87	23 / 30
PBT #2	6.06	0.67	11.06	62 / 80	5.08	0.34	6.69	23 / 30
PC #2	6.29	0.34	5.41	56 / 72	6.02	0.30	4.98	20 / 24
PC #1	6.45	0.32	4.96	56 / 72	6.40	0.49	7.66	20 / 24
							0.05	0.78

Table 4 - Tensile Stress at Break, MPa

Resin	ASTM D 638				ISO 527				Difference of the Means	
	Mean	BL Std Dev	COV	Labs (I/R)	Mean	BL Std Dev	COV	Labs (I/R)	(ASTM - ISO)	
HIPS #1	19.29	0.74	3.78	68 / 80	18.41	0.88	4.78	30 / 30	0.88	
HIPS #2	25.47	0.77	3.02	68 / 80	24.84	1.07	4.31	30 / 30	0.63	
PBT #1	29.10	4.74	16.29	58 / 68	32.08	5.50	17.14	27 / 29	-2.98	
PBT #2	30.09	2.58	8.57	58 / 68	26.19	2.38	9.09	27 / 29	3.90	
ABS #1	32.34	1.68	5.19	64 / 76	31.37	1.31	4.18	80 / 92	0.97	
ABS #2	36.93	1.77	4.79	64 / 76	34.63	1.40	4.04	80 / 92	2.30	
PC #1	64.18	2.44	3.80	62 / 69	70.96	2.20	3.10	18 / 19	-6.78	
PC #2	70.62	3.90	5.52	62 / 69	69.88	2.74	3.92	18 / 19	0.74	

Table 5 - Modulus of Elasticity, MPa

Resin	ASTM D 638						ISO 527						Difference of the Means	
	Mean	BL Std Dev	COV	Labs (I/R)	Mean	BL Std Dev	COV	Labs (I/R)	Mean	BL Std Dev	COV	Labs (I/R)	(ASTM - ISO)	
PBT #2	1642	185	11.27	51 / 59	1674	119	7.11	18 / 23	-32					
HIPS #1	1926	221	11.47	55 / 65	1956	166	8.49	20 / 24	-30					
HIPS #2	2200	268	12.18	55 / 65	2110	222	10.52	20 / 24	90					
PC #1	2264	241	10.64	53 / 59	2389	161	6.74	16 / 19	-125					
ABS #1	2297	280	12.19	59 / 64	2264	159	7.02	53 / 65	33					
PC #2	2370	224	9.45	53 / 59	2466	176	7.14	16 / 19	-96					
PBT #1	2384	273	11.45	51 / 59	2544	166	6.53	18 / 23	-160					
ABS #2	2579	335	12.99	59 / 64	2543	177	6.96	53 / 65	36					

ASTM D 638 and ISO 527 test methods: the stress at which an increase in strain occurs without an increase in stress. This is the point of zero slope on the stress-strain curve. Since the speeds of testing and materials were the same for both ASTM and ISO data, any differences found were most likely due to molding and specimen geometry. All of the results for Tensile Stress at Yield were within two standard deviations except for the ABS resins and HIPS #1. There was slightly more than two standard deviations difference for HIPS #1 and more than four standard deviations difference for both ABS resins. This is interesting given that there is better agreement for the ABS resins among the other properties. It is also interesting that for all of the resins, the means for the ASTM specimens were higher than the means for the ISO specimens. This is consistent with the previously mentioned effects of specimen geometry. The coefficient of variances were similar for both test methods.

Elongation at Yield (Table 3) results for the ASTM specimens were also slightly higher than the ISO specimens. As mentioned previously for the Tensile Stress at Yield data, this is most likely due to molding and specimen geometry. The difference was less than one standard deviation for five of the eight materials. The results for ABS #1 were less than two standard deviations apart. Larger differences existed for ABS #2 and PBT #2. Excepting PBT #2, the two test methods had similar variability. Overall, one method did not appear more consistent than the other for Elongation at Yield.

Break properties are generally less consistent than yield properties. This was particularly true for the Tensile Stress at Break (Table 4) of both grades of PBT. These specimens had a strong tendency to “neck” or “draw” after the yield point. The coefficient of variances for these resins is more than twice that of the others. The difference between the test methods was less than two standard deviations for all materials except PC #1. Less than one standard deviation difference exists for the remaining properties for PC #1.

The results for ASTM D 638 and ISO 527 are surprisingly close for Modulus of Elasticity (Table 5) given the technical differences between the two methods. The speed of testing for all materials was 1 mm/min for the ISO specimens, while Modulus of Elasticity for the ASTM specimens was measured using 5 mm/min for ABS and 50 mm/min for HIPS, PC, and PBT. Theoretically, the viscoelastic nature of these thermoplastics should have resulted in higher modulus values when tested at a higher strain rate [1,2,3]. The anisotropy of the test specimens should have also resulted in higher values for the ASTM specimens. Neither of these factors seemed significant for the Modulus of Elasticity of these materials. For all eight materials in this study, less than one standard deviation of difference was found between the means for the ASTM D 638 and ISO 527 test methods. This may be due in part to the difference in modulus calculations for each test method. For the ASTM specimens, the slope of tangent method was used. The participants either manually calculated the modulus from the stress-strain curve or used software to determine the slope of the initial linear portion of the curve. The participants testing the ISO specimens calculated the chord modulus using the two strain points, 0.05 % and 0.25%, as specified in ISO 527. Modulus of Elasticity as calculated by the ISO method resulted in better agreement between labs. This is evident in the lower coefficient of variances for the ISO test method for all eight materials. The closer agreement between labs using the ISO Method is most likely the result of the labs using the same two points on the curve for the modulus calculation instead of determining

the slope of a portion of a stress-strain curve.

Common Errors in Testing

The numerical analysis of the tensile properties was conducted by comparing the results from laboratories included in the statistics. The correlation continues with the outliers for both test methods. On an anecdotal basis, several typical testing errors made during testing were investigated and found to occur in labs using either test method.

Most of the outliers for Elongation at Yield typically test high for both samples. One common mistake made by these laboratories is the use of cross-head deflection or grip separation to measure elongation. Any initial seating of the specimen in the grips at the start of the test will cause a "toe" on the stress-strain curve. This toe region is a small section of very low slope before the initial linear portion of the curve. A procedure for toe compensation can be found in the annexes of ASTM D 638 however, there is no provision for toe compensation in ISO 527. If no compensation is made for this toe region, elongation measurements will be falsely high. Since elongation of the specimen will be less in the radius and grip areas compared to the narrow section, selection of an initial gage length is critical and will affect elongation measurements significantly. The accuracy of this type of elongation measurement is not suitable to measure Elongation at Yield. Both ASTM D 638 and ISO 527 only permit the use of grip separation to measure strain after the yield point.

A correlation was found between outlying laboratories reporting high Elongation at Yield results and low Modulus of Elasticity results. This could be the result of including the initial low sloped toe region of the stress-strain curve in the calculation of tangent modulus using ASTM D638. The 0.05% strain point used in the calculation of chord modulus for ISO 527 would fall in the toe region causing erroneous data. These laboratories often report Yield and Break Stress values that are consistent with the other participants. This is not surprising since these values can be determined from the shape of a stress-strain curve without accurate strain measurements.

Several labs have on occasion reported data for the wrong yield point. This was most prevalent for the polycarbonate specimens. These materials yielded, then continued to elongate with an increase in stress before break. As a result, several labs reported Tensile Stress at Yield results that were similar to Tensile Stress at Break. Elongation at Yield results for these labs were greater than 100% instead of approximately 6%. Clearly they had selected a point just before break as the yield point. These mistakes are often due to reliance on computer software for calculations. Laboratories who have experienced these problems are encouraged to periodically verify automatically calculated results using stress-strain curves and manual computations. This is particularly true when testing an unfamiliar material that may have an unusually shaped stress-strain curve.

Summary

The results from this comparison have shown that the strength of correlation between ASTM D 638 and ISO 527 test methods can vary for materials and properties. Of particular interest was the agreement for Modulus of Elasticity. The labs testing the

42 LIMITS OF TEST METHODS FOR PLASTICS

ASTM and ISO specimens were different populations. A future study could require one group of labs to test both types of specimens. The data presented in this study provides a foundation for further research into the relationship between the ASTM D 638 and ISO 527 test methods.

References

- [1] Turner, S., "Tensile Testing of Plastics," *Tensile Testing*, P. Han, Ed., ASM International, Materials Park, OH, 1992, pp. 105-133.
- [2] Daniels, C. A., Ph.D., P.E., *Polymers: Structure and Properties*, Technomic Publishing Company, Inc., Lancaster, PA, 1989.
- [3] Harper, C. A., *Handbook of Plastics, Elastomers, and Composites*, Second Edition, Technology Seminars Inc., Lutherville, MD, McGraw-Hill Inc., 1992.

DISCUSSION

Nanying Jia¹ (written discussion)—Are there companies that subscribed both ASTM and ISO tests on tensile properties? Presumably the comparison limited to these companies would eliminate certain variabilities that may contribute to the difference between the ASMT and ISO results.

M. A. Friday (author's closure)—There was an insufficient number of laboratories participating in both the ASTM and ISO tests to conduct a thorough comparison of test results. Although the use of one group of labs would eliminate certain variables, the summary statistics from a very small group could be significantly influenced by one or two labs. The purpose of this study was to use larger populations more representative of the industry to compare the summary statistics for the two test methods.

¹Allied Signal Inc., 101 Columbia Rd., Morristown, NJ 07962-1021.

Michael P. Sepe¹

The Usefulness of HDT and a Better Alternative to Describe the Temperature Dependence of Modulus

Reference: Sepe, M. P., "The Usefulness of HDT and a Better Alternative to Describe the Temperature Dependence of Modulus," *Limitations of Test Methods for Plastics, ASTM STP 1369*, J. S. Peraro, Ed., American Society for Testing and Materials, West Conshohocken, PA, 2000.

Abstract: The vast majority of the short-term properties that appear in a material data sheet are measured at room temperature. The heat deflection temperature (HDT) represents the only systematic attempt to characterize elevated temperature performance. The HDT test describes a particular response to temperature under a very specific set of conditions, however it is often used in the material selection process as a maximum continuous use temperature. As the trend toward the computerization of property data has progressed, the tendency to rank order properties for a large number of materials from different families has increased the separation between the property value and its significance to the design engineer.

This paper will briefly review the HDT test as defined in the ASTM Test Method for Deflection Temperature of Plastics Under Flexural Load (D 648) and the International Standards counterpart, ISO 75. It will then discuss an alternative method for capturing a more complete picture of the effect that temperature has on modulus. This technique, known as dynamic mechanical analysis (DMA), provides an excellent tool for evaluating materials and comparing their mechanical performance over a wide range of temperatures.

Keywords: heat deflection, DMA, properties

Background

ASTM D 648 describes a method for determining the heat deflection temperature (HDT) or deflection temperature under load (DTUL). With the trend toward globalization, this method is reflected in and refined by ISO 75. Both tests seek to define the temperature at which a given degree of bending is achieved in a sample placed under a fixed flexural stress. The apparatus used to conduct the test is shown (Figure 1). The working portion of the instrument is immersed in an oil-based fluid, which is used as the heat transfer medium. A specimen is placed in a 3-point bend fixture and the desired stress

¹Technical Director, Dickten & Masch Mfg. Co., Watertown Plank Road, Nashotah, WI 53058.

is applied to the center of the bar. The temperature of the oil bath is then raised at a rate of 2°C/minute until the limiting deflection point is reached. This temperature is defined as the heat deflection temperature. Typically the test is run at two different stresses. In the ASTM method the stresses are specified at 0.455 MPa (66 psi) and 1.820 MPa (264 psi). ISO 75 has added a third condition that employs a stress of 8.00 MPa (1160 psi). Sample thickness, fabrication technique, and post-molding treatments such as annealing will influence the results of the test. This has been addressed in previous work [1]. The focus of this work is the relationship of the HDT to the load-bearing properties of a material at elevated temperatures.

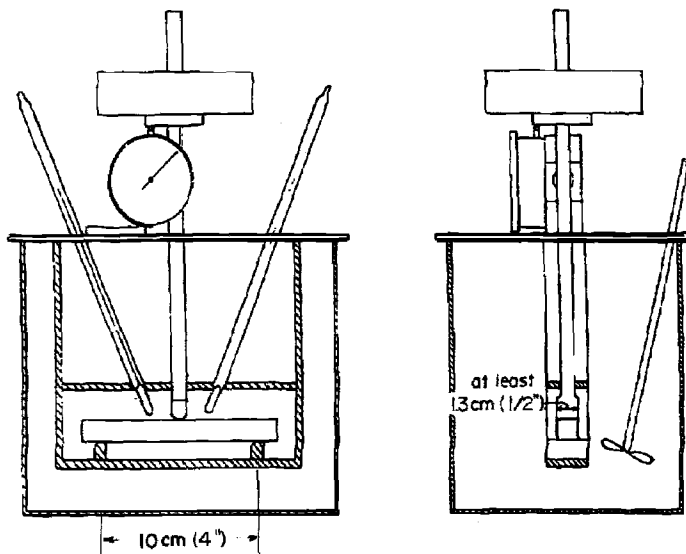


Figure 1 – Apparatus for Deflection Temperature Test

Discussion

Since the HDT defines a temperature at which a given sample geometry exhibits a specific deformation under a fixed stress, the test essentially measures the temperature at which a material achieves a certain modulus [2]. An examination of property sheets from different materials reveals some interesting patterns which can be misleading to an engineer or designer who is uninitiated in the peculiarities of polymer structure. The most important difference in defining the response of a polymer to increased temperature is the distinction between semi-crystalline and amorphous structure. The HDT values for unreinforced and glass fiber-reinforced grades of nylon 6, a semi-crystalline polymer, and polycarbonate, an amorphous material, are shown (Table 1). Note that in the unfilled nylon 6 the HDT values at the high and low stress are 110°C apart while the values for the unfilled polycarbonate differ by only 6°C. The introduction of glass fiber raises the HDT of

the polycarbonate by only 10°C at both stress levels. The improvement in the nylon 6, however, is much more dramatic. Even with the addition of a small amount of reinforcement, the value at 0.455 MPa increases by 35°C. However, at 1.82 MPa it increases by 135°C and becomes almost equal with the test value for the lower stress. The incorporation of additional reinforcement has little or no effect on the HDT in either material. These patterns are apparent for most materials that fall into either the amorphous or semi-crystalline family.

Table 1- *HDT Values for Nylon 6 and Polycarbonate*

Material	HDT Values (°C)	
	@ 0.455 MPa	@ 1.82 MPa
PC-Unfilled	138	132
PC-10% Glass	148	142
PC-40% Glass	154	146
Nylon 6- Unfilled	175	65
Nylon-14% Glass	210	200
Nylon-44% Glass	215	210

Nylons and other semi-crystalline resins such as polyesters make extensive and very efficient use of a wide variety of fillers and reinforcements. While glass fiber is perhaps the most important of these, mineral systems and glass bead are also used to reduce warpage and cost. Often the differences in elevated temperature performance are not detectable through the HDT. HDT measurements at 1.82 MPa for an unreinforced nylon 6, and a PBT polyester along with several filled analogs are shown (Table 2). All of the filled varieties appear to benefit equally from the addition of the inorganic material. In order to make sense of this data; a method is needed that examines the modulus of the material before and after the HDT. A powerful technique that accomplishes this objective is dynamic mechanical analysis (DMA).

Table 2 – *HDT for Nylon 6 and PBT Polyester with Various Fillers*

Filler Type & Amount	HDT @ 1.82 MPa (°C)	
	Nylon 6	PBT
None	65	54
14% Glass	200	191
33% Glass	210	207
44% Glass	210	204
40% Glass/Mineral	206	199

The principles of DMA are beyond the scope of this paper and are covered in various publications [3,4] as well as in the literature of companies that supply dynamic mechanical analyzers [5]. In its simplest form the output from a DMA gives a plot of the elastic and viscous modulus as a function of temperature. The elastic modulus provides a measurement of the load-bearing properties while the viscous modulus assists in

pinpointing important transitions and provides an assessment of a material's tendency to creep under load.

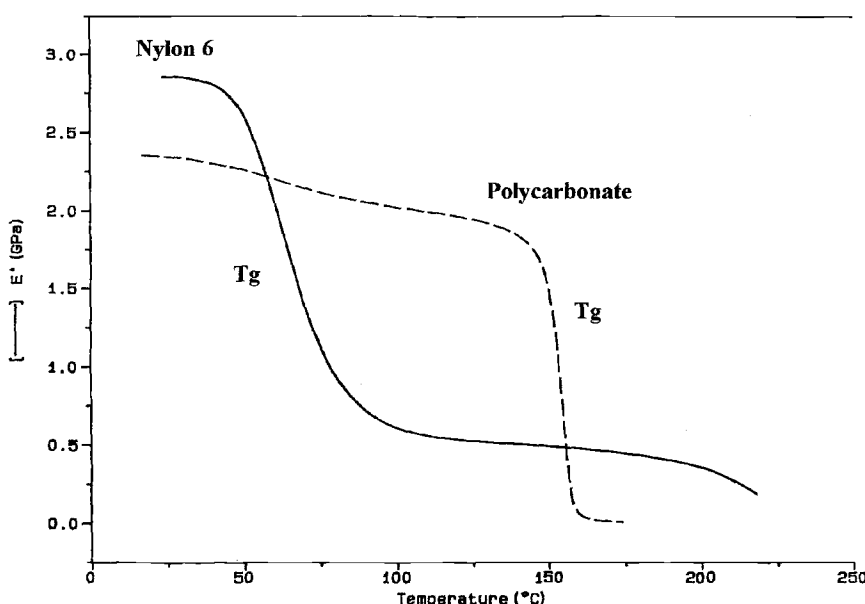


Figure 2 – Comparative Modulus Plot of Nylon 6 and Polycarbonate

A plot of elastic modulus versus temperature for the nylon 6 and the polycarbonate listed in Table 1 is shown (Figure 2). Several important features appear in this graph. First, the plot gives a modulus at any temperature between room temperature and the softening point of the material. Engineers who work with finite element analysis (FEA) know the importance of being able to provide the software with a meaningful modulus value for the application. Typically, the only value available is the room temperature value measured by the ASTM Test Methods for Flexural Properties of Unreinforced and Reinforced Plastics and Electrical Insulating Materials (D 790). Second, both materials exhibit temperature regions where the modulus is very stable. These are punctuated by relatively narrow regions where properties change dramatically. These temperature ranges are known as glass transitions. At these temperatures the mobility of the polymer chains increases to the point where any material that does not form crystals will soften. In polycarbonate, which is amorphous, the glass transition results in a loss of over 99% of its stiffness. From an engineering standpoint the material has softened and is no longer usable in a load-bearing manner. In nylon 6, which is semi-crystalline, the modulus declines significantly but the polymer is still solid above the glass transition due to the presence of the crystalline structure. This crystalline structure does not fall apart until the material reaches the melting point, approximately 155°C above the glass transition temperature (T_g).

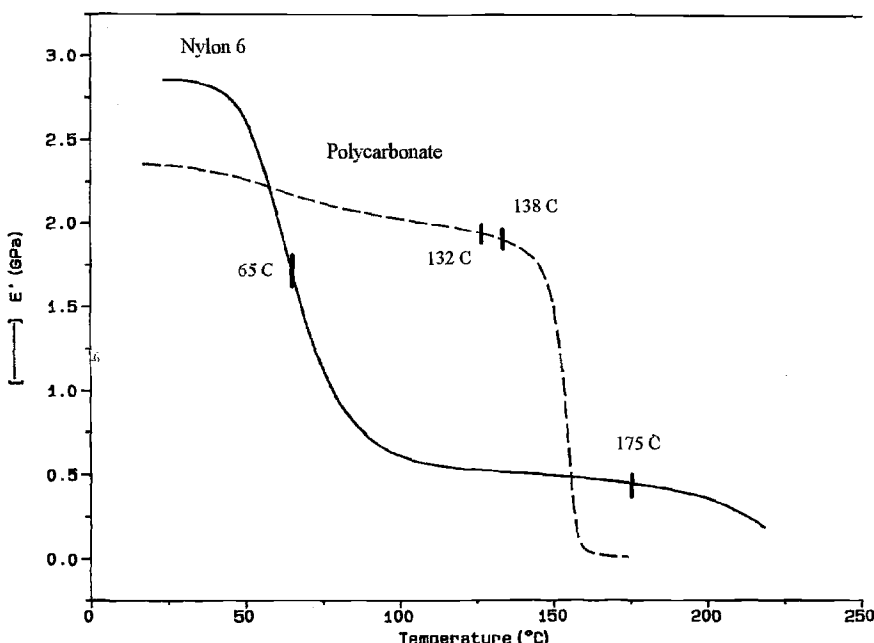


Figure 3 – Modulus Plots from Figure 2 Showing HDT Values

The plots in Figure 2 are shown with the HDT values included on the curves (Figure 3). In polycarbonate, the modulus decline is a single-step process, everything is lost all at once and the magnitude of the applied load has little bearing on the temperature at which the prescribed deflection is reached. In the nylon 6, the progress from room temperature to softened material is a two-step process; 80% of the modulus is lost at the glass transition and the remaining 20% is lost at the melting point. The high-load HDT corresponds to the T_g because the modulus declines sufficiently to achieve the necessary deflection. However, at the low load of 0.455 MPa the crystal structure resists deformation and the temperature must be raised to within 45°C of the melting point before it will deflect sufficiently to register failure.

The effect of the reinforcement also becomes more easily understood through these curves. Fillers and reinforcements do not alter transition temperatures; they merely stiffen the matrix and increase the utility of the material as a load-bearing member. A comparative modulus plot of an unreinforced polycarbonate and a 10% glass-reinforced analog are shown (Figure 4). Note that while the reinforced system is significantly stiffer at virtually any temperature at which the polymer is still solid, the effect of the glass transition remains a critical factor in the temperature limitations of the material. This explains the reason for the relatively small improvement in the HDT values. The same comparison for the unfilled nylon 6 and a 14% glass fiber-reinforced grade is shown (Figure 5). Again it can be seen

that the critical transition temperatures are unchanged since they are properties of the polymer matrix. However in this case the glass fiber raises the modulus of the crystalline plateau to a point where the material resists deformation under load until the material is near the melting point. This accounts for the apparently phenomenal increase in HDT when reinforcement is added to a semi-crystalline material.

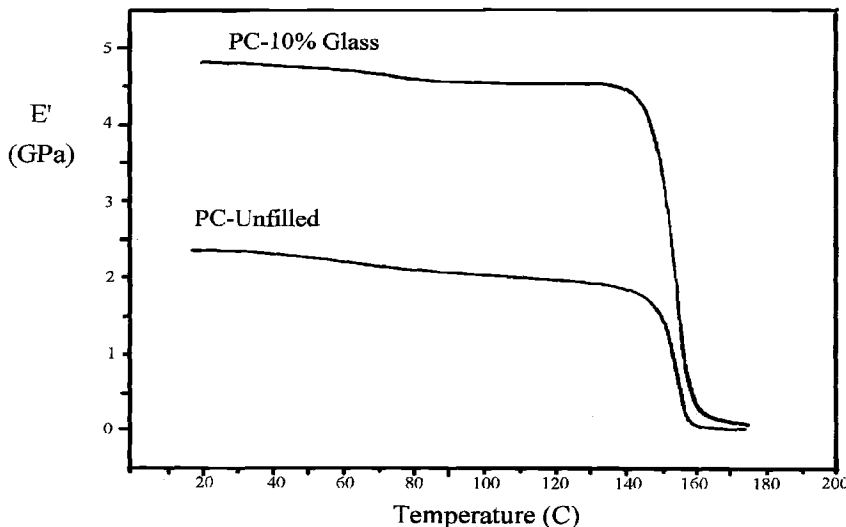


Figure 4 – Comparative Modulus Plot of Unfilled and Filled Polycarbonate

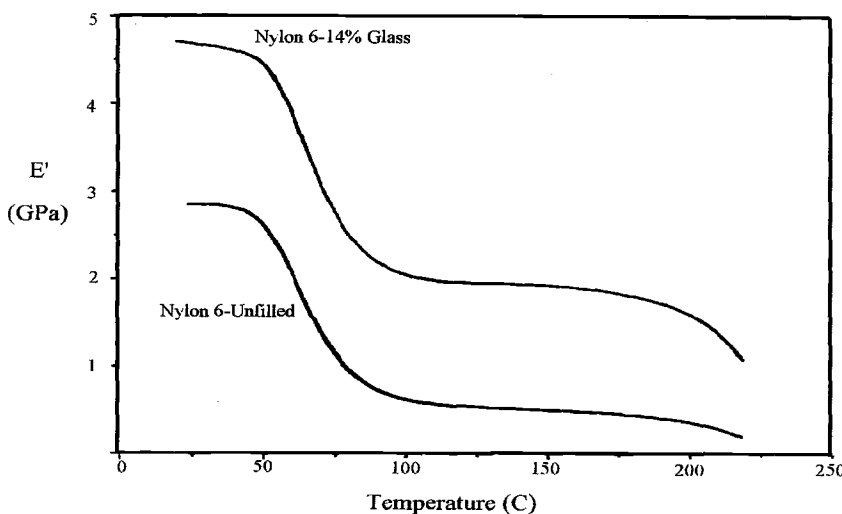


Figure 5 – Comparative Modulus Plot of Unfilled and Filled Nylon 6

The modulus vs. temperature plots for all of the nylon 6 materials listed in Table 2 are shown (Figure 6). Note that while all of the HDT values are very nearly equivalent, the actual modulus of the materials and the effect of T_g on the modulus of each material differ significantly depending upon the amount and type of reinforcement used. These distinctions are transparent to the user of tabular data. An expanded set of values that summarizes the plots in Figure 6 is shown (Table 3). Note that the T_g does not change appreciably regardless of how much reinforcement is used. However, the percent decline in the modulus as the materials pass through the glass transition varies substantially. It is these details that are so important to the material selection process but are missed by the standard property table values.

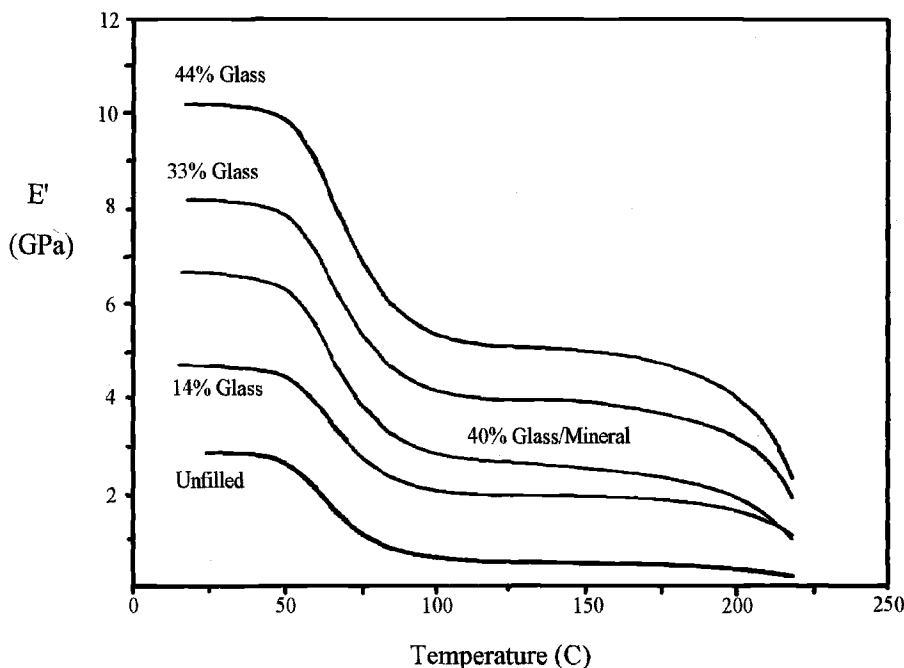


Figure 6 – *Effect of Filler Type and Content on Modulus of Nylon 6*

These differences become even more difficult to assess when the process of material specification becomes focused on rank-ordered tabular values for particular properties. We have seen in Table 3 how materials with different load-bearing characteristics can appear to have the same elevated-temperature performance when ranked by HDT. The following case study illustrates the hazards of attempting to solve performance problems with tabular data. An application in acetal homopolymer (POM) is failing at elevated temperatures. The temperature of the application is not known, only that it is above 90°C and below 130°C. Acetal had been selected originally because it has an HDT above 130°C.

Table 3 - Combined HDT and DMA Data for Nylon 6

Filler Type & Amt.	HDT @ 1.82 MPa (°C)	T _g (°C)	Pre-T _g Modulus (GPa)	Post-T _g Modulus (GPa)
None	65	65	2.81	0.56
14% Glass	200	69	4.46	1.96
33% Glass	210	70	7.87	3.99
44% Glass	210	71	10.04	5.13
40% Glass/Mineral	206	69	6.44	2.69

In the opinion of the engineers involved in the project, the failure is associated with the load-bearing characteristics of the material at the application temperature. In their view, this automatically translates to a problem with HDT. The HDT of the material being used is 142°C. The next step up the ladder of a rank-ordered HDT table is a polysulfone (PSF) material with an HDT of 174°C. The decision is made to convert the application to the polysulfone material.

A DMA plot of modulus versus temperature for the two materials under consideration is shown (Figure 7). The acetal is a semi-crystalline material with a rather unusual modulus-temperature response; the modulus of the acetal declines gradually as a function of temperature. The polysulfone exhibits behavior typical of an amorphous material with a very stable modulus up to the glass transition. Because of the higher modulus of the polysulfone at temperatures above 65°C, it is likely that the change in material will solve the problem. However, several considerations become apparent once the modulus-temperature behavior of the two materials is understood.

First, if we assume a worst-case application temperature of 130°C it can be seen that the modulus of the acetal has declined by 70% from the room-temperature value on the property chart. Second, the difference in modulus at 130°C between the acetal and the polysulfone is 1.8 GPa (261,000 psi). An examination of a collection of DMA curves is likely to uncover several options that improve the modulus at temperature without raising the material cost/cubic inch by 125%. Third, while modulus at temperature will improve by switching to the polysulfone, a host of other properties will decline including chemical resistance, fatigue resistance, and environmental stress crack resistance (ESCR). Finally, this is an application where tooling has already been built. Flow paths have been sized for a material with the viscosity and shear-responsiveness of acetal and cavities and cores have been cut for an anticipated shrinkage of 2%. The polysulfone is a much higher viscosity material that shear thins less efficiently, requires much higher processing temperatures and pressures, and only shrinks 1/2%. In short, the conversion from acetal to polysulfone may be costly and ultimately unsuccessful because of an inappropriate focus on tabular data.

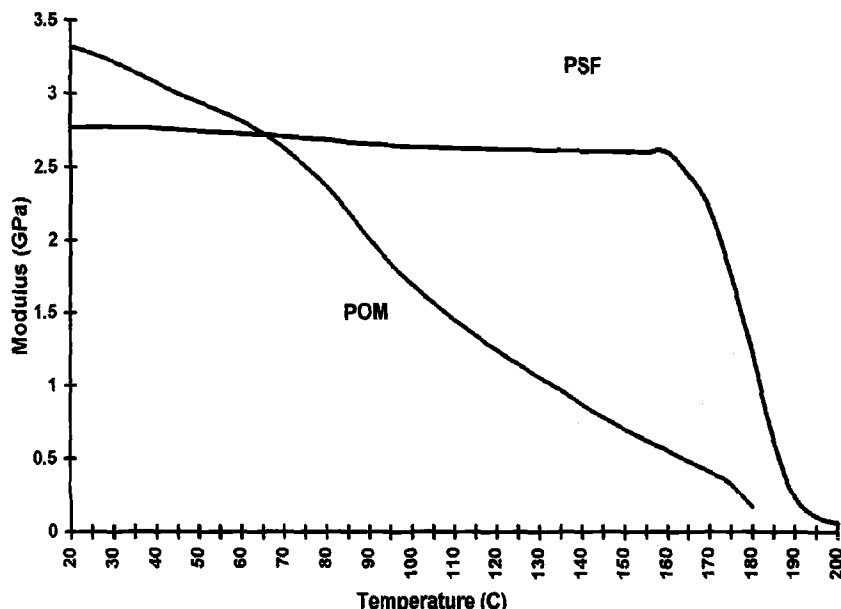


Figure 7 – Modulus Comparison (PSF vs. POM)

Conclusions

The heat deflection test has been a familiar fixture in the material property chart for many years. Many designers and engineers treat this value as a measure of long-term elevated-temperature performance and specify materials accordingly. This leads to product failures in some cases and costly overengineering in others. Dynamic mechanical analysis (DMA) provides a means of evaluating and understanding the behavior of modulus with temperature and provides a context for the tabular data provided by the HDT test. With this new data, more informed decisions can be made regarding the high-temperature performance aspects of plastic materials.

Acknowledgments

The author wishes to express his sincere thanks to Mary Hesprich and Michael Tahtinen for their assistance in performing some of the tests used in this paper.

References

- [1] Bozzelli, J. and Tiffany, P., SPE Antec, Vol. 32, 1986, p. 120.
- [2] Takemori, M., SPE Antec, Vol. 24, 1978, p. 216.

- [3] Ferry, J. D., *Viscoelastic Properties of Polymers*, 3rd edition, John Wiley & Sons, New York (1980).
- [4] Aklonis, J. J. and MacKnight, W. J., *Introduction to Polymer Viscoelasticity*, 2nd edition, Wiley-Interscience, New York (1983).
- [5] TA Instruments Bulletin TA-029, DMA 983 Dynamic Mechanical Analyzer (1994).

Nanying Jia¹ and Val A. Kagan²

Interpretations of Tensile Properties of Polyamide 6 and PET Based Thermoplastics Using ASTM and ISO Procedures

Reference: Jia, N. and Kagan, V. A., "Interpretations of Tensile Properties of Polyamide 6 and PET Based Thermoplastics Using ASTM and ISO Procedures," *Limitations of Test Methods for Plastics, ASTM STP 1369*, J. S. Peraro, Ed., American Society for Testing and Materials, West Conshohocken, PA, 2000.

Abstract: As more and more U.S. companies are looking to convert from ASTM to ISO standards for materials development, testing, and analysis in order to gain greater opportunities and compete more effectively in the global market, it has become increasingly important to deal with the concerns raised during the conversion process, so that the differences can be reconciled and harmonies can be brought into the two sets of standards.

This article presents our investigation on several technical issues in the ASTM and ISO standards on the tensile properties of plastics. Using polyamide (PA) 6 and polyethyleneterephthalate (PET) based thermoplastics as examples, our analysis revealed a range of similarities and differences in these two testing procedures. With either procedure – ASTM or ISO – similar results were obtained for material parameters such as tensile strength, tensile strain, and modulus of elasticity, in nonreinforced and short glass fiber reinforced plastics.

The investigation also focused on the role of the system compliance on the tensile strain and modulus measurements, and the effect of grips (wedge- and side-action grips) and gripping on the tensile behavior of the materials. Among the two types of grips, the wedge-action grip was found to cause greater measurement variability, especially in Young's modulus. The analysis of system compliance, on the other hand, reinforced the statements in both testing standards that an accurate strain and modulus measurement would require the use of extensometer. The results in this article went further to indicate how to improve the accuracy in the Young's modulus using the system compliance when the extensometer was not applied during testing. Recommendations were made on the effective use of the testing procedures in product development and design.

¹ Sr. Staff Scientist, Analytical Sciences Skill Center, AlliedSignal Inc., Morristown, NJ 07962-1021.

² Applied Technology Leader, Engineering Plastics, AlliedSignal Inc., Morristown, NJ 07962-1021.

Keywords: polyamide (PA), polyethyleneterephthalate (PET), tensile properties, stress, strain, tensile strength, break, Young's modulus, elasticity, system compliance, grips, ASTM, ISO, design, test

Introduction

In recent years, demands have increased in using polyamide (PA) and polyethyleneterephthalate (PET) products to replace certain metal structures in the automotive vehicle air induction and power train systems, lawn/garden and power tools [1-2]. An average car uses 18 kg of PA and 3 kg of PET. With the annual vehicle production at nearly 12 million, the needed amount of PA is more than 200 million kg and more than 45 million kg for under-the-hood applications alone [3]. The design of these components, especially those critically stressed parts such as vibration welded air intake manifolds [3-4], door and instrument panels, requires advanced analyses of structure [5-6], NVH (noise, vibration, and harshness), welded joints [3], and service life [7].

Concurrent engineering design involving thermoplastic materials relies on information concerning short- and long-term mechanical properties under a wide range of loading and environmental conditions [2] and correct methods of analysis [5] for predicting the mechanical performance of the injection molded parts [8-9].

The influence of time-temperature effects on the tensile strength and tensile-tensile fatigue behavior of short-fiber reinforced polyamides (PA 6 and PA 66) has been reported before [7], and it was found that at room temperature (23°C), the tensile strength of these two thermoplastics are virtually the same. This result has made it possible to simplify our analysis by focusing the compatibility study of tensile properties on one of the two PA plastics mentioned above. The focused tensile property analysis of PA 6 based thermoplastics was presented before [10]. The current paper has extended the scope of that study to include other important information from the tensile property testing and analysis.

ISO or ASTM

In the environment of a worldwide economy, it is increasingly critical for companies with international businesses to have access to reliable and comparable material properties data [6, 11-12] for the product re-design and new product development [13-14]. As the complexity in thermoplastic products is growing, the role of material property testing is gaining importance as well. Today's product designers and toolmakers must consider not only the performance requirements for the injection-molded parts, but also the properties of thermoplastics with which the products are made. Certain goals in product design, such as weight reduction, time and cost savings, can only be achieved when considerations in different design areas are combined and optimized [5-6, 13-16].

In this situation, global standardization is playing a more important role than ever in facilitating product manufacturing, marketing, and sales [17]. The widely published testing procedures and specifications for plastic materials by the American Society for Testing and Materials (ASTM, Committee D-20 on Plastics) and the International

56 LIMITS OF TEST METHODS FOR PLASTICS

Standard Organization (ISO) have helped product developers, designers, and molders to establish correct and useful baselines. An important development in the standardization area is the fact that the American automotive industry has become one of the first to require ISO test procedures for material and product qualifications [18] when the majority testing in the North America is still conducted using ASTM standards. The United States Council for Automotive Research (USCAR) recommended the manufacturers of thermoplastic products to fully convert to ISO test procedures by June 1998.

The decision for this conversion will no doubt have a major impact on material suppliers, molders, designers, and end users when most of the material and product information accumulated for decades and still in use was obtained using ASTM procedures [18]. The current investigation is part of our effort in assisting this transition. The tensile properties of thermoplastics were analyzed not only for the purpose of comparing the ASTM and ISO tensile test procedures, but also for the importance of these properties in the product design.

The current investigation has been focused on the tensile property measurements of PA and PET based thermoplastics. Material parameters obtained using ISO and ASTM specimens and test procedures were compared for their similarities and differences. Analyses were also made on two important aspects of the tensile property measurements, one was the use of extensometer, and another, the effect of grips and gripping on the accuracy of Young's modulus. The purpose of the investigation and analyses is to provide the product designers, product developers, and testing community alike with a guidance in correctly obtaining and interpreting their test results.

Materials

The thermoplastics used in this investigation were heat stabilized, unfilled and glass and/or mineral filled polyamide (PA) 6 and polyethyleneterephthalate (PET). Materials were injection molded into ISO multipurpose and ASTM Type 1 and Type 2 specimens described in ISO Multipurpose test specimens (ISO 3167:1993 (E)) and ASTM Standard Test Method for Tensile Properties of Plastics (ASTM D 638-97). The injection molding was carried out according to ISO Injection moulding of test specimens of thermoplastic materials (ISO 294:1995), ASTM Standard Practice for Injection Molding Test Specimens of Thermoplastic Molding and Extrusion Materials (ASTM D 3641-97), and ASTM Standard Classification System for Nylon Injection and Extrusion Materials (PA) (ASTM D 4066-96a). All specimens were sealed (see ASTM Standard Practice for Packaging/Packing of Plastics, or ASTM D 3892-93) prior to testing in order to maintain their dry-as-molded (DAM) conditions.

Test Procedures

The tensile property tests were conducted using Instron 4505. Most tests were conducted under standard laboratory conditions (temperature = $23 \pm 2^\circ\text{C}$; relative humidity = $50 \pm 5\%$) on dry-as-molded samples. Some samples were also tested at different temperatures (-40°C and 150°C) using an environmental chamber attached to the Instron. The temperature inside the chamber was controlled at $\pm 2^\circ\text{C}$ within the set

point.

Each sample was tested at two crosshead speeds: 1 and 5 mm/min for filled materials, and 1 and 50 mm/min for unfilled materials. The 1 mm/min speed was used to obtain the Young's modulus, while the 5 or 50 mm/min speed was used to obtain other tensile properties such as tensile strength, stresses and strains at yield and break. The tensile strain was measured from the narrow section of each specimen using a clip-on extensometer (Instron 2630-115) with a gage length of 50.8 mm. In some cases the crosshead position was also recorded and used to calculate the apparent strain and modulus, as discussed later.

The test control and data acquisition were achieved using Instron Series 9 software. The material parameters for tensile properties, such as tensile strength (σ_M), tensile strain at tensile strength (ε_M), stress at break (σ_B), and strain at break (ε_B), were obtained according to the definitions in ASTM D 638 and ISO Determination of tensile properties (ISO 527-1, 2:1993 (E))³. The Young's modulus, E , was calculated according to the definition in ISO 527-1, which gives

$$E = \frac{\sigma_2 - \sigma_1}{\varepsilon_2 - \varepsilon_1} \quad (1)$$

where $\varepsilon_1 = 0.0005$, $\varepsilon_2 = 0.0025$, and σ_1 , σ_2 = stresses at ε_1 and ε_2 , respectively.

For each sample, a minimum of five specimens were tested under a given condition. The sample mean and sample standard deviation were calculated for each parameter of tensile properties (Table 1).

Results and Discussions

Tensile Properties by ISO and ASTM Standards

In Figures 1 to 3, properties obtained using ISO specimens were plotted against those obtained using ASTM (Type 1) specimens. The solid line, $Y = X$, indicates on the graph where the two sets of property values are equal to each other. For the tensile strength (Figure 1) and strain at tensile strength (Figure 2), the closeness of the data points to this line suggests that the properties obtained using the two standards are practically the same. In fact this was found to be the case for the entire stress-strain relationship [10].

The difference, on the other hand, apparently exists in the Young's modulus where numbers from ISO specimens are often higher than those from ASTM specimens (Figure 3). This difference can be quantified by calculating the ratio between the two sets of modulus numbers using linear regression (Table 2). Ratios were also calculated in the same way for other properties (Table 2). The results indicate that, among the materials in the investigation, the ultimate stresses (σ_M and σ_B) obtained from ISO specimens are on average 2 ~ 3% higher than those from ASTM specimens, and the modulus can be up to

³ The definitions of these parameters were considered equivalent in these two standards.

Table 1 – Materials and Their Tensile Properties, 23°C

Material	σ_m , MPa	ϵ_m , %		σ_b , MPa		ϵ_b , %		E , MPa	
	ASTM	ISO	ASTM	ISO	ASTM	ISO	ASTM	ISO	ASTM
PA 6, 0% G.F. ¹	84.98	87.09	4.24	4.38	—	—	—	—	3140.0
St.Dev.	0.66	0.29	0.06	0.10	—	—	—	—	199.2
PA 6, 15% G.F., 20% M. ¹	117.39	125.01	2.31	2.36	117.37	125.01	2.32	2.36	8846.6
St.Dev.	0.32	0.38	0.02	0.04	0.33	0.38	0.04	0.04	136.2
PA 6, 15% G.F., 20% M. –40°C	163.77	169.70	2.78	2.90	163.77	169.70	2.78	2.90	10578.6
St.Dev.	1.92	2.23	0.04	0.10	1.92	2.23	0.04	0.10	204.2
PA 6, 15% G.F., 20% M. 150°C	45.60	47.59	8.39	7.90	45.32	47.39	8.79	8.40	3227.1
St.Dev.	0.44	0.37	0.20	0.30	0.40	0.36	0.29	0.50	119.8
PA 6, 30% G.F., Recycled	150.11	166.30	2.20	2.29	149.21	166.14	2.33	2.32	10522.7
St.Dev.	0.34	0.23	0.04	0.04	0.61	0.40	0.07	0.07	436.2
PA 6, 33% G.F.	176.66	180.70	2.83	2.86	175.62	179.90	3.02	3.00	9788.8
St.Dev.	1.14	1.02	0.05	0.11	1.00	1.19	0.07	0.25	493.0
PA 6, 33% G.F., I.M. ¹	143.59	151.71	2.60	2.67	142.50	149.75	2.79	2.89	9372.0
St.Dev.	0.27	0.70	0.04	0.01	0.36	0.81	0.06	0.07	297.4
PA 6, 40% M. & G.F.	119.17	129.09	2.31	2.30	119.15	129.09	2.32	2.31	10584.3
St.Dev.	0.90	0.45	0.02	0.05	0.91	0.45	0.04	0.06	333.6
PA 6, 50% G.F.	212.58	220.84	2.62	2.51	212.46	220.76	2.66	2.54	14890.0
St.Dev.	1.09	2.46	0.07	0.14	1.33	2.46	0.10	0.15	1085.9
PET, 30% G.F.	156.78	153.09	2.57	2.43	156.78	153.03	2.58	2.45	11586.3
St.Dev.	0.98	0.29	0.03	0.04	0.98	0.37	0.04	0.07	156.2
PET, 35% M. & G.F.	127.66	126.45	1.73	1.57	127.66	126.45	1.73	1.57	12570.5
St.Dev.	1.06	1.62	0.05	0.09	1.06	1.62	0.05	0.09	213.5

¹ G.F., M., I.M.: glass fiber reinforced, mineral reinforced, and impact modified, respectively.

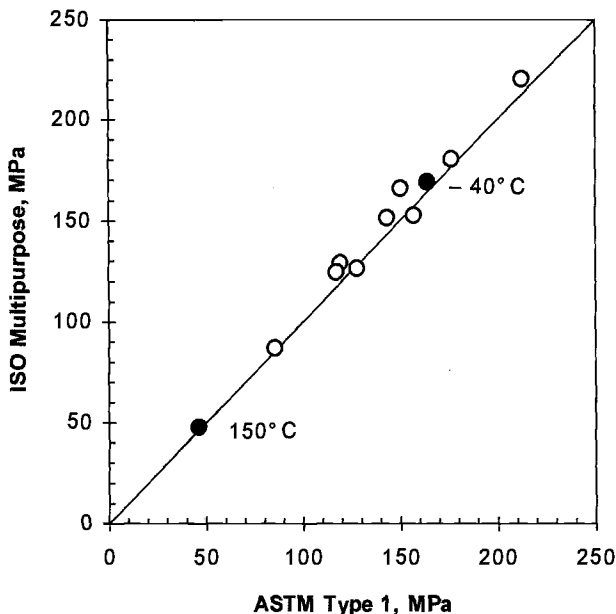


Figure 1 – *Tensile Strength of Materials, σ_M . $T = 23^\circ\text{C}$ unless otherwise indicated.*

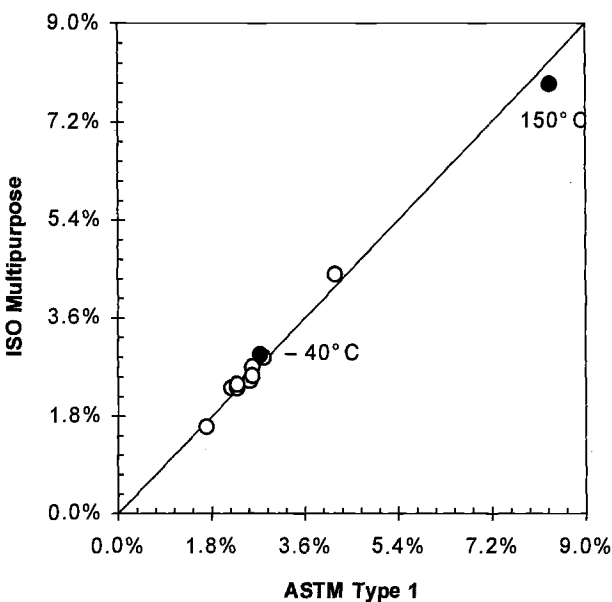


Figure 2 – *Tensile Strain at Tensile Strength, ϵ_M . $T = 23^\circ\text{C}$ unless otherwise indicated.*

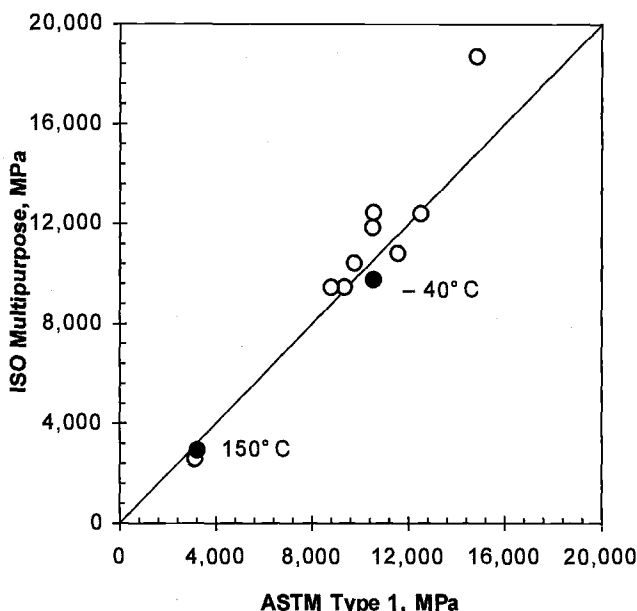


Figure 3 – *Young's Modulus, E. T = 23°C unless otherwise indicated.*

Table 2 – *Ratios between ISO and ASTM Property Parameters*

	σ_M	ϵ_M	σ_B	ϵ_B	E^1
ISO ÷ ASTM ²	1.028 ± 0.04	0.934 ± 0.024	1.022 ± 0.039	0.947 ± 0.019	1.082 ± 0.126
r^2 (coef. corr.)	0.987	0.994	0.984	0.997	0.924

¹ The modulus value for PA 6, 50% G.F. was not used in calculating this ratio.

² ISO ÷ ASTM = (slope in regression) ± 1 (standard error).

8% higher for the ISO specimens. On the other hand, the opposite trend was found in tensile strains where in many cases the numbers for ϵ_M and ϵ_B are lower in ISO specimens.

Despite the small difference in the nominal cross-sectional areas ($10\text{ mm} \times 4\text{ mm} = 40\text{ mm}^2$ for ISO, $12.7\text{ mm} \times 3.18\text{ mm} = 40.4\text{ mm}^2$ for ASTM Type 1), the different linear dimensions of the two specimens (e.g., the ASTM specimen is wider but thinner than the ISO specimen) might have had an impact on the injection molding process and the distribution of the reinforcement, especially the orientation and distribution of glass fibers. If so, this may be enough to cause a difference in the measured properties. The fact that the deviation from the $Y = X$ line in the modulus data tends to increase with the amount of glass fibers (Figure 3) further suggests such a possibility.

System Compliance and Its Effect on Tensile Strain and Modulus Measurements

Despite the statement in both standards that an extensometer should be used in elongation measurement, use of such device may not always be possible or convenient. At low temperature (e.g., -40°C), certain mechanisms in the extensometer tend to be frozen and the surface of the specimen can be slippery, making the extensometer difficult to attach or operate. At high temperature, handling of the extensometer may also be difficult for the lab operator, especially when limited by the tight space in the chamber [20]. Without an extensometer, however, one must find alternatives with which the elongation, strain, and modulus can be calculated. The purpose of this section is to analyze such an alternative and estimate the errors associated with the measurement method.

Next to the use of extensometer, the obvious way of obtaining tensile strain is to calculate the change in so-called grip to grip distance, ΔL , as shown in Figure 4. In reality, however, ΔL rarely gets measured directly; instead it is the change in the crosshead position, ΔX , that is recorded and used in the strain calculation. For the purpose of the current discussion, the strain based on ΔX is called apparent strain, which is defined as $\varepsilon_a = \Delta X / L$. The apparent modulus, on the other hand, can be defined as

$$E_a = \frac{\sigma_{a2} - \sigma_{a1}}{\varepsilon_{a2} - \varepsilon_{a1}} \quad (2)$$

where $\varepsilon_{a1} = 0.0005$, $\varepsilon_{a2} = 0.0025$, and σ_{a1} and σ_{a2} are stresses at ε_{a1} and ε_{a2} , respectively.

To substitute ε and E with ε_a and E_a , one may encounter errors in two ways: (1) Unlike in the section defined by the gage length L_0 , the stress and strain in L is not always simple and uniaxial, especially at the vicinity of the grips where complex stress and strain distribution is expected; (2) Use of ΔX will include the deformation of the testing machine in the strain calculation, making the results machine dependent, therefore less reliable and less reproducible.

To quantify the above analysis, notice first that the ΔX can be expressed as

$$\Delta X = \Delta S + \Delta L \quad (3)$$

where ΔS is the total machine deformation which may include deformation from the loadcell, the crosshead beam, and the grips and connectors. Assume further that the stress and strain are uniform across any cross-section in L , and the contributions by other stress components to the specimen elongation are negligible. In this case one may have

$$\Delta L = 2 \int_0^{L/2} \varepsilon(x) dx = 2 \int_0^{L/2} \frac{\sigma(x)}{E} dx = \frac{2P}{Eh} \int_0^{L/2} \frac{dx}{b(x)} \quad (4a)$$

or

$$\Delta L = m \cdot \Delta L_0 \quad (4b)$$

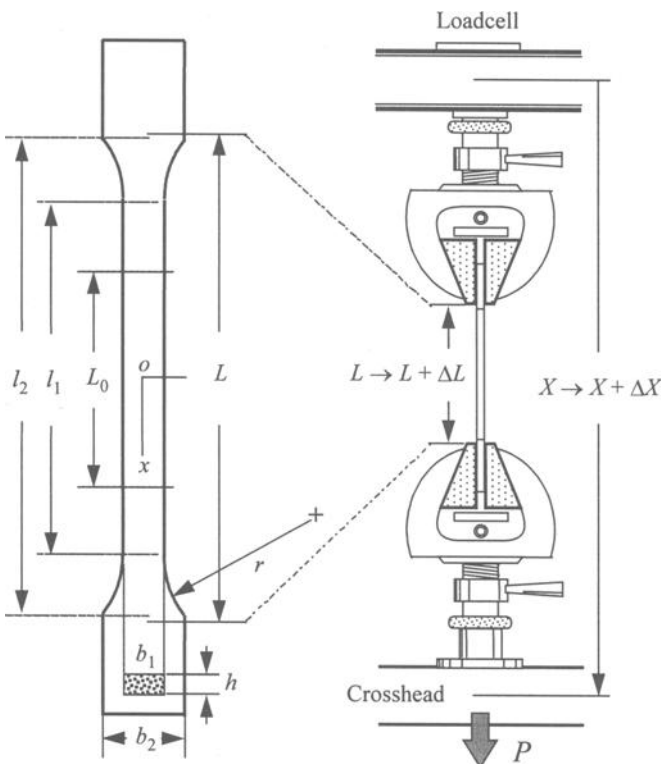


Figure 4 – Tensile Specimen and Test Setup (ISO 527-2:1993(E); Table 4).

where P = applied load, $b = b(x)$ ($b_1 \leq b(x) \leq b_2$) and h = constant are the width and thickness of the specimen, ΔL_0 is the change in gage length. The ratio between ΔL and ΔL_0 is expressed by a deformation parameter m ,

$$m = \frac{1}{L_0} \left\{ l_1 + \frac{b_1}{b_2} (L - l_2) + b_1 \left[\frac{1 + 2r/b_1}{\sqrt{1 + 4r/b_1}} \cos^{-1} \sqrt{\frac{b_1}{b_2} \left(1 - \frac{b_2 - b_1}{4r} \right)} - \frac{1}{2} \cos^{-1} \left(1 - \frac{b_2 - b_1}{2r} \right) \right] \right\}. \quad (5)$$

The definitions of parameters in Eq.(5), b_1 , b_2 , l_1 , l_2 , and r , are consistent with those given in ISO 527-2:1993(E) (Figure 4). To derive Eq.(5) it was also assumed that ΔL and ΔL_0 are both proportional to the applied load, i.e. the material is essentially elastic. The analysis below is therefore restricted in the region where the stress and strain are linearly related⁴. The numerical values for m for different types of tensile specimens are shown in

⁴ It is possible to extend the current analysis to the entire stress-strain region by replacing

Table 3.

Table 3 – Parameter m for ISO and ASTM Specimens¹

Type of Specimen	m	L_0 (mm)	L (mm)	l_1 (mm)	l_2 (mm)	b_1 (mm)	b_2 (mm)	r (mm)
ISO	1.60	50.8	115	59.0	115	9.86	19.7	82
ASTM Type 1	1.72	50.8	115	60.8	102	12.56	18.9	68
ASTM Type 2	1.68	50.8	135	60.3	118	6.23	19.0	68

¹ The geometric parameters used in calculating m can be found in ISO 527-2:1993(E) and in Figure 4.

Furthermore, assume that the overall deformation of the machine, ΔS , is proportional to P , Eq.(3) can then be written as

$$\Delta X = s \cdot P + m \cdot \Delta L_0 \quad (6)$$

where s is defined as system compliance.

With the help of Eq.(6), the apparent strain can be expressed in terms of the “real strain” ε as

$$\varepsilon_a = \frac{s \cdot P + m \cdot \Delta L_0}{L} = \left(\frac{s \cdot A}{L} \right) \sigma + m \cdot \left(\frac{L_0}{L} \right) \varepsilon \quad (7)$$

where $A = b_1 \cdot h$ = initial cross-sectional area.

Using Eq.(7), the change in ε_a can be related to changes in σ and ε , i.e., $\Delta \varepsilon_a = (s \cdot A / L) \Delta \sigma + m \cdot (L_0 / L) \Delta \varepsilon$. This relationship can be applied to express the apparent Young’s modulus in terms of the “real modulus” E :

$$E_a = \frac{\Delta \sigma}{\Delta \varepsilon_a} = \frac{\Delta \sigma}{\Delta \varepsilon} \div \frac{\Delta \varepsilon_a}{\Delta \varepsilon} = \frac{E}{(s \cdot A / L) E + m \cdot (L_0 / L)} \quad (8)$$

where the assumption is made for $\Delta \sigma / \Delta \varepsilon = (\sigma_2 - \sigma_1) / (\varepsilon_2 - \varepsilon_1) = E$. In situations where E_a , rather than E , is obtained, Eq.(8) can be rearranged to give an estimate on E once the system compliance s is known. In this case, one has that

$\varepsilon = \sigma/E$ in Eq.(4a) with a more general relationship $\varepsilon = \varepsilon(\sigma)$ that can be established experimentally. The consequence, however, is that one must deal with a parameter m that is likely to be stress dependent, and the overall calculation may no longer be simple enough to make the effort practical.

$$E' = \frac{m(L_0 / L)E_a}{1 - (s \cdot A / L)E_a} = \frac{(m \cdot L_0)E_a}{L - (s \cdot A)E_a}. \quad (9)$$

In this equation, the symbol E' has been used in order to differentiate its value from the original E obtained in Eq.(1).

To see how the above analysis can be applied, one may follow the steps outlined below:

(1) Obtain the numeric data for ΔX_i , $\Delta L_0 i$, and P_i , where $i = 1, 2, \dots, n$, and n is the total sampling points;

(2) Calculate a new data series, $\Delta X_i - m \cdot \Delta L_0 i = (\Delta X - m \cdot \Delta L_0)_i$, where m is obtained from Table 3 according to the type of the specimen (ISO or ASTM);

(3) Run a linear regression on P_i and $(\Delta X - m \cdot \Delta L_0)_i$ in a region roughly defined by $0.0005L < \Delta X_i < 0.025L$, or $0.0005 < \epsilon_a < 0.0025$;

(4) Use the slope calculated in step (3) as the system compliance, s ;

(5) Calculate E and E_a from Eqs.(1) and (2), and calculate E' from Eq.(9) using s and E_a .

The calculated system compliance s , is shown in Table 4 for a number of samples. Interestingly enough, the number s was found to be actually dependent on modulus E_a or E , as demonstrated clearly in Figure 5. An empirical relationship can be easily found to be

$$s = 86.592 \times E_a^{-0.6269}. \quad (10)$$

Using Eq.(10), the system compliance for each material sample was recalculated and the results (s^*) can be found in Table 4 for a direct comparison with s .

Table 4 – Calculation of System Compliance

Material and Specimen Type	s (mm/kN)	$s^* =^1$ $86.592 \times E_a^{-0.6269}$
PA 6, 0% – ASTM Type 1	0.775	0.789
PA 6, 14% G.F., I.M. – ISO	0.616	0.595
Same as above, 120°C	0.850	0.849
PA 6, 33% G.F., I.M. – ASTM	0.481	0.487
Same as above, ASTM Type 2	0.470	0.328
PA 6, 40% G.F. – ISO	0.383	0.390
PET, 45% G.F. – ISO	0.383	0.382
PET, 15% G.F. – ISO, 150°C	0.728	0.977

¹ The numeric values for E_a can be found in Table 5.

The dependence of s on E_a or E raised an interesting question concerning the nature of the system compliance which was thought originally to reflect only the deformation of

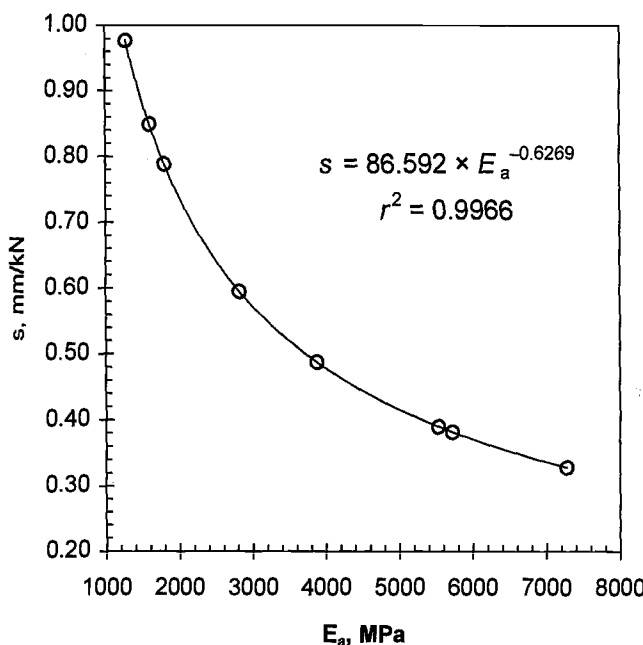


Figure 5 – System Compliance vs. Apparent Young's Modulus (Table 4). r^2 = coefficient of correlation.

Table 5 – Correction of Young's Modulus Using System Compliance

Material and Specimen Type	s^* (mm/kN)	E_a (MPa)	E (MPa)	E'^1 (MPa)	$\Delta(E_a, E)^2$	$\Delta(E', E)^2$
PA 6, 0% G.F. – ASTM ³	0.789	1798.5	2658.6	2729.2	-32.4%	2.65%
PA 6, 14%G.F., I.M. – ISO ³	0.595	2821.2	4685.7	4628.8	-39.8%	-1.21%
Same as above, 120°C	0.849	1598.6	1918.3	2092.1	-16.7%	9.06%
PA 6, 33%G.F., I.M. – ASTM	0.487	3878.2	9606.7	8797.8	-59.6%	-8.42%
Same as above, ASTM Type 2	0.328	7280.6	9813.3	9244.4	-25.8%	-5.80%
PA 6, 40%G.F. – ISO	0.390	5531.0	13137.7	14621.8	-57.9%	11.3%
PET, 45% G.F., – ISO	0.382	5724.0	15833.5	15687.8	-63.9%	-0.92%
PET, 15% G.F., – ISO, 150°C	0.977	1278.9	1918.3	1566.4	-33.3%	-18.3%

¹ The corrected Young's modulus based on Eq.(9).

² $\Delta(E_a, E) = (E_a - E) / E \times 100$; $\Delta(E', E) = (E' - E) / E \times 100$.

³ ASTM Type 1 and ISO multipurpose specimens, respectively (see Table 3).

the testing machine, not the material properties. By measuring directly the grip

separation during the course of elongation rather than relying on the return of the crosshead position ΔX , we found that most of the machine deformation, $(\Delta X - m \cdot \Delta L_0)$, actually occurred within the area where the specimen was clamped. It was believed that the portion of the specimen between the gripping faces contributed significantly to the overall deformation ΔX . Little surprise then that the quantity represented by $(\Delta X - m \cdot \Delta L_0)$, and eventually s , would be material property dependent since the grip-to-grip elongation, $\Delta L = m \cdot \Delta L_0$, did not take into account the deformation of the specimen between the gripping faces.

An important implication from Eq.(10) is that one may obtain the correction for E_a (i.e., E') even if the system compliance cannot be obtained from the materials to be tested. To do so, one needs to obtain at first the numerical expression in Eq.(10) by testing several controlled materials with known stress-strain relationships that allow s to be derived from steps (1) ~ (5) outlined above. Once s is known and $s \cdot E_a$ relationship is established, E' can be calculated using Eq.(9) for any material sample with E_a obtained experimentally. E' represents the correction for E_a and its numeric value is expected to be close to that of E , the "real modulus" obtained from Eq.(1) using an extensometer. The step-by-step procedure to obtain E' from s and E_a is summarized as follows:

- (A) Test controlled samples without extensometer, and obtain P_i , ΔX_i , and $(\Delta X - m \cdot \Delta L_0)_i$, where ΔL_0 can be calculated from the known stress-strain relationship;
- (B) Follow steps (3) to (5) above to calculate the apparent modulus E_a and the system compliance s ;
- (C) Plot s against E_a , and establish the empirical relationship such as the one shown in Eq.(10)⁵;
- (D) Test new samples using the same setup, and calculate E_a ;
- (E) Calculate E' from Eq.(9), using s obtained from Eq.(10).

A few examples of such calculations have been given in Table 5. The effectiveness of the above procedures can be seen clearly from the calculated errors $\Delta(E_a, E) = (E_a - E) / E \times 100$, and $\Delta(E', E) = (E' - E) / E \times 100$.

The Effect of Grips and Gripping on Modulus Measurement

One of the observations from the tensile test was that although the sample standard deviation for stress (e.g., σ_M and σ_B) is normally very small, the same deviation is greater for strain, and greater still for Young's modulus. Using the coefficient of variation (CV) to characterize the data scattering, where $CV = (\text{sample standard deviation}) \div (\text{sample mean})$, it was found that CV is 0.2 ~ 1.5% for stress, 2 ~ 5% for strain, and 2 ~ 10% for modulus.

In order to understand the progressive increase in CV from stress to strain, and from strain to modulus, a closer examination was made on the stress-strain relationship between $\varepsilon = 0$ and 0.3% where the modulus was calculated. It was found that in many

⁵ Since the relationship in Eq.(10) is purely empirical, one should be able to choose any mathematical expression deemed to best fit the data at hand.

cases the initial behavior of the stress-strain curve near $\varepsilon = 0$ was rather complicated (Figure 6, the left half). The CV for the modulus could increase significantly when this initial region extended beyond $\varepsilon = 0.05\%$. This situation was found to be worse in some samples than in others.

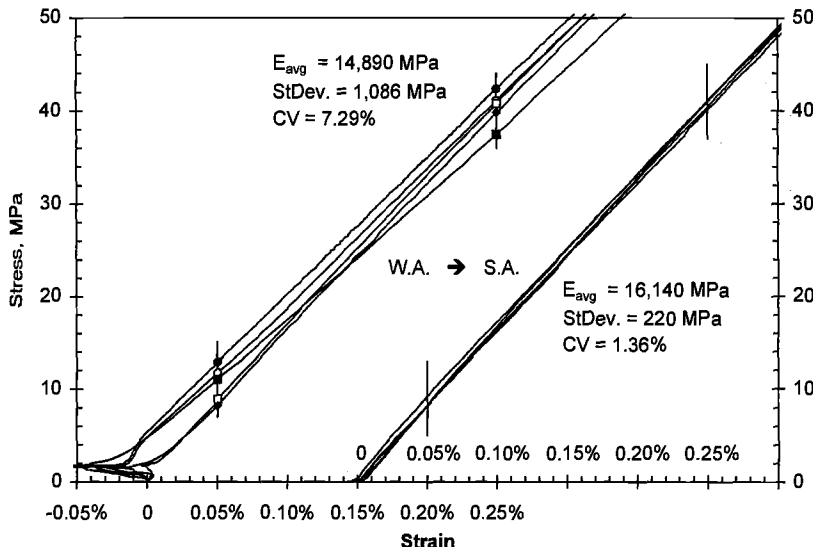


Figure 6 – *Effect of Grips on the Tensile Behavior of Thermoplastics (PA 6, 50% G.F.). The variation in modulus measurement associated with the wedge-action grips (W.A.) is seen to be reduced significantly with the use of side-action grips (S.A.).*

To find out why this was the case, the specimen elongation and the applied force were compared from one sample point to the next, as shown in Figure 7. It was noticed that, at the beginning of the tensile test, the applied force does not always increase as the position of the crosshead changes. Instead the force remains unchanged or even decreases following an initial increase. But soon it increases again and this time the change is more rapid. Corresponding to the force, the elongation measured by the extensometer also exhibits a strange pattern in the same region.

An explanation for this phenomenon can be given knowing that the force has been transferred to the specimen through a pair of wedge-action, or self-tightening, grips. The decrease in force following an initial increase can be considered to be a result of the grips biting into the material (Figure 7). The indentation by the serrated grip faces may have caused certain plastic flow on the surface of the specimen, and it apparently has been sensed by the extensometer as suggested by the elongation behavior seen in Figure 7. The combination of the surface indentation and the surface plastic flow appears to be what gave the erroneous stress-strain behavior that in turn caused large variations in strain and modulus.

To verify this hypothesis, tensile tests were conducted on a few samples using a pair

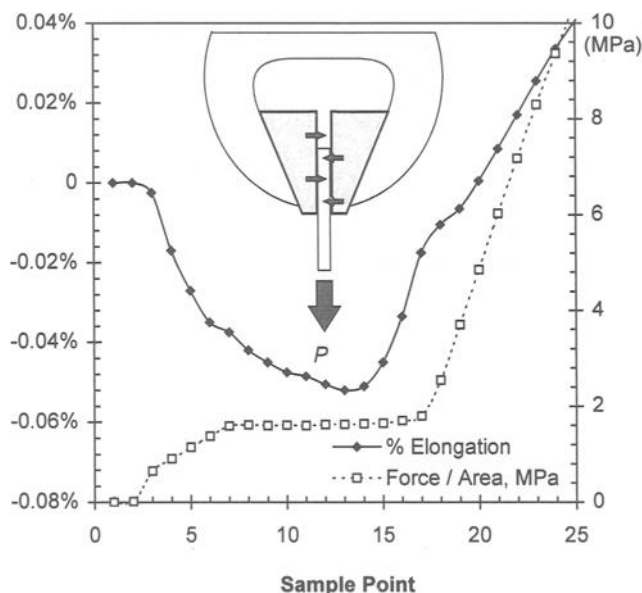


Figure 7 – The Self-Tightening of the Wedge-Action Grips Was Considered to be Responsible for the Large Variability in Strain and Modulus Measurement (Figure 6).

of side-action grips in which the on-going surface indentation is not an issue due to the lack of self-tightening. Figure 8 shows the stress-strain in the same region as Figure 7. Sure enough, the force and elongation behavior that caused large errors is no longer there. The significantly reduced variability is obvious in Figure 6 where the stress-strain curves with wedge-action and side-action grips are compared. The comparison between the CV's from samples using two types of grips is given in Table 6.

The problem with using the side-action grips is that specimens with high tensile strength often slip between the grips in the middle of testing. This problem, however, should not affect the modulus measurement since the slipping usually occurs far beyond $\epsilon = 0.0025$.

Conclusions

(1) Tensile strength and deformation parameters of PA 6 and PET obtained by ISO and ASTM methods are generally compatible; both can be used for the design of injection molded, non-reinforced and glass fiber reinforced parts and the material pre-selection.

(2) For the structural design of critically stressed plastic components, design optimization for mechanical performance, weight reduction, and so on, it is very important to ensure that accurate ISO or ASTM tensile property data are utilized.

(3) The ISO tensile test data for stress and modulus are found to be slightly higher than that of ASTM for reinforced and non-reinforced semicrystalline PA 6, PET, and

amorphous PP [18].

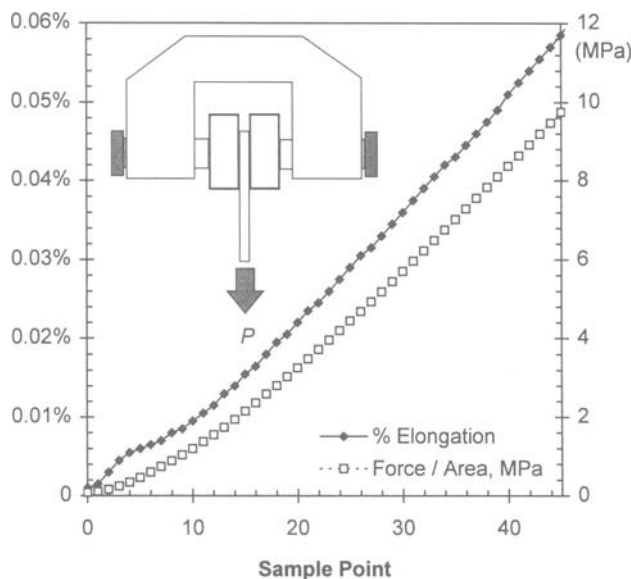


Figure 8 – “Well-Behaved” Stress and Strain Curves with the Use of Side-Action Grips.

Table 6 – Coefficient of Variation for Young’s Modulus and the Effect of Grips on Measurement Variability

Material and Specimen Type	Grips	<i>E</i> (MPa)	St.Dev. (MPa)	CV
PET, 30% G.F. – ISO ¹	W.A. ²	12,101	996.4	8.23%
	S.A. ²	12,592	166.1	1.32%
PA 6, 0% G.F. – ASTM ¹	W.A.	3,140	199.2	6.34%
	S.A.	3,150	109.4	3.47%
PA 6, 0% G.F. – ISO	W.A.	2,540	300.3	11.82%
	S.A.	2,850	117.8	4.13%
PA 6, 12% G.F. – ISO	W.A.	6,292	705.5	11.21%
	S.A.	5,805	107.5	1.85%
PA 6, 33% G.F. – ASTM	W.A.	9,790	493.0	5.04%
	S.A.	10,600	370.0	3.49%
PA 6, 33% G.F. – ISO	W.A.	10,410	1,666.0	16.01%
	S.A.	9,630	360.4	3.74%

¹ ISO multipurpose and ASTM Type 1 specimens, respectively.

² W.A. – wedge-action grips; S.A. – side-action grips.

Table 6 (*Continued*)

Material and Specimen Type	Grips	E (MPa)	St.Dev. (MPa)	CV
PA 6, 50% G.F. – <i>ASTM</i>	W.A.	14,890	1,086.0	7.29%
	S.A.	16,140	220.0	1.36%
PA 6, 50% G.F. – <i>ISO</i>	W.A.	18,700	3,465.0	18.53%
	S.A.	16,100	668.0	4.15%

(4) The value of Young's modulus can be significantly affected by the method of tensile strain calculation, which can be obtained with or without an extensometer.

(5) Use of wedge-action grips may cause large variability in strain and modulus calculation, and this variability can be reduced significantly by using the side-action grips.

References

- [1] "Composites Makes Progress Under the Bonnet", *Reinforced Plastics*, May 1997, pp. 28-32.
- [2] Roast, D. and Di Mattia, D., *Designing with Plastics and Composites: A Handbook*, Van Nostrand Reinhold, New York, 1993, 979 pages.
- [3] Carlson, E. and Nelson, K., "Nylon Under-the-Hood: A History of Innovation", *Automotive Engineering*, December, 1996, pp. 84-89.
- [4] Kagan, V., "Vibration Welding of Glass Fiber Reinforced Polyamide Plastics", *Kunststoffe, European Plastics*, December, 1997, pp. 1804-1807.
- [5] Trantina, G. and Nimmer, R., *Structural Analysis of Thermoplastic Components*, McGraw-Hill, Inc., 1994, 366 pages.
- [6] Beiter, A., Cardinal, J. M., and Ishii, K., "Preliminary Plastic Part Design: Focus on Material Selection and Basic Geometry While Balancing Mechanical Performance and Manufacturing Cost", *Journal of Reinforced Plastics and Composites*, Vol. 16, No. 14/97, pp. 1293-1302.
- [7] Jia, N. and Kagan, V. A. "Effects of Time and Temperature Conditions on the Tensile-Tensile Behavior of Short Fiber Reinforced Polyamides", *ANTEC'97, SPE Conference Proceedings*, Vol. 2, pp. 1844-1848.
- [8] Kwok, W. and Choy, C. L., "Elastic Moduli of Injection-Molded Short-Glass-Fiber-Reinforced Poly (ethylene terephthalate)", *Journal of Reinforced Plastics and Composites*, Vol. 16, No. 4/1997, pp. 290-305.

- [9] *Engineering Plastics*, Engineering Materials Handbook, Vol. 2, ASM International, 1988, 883 pages.
- [10] Jia, N. and Kagan, V. A., "Compatibility Analysis of Tensile Properties of Polyamides Using ASTM and ISO Testing Procedures", *SPE Conference Proceedings*, ANTEC'98, Vol. 2, *Materials*, pp. 1706-1712.
- [11] Reinnertsen, C., "Testing Requires a Delicate Balance", *Machine Design*, May 28, 1993, pp. 62-71.
- [12] "Testing, Testing", *Reinforced Plastics*, June 1993, pp. 48-52.
- [13] Oehler, R., Graichen, C., and Trantina, G., "Design-Based Material Selection", *Plastics Engineering*, January 1995, pp. 25-28.
- [14] Wigodsky, V., "Plastics Testing", *Plastics Engineering*, October 1997, pp. 22-26.
- [15] Rackowitz, R., "Looking Beyond the Materials Data Sheet", *Plastics Design Forum*, May 1994, pp. 28-31.
- [16] Wigodsky, V., "The Road to Standardization", *Plastics Engineering*, April 1995, pp. 22-28.
- [17] Gabriele, C., "Global Standards Could Resolve Inconsistencies", *Plastics Technology*, June 1993, pp. 48-55.
- [18] *Uniform Global Testing Standards: A Technical Primer*, The Society of the Plastics Industry, Inc., 1996, 52 pages.
- [19] Verne, L. "Comparable Data for Plastic Materials – Help is on the Way", *Plastics Design Forum*, January-February 1993, pp. 37-40.
- [20] Turek, E., "On the Tensile Testing of High Modulus Polymers and the Compliance Correction", *Polymers Engineering Science*, Vol.33, 1993, pp. 328-333.

Pedro Albrecht,¹ Jianmin You,² Mark Albrecht,³ and Kathy Eley³

Tension Testing of Thin Bulk Adhesive Specimens

Reference: Albrecht, P., You, J., and Albrecht, M., "Tension Testing of Thin Bulk Adhesive Specimens," *Limitations of Test Methods for Plastics, ASTM STP 1369*, J. S. Peraro, Ed., American Society for Testing and Materials, West Conshohocken, PA, 2000.

Abstract: This paper describes a method of measuring the tensile properties of a bulk adhesive — including modulus of elasticity, yield stress and strain, and tensile strength and strain. The authors developed the method unaware of ASTM Test Method for Tensile Properties of Thin Plastic Sheeting (D 882). Not surprisingly, requirements founded on common sense are the same in the ASTM Standard as in the present study.

Augmenting ASTM D 882, this paper offers suggestions on (1) building tensiometers for low-load tests including a load cell and displacement-controlled loading apparatus, (2) building environmental chambers housing multiple tensiometers per chamber, (3) controlling relative humidity and temperature, (4) casting adhesive sheets, (5) cutting strip specimens from the sheets and preparing them for testing, (6) conditioning the specimens, (7) applying displacements with a computer-controlled stepper motor, and (8) acquiring data automatically.

The need to carefully control the environment and strain rate is shown with stress-strain curves that were measured at different relative humidities (15, 50 and 85%), temperatures (-15, 30 and 50 °C) and initial strain rates (10^{-2} , 10^{-4} , 10^{-6} and 10^{-8} s^{-1}).

Five series of tests were conducted to determine the effects of batch, loading method, environment, strain rate, and adhesive. The results show that the testing system is highly reliable. Stress-strain curves of replicate specimens tested in the same environment and at the same strain rate are highly reproducible.

The testing system is suited particularly well for thin film specimens of any material whose tensile properties are affected by relative humidity and temperature such as epoxy, acrylic, gelatin, photographic emulsion, and many kinds of paints and plastics.

Keywords: tension testing, tensiometer, environmental chamber, structural adhesive, FM 300K, hygro-thermo-mechanical properties, strain rate.

¹Professor, Department of Civil Engineering, University of Maryland, College Park, MD 20742.

²Graduate Assistant, Department of Mechanical Engineering, University of Maryland, College Park, MD 20742.

³PAA Consultant, 4201 Woodberry Street, Hyattsville, MD 20782.

Introduction

Special testing equipment is needed to measure the tensile properties of structural adhesives because the adhesive in a bondline is very thin and its strength is greatly affected by relative humidity (RH), temperature, and strain rate.

The original version of the method for testing thin bulk adhesive specimens in tension described in this paper was conceived by Mecklenburg and used extensively by Mecklenburg et al. [1] and Albrecht et al. [2]. Building on the original version, the authors in the last three years perfected the tension testing device, hereafter called *tensiometer*, added computer-controlled loading, and implemented automated data acquisition. This resulted in an efficient and cost-effective testing system for measuring stress-strain curves with very good reproducibility, allowing more accurate and reliable measurement of tensile properties than was possible in previous manually operated tests. The method is described in three parts below: specimen preparation, equipment and application.

Specimen Preparation

Structural Adhesive FM 300K

Mecklenburg et al. [1] measured stress-strain curves of 23 commercial adhesives in two environments — 90% RH/49 °C and 50% RH/22 °C — to determine their applicability to bonding steel bridges. The three best adhesives were found to be FM 300K, Eccobond 91-9, and AF-111; they were then selected for detailed characterization of their properties in bulk (neat) and in steel-steel bonds [2]. The structural adhesive FM 300K was retained subsequently for characterization of its hygro-thermo-mechanical properties and long-term durability [3]. Partial results are included herein to illustrate the capabilities of the testing system.

The hot-cured structural adhesive FM 300K manufactured by Cytec Fiberite is a modified epoxy adhesive film available with three different moisture-resistant polyester carriers. The manufacturer recommended the tight-knit, tricot, polyester carrier for ease of controlling bondline thickness and for its good blend of structural and handling properties during lay-up. According to the manufacturer, FM 300K has superior metal-to-metal peel strength, can be used at service temperatures of -55 to 150 °C, and resists moisture and corrosion in high humidity environments with little reduction in mechanical properties. Its glass transition temperature varies from 150 °C in a dry environment to 123 °C when fully saturated. Standard weight and nominal film thickness before curing are 0.4 ± 0.025 kg/m² and 0.33 mm, respectively.

Curing

Thirteen 200×150 mm films of FM 300K adhesive were cured in the present study. Each film was placed between two aluminum plates 300 mm long, 230 mm wide, and 16 mm thick. Both film surfaces were covered with Mylar sheets to prevent the adhesive from bonding to the aluminum plates. Narrow metal shim strips of 0.32 mm thickness

were placed along the four edges to control the thickness of the cured film. The assembly was clamped and placed in a THELCO laboratory oven, Precision Scientific Model 70. The temperature was incrementally raised over a period of 60 minutes to the target curing temperature of 177 °C. After one hour of curing at that temperature, the assembly was removed from the oven, cooled for three hours at ambient room temperature, and then disassembled.

Cutting

The specimens were cut from a central area of a film about 25 mm away from all four sides. Each cut was made by running a 0.017 heavy duty carpet blade about 10 times at medium hand pressure along a rigid, machined aluminum bar resulting in specimens with straight and parallel edges. Utmost care was exercised in cutting the specimens to prevent nicks and tears at the edges that could cause specimens to fail prematurely. All specimens cut from the same film are referred hereafter as a *batch*.

Sanding

After cutting, the specimen edges were sanded with 3M 326U Aluminum Oxide Resin Paper 220 to remove cracks and scratches and fully straighten the edges. To this end several specimens were clamped between two machined plates for ease of sanding.

Measuring

Specimen thickness and width were measured with a digital micrometer and a 50X traveling microscope. The digital micrometer and traveling microscope are accurate to ± 0.0025 mm. Thickness and width were measured at five cross sections spaced 30 mm apart and centered about the mid-point of the 127-mm gage length between the two grips. The area is the product of thickness and width. The minimum smallest of the five areas was used to calculate the stress for the stress-strain curves.

Table 1 — *Cross Sections of Three Random Specimens*

Batch-Specimen No.	Width		Thickness		Area	
	Mean (mm)	COV (%)	Mean (mm)	COV (%)	Mean (mm^2)	COV (%)
X11-1	5.949	0.63	0.281	1.61	1.674	1.69
X12-11	5.908	0.38	0.330	3.69	1.951	3.90
X13-20	5.862	0.56	0.291	2.94	1.703	3.01

Table 1 lists, as an example, the mean thickness, width, and area as well as the corresponding coefficients of variation (COV) of three randomly selected specimens. For all 124 FM 300K specimens tested in the present study, the mean COVs were 2.57% on thickness, 0.57% on width, and 3.00% on area.

After a specimen was installed in the tensiometer and the grips tightened, its gage length between grips, L_0 , was measured with a caliper accurate to 0.05 mm. The gage length was subsequently used to calculate strain.

Conditioning

RH and temperature greatly affect the physical properties of polymeric materials. To properly account for these effects of environment, the moisture content in the specimen must be in equilibrium with the RH of the air in the chamber — RH is a partial pressure of water divided by the vapor pressure of water at the temperature. Likewise the specimen's temperature must be the same as that inside the chamber. The former takes a long time to equilibrate, the latter a short time. According to ASTM Test Method for Tensile Properties of Thin Plastic Sheeting (D 882) and ASTM Practice for Conditioning Plastics and Electrical Insulation Materials for Testing (D 618), specimens should be conditioned to the environment for 40 or more hours prior to testing.

The required moisture conditioning time depends on specimen thickness, diffusion coefficient, and temperature. While it can be calculated, it is best measured. Fig. 1 shows the free moisture swelling strain as a function of time for FM 300K at 50 °C. The specimen was equilibrated for two weeks at 17% RH at which time the silica gel was then replaced with new gel pre-conditioned to 92% RH. After 24 hours the specimen had reached about 95% of its final moisture content. Still, in the present study all (0.3 mm thick) specimens were conditioned in environmental chambers for two weeks prior to testing. In comparison, Ishida and Allen [4] and Ishida [5] reported that about 100 days

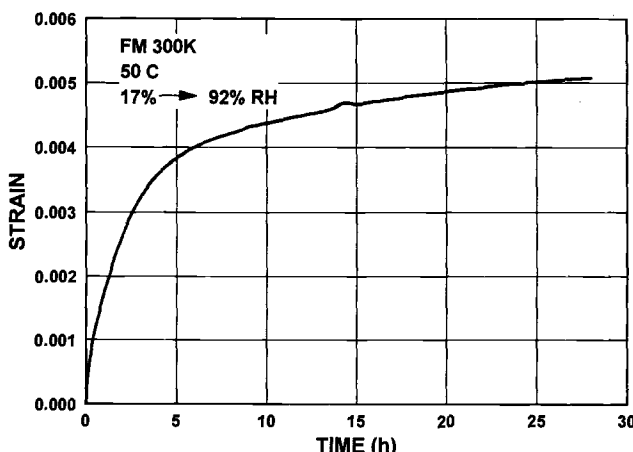


Figure 1 — *Free Swelling Strain of FM 300K with Time*

were needed to condition their disk-shaped epoxy specimen of 50-mm diameter and 3.2-mm thickness. Conditioning time should be chosen for each specimen/material combination.

Equipment

Automated System Testing

With the advent of electronics and computers, automated materials testing is progressing fast. Today computer-controlled equipment can be built in-house, as was done in the present study. As a result of these advancements, tests of thin bulk adhesive specimens can now be performed with greater precision and reproducibility than previously possible.

As shown in Fig. 2, a testing system consists of tensiometers, environmental chamber, switch and balance unit, strain indicator, loading system, data acquisition (DAQ) board, and a personal computer (PC). A tensiometer is a small, low-load, displacement-controlled, screw-driven tensile testing device. Up to six of them are placed in an environmental chamber in which RH and temperature are controlled. A stepper motor, controlled via the parallel (printer) port of the PC, turns the threaded loading rod that pulls the movable grip holding the specimen. The switch and balance unit receives the signals from the strain gages mounted on the load cell of each tensiometer; the strain indicator conditions and amplifies the signals. These signals are converted to applied load and specimen elongation. The PC reads the output from the load cell through a DAQ board connected to the strain indicator's analog output.

The conditioned signals are sampled at a specified rate and stored on the hard disk. An exception to this computer-controlled loading and data acquisition were the tests performed at 10^{-8} s⁻¹ strain rate, which lasted up to 8 months. In these tests, the loading

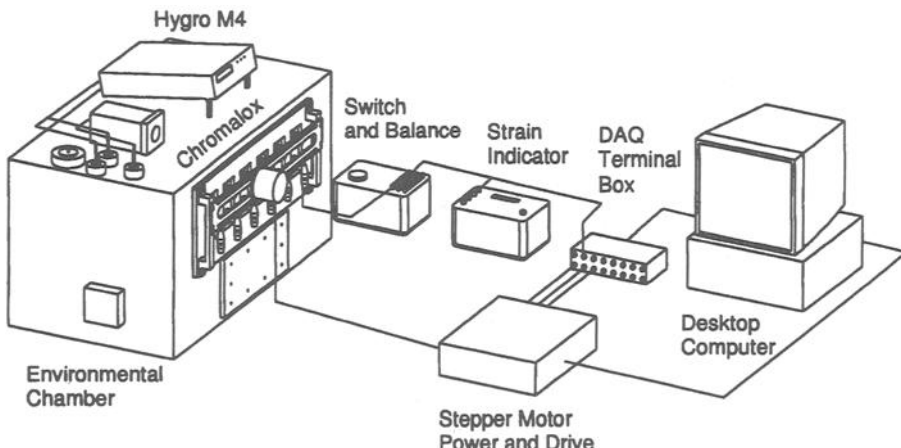


Figure 2 — *Testing System*

rod was turned manually with a dial gage mounted on the front face of the tensiometers and the data were recorded manually. The data were analyzed in a spreadsheet.

Tensiometer

A tensiometer, shown in Figs. 3 and 4, consists of five major components: (1) two $457 \times 152 \times 1.6$ mm stainless steel side plates, (2) a $184 \times 73 \times 25$ mm acrylic face plate, (3) a $432 \times 73 \times 25$ mm acrylic spacer bar, (4) a $145 \times 19 \times 3.2$ mm aluminum load cell, (5) a $73 \times 50 \times 50$ mm two-piece aluminum load cell clamp, and (6) a loading device. The above dimensions are listed in the order of length, width, and thickness.

Side Plate — The side plates hold the face plate, spacer bar and load cell clamp in place, all three being attached with eight bolts of 6.2-mm diameter and 93-mm length through the full width of the tensiometer.

Face Plate — Mounted on the face plate are the connector for the wires leading to the strain gages on the load cell and the dial for manually rotating the loading rod. When the specimen is loaded automatically with a stepper motor, the dial is replaced with an attachment for the shaft of the stepper motor.

Spacer Bar — The horizontal spacer bar, which extends from the face plate to the end of the tensiometer, supports the loading rod, the specimen grips, and the link plate between the quasi-fixed grip and the load cell.

Load Cell — The load cell, in the shape of a cantilever bar, extends 95 mm above its clamp. It is instrumented with two strain gages mounted on each side and wired as a Wheatstone bridge resistance circuit. It has a capacity of 120 N, a limit set to prevent yielding of the aluminum bar at the base. Bar thickness can be increased when more load capacity or load cell stiffness is needed. Load capacity increases with the square and load cell stiffness with the cube of the thickness.

Loads Cell Clamp — At its bottom, the load cell is clamped between two jaws, one of which has a groove slightly wider and slightly shallower than the width and thickness of the load cell. The grooved jaw is bolted to the side plates while the flat jaw is, in turn, bolted to the grooved jaw.

Loading Device — The loading device is screw-driven by a 230 mm long stainless steel rod of 12.7-mm diameter and 20 threads per 25.4-mm length. This loading rod is supported at the face plate on the left end and at the aluminum bearing block mounted on the spacer bar on the right (Fig. 4). A Miniature Precision Bearing of dimensions $12.7 \times 25.4 \times 0.125$ mm is inserted at the left support of the rod and a 6.35×12.7 mm bearing at the right support. These stainless steel ball bearings allow the rod to turn effortlessly.

The left end of the rod was machined down to 6.4 mm over a 19-mm length so that the dial gage or the shaft of the stepper motor could be attached.

The loading rod passes through the movable aluminum grip that has matching female threads. The grip moves as the rod is turned thus loading the specimen. The quasi-fixed grip — so called because it moves as the load cell deflects — is mounted on a stainless steel plate supported on two four-wheel trucks taken from a miniature toy train. The load cell protrudes through a hole in the link plate and resists the applied load, which

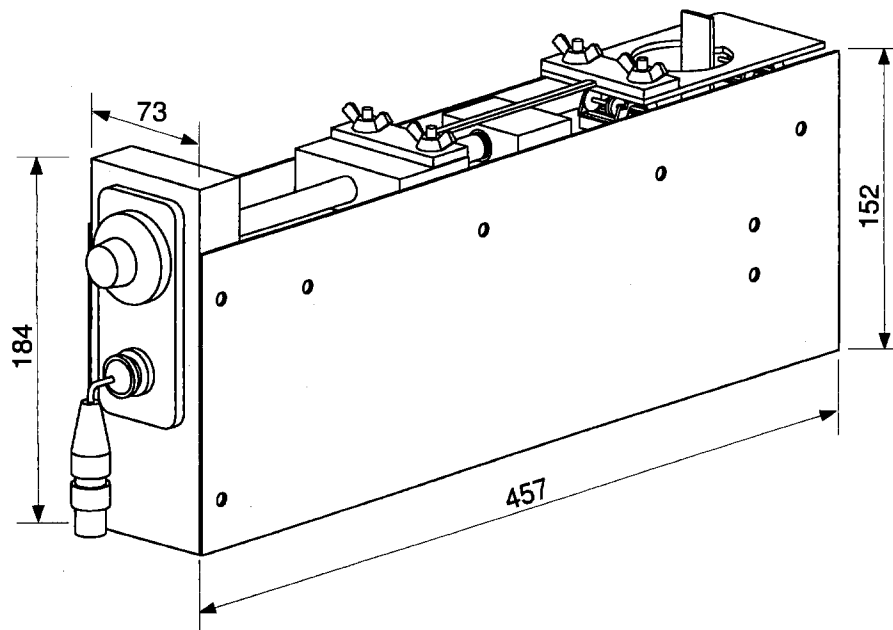


Figure 3 — Three-dimensional View of Tensiometer

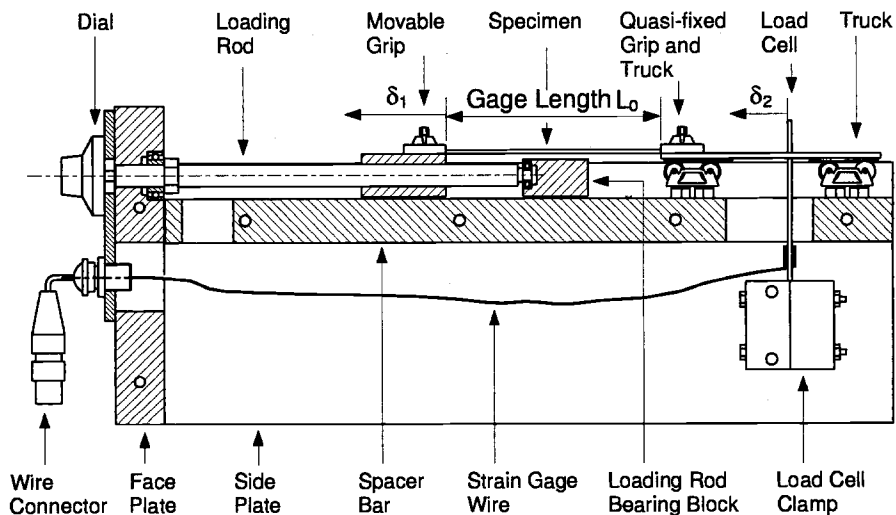


Figure 4 — Longitudinal Cross Section of Tensiometer

is transferred through a notched stainless steel ball of 6.4-mm diameter pressed onto the hole edge.

The loading rod is turned manually with a 46-mm diameter turns-counting dial, model RB manufactured by McMaster-Carr; or automatically with a computer-controlled stepper motor. The dial is accurate to $\pm 1/200$ rev = $\pm 1.8^\circ$ which, for 127-mm specimen length and loading rod threads of 25.4 mm/20 threads, converts to $\pm 50 \mu\text{e}$. The stepper motor is accurate to $\pm 1/400$ rev = $\pm 0.9^\circ = \pm 25 \mu\text{e}$.

Specimen Grips — The specimen is gripped at each end with a 50×25×6.4 mm acrylic plate and two 4.7-mm diameter screws with wing nuts. The plate edges were slightly rounded. Specimens tested in the present study ruptured at various places along the length, and only rarely at a grip edge.

The face of the acrylic grip plate and the ends of several specimens were brushed with fingernail polish. Since the coating did not crack along the line where the specimen enters the grip plate, these specimens did not slip.

Specimens can be prismatic along the full length between grips. Dog-bone-shaped specimens are not needed for tensile testing of thin bulk adhesive specimens, thus reducing fabrication cost and simplifying the measurement of extension and thus strain.

Calibration for Load Cell Displacement — The tensiometers were carefully calibrated for load cell displacement and applied load as follows. First, a 150×7×1.3 mm steel strip was installed between the grips to calibrate the load cell displacement δ_2 as a function of measured load cell strain ε_{LC} . The movable grip displaces in proportion to the number of revolutions r of the dial gage:

$$\delta_1 = rp \quad (1)$$

where

r = number of revolutions, and

p = 25.4 mm/20 threads = 1.27 = pitch of threaded loading rod.

Since the steel strip is about 300 times stiffer than the bulk adhesive specimen, the load cell displacement δ_2 is about equal to the displacement of the movable grip δ_1 , which in turn is equal to rp from Eq. 1. It is noted that the loading rod and the link plate connecting the quasi-fixed grip to the load cell are 4000 and 8000 times stiffer than an adhesive specimen. Hence $\delta_1 = \delta_2 = \delta_{LC}$. In essence, inserting the rigid steel strip makes the displacement of the load cell equal to the displacement applied by turning the dial. The load cell displacement δ_2 is calibrated as follows:

1. Install the steel strip, turn the dial until the link plate on the quasi-fixed grip just touches the load cell, and set the strain indicator to zero.
2. Turn the dial by 0.2 revolutions, record the revolution r , and calculate the load cell displacement $\delta_2 = rp$.
3. Read the strain indicator value R and calculate the load cell strain $\varepsilon_{LC} = (R/4) \times 10^{-6}$.
4. Repeat steps 2 and 3 until the maximum allowable displacement of the load cell $\delta_2 = \delta_{2, \text{allow}}$ is reached, that is, from the displacement equation of a cantilever:

$$\delta_{2,allow} = 2\sigma_{allow}L^2/3hE \quad (2)$$

where

σ_{allow} = allowable bending stress of load cell from yield stress of aluminum and chosen safety factor,

L = length of load cell,

h = thickness of load cell, and

E = modulus of elasticity of aluminum.

5. Plot δ_2 versus ε_{LC} and verify that the relationship is linear.
6. Fit the following linear equation to the data:

$$\delta_2 = K_d \varepsilon_{LC} \quad (3)$$

The slope of the line is the desired calibration factor for load cell displacement K_d in units of mm/strain.

Calibration for Load — After calibrating the load cell for displacement, the tensiometer was calibrated for load. To this end, a steel spring was used that had 106-mm overall length, 1.2-mm wire diameter, 66 loops of 11-mm outside diameter, and known stiffness K_s . The length change of the spring, like that of an adhesive specimen tested in the tensiometer, is the difference between the displacements of the movable grip and the load cell (Fig. 4). It is also equal to the grip separation because the link plate connecting the quasi-fixed grip to the load cell is about 8 000 times stiffer than a typical adhesive specimen:

$$\Delta L_0 = \delta_1 - \delta_2 \quad (4)$$

The left side of Eq. 4 is replaced by the unknown load and known spring stiffness, P/K_s , while Eqs. 1 and 3 are substituted for δ_1 and δ_2 . This yields the applied load as a function of the measured load cell strain:

$$P = K_s(r\rho - K_d \varepsilon_{LC}) \quad (5)$$

The load cell is then calibrated for load as follows:

1. Install the spring, turn the dial until the link plate on the quasi-fixed grip just touches the load cell, and set the strain indicator to zero.
2. Turn the dial by 0.2 revolutions and record the revolution r .
3. Read the strain indicator value R and calculate the load cell strain $\varepsilon_{LC} = (R/4) \times 10^{-6}$.
4. Calculate P with Eq. 5.
5. Repeat steps 2 to 4 until the maximum allowable displacement of the load cell is reached, Eq. 2.

6. Plot P versus ε_{LC} and verify that the relationship is linear.
7. Fit the following linear equation to the data:

$$P = K_p \varepsilon_{LC} \quad (6)$$

where K_p = calibration factor for load in units of N/strain.

The load calibration factor was verified independently with incremental weights attached to a wire that pulled directly on the load cell and was guided by pulleys.

Tensiometers should be recalibrated when used at temperatures much lower or higher than the ambient temperature. Table 2 lists values of K_d and K_p of a tensiometer calibrated at 15% RH and three different temperatures of -15, 30, and 50 °C.

Strain and Stress — Once K_d and K_p are determined, the strain and stress in the specimen are calculated from:

$$\varepsilon = (\delta_1 - \delta_2) / L_0 \quad (7)$$

and

$$\sigma = P / A \quad (8)$$

where δ_1 , δ_2 , and P are given by Eqs. 1, 3, and 6.

Environmental Chamber

The environmental chambers for six tensiometers have overall dimensions of 915-mm length, 500-mm width, and 500-mm height (Fig. 5). They are made of 9.5 mm thick acrylic plates held together with methylene chloride and screws. A 785 mm long platform subdivides the chamber into an upper half for the tensiometers and a lower half for the light bulbs and the pans containing the silica gel.

Two doors on the front of the chamber provide access to the tensiometers (686×267 mm) and the pans (381×178 mm). The former has six 50×27 mm cutouts for the dial and the wire connector as shown in Fig. 5. Bolts with wing nuts spaced about 100 mm on centers hold the doors in place. The bolts are countersunk in the chamber wall; an acrylic strip bonded to inside wall prevents the bolts from falling in. All door and cutout edges are sealed with 25 and 12 mm strips of 0.37 mm thick silicon rubber laminate. The spongy laminate effectively minimizes air leaks.

Table 2 — *Calibration Factors at Three Temperatures and 15% RH*

Parameter	-15 °C	30 °C	50 °C
K_d (mm/strain)	1,199	1,193	1,190
K_p (kN/strain)	49.58	48.32	47.55

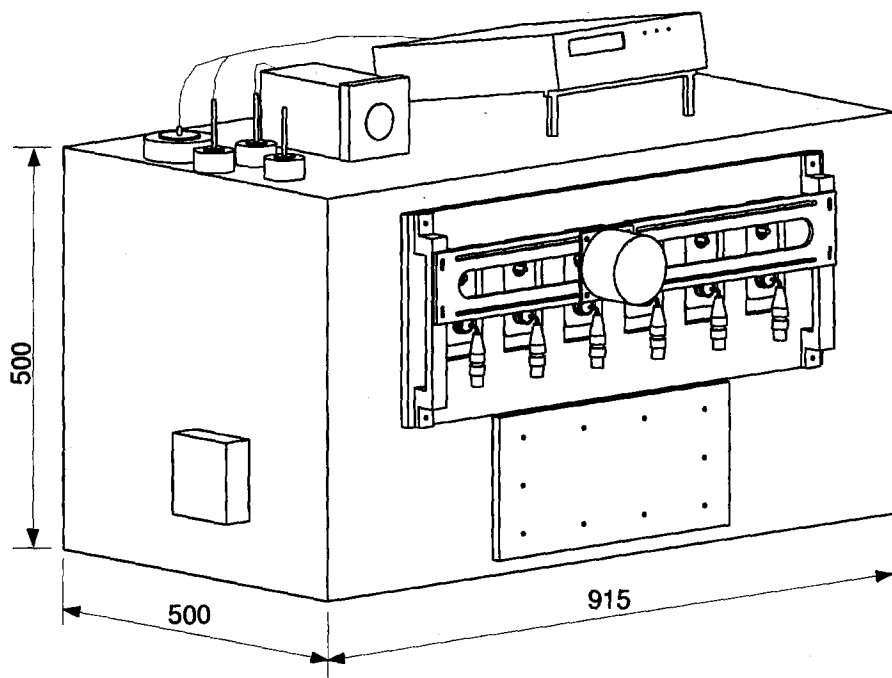


Figure 5 — Three-dimensional View of Environmental Chamber

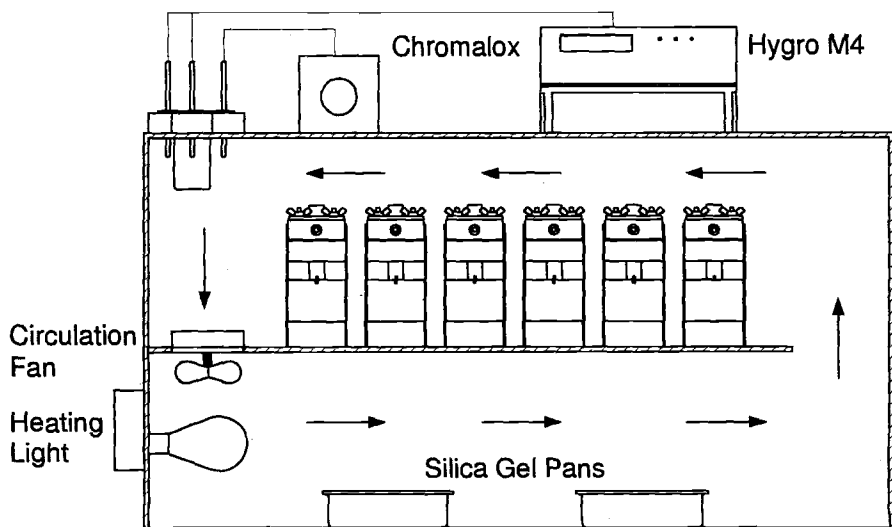


Figure 6 — Longitudinal Cross Section of Environmental Chamber

Two 80-mm diameter fans continuously pump air from the upper to the lower half of the chamber through circular holes in the platform. Together the fans move air at a rate of 1.8 m³/min. That is, about every 10 s the air is moved around the chamber — over the silica gel, up the 130×500 mm opening in the platform, and over the specimens following the arrows in Fig. 6.

Two light bulbs for heating the chamber are installed below the fans and circular holes in the platform. The chambers used in the 50 °C tests were insulated all around with 38 mm thick boards of Styrofoam. The joints were sealed with 75 mm wide transparent packing tape. A thermometer and probes for the dew-point meter and Chromalox were inserted through conical one-hole rubber stoppers that fitted into matching reinforced holes in the top plate of the chamber (Fig. 5).

RH Control — ASTM Practice for Maintaining Constant Relative Humidity by Means of an Aqueous Glycerin Solution (D 5032) and ASTM Practice for Maintaining Constant Relative Humidity by Means of Aqueous Solution (E 104) limit tests to RHs ranging from 30 to 98% at temperatures of 0 to 70 °C and dryness to saturation at temperatures of 0 to 50 °C — both in relatively small containers. These practices are not suitable for the present tests conducted in large chambers at RHs of 15 to 85% and temperatures of -15 to 50 °C. While moisture saturated salt solutions [6] can create different RHs, this method does not seem practical for use with the present equipment.

In the present study, RH was controlled with 2.5 kg of silica gel desiccant (mesh size 3-9) evenly spread out in two pans of dimensions 400×260×50 mm placed on the bottom of the chamber (Fig. 6). Dry silica gel was previously conditioned in a separate chamber by incrementally adding water until the air in the chamber reached the desired RH.

RH was measured with a Hygro-M4 (General Eastern) hygrometer moved from chamber to chamber as needed. The Hygro-M4 is a general purpose chilled mirror hygrometer, a bench top indicator. Mated with General Eastern's chilled single-stage sensors Model 1111H-SR and T-100, it provides an overall measurement range of -40 to +60 °C dew/frost point and 0.002 to 100% RH according to the manufacturer. RH can be read with an accuracy of ±0.1% RH. Each chamber was equipped with a mini hygrometer for convenience.

In the 15 and 50% RH tests, about 12 mL of water was added to raise the RH by 1%. Any deviations from the desired value were compensated by adding water to raise RH or dry silica gel to lower RH. Fans continuously circulated the air, providing an uniform environment in the chamber and shortening the time to moisture equilibrium. The RH was easily held to ±1% over periods of several weeks.

In the high 85% RH tests, some moisture leaked out of the chamber. About 140 mL of water were injected into the chamber every four days to maintain 85% RH.

Temperature Control — The temperature in the chambers was controlled in two ways. In the tests conducted below room temperature (-15 °C), the small environmental chamber was kept in a refrigerator. The Chromalox on-off controller, with a temperature sensor installed inside the chamber, was located outside the refrigerator. It automatically turned the refrigerator on when the temperature in the chamber was higher than needed and off otherwise. If left running all the time, the temperature in the refrigerator would bottom out at -15 °C.

In the tests conducted above room temperature (30 and 50 °C), the environmental chamber was placed on a table in the ambient environment. The Chromalox controller sitting on top of the chamber turned two 25-W light bulbs on and off as needed to maintain the desired temperature (Fig. 6). Only in the tests conducted at 50 °C were all sides of the environmental chambers insulated with Styrofoam boards to reduce heating loss.

The total power of the bulbs should not exceed 50 W to prevent overheating of the chamber if the Chromalox controller fails and the bulbs remain on. With bulb power higher than 50 W, the accumulated heat could deform the acrylic components of the chamber.

The temperature was measured in all tests with the high precision Hygro-M4 hygrometer, with an accuracy of ± 0.1 °C. The Chromalox controller held the temperature to ± 0.5 °C.

Automatic Loading System

The specimens tested at initial strain rates of 10^{-4} and 10^{-8} s⁻¹ were loaded manually. Those tested at 10^2 and 10^6 s⁻¹ were loaded automatically with a stepper motor controlled through a drive and power supply unit, an attachment fixture, and a C++ program.

Stepper Motor — Stepper motors can be used in simple open-loop control systems and are generally suited for systems operated at low acceleration and static load. Closed-loop control may be needed for high dynamic loads, particularly when loads vary. If a stepper motor in an open-loop control system is overtorqued, all knowledge of rotor position is lost and the system must be reinitialized. To prevent this, the torque capacity of the stepper motor must not exceed the maximum running torque calculated from:

$$M_T = PR(\tan \alpha + \mu) / (1 - \mu \tan \alpha) \quad (9)$$

where

P = maximum force applied to specimen,

R = radius of threaded rod,

μ = friction coefficient between steel rod and movable aluminum grip, and

α = angle of helical rod thread.

In this study, $\alpha = \text{atan} (d/2\pi R) = \text{atan} (1.27/2 \times 3.14 \times 12.7) = 0.016$ rad; $P = 120$ N; and $\mu = 0.2$. Thus $M_T = 0.33$ N-m. Given an ample safety factor, a stepper motor with a running torque of 1.3 N-m was chosen — Sigma Model #21-3424D-29058, 1.8/0.9 degree per step, corresponding to $6.35 \times 10^{-3}/3.175 \times 10^{-3}$ mm displacement per step.

Stepper Motor Drive and Power Supply — Required drive and power supply are determined by the stepper motor. Selected in the present study were a miniature high performance bipolar stepper motor drive Model IB 106 from Intelligent Motion System and a 48 VDC @ 4 amps power supply Model E48-4.0.

Attachment Fixture — A specially designed guide, mounted on the front of the chamber (Fig. 5), was used to attach the stepper motor and slide from one tensiometer to another. The stepper motor was connected to the loading rod of a tensiometer with a universal joint of stainless steel to facilitate rod alignment.

Control Program — The stepper motor can be controlled in various ways; for example, via the parallel port of a PC or the digital output port of a DAQ board. In the Windows multitasking operating system, a special lower level program would have to be written to achieve accurate millisecond stepping time. Instead, the authors achieved that with a parallel port and a C++ program running in DOS — an inexpensive yet powerful platform for implementing projects dealing with the control of real world peripherals.

A standard parallel port has 25 pins: 8 for output (DATA port), 5 for input, (STATUS port), and 4 four bidirectional leads (CONTROL port), thus providing a simple means of using the PC interrupt structure. The remaining 8 pins are grounded.

The following function “RunMotor” generates three signals at the output pins 1, 2 and 14, which are connected to the stepper motor drive:

```
void RunMotor(int DirMode, long NumSteps, unsigned long DelayTime){  
    unsigned long register i;  
    outportb(CONTROL,DirMode); /* direction and stepping mode */  
    for(i=0; i<NumSteps; i++){ /* use DATA port to turn motor */  
        outportb(DATA,0x00); /* make Data 0 (pin2) high */  
        delay(DelayTime); /* delay "DelayTime" in milliseconds */  
        outportb(DATA, 0x01); /* make Data 0 (pin2) low */  
    }  
}
```

Parameter “DirMode” controls the direction and stepping mode, “NumSteps” controls the number of steps, and “DelayTime” controls the time between each step and hence the speed of the stepper motor. Function “RunMotor” is integrated into a C++ program that describes the desired loading path and speed.

Pins 1 and 2 connect to the step clock and direction pins of the stepper motor drive respectively. Pin 14 connects to the drive’s stepping mode pin.

Data Acquisition System

Time, stepper motor position, and load cell voltage were recorded with a DAQ board and a LabVIEW program. The DAQ board, National Instruments Model PC-LPM-16PnP, is featured as follows: XT or AT Bus; a 12-bit, successive-approximation, self-calibrating analog to digital converter (ADC) with 16 analog inputs; 50 kS/s maximum sampling rate; 8 lines of TTL-compatible digital input; 8 lines of TTL-compatible digital output; and two 16-bit counter/timer channels for timing I/O.

A Virtual Instrument (VI), a LabVIEW program whose appearance and operation imitate actual instrumentation, was written in the present study to acquire and process data. LabVIEW is a program development application, much like various commercial C/C++ or BASIC programming languages. It differs from those other languages in one

important respect: the others create lines of codes with text-based languages, whereas LabVIEW creates programs in block diagram form with the graphical programming language G. Functionally analogous to a conventional language program, it is much easier and faster for developing instrumentation applications. A VI can contain many sub-VIs, just as a C/C++ program contains many functions.

Application

To demonstrate the reliability of the testing system and the reproducibility of the data, stress-strain curves were measured in five series of tests with batch, loading method, environment, strain rate and adhesive type as variables. All tests were performed in environmental chambers in which RH and temperature were carefully controlled. Loading and data acquisition were computer controlled unless noted otherwise. In the following, the authors use the term "initial strain rate" as defined in the ASTM Test Method D 882.

Effect of Batch

In the first series of tests, one specimen each from 13 batches were tested in the 50% RH/30 °C environment and at 10^{-4} s⁻¹ initial strain rate. Figure 7 shows very good correlation between the 13 stress-strain curves. Clearly, batch and specimen preparation were not significant variables in the present study.

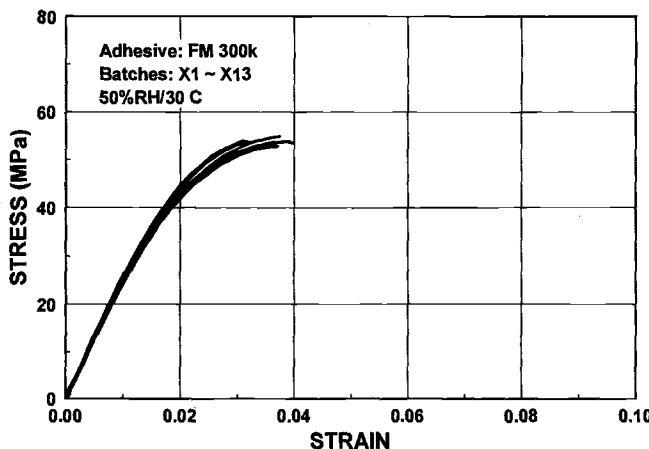


Figure 7 — *Effect of Batch on Stress-strain Curves*

Table 3 lists the average tensile properties of the 13 specimens, including standard deviation (STD) and coefficient of variation (COV) with symbols of: E = modulus of elasticity, $\sigma_{y, 0.2\%}$ and $\epsilon_{y, 0.2\%}$ = yield stress and yield strain at 0.2% offset, σ_u = tensile strength, and ϵ_u = elongation at break.

Table 3 — *Effect of Batch on Tensile Properties*

Statistic	E (GPa)	$\sigma_y 0.2\%$ (MPa)	$\varepsilon_y 0.2\%$	σ_u (MPa)	ε_u
Average	2.59	38.8	0.0168	52.8	0.0330
STD	0.08	1.5	0.0013	1.8	0.0045
COV (%)	3.1	3.7	7.7	3.5	13.6

The greatest variation was found in the elongation at break, a value influenced by slight imperfections along the specimen edges. This variation would likely decrease if specimens of greater cross section were tested.

Ideally such a test should be performed with multiple specimens per batch to determine separately the between-batch and within-batch variations. But this seemed hardly necessary, given the very good correlation shown in Fig. 7. Considering also that the 13 specimens were tested in 6 tensiometers within a chamber, the results are actually excellent. In the authors' opinion, there is no need for a three-way factorial experiment design and analysis of variance. The results speak for themselves.

Effect of Loading Method

In the second series of tests, the effect of loading path was examined with five specimens tested in the 85% RH/50 °C environment and at 10^{-4} s⁻¹ initial strain rate. As shown in Fig. 8, specimen A was strained continuously. Specimen B was strained in initial strain increments of 0.001 applied over 0.4 s followed by stress relaxations of 9.6 s duration, for a loading time of 10 s per step. The steps were repeated until the specimen

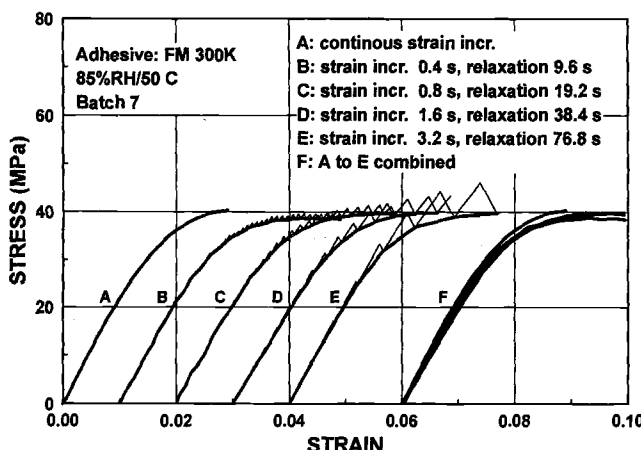


Figure 8 — *Effect of Loading Method on Stress-strain Curves,
Initial Strain Rate 10^{-4} s⁻¹*

failed. Initial strain increments and times were doubled for specimen C, again doubled for specimen D, and once more doubled for specimen E. Still, in all tests the initial strain rate remained constant at 10^{-4} s⁻¹. Figure 8 shows the saw-tooth-shaped strain-relaxation increments. Connecting the bottom points of the relaxation segments yields the stress-strain curve. The stress relaxation segments are not vertical because the load cell deflects by δ_2 . The stiffer the load cell relative to the specimen, the more the relaxation line would approach the vertical.

All five curves A through E were replotted as F in Fig. 8 — without the saw teeth. The curves are in no particular order. Near the top — approaching 40 MPa stress — curve A is highest, curve B lowest and the other three fall in between. The correlation is as good as that found for effect of batch in Fig. 7. It appears that the same stress-strain curve is obtained whether the strain is increased continuously or in steps.

This finding opened the door to testing specimens in the present study at the extremely low initial strain rate of 10^{-8} s⁻¹ without having to dedicate the stepper motor to one specimen at a time for about 8 months. Instead, the strain was incremented manually by 0.003 every 3.5 days, for an initial strain rate of $0.003 / (3.5 \times 24 \times 3,600) = 1 \times 10^{-8}$ s⁻¹.

Table 4 lists the average tensile properties of the 5 specimens, including standard deviation (STD) and coefficient of variation (COV). The STD and COV values are higher than those for effect of batch (Table 3). The COV of elongation at break is again large — 19.5%.

Table 4 — *Effect of Loading Method on Tensile Properties*

Statistic	E (GPa)	$\sigma_{y,0.2\%}$ (MPa)	$\varepsilon_{y,0.2\%}$	σ_u (MPa)	ε_u
Average	2.14	33.2	0.0176	39.1	0.031
STD	0	1.6	0.0013	1.5	0.006
COV (%)	4.6	4.9	7.4	3.9	19.5

Effect of Hygro-thermal Environment

In the third series of tests, 3 specimens were tested in the dry-cold (15% RH/-15 °C), 6 in the mild (50% RH/30 °C), and 6 in the humid-hot (85% RH/50 °C) environments. The initial strain rate was 10^{-4} s⁻¹. Figure 9 shows the 15 stress-strain curves. The correlation within each set was again very good.

Figure 9 shows how sensitive adhesives — and polymers in general — are to changes in RH and temperature in ambient environments. The behavior changes from

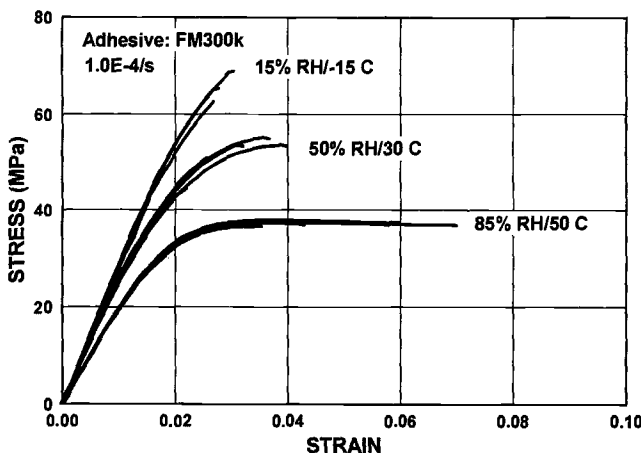


Figure 9 — *Effect of Environment on Stress-strain Curves*

very brittle in the dry-cold to very ductile in the humid-hot environment. Increasing RH, temperature, or both, greatly reduce the modulus of elasticity, yield strength, and tensile strength but increase the elongation at break. It is noted that FM 300K ranks in the top 3 of 28 structural adhesives the authors have tested over the years in the humid-hot (85% RH/50 °C) environment. This comparison is based on adhesive strength.

Effect of Strain Rate

In a fourth illustration of the capabilities of the testing system described herein, five specimens were tested at 10^{-2} initial strain rate and six specimens each at 10^{-4} , 10^{-6} and 10^{-8} s^{-1} initial strain rates — all 23 in the humid-hot environment (85% RH/50 °C). To

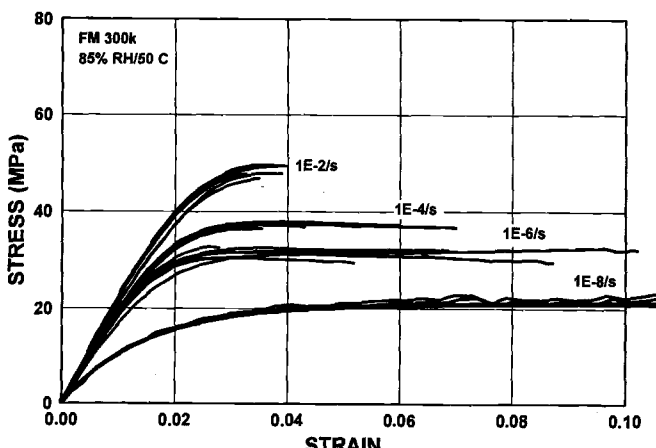


Figure 10 — *Effect of Strain Rate on Stress-strain Curves*

measure stress-strain curves at these rates took about 4 s at 10^{-2} s⁻¹ to 240 days at 10^{-8} s⁻¹. Variability between replicate specimens tested at a given strain rate, Fig. 10, is comparable to those in the tests on the effects of batch, loading method, and hydro-thermal environment.

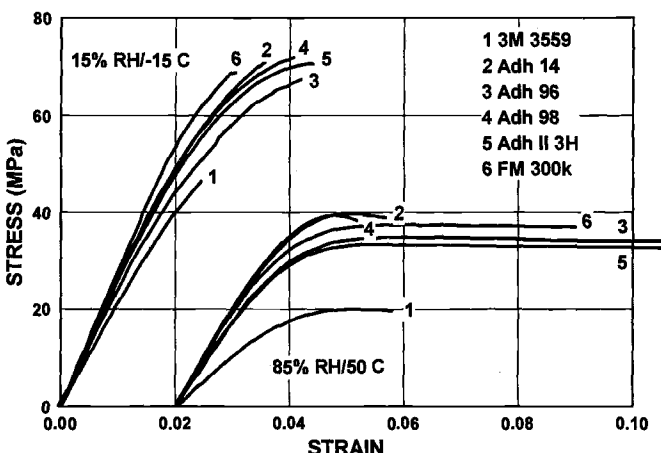


Figure 11 — *Effect of Adhesive on Stress-strain Curves*

Effect of Adhesive

Finally, to determine whether FM 300K is comparable to other adhesives, five more were tested: adhesive 3M 3559 made by 3M; and adhesives No. 14, No. 96, No. 98, and No. II3H made by Martin-Marietta for use in U.S. Army bridges. One specimen of each adhesive was tested in the dry-cold (15% RH/-15 °C) and one in the humid-hot (85% RH/50 °C) environment. Figure 11 compares the stress-strain curves of FM 300K with those of the other five adhesives. Table 5 lists the tensile properties in the two environments. Clearly, FM 300K behaves similarly to the Martin-Marietta adhesives. All are greatly affected by RH and temperature.

Table 5 — *Effect of Adhesive on Tensile Properties Environments: 15% RH/-15 °C and 85% RH/50 °C*

Adhesive	E (GPa)	$\sigma_{y,0.2\%}$ (MPa)	$\varepsilon_{y,0.2\%}$	σ_u (MPa)	ε_u
3M 3559	2.15 & 1.03	43.2 & 16.4	0.022 & 0.018	46.4/20.0	0.025 & 0.038
Adh 14	2.76 & 2.01	47.6 & 32.0	0.019 & 0.018	71.1/39.8	0.036 & 0.037
Adh 96	2.46 & 1.80	44.5 & 26.7	0.020 & 0.017	67.5/34.9	0.042 & 0.107
Adh 98	2.64 & 2.08	53.7 & 31.6	0.022 & 0.017	72.0/39.4	0.041 & 0.032
II 3H	2.60 & 1.72	49.6 & 27.5	0.021 & 0.018	70.7/33.3	0.044 & 0.093
FM 300K	2.94 & 2.03	56.7 & 28.8	0.021 & 0.016	65.3/36.6	0.028 & 0.035

Conclusions and Recommendations

Highly repeatable and reproducible tensile stress-strain curves for thin bulk adhesive specimens can be measured with the testing system described in this paper. The authors attribute this capability to careful specimen preparation, accurate RH and temperature controls, and computer-controlled loading and data acquisition.

It was shown that RH, temperature, and strain rate greatly affect tensile properties. To properly account for their effects, the three parameters must be carefully controlled. Most important is the need to allow enough time for the moisture content in a bulk adhesive specimen to equilibrate with the RH of the environment before the test is started. To this end, specimens of 0.025 mm or less thickness — typical of bondlines — should be conditioned for at least 48 hours.

Instruments for measuring RH and temperature should be accurate to $\pm 0.2\%$ RH and $\pm 0.1^\circ\text{C}$. Specimens should be conditioned and tested in environments controlled to $\pm 1.5\%$ RH and $\pm 0.75^\circ\text{C}$.

In tests designed to determine the effect of temperature, RH should be kept constant. In a closed system, RH drops as temperature is increased. So the temperature rise decreases strength while the concomitant drop in RH increases strength, thus masking the true temperature effect.

The stress-strain needed to design a bonded joint should be measured at the same rate at which the structure is loaded in service. For typical grade separation bridges on highway intersections, the rate for dead load (bridge weight) is even smaller than 10^{-8} s^{-1} while the rate for live load (truck weight) is about 10^{-2} s^{-1} .

Noting the general lack of stress-strain curves in the product literature as well as the large effects of environment and strain rate, the authors wonder what tensile properties engineers use to design bonded components and structures.

Acknowledgments

The authors gratefully acknowledge the generous advice they received from Dr. Marion F. Mecklenburg during the course of this project. Dr. Mecklenburg is Senior Research Scientist at the Smithsonian Center for Materials Research and Education, 4210 Silver Hill Road, Suitland, MD 20746-2863.

References

- [1] Mecklenburg, M. F., Albrecht, P., and Evans, B., "Screening of Structural Adhesives for Application to Steel Bridges," Interim report, NTIS No. PB 86 142 601, available from National Technical Information Service, Department of Civil Engineering, University of Maryland, College Park, MD, 1985.
- [2] Albrecht, P., Mecklenburg, M. F., Wang, J., and Hong, W., "Effect of Environment on Mechanical Properties of Adhesives," Report FHWA/RD-87/029, Department of Civil Engineering, University of Maryland, College Park, MD, 1987.

- [3] Albrecht, P., You, J. M., Albrecht, M., and Eley, K., "Tensile Properties of FM 300K Adhesive," Final Report, Department of Civil Engineering, University of Maryland, College Park, MD, 1998.
- [4] Ishida, H., and Allen, D.J., "Physical and Mechanical Characterization of Near-Zero Shrinkage Polybenzoxazines," *Journal of Polymer Science: Part B: Polymer Physics*, Vol. 34, 1996, pp.1019-1030.
- [5] Ishida, H., "Development of Polybenzoxazines: a New Class of High Performance, Ring-opening Phenolic Resins with Superb Balance of Physical and Mechanical Properties," *Proceedings, International Composites Expo '98*, Nashville, TN, January, 1998, pp.1/14-B-8/14-B.
- [6] Shirrell, C. D., "Diffusion of Water Vapor in Graphite/epoxy Composites," *Advanced Composite Materials — Environmental Effects, ASTM STP 658*, J. R. Vinson, Ed., American Society for Testing and Materials, West Conshohocken, PA, 1978, pp. 21-42.

James R. Paschal¹

A Study of Bond Strength Testing for Solvent Cement Joints in PVC Piping Systems

Reference: Paschal, J.R., "A Study of Bond Strength Testing for Solvent Cement Joints in PVC Piping Systems," *Limitations of Test Methods for Plastics, ASTM STP 1369*, J.S. Peraro, Ed., American Society for Testing and Materials, West Conshohocken, PA, 2000.

Abstract: To evaluate the strength of the bond area formed by solvent-cementing of thermoplastic pipe and fittings, tests are conducted at 2 hours, 16 hours and 72 hours. Because the data is statistical in nature, more than a single specimen must be tested to provide a representative strength at each cure time. Considering that 3 tests are run, each consisting of multiple specimens, a method was developed for testing joined plaques rather than pipe and fittings. This method, known in the industry as "lap-shear" is much less time intensive than actual pipe joint preparation, and in theory, provides a good approximation of the anticipated strength of a pipe/fitting joint. A study of this test method was conducted to investigate variables in preparation technique and their effect on strength. The results indicate an extreme sensitivity to minor variations in preparation. The interpretation of this data with respect to joint strength is also discussed. An explanation of these significant deviations encountered due to the changes in preparation is provided, based on thermodynamic considerations of the mixing/dissolution process and work input to sample/solvent system. This paper presents an analysis of the sample preparation technique, in both a theoretical and qualitative context of solution thermodynamics and an evaluation of the minor changes in methodology that can cause major differences in test results. Notable results of the study include changes in shear strength on the order of 12-100% based solely on sample handling within the first 30 seconds, and a lack of sensitivity to the composition of the cement within normal ranges. The solution thermodynamics analysis provides some insight as to the relative significance of the variables in the preparation method.

Keywords: solvent-cement, PVC, poly(vinyl chloride), shear, bond, diffusion

Introduction

Poly(vinyl chloride) (PVC) pipe and fittings are often joined using what is termed a solvent-cement. This solvent-cement is a mixture of solvents, PVC resin, and possibly an inert filler material. The cement is applied to the surface of both the pipe and fitting socket, dissolving a thin layer of the PVC at each surface. The resulting surface consists of a solvent-rich region containing some PVC, a swollen rubbery PVC region with high

¹ Director, Physical & Mechanical Testing, NSF International, Ann Arbor, MI 48105.

solvent concentration, supported by the glassy PVC region with negligible solvent content. While in this dissolved state, the surfaces are brought into contact mechanically, typically using a combination of bi-directional motion and pressure. This mechanical mixing of the two surfaces, evaporation of the solvents, and diffusion of the PVC provides the bonding mechanism for the pipe/fitting joint.

When implemented as an actual installation process, the effectiveness of a solvent-cement relies on its ability to provide a sufficiently strong bond at varying ambient temperatures and within acceptable time limits. The time for curing of the joint must be long enough to allow completion of the assembly, while providing some strength in relatively short times for handling and testing purposes. These factors led to the development of a test method known in the industry as "lap-shear". The lap shear method is used to determine the resulting bond strength and efficiency of the solvent system. This test has been utilized in the PVC piping industry for over 15 years, with a generally good history until relatively recent changes in the solvent cement systems magnified differences between labs and worsened repeatability even within a single lab. The solvent systems were changing due to legislation governing volatile content of products and air quality standards. Cements, which historically may have contained up to 97% solvents, were now being forced to meet the same performance standards with much lower solvent content. The solvent content was reduced in many cases by adding inert fillers. This, in turn, led to labs reporting data with significant variations on the same cement. However, because the cement could be tested at one lab and meet the requirements, while results from another lab were much lower, it was considered to be a testing method issue rather than an indication of a poor cement.

Many of the testing details have been investigated, and are discussed in the Experimental Method section. An analysis was also done to compare the lap-shear requirements with actual pipe joint dimensions and loading. This work is shown in the Pipe Joint Evaluation section. The Thermodynamic Considerations section considers the mixing/dissolution process and provides a qualitative explanation for some of the significant deviations experienced.

Experimental Method

Lap-shear Test Method

ASTM Reference – Standard Specification for Solvent Cements for Poly(Vinyl Chloride) (PVC) Plastic Piping Systems (D2564)

Specimens – The test specimen consists of two plaques of PVC joined using the solvent cement to be tested, as shown in Figure 1. The PVC used to fabricate the plaques is specified as a Type 12454, as per ASTM Specification for Rigid Poly(Vinyl Chloride) (PVC) Compounds and Chlorinated Poly(Vinyl Chloride) (CPVC) Compounds (D1784). The PVC compound is two-roll milled into a sheet form, and then compression molded into the basic plaque used to fabricate the specimen plaques. Originally, the plaque as-molded would be cut to the dimensions shown in Figure 1. However, this was identified as a potential source of inconsistency due to irregularities in the plaque surface after molding. To eliminate

this, the plaques were machined to be flat and parallel within 0.01 mm across the surfaces. This modification to the method did not, in and of itself, provide any statistically significant improvement in the test repeatability (see Table 1).

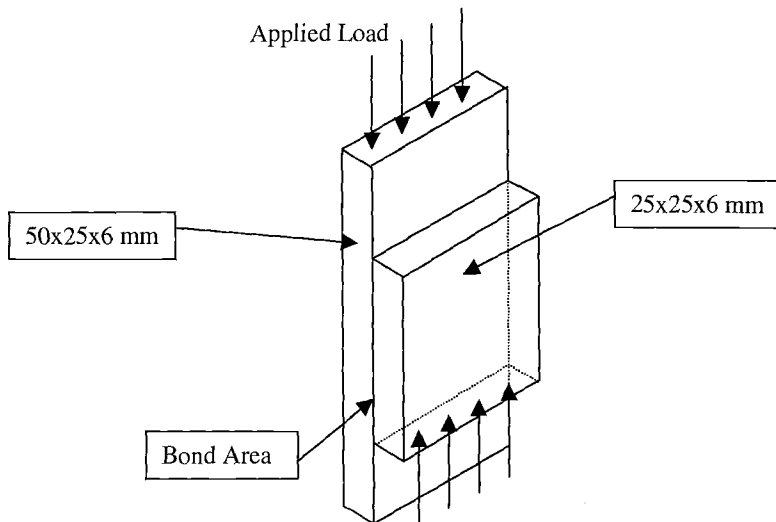


Figure 1 – *Lap Shear Test Assembly*

Cleaning – After preparing the PVC plaques, the surfaces to be joined are then cleaned with methyl-ethyl-ketone (MEK). While not especially aggressive, MEK is a solvent for PVC, and the amount used for cleaning could affect the surface characteristics. This was considered for the shorter cure times, with excessive amounts of MEK applied immediately prior to the solvent cement. In this scenario, it was hypothesized that the MEK would interfere with the evaporation of the more aggressive solvents, thereby lowering the short-term shear strength. Testing was conducted with both excessive MEK applied with heavy brush strokes immediately prior to testing, and specimens cleaned with MEK on a damp cloth which were dried for 24 hours before testing. Additionally, surface abrasion in conjunction with the MEK cleaning was evaluated. The abrasion was achieved by manually wiping 80-grit sandpaper across the surfaces. As shown in Table 1, the MEK application method did not significantly affect the test data. However, the abraded surfaces did exhibit a slightly depressed shear strength.

Specimen Assembly – The assembly process for the two plaques involves application of the solvent cement to each plaque using a soft-bristle brush, bringing the two surfaces into contact, rotating the 25x25 mm plaque 180°, and subsequently applying a 2 kg mass. The device used for uniform application of the 2-kg mass is shown in

Figure 2. The existing test method specifies the use of approximately 2 N force when rotating the 25x25 mm plaque, followed by a 30 s period before application of the 2 kg mass.

Table 1 – *Shear Strength versus Specimen Preparation Parameters*

Description		Average ^a Shear, N/mm ²	Std. Dev ^a , N/mm ²
Specimen Surface	Machined	2-hr	2.00
	As-molded	2-hr	1.94
	Machined	16-hr	3.90
	As-molded	16-hr	4.23
Cleaning/Abrasion			
	Brush MEK #1	2-hr	1.07
	Cloth MEK #1	2-hr	1.08
	Abraded, cloth #1	2-hr	1.00
	Brush MEK #2	2-hr	1.36
	Cloth MEK #2	2-hr	1.45
	Abraded, cloth #2	2-hr	1.30

^a5 specimens used for each test

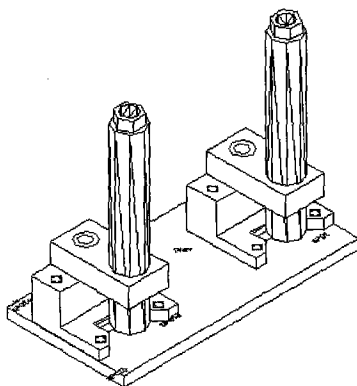


Figure 2 – *Loading Device*

The potentially critical parameters identified in this process are the amount of solvent cement used in the bond area, and the elapsed time before application of a compressive load on the joint. To evaluate these differences, the method was modified to include measuring the mass of solvent cement 3 minutes after

application, and further modified to include the application of a compressive load during the 30 s waiting period. Testing indicated the time delay from application of the cement to loading was critical, rather than the actual value of the applied load. As such, the most efficient and cost-effective means to achieve this is the hands of the analyst. That is, immediately after rotating the plaque, the analyst would use both thumbs to apply a relatively even pressure across the surface, while using the index fingers to hold the plaque in place. The results of this testing are given in Tables 2a and 2b. It should be noted that the amount of solvent cement applied is difficult to predetermine. The surface must be covered, which indirectly provides a lower limit, while the compressive load forces any excess cement out of the bond area, thereby establishing an upper limit. For purposes of this study, the effective range was 60-170 mg.

Table 2a – Shear Strength versus Mass of Solvent Cement

Cure Time, hr	Cement, mg	Average ^a Shear, N/mm ²	Std. Dev ^a , N/mm ²
2	66	1.97	0.44
2	71	2.05	0.42
2	118	2.08	0.48
2	123	1.87	0.46
16	97	3.74	0.79
16	117	3.78	0.57
16	119	3.54	0.55
16	172	3.58	0.63
72	70	7.24	1.32
72	97	5.28	0.30
72	118	4.97	0.82
72	134	5.58	0.59

^a5 specimens used for each test

The data in Table 2b represents the differences between shear strengths as a result of applying a compressive load during the 30 s interval. This interval occurs directly after the cement is applied to the plaques, but prior to the 2 kg load being placed on the joint. Figure 3 provides a graphic representation of the change in the test method. The “loading” is provided by the analyst immediately after brushing the cement onto the plaques, and held for 30 seconds. For the data given in Table 2b each row represents testing of 10 specimens, 5 with immediate compression loading held for 30 s, and 5 held for 30 s without the load. For each set of 10 specimens, the solvent cement was identical, taken from a single thoroughly mixed container. However, the separate samples for each cure time (e.g. 2-hr #1 versus 2-hr #2) were each a different cement formulation. The solvents and resin are generally the same, but in varying proportions and each cement is sufficiently unique to be sold under its own

trade designation. Furthermore, the cements not only differed in formulation but also manufacturer. This testing represents cements from four different producers.

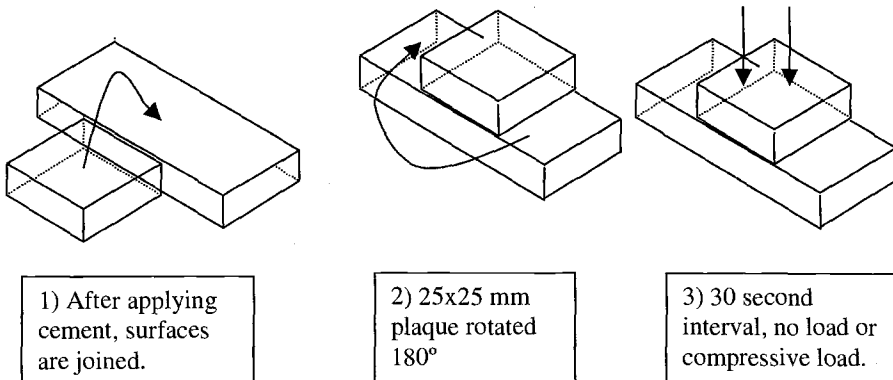


Figure 3 – Assembly Method and Modification

Table 2b – Shear Strength versus Immediate Loading

Cure Time, hr	Shear w/o load, N/mm ²	Cement, mg	Shear w/ load, N/mm ²	Cement, mg	Increase
2, #1	1.52	73	1.74	102	14%
2, #2	1.69	98	1.89	94	12%
16, #1	2.83	77	3.78	117	34%
16, #2	3.39	80	4.61	89	36%
16, #3	3.14	75	4.45	85	42%
72, #1	4.21	92	8.60	118	104%
72, #2	4.42	84	8.14	94	84%
72, #3	4.62	82	7.90	93	71%
72, #4	3.85	121	9.91	133	157%

Pipe Joint Evaluation

Shear Stress in Pipe Joint

Most solvent-weld joints of PVC pipe in the United States are formed using conical or “taper” sockets. That is, the socket area of the fitting, to which the pipe is joined, is tapered with a larger diameter at the entrance than the diameter at the bottom of the

socket. A schematic of this is shown in Figure 4. The taper is exaggerated for purposes of demonstrating the "interference fit". It is this interference fit that provides the compressive loading during assembly. As the data in Table 2b indicate, this initial compression of the bonding surfaces can significantly improve the strength of the joint. The taper of the socket increases the complexity of modeling the joint, and using data from a planar plaque joint is much more susceptible to misinterpretation. This is demonstrated in the modeling detailed in the following sections.

Case 1, Cylindrical Socket Model – In the most simplistic case, the fitting socket could be modeled as a cylinder, with entrance diameter A equal to bottom diameter B. Further, it is assumed the bonding of the pipe surface to the fitting socket is uniform throughout, and encompasses the entire length of the fitting socket. For purposes of analysis, the fitting is assumed to be an end-cap, such that the loading of the joint is induced by internal pressurization of the pipe/end-cap assembly. This idealistic case also assumes the cut end of the pipe is in contact with the pipe stop of the cap, such that the cap area, which is pressurized, has the same diameter as the inside diameter of the pipe. The total load carried by the solvent-weld joint is then given by (1).

$$F = (P)[\pi d^2/4] \quad (1)$$

where:

F = total load exerted on pipe joint, N

P = internal pressure of the pipe/end-cap assembly, N/mm²

d = internal diameter of the pipe, mm

The shear stress on the joint is given by (2).

$$\sigma_s = F / (\pi D L) \quad (2)$$

where:

σ_s = engineering shear stress, N/mm²

D = external diameter of the pipe, mm

L = length of the fitting socket, mm

Testing was conducted using both lap shear samples and pipe/fitting joints. The 72-hr cure lap shear samples had an average shear strength of 6.95 N/mm². Using this value for σ_s , and dimensions from 3/4 Schedule 40 pipe and fittings (D = 26.7, d = 20.9, L = 18.3), results in a pressure of 31.1 MPa at failure. When pipe/fitting samples were tested with this solvent cement the joint failed at pressures of 12.9, 12.4 and 12.6 MPa. Obviously this simple model is far from accurate in predicting the joint strength at longer cure times, based on lap shear test data. The model did, however, predict the short cure time (2-hr) pressure quite well (10.7 versus 10.8, Table 3).

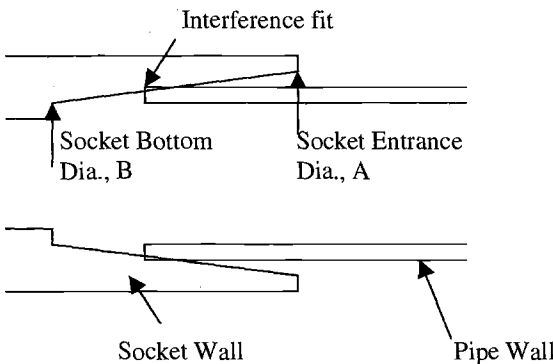


Figure 4 – Taper Socket/Pipe Geometry

Case 2, Conical Socket Model, 1st Approximation – For the conical socket, a simple approximation would be to assume the load carrying capability of the joint is entirely within the interference fit area. Because the socket is tapered, some deformation of the pipe or socket must occur to fully insert the pipe. The materials in general use for pipe normally have a higher molecular weight than the fitting materials. This will directly affect the relative diffusion rates at each surface, as well as the lowering of the glass transition temperature (T_g) due to the plasticizing effect of the solvents. In this approximation it is assumed that in the short time during joint assembly, the fitting material is much more aggressively modified by the solvent and fully accounts for all material deformation. This assumption then reduces the model to that of Case 1, with socket length becoming the length of interference fit rather than the full socket. For outside-diameter controlled PVC pressure pipe and fittings, the interference fit is specified as being 1/3 of the total socket length. This reduces the expected failure pressure of a joint to 1/3 that given in Case 1. Again using the data for the 72-hr cure, ¾ Schedule 40 assembly, the predicted failure pressure would be 31.1/3 or 10.4 MPa. The model is now much closer to the actual pressures, but underestimates what would be expected performance for typical cement, at all three cure times.

Case 3, Conical Socket Model, 2nd Approximation – In this model, it is assumed that the interference portion of the socket has the same load-carrying capability as the lap shear conducted with compressive loading. Furthermore, the remaining 2/3 of the socket length has some measure of shear resistance. At the point just beyond the interference fit, the shear strength is the “no-compression” strength from Table 2b, then dropping linearly with distance along the socket length. The magnitude of the drop in shear for this region varies with cure time, and is based on the data from Table 2b. The assumed decrease is the average of the decrease in values for each cure time. That is, -12% at 2-hr, -27% at 16-hr, and -54% at 72-hr. Figure 5 provides a schematic of the shear strength as a function of location along the socket length. The starting values for each cure time are typical, but not representative of any single solvent cement.

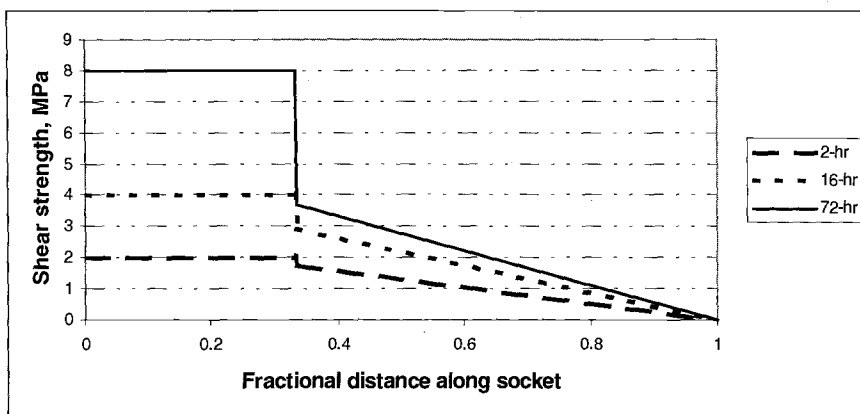


Figure 5 – Shear versus Socket Length Distance for Case 3

This model also uses the conical area of the bond for the 2/3 of the socket extending beyond the interference fit. The interference fit area is assumed cylindrical. To determine the total load that can be carried by this linearly decreasing shear strength, along the conical area, (3) must be integrated.

$$F_x = \int \sigma_{sx} dA \quad (3)$$

where:

F_x = force carried by conical section away from interference fit

σ_{sx} = $\sigma_0 - Sx$ = linearly decreasing shear strength

σ_0 = step-reduced shear strength (e.g. $0.88\sigma_s$ for 2-hr cure)

x = distance along socket length

S = rate of change of shear strength with distance = $\sigma_0/(x_2 - x_1)$

dA = differential area

The lateral area of a frustum of a right circular cone of length dx is given by (4).

$$dA = \pi/2 [Z + Yx] dx \quad (4)$$

where:

$Z = D + B$

$Y = (A-B)/L$

Substitution of (4) into (3) and integrating yields:

$$F_x = \pi/2 [(\sigma_0 Z)x + (\sigma_0 Y - SZ)x^2/2 - (SY)x^3/3] \quad (5)$$

evaluated from x_1 to x_2 . In this case, x_1 is 1/3 the distance from socket bottom to entrance, and x_2 is the socket length. The load carried by the interference fit portion is determined by (6).

$$F_I = \sigma_s (\pi D L/3) \quad (6)$$

The total load, F_T is then given by:

$$F_T = F_I + F_x \quad (7)$$

From which a failure pressure can be calculated as:

$$P = (F_T) / [\pi d^2/4] \quad (8)$$

Calculated results for this case, as well as 1 and 2 are given in Table 3.

Table 3 – *Comparison of Models*

Cure Time, hr	Lap Shear, N/mm ²	Case 1 Pressure, Mpa	Case 2 Pressure, Mpa	Case 3 Pressure, Mpa	Fail Pressure, Mpa
2	2.39	10.7	3.57	5.25	10.8
16	5.19	23.2	7.73	11.3	13.1
72	6.95	31.1	10.4	14.8	12.6

Thermodynamic Considerations

The work presented thus far has shown the critical parameter in this test to be the elapsed time prior to compression. To further understand this, a review of the competing mechanisms at work is necessary. Upon application of the solvent cement system to the PVC surface, the solvent will immediately begin to penetrate the PVC, while at the same time excess solvent is evaporating. Dissolution of the PVC must occur prior to significant evaporation of the solvent, and yet final evaporation of the solvent must also occur relatively rapidly to provide a strong bond.

Diffusion in the PVC Plaque

Diffusion in polymers is generally divided into at least two categories, Fickian and non-Fickian or anomalous. Some authors further divide the non-Fickian regime based on the type of transport [1]. For glassy polymers below their T_g , the departure from Fickian diffusion is generally considered the result of the diffusion rate being much higher than the relaxation process in the polymer. PVC at 23°C is well below its T_g , but the solvent cements used are specifically formulated with less aggressive solvents and a

small percentage of dissolved PVC resin for purposes of hindering the dissolution process. This, coupled with the obvious rubbery region formed during the assembly procedure would indicate the diffusion is Fickian. In this case, the diffusivity is a function of pressure as well as concentration and temperature. This pressure dependence could then be the governing factor contributing to the significant deviations in test data. Microscopic examination of the test specimens shows a very distinct advancing solvent boundary, which can be analyzed by the method given in [2]. A complete analysis is beyond the scope of the current work and is planned as future work. However, some general statements can be readily made based on a review of this work. The coordinate system used in [2] is shown in Figure 6.

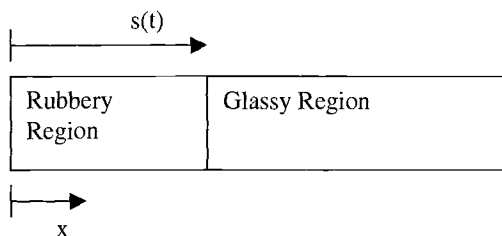


Figure 6 – *Coordinate System for One-dimensional Diffusion*

The governing differential equation is

$$\frac{\partial C}{\partial t} = \frac{\partial}{\partial x} \left(D \frac{\partial C}{\partial x} \right) \quad 0 \leq x \leq s(t) \quad (9)$$

where:

C = concentration

D = diffusivity

t = time

x, s(t) as shown in (Figure 6)

Initial Conditions: $C = 0$ at $t = 0$, for all x

Boundary Conditions: $C = C_o$ at $x = 0$, for $t > 0$

For the case of constant diffusivity, which is assumed over the first 30 seconds of sample preparation, the solvent penetration into the PVC can be expressed as

$$s(t) = k \sqrt{Dt} \quad (10)$$

where k is a constant. This provides some insight as to the expected change in bond strength as a function of time. The underlying rationale being that increased solvent penetration will result in a more uniform and stronger bond. However, the plasticizing effect of the solvent will weaken the bond if the solvent is not then allowed to diffuse out of the polymer within the timeframe for testing. For the 2-hr cure time, t and $t^{1/2}$ are of the same order of magnitude, whereas the difference at longer cure times is more pronounced. This then, contributes to the rationale for the 2-hr cure being more closely modeled by Case 1.

Solvent Vaporization

During assembly the solvents will be diffusing into the surrounding air much more quickly than into the PVC surface. This is considered to be critical to understanding the results presented earlier. To form a sufficiently strong bond, a highly concentrated solution of PVC in solvent must exist prior to the solvent dissipating into the atmosphere. For this to occur, the separation distance between PVC layers must be kept small to minimize transport of solvent to air and maximize chain diffusion and entanglement between surfaces. The use of compressive loading during specimen assembly reduces the bond thickness by an average of 0.10 mm from its non-compressed average thickness of 0.22 mm. The solvent diffusion into the air is directly proportional to the area of the solvent surface exposed to the air, which is reduced by 45% due to this compression.

When considering diffusion of polymers and organic compounds, the diffusion coefficient is often assumed to take the form

$$D = k M^a \quad (11)$$

where k and a are constants [3]. Without citing data for the specific PVC and solvents used in this study, but based on the typical ranges of data for these materials, the diffusivity for the solvent to air will be on the order of 10^5 higher than that of the polymer to solvent.

Summary

A review of the test method for lap shear strength of PVC solvent cements was conducted to evaluate the relative importance of various parameters in the assembly process. The parameters included surface roughness and cleaning, pressure application to the bond area immediately after joining, and pressure loading after a 30-s waiting period. The most significant factor was determined to be the immediate loading, which resulted in shear strength increases from 12% at a 2-hr cure, to 100% at a 72-hr cure. It was also found that the continued application of the load beyond the first 30 s had very little effect on the lap shear results.

Several models were presented to approximate the expected strength of a pipe/fitting joint based on lap shear test data. The Case 1 model, which assumed the entire socket length contributed fully to the strength, most accurately predicted the pipe/fitting failure

pressure for the short-term cure (2 hr). This is consistent with the penetration dependence on the $t^{1/2}$ term, at cure times having t on the same order of magnitude as $t^{1/2}$. The amount of solvent present at these early times is also sufficiently high that mass transport to air has not yet lowered the solvent concentration at the polymer surface. The Case 3 model, which assumed the interference fit portion contributed fully, with a step decrease at 1/3 the socket length and linear decrease across the remaining socket length most closely predicted the failure pressure for longer cure times (16 hr and 72 hr).

A review of diffusion thermodynamics for this type of system was presented to provide at least a general indication of the mechanisms involved, and provide a basis for future work.

Acknowledgments

The author gratefully acknowledges the assistance of Willie Bush, NSF International, in the sample preparation and testing; George Blanco, IPS Corp., for his diligent review of the work while in progress; and Paul Naton, Oatey Co. (retired), for his work both in design of the device shown in Figure 2 and providing collaborative test data.

References

- [1] Frisch, H.L., "Sorption and Transport in Glassy Polymers - A Review," *Polymer Engineering and Science*, Mid-January, 1980.
- [2] Tosun, I. and Yilmaz, L., "On the Fickian Diffusion of Organic Penetrants in Glassy Polymers," *Polymer Engineering and Science*, November, 1982, Vol. 22, No. 16.
- [3] Brandrup, J. and Immergut, E.H., Ed., *Polymer Handbook*, 2nd Ed., John Wiley and Sons, New York

DISCUSSION

Nanying Jia¹ (written discussion)—Have you tried to test the bond strength directly on the joints?

James R. Paschal (author's closure)—For the purposes of this paper, the only testing done directly on piping joints was the hydrostatic burst testing, shown as the “Fail Pressure” in Table 3. Conducting a controlled shear test on a joint is being considered as an alternative method within a separate project at ASTM.

Nanying Jia¹ (written discussion)—Have you had a chance to examine the bonding under (optical, SEM) microscope? If so, how do you think the characteristics of the bond (or any defects) would affect the results of the standard shear test on the actual piping systems?

James R. Paschal (author's closure)—The bonding surfaces have been examined under an optical microscope only. When examined, it is apparent that any flaws in the surface which provide a gap between plaques will decrease the shear strength. This was confirmed by subtracting this area from the strength calculations and the resulting value being very consistent with data from plaques without flaws. This could become quite critical in piping applications, which is the reason the pipe and fittings standards have tolerances on both diameter and out-of-roundness, as well as the installation standard requiring a dry check of the interference fit before joining the pipe and fittings.

¹AlliedSignal, Inc., 101 Columbia Road, Morristown, NJ 07962-1021.

Impact/Fracture

Patrick S. Leevers and Mark Douglas¹

Notched Impact Testing of Thermoplastics: A New Perspective

Reference: Leevers, P. S. and Douglas, M., "Notched Impact Testing of Thermoplastics: A New Perspective," *Limitations of Test Methods for Plastics, ASTM STP 1369*, J. S. Peraro, Ed., American Society for Testing and Materials, West Conshohocken, PA, 2000.

Abstract: The toughness of unreinforced thermoplastics is often high, but limited by a transition to brittle behaviour with increasing impact speed and decreasing temperature. Izod or Charpy impact strength data are widely regarded as a primary performance index for these materials, but cannot be used for quantitative design. Although fracture mechanics analysis offers a substantial advance, the impact fracture resistance for some polymers varies substantially with configuration (the shape and size of the body and the impact speed) rather than being a material constant as expected. A model of brittle impact fracture as a process of local fusion within a rapidly-loaded crack-tip craze explains this variation quantitatively. The model leads to a method of correlating impact fracture in different configurations, which is demonstrated here using a case study.

Keywords: fracture mechanics, thermoplastics, impact fracture, dynamic fracture, rate, geometry, correlation

Introduction

The widespread use of Izod and Charpy impact tests to evaluate plastics is, to an unprejudiced eye, rather difficult to justify. Many structural polymers used in load-bearing applications do show a range of fracture behaviour from 'ductile' to 'brittle'. Most thermoplastics can show either kind of behaviour, and may suffer an abrupt tough-to-brittle transition with any of a number of parameters — one of which is the rate of loading at a notch. In order to select a polymer for a specific application it may be important to know its sensitivity to this kind of impact embrittlement. However, it is difficult to see how one might learn this from conventional impact strength data.

Impact failures of engineering components are not uncommon, but they are probably outnumbered by those from other brittle modes: fatigue and slow crack growth. The fracture surfaces which witness all three modes are superficially similar, but profoundly different rate and temperature dependencies emphasise that different mechanisms are at work. Slow crack growth failures are favoured by long periods under static load at higher temperatures, whilst impact failures are favoured by rapid loading at lower temperatures.

Impact tests may well be as popular as they are simply because they offer the quickest and easiest method of inducing brittle fracture. For tough thermoplastics (e.g. polyolefins) impact at a notch may be the *only* practical way to generate a brittle surface in the laboratory which resembles those seen (or feared) in product failures. It may be very misleading, however, to regard impact strength as a general measure of resistance to brittle fracture.

¹ Reader in Polymer Engineering and Research Student respectively, Mechanical Engineering Department, Imperial College, London SW7 2BX, UK.

Even in their own sphere, impact tests convolute at least two distinct properties. For historical reasons, the result of a test is expressed as a 'strength' on dividing the absorbed energy by the fracture surface area. Thus discrimination is lost between the resistance of the material to crack growth initiation during rapid loading, and its resistance to crack propagation rapid enough to outrun the subsequent driving force. To isolate geometry-independent material data from either is very difficult and indeed, as we shall argue, their geometry dependencies may differ.

Thus the widespread currency of impact data can be questioned on a more direct basis: lack of portability to other geometries. Charpy or Izod impact strength cannot be used for design. As a result many species of *ad hoc* test methods have flourished without competition. Such methods range from impact tests on specimens having other elementary shapes (e.g. discs) to product tests (Drop Tests for containers, Falling Weight Impact Tests for appropriately vulnerable products such as pipe).

Fracture Mechanics Treatment of Impact Data

Fracture mechanics offers the most generally satisfactory of alternative currencies for impact strength assessment. The fracture mechanics approach begins conservatively by insisting that the material be tested in the presence of the sharpest possible notch: a crack. It was recognised by earlier authors that an impact bend test on a sharply notched specimen was merely a notched bend test done quickly; the absorbed energy was measured, rather than the failure load, because — until instrumented high-rate test machines became available — there was no alternative. Instrumented tests could therefore yield a fracture toughness result, as first shown for plastics by Williams [1].

The method developed to its highest state in the ESIS test protocol [2] can be seen as a rigorous geometric correction which can give a test result (G_c) portability to other geometries. The load/displacement trace up to the peak load point is characterised by an area U_p . The impact fracture resistance G_c is given as:

$$G_c = \frac{U_p}{BW\Phi(\alpha)}, \quad (1)$$

where B is the width of the crack front; W is the length of its path from one free surface to the other (and a useful parameter for the *size* of the body); and Φ is a dimensionless function of the *shape* of the body — including α , the ratio of crack length to W . It is useful to remember that for a given shape of two-dimensional body (e.g. a three-point bend geometry of fixed span/depth ratio), the normalised load point compliance C^* is given as a function of α by:

$$C^*(\alpha) \equiv E'WC(\alpha), \quad (2)$$

is invariant with size W , C being the load point compliance and E' the 'reduced' (constraint dependent) tensile modulus.

The present paper, whilst leaning heavily on data gathered using ESIS-type methods, concentrates on the unwelcome fact that for many polymers of technological importance, G_c varies strongly with impact speed. Of course, this was already known: if it were not so, impact tests would be unnecessary. Unfortunately, however, speed-dependence re-introduces geometry-dependence through the back door [3], since the same impact speed can translate into different 'effective' crack loading rates in different geometries.

The most credible explanation for rate-dependence of G_c lies in a model which attributes impact fracture initiation to local adiabatic melting. Reviewing current and newly acquired data we suggest, on the basis of this model, a way of presenting impact fracture data which

may improve its 'portability' from specimen to engineering component. The method is illustrated briefly on the basis of a service failure problem.

Adiabatic Failure of a Cohesive Zone

Contemporary Fracture Mechanics recognises the crack-tip stress singularity represented by the stress intensity factor as a fiction — emphasising, in its place, the role of the crack-tip cohesive zone which annuls it. This movement in Fracture Mechanics conveniently reconciles physically-based models of damage and cohesion with computational models which represent cohesion as a 'holding-back force' in order to calculate the energy release rate.

In both glassy and semi-crystalline polymers the cohesive zone often takes the physical form of a craze: a colinear 'crack extension' whose surfaces are bonded by micro-fibrillar or film material. Following the work of Williams [1] we represent such a zone most simply as a Dugdale-Barenblatt zone bearing a uniform stress.

If the crack with such a craze at its tip suffers an increasing load without extending, or if it propagates carrying the craze before it, every craze fibril is extended. Almost always, the fibril at the craze mouth (i.e. the crack 'tip') extends most rapidly. It is generally accepted that fibrils extend by a process whereby material is 'cold-drawn' from the bulk, so that the cohesive surface corresponds to the shoulders of a classic propagating tensile neck. If it takes place quickly, such a process will concentrate adiabatic heating at the cohesive surface.

Fracture Initiation and Propagation by Thermal Decohesion

Using the Dugdale model, Leevers [4] calculated the conditions under which the cohesive surface in a thermoplastic could melt, to a depth sufficient to liberate every chain (within a statistically averaged sample) crossing it. The results were expressed as fracture criteria for both rapid crack propagation and impact crack initiation.

The results can be summarised in equations for the minimum value of dynamic fracture resistance G_D (with respect to crack speed):

$$G_{D,\min} = \rho \bar{s}_w [5C_p(T_m - T) + 2\Delta H_f], \quad (3)$$

and for the impact fracture initiation resistance as a function of impact speed (i.e. displacement rate) \dot{v} :

$$G_{ca} = E^{-1/3} \left[\frac{3}{2} \rho C_p (T_m - T) \right]^{4/3} (\pi \kappa)^{2/3} \Psi(\alpha) W^{1/3} \dot{v}^{-2/3}, \quad (4)$$

G_{ca} gains a subscript denoting 'apparent', having lost its claim to be a material property. In these equations ρ is the mass density, E the elastic modulus, \bar{s}_w the weight-average chain contour length, C_p the specific heat, ΔH_f the latent heat of fusion, T_m the melting temperature and κ the thermal diffusivity of the material; T is the test temperature. Another geometry factor Ψ represents the shape of the body; its determination has been outlined elsewhere [3] and its use will be illustrated using an example below.

For crystalline polymers, materials for which both \bar{s}_w and the melting point T_m are clearly definable, some of the other parameters are not. E must represent both the bulk material and the crack tip zone — at which strain rates are much higher — whilst both C_p and κ vary strongly between a typical T and T_m . In this context the $\frac{3}{2}$ factor in Eqn. (4), which was omitted in error from earlier expositions [3-5], has not been greatly missed.

Nevertheless, Eqn. (3) has proved to be remarkably successful in determining the minimum resistance G_D of a number of polymers. The simplest measurement method for G_D uses a tube or pipe specimen internally pressurised by an annular layer of liquid surrounding a solid mandrel [6]. Using this method, the crack chooses its own speed and can be assumed to run at $G_{D,\min}$ when driven by the minimum pressure at which it will run at all.

Equation (4), in contrast, rests on altogether less secure foundations. The doubts will be discussed below, but they can be sidestepped by regarding the test temperature as a parameter and combining the bulk properties in Eqn. (4) into a single material parameter Γ :

$$G_{ca} = \Gamma \Psi(\alpha) W^{1/3} v^{-2/3}. \quad (5)$$

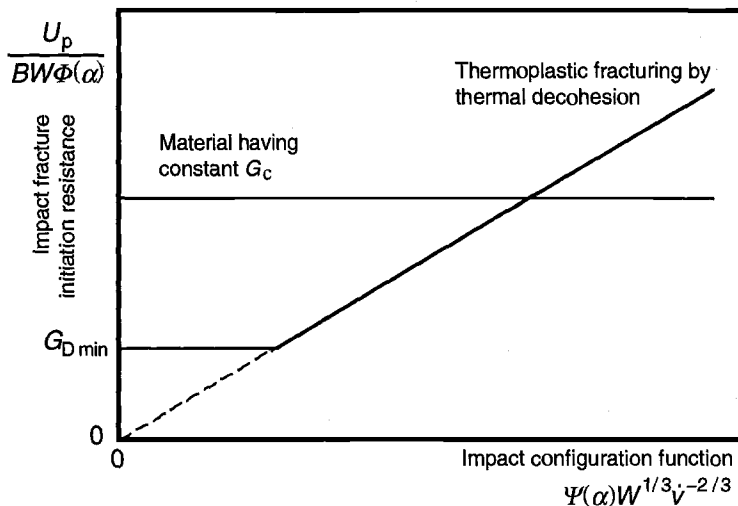


Figure 1 — *Schematic of impact data for LEFM and thermal-decohesion materials.*

Thus, invoking Eqn. (1) shows that the application of the thermal decohesion model to impact of a thermoplastic can be summarised as a plot of $\frac{U_p}{BW\Phi(\alpha)}$ against an 'impact configuration function' $\Psi(\alpha)W^{1/3}v^{-2/3}$ (Fig. 1). Linear elastic fracture mechanics asserts that failure data from sharply notched bodies of any shape (expressed by the dimensionless functions $\Phi(\alpha)$ and $\Psi(\alpha)$), of any size W and impacted at any speed v will lie on a horizontal line: constant G_c . The thermal decohesion model predicts that they will lie on a straight line through the origin. However, as Fig. 1 illustrates, this line should be limited by a lower plateau at constant $G_{D,\min}$ since this is the minimum driving force at which the 'initiated' crack can propagate sufficiently far, and sufficiently rapidly, to unload the driven specimen and define a 'peak load'.

The Effect of Impact Speed in a Specific Geometry

Using a method based on the ESIS impact fracture toughness test, the effect of impact speed on a thermoplastic can be isolated for a Charpy-like impact bend geometry.

In pressure-pipe grade medium density polyethylene (MDPE), for example, at low rates the initial notch blunts and the specimen yields or tears, absorbing considerable energy, by craze propagation and net-section yielding. G_c can still be calculated from the peak-load energy via Eqn. (1), but the result is not in any sense valid. At higher displacement rates, peak load corresponds to initiation of a *rapid crack propagation* event which leaves a glassy surface and almost instantaneously unloads, or partially unloads, the specimen. This absorbs so little energy that no further external work is needed to drive it. Stick-slip crack propagation — repeated cycles of arrest and re-initiation — may occur, but the intermediate crack arrests usually disappear as the rate increases further.

Above the low-speed ductile plateau, data for tough pipe-grade MDPEs show very clearly the predicted $-2/3$ power dependence on impact speed (Fig. 2). For this material $G_{D,\min}$ about 2.5 kJ m^{-2} . It is very difficult to achieve the speeds needed to observe such a low fracture resistance in this geometry, the results being widely scattered by dynamic effects. This topic will be discussed further below.

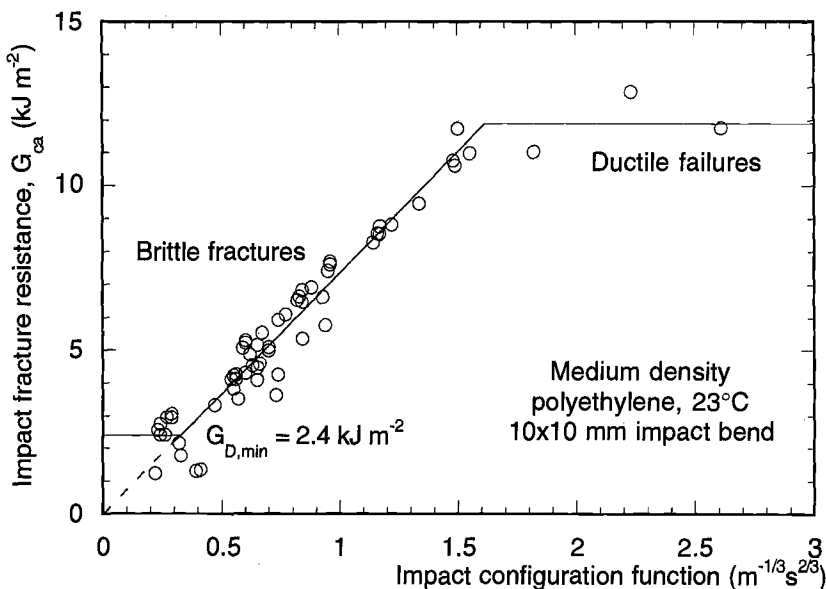


Figure 2 — Impact fracture resistance data from MDPE bend specimens as a function of the impact configuration function.

Other materials for which the thermal decohesion model appears to work well include polyamide 6 and unplasticised poly(vinyl chloride) — surprisingly, in the latter case, since this polymer does not have a very well-defined melting point.

For a polyoxymethylene (POM), on the other hand, impact data (Fig. 3) do not conform to the thermal decohesion model at all. The minimum predicted impact fracture resistance of this material is $G_{D,\min} = 2.21 \text{ kJ m}^{-2}$ at 23°C , but most impact fracture toughness results (Fig. 3) are at least 50% higher than this and there is no sign of a region of $-2/3$ power impact speed dependence. There is a further increase in G_c at displacement rates far too low to be considered as ‘impact’ or for the thermal decohesion mechanism to be viable. Viscoelastic crack blunting is a much more likely explanation. It seems most likely that the craze mechanics assumed by the thermal decohesion model simply do not apply to POM.

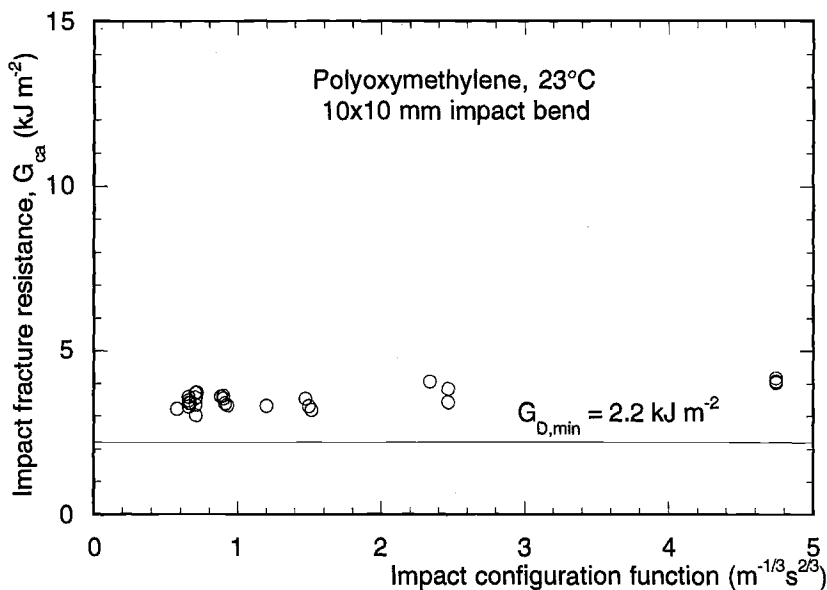


Figure 3 — Impact fracture resistance data for POM bend specimens as a function of the impact configuration function.

Translation of Impact Fracture Data Between Geometries

In general, the geometry functions $C^*(\alpha)$, $\Phi(\alpha)$ and $\Psi(\alpha)$ will also differ between the Izod or Charpy geometry tested in the laboratory at one impact speed, and the component struck in service at another. In this section we outline a practical example which illustrates the potential portability of impact strength data for plastics whose G_c is manifestly not constant. The practical problem from which this example arose about three years ago in Europe was, typically, distinguished by a lack of service failure details. Its principal features, however, were reproducible in the laboratory.

Most of the pipe used for water and fuel-gas distribution in Europe is extruded from medium-density polyethylenes (MDPE). These lightly branched ethylene-hexene or ethylene-butene copolymers are extremely tough materials and can withstand a great deal of abuse during installation. Loaded cracks readily form strong crazes which extend for millimetres. At the minimum service temperature of 0°C, these materials exhibit brittle failure in sharply-notched Charpy bend specimens impacted at speeds exceeding about 0.1 m s^{-1} , and they can sustain rapid crack propagation. As Fig. 2 confirms, they conform very well to the thermal decohesion model.

The problem considered here arose from the common practice of shipping extruded MDPE pipe as large as 125 mm in diameter on large-diameter coils. On site, the pipe is uncoiled, straightened in four-point bending, and rough-cut to length using an electric saw. Pipe extruded from one of two candidate MDPE grades was sometimes observed, when carrying out this procedure during cold weather, to suffer clean, brittle fractures which 'guillotined' the pipe in the circumferential plane. Since this event achieved precisely the result sought by the operator, it was hardly a problem in itself, but there was customer concern that it might symptomise other problems to come.

The investigation compared the susceptible material to a control grade. Both properties exposed by an impact test were separately at issue here:

- 1 Rapid crack propagation resistance, G_D . If the susceptible material had a significantly lower $G_{D,\min}$, a given static stress induced by straightening of the coil could sustain rapid crack propagation in one material but not in the other.
- 2 Impact fracture resistance, G_c . The most probable trigger for initiation was identified as high-frequency vibration induced by the power saw blade. Even if both materials had the same resistance to rapid crack propagation, the susceptible material might have failed due to its lower resistance to initiation.

The investigation concluded that it was the first rather than the second explanation which accounted for the fracture events. However, here we consider only the issue of geometry dependence in a single material. G_c is always to be calculated using Eqn. (1); the question is whether it is constant and, if not, whether its geometry dependence can be accounted for using the thermal decohesion model.

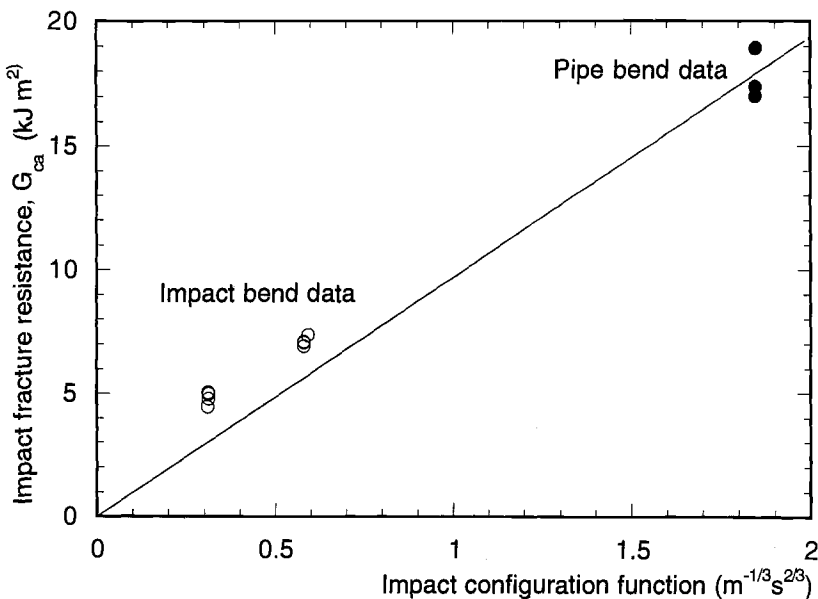


Figure 4 — Impact data for two geometries.

For each material, two specimen geometries were tested in the laboratory. The first was a small ($W = 10$ mm), 'sharply-notched Charpy' specimen, cut from the pipe wall and tested according to the ESIS standard [2], but at two speeds: 1.0 and 2.5 m s^{-1} . The second was a length of extruded pipe (diameter $D = W = 125$ mm), with a diameter/thickness ratio of 11, notched at mid-length with a razor-sharpened straight-fronted cut to a depth of 20% of the diameter. This was simply supported with a span of 0.5 m and struck opposite the notch (Charpy style) at 2.2 m s^{-1} , using a drop-weight machine.

The notched pipe bend configuration has not previously been studied and its geometry correction functions $C^*(\alpha)$, $\Phi(\alpha)$ and $\Psi(\alpha)$ had to be computed. The scheme for doing so has been outlined elsewhere [3] and will not be repeated here. The starting point, as for conventional linear-elastic fracture mechanics, was a compliance calibration

$$C^*(\alpha) = E'D \frac{v}{P}.$$

An arbitrarily-sized finite-element model of the pipe span, made from a linearly-elastic material of arbitrary modulus E' , was subjected to an arbitrary mid-span load P to determine the resulting load-point displacement v . This was repeated for a number of crack lengths α . An interesting feature of this geometry is that the crack front length B changes, sometimes discontinuously, with α .

The results are shown in Fig. 4. Clearly for MDPE they favour correlation on the basis of the thermal decohesion model rather than on the basis of a unique G_c value.

Impact Specimen Size Effects for Craze-Forming Plastics

The closed-form expression for impact fracture resistance given here as Eqn. (4) was derived [4] on the basis of assumptions which were always recognised as restrictive. In particular, the specimen loading was assumed to be linear, at a rate given by the compliance of the initial crack, whilst the craze at its tip was assumed to be small and to correspond to that at the tip of a crack in a centre-cracked plate.

Neither of these assumptions is remotely applicable to an impact bend specimen; they would only be approximately true even if the craze stress were extremely high, so that the craze size were very small. If a Charpy-type specimen of MDPE is sharply notched to a depth of $0.2W$ and subjected to a constant quasi-static displacement rate (say, 10 mm s^{-1}), the craze which grows from the notch tip will quickly reach millimetres in length. As it does so the specimen softens — an effect distinct from elastic non-linearity, which is also likely to intervene. Whilst this softening reduces the rate at which the craze must grow (since the stress intensity factor which it opposes falls), the reduction in ligament size increases it. The net effect on the rate of fibril extension at the craze mouth — which determines the survival time — is difficult to assess. Meanwhile, load/displacement non-linearity affects the apparent energy.

A further complication arises as the impact speed increases and the inertia of the specimen modifies the rate at which the craze is loaded. From the quasi-static case described above, the system enters a regime in which it is well described by a lumped mass-spring model [7] before finally approaching a dynamic regime in which wave propagation effects dominate.

The effect of these factors is that Eqn. (4) becomes a poor description of behaviour as the craze size and impact speed increase. Nevertheless, the underlying fracture criterion can still be applied within a simulation of the test which accounts for craze growth under load, the corresponding increase in compliance and mass-spring oscillations of the specimen.

Simulations of this kind were first carried out by Morgan [5], but have been greatly extended by the use of mass-spring models and of new Dugdale solutions for large crazes in finite bend specimens [8]. The extent of craze growth which takes place before fracture is predicted by the simulation and can be measured from the fracture surface to provide independent verification. Previously, the fall in craze growth with impact speed was seen as evidence that it is the rate-dependence of craze formation which determined fracture resistance. From the thermal decohesion perspective, the craze simply grows to balance the applied load; it grows less with increasing impact speed because it fails earlier and the fracture resistance diminishes.

Conclusions

The enduring popularity of Charpy and Izod impact tests for thermoplastics seems unjustified. If many components were at risk of failure by impact, it would be difficult to

argue that impact strength data could be used to reduce the risk. There is a suspicion that such data are regarded as an index of resistance to brittle fracture in general.

The use of fracture mechanics analysis to convert impact strength to fracture resistance offers the possibility of portability to other geometries, but relies on fracture resistance being a geometry-invariant material property.

The thermal decohesion model for impact and dynamic fracture in thermoplastics asserts that fracture resistance is *not* constant, and is strongly supported by experimental data. It also emphasises that the nature of resistance to impact brittle fracture is profoundly different from that to other brittle fracture modes. The model can be used, however, to construct an alternative scheme for transferring data between impact configurations. This scheme has been demonstrated for a practical impact failure problem.

Acknowledgments

The authors wish to thank the UK Engineering and Physical Science Research Council and Du Pont for funding this work. Some of the experimental work was carried out by Robert Payne as part of his final-year undergraduate project, helped by Paul Davis (S4 testing) and Hugh MacGillivray (drop-weight testing).

References

- [1] Williams, J.G., *Fracture Mechanics of Polymers*, Ellis Horwood, Chichester, UK, 1987.
- [2] Pavan, A. and Williams, J.G., "Development of a Standard for Determining K_{IC} and G_{IC} for Plastics at High Loading Rates: the ESIS Protocol for 1 m s^{-1} Testing," *Limitations of Test Methods for Plastics, ASTM STP 1369*, J. S. Peraro, Ed., American Society for Testing and Materials, West Conshohocken, PA, 1999.
- [3] Leevers, P.S., "Impact and Dynamic Fracture Resistance of Crystalline Thermoplastics: Prediction from Bulk Properties," *Polymer Engineering and Science*, Vol. 36, No. 18, 1996, pp. 2296-2305.
- [4] Leevers, P.S., "Impact and Dynamic Fracture of Tough Polymers by Thermal Decohesion in a Dugdale Zone", *International Journal of Fracture*, Vol. 73, No. 2, 1995, pp. 109-127.
- [5] Leevers, P.S. and Morgan, R.E., "Impact Fracture of Polyethylene: a Non-linear-elastic Thermal Decohesion Model", *Engineering Fracture Mechanics*, Vol. 52, No. 6, 1995, pp. 999-1014.
- [6] Greenshields, C.J. and Leevers, P.S., "Rapid Crack Propagation in Plastic Water Pipes: Measurement of Dynamic Fracture Resistance", *International Journal of Fracture*, Vol. 79, 1996, pp. 85-95.
- [7] Williams, J.G. and Adams, G.C., "The Analysis of Instrumented Impact Tests Using a Mass-spring Model", *International Journal of Fracture*, Vol. 33, 1987, pp. 209-222.
- [8] Douglas, M. "*Impact Fracture of Engineering Polymers*", PhD Thesis, University of London, 1998.

Michael P. Manahan, Sr.,¹ Carlos A. Cruz, Jr.,² and Harold E. Yohn³

Instrumented Pendulum Impact Testing of Plastics

Reference: Manahan, M. P. Sr., Cruz, C.A. Jr. and Yohn, H. E., "Instrumented Impact Testing of Plastics," *Limitations of Test Methods for Plastics, ASTM STP 1369*, J. S. Peraro, Ed., American Society for Testing and Materials, West Conshohocken, PA, 2000.

Abstract: Conventional impact tests (without instrumentation) are performed to measure the energy required to break a notched specimen under dynamic loading. Instrumented impact tests not only measure the notched specimen breaking energy but also quantify the energy required to form a crack at the root of the notch and the energy required to propagate the crack through the material. Instrumented test systems use strikers which have strain gages so that the load-deflection curve during the impact event can be derived. These data provide load, deflection, and energy data which can be correlated with engineering parameters such as fracture toughness, ductility, and fracture resistance.

This paper compares instrumented impact results obtained using both the Charpy and Izod test procedures. Several possible limitations of the instrumented test procedure have been identified and test procedures to overcome these limitations have been proposed. In addition, an important potential limitation of the Izod test, specimen clamping pressure, has been studied.

Keywords: instrumented impact test, Charpy test, Izod test, fracture resistance, striker, strain gages, dynamic testing

Introduction

The most common laboratory impact test configurations are the pendulum

¹ President, MPM Technologies, Inc., 2161 Sandy Drive, State College, PA 16803.

² Research Fellow, Rohm and Haas Company, PO Box 219, Bristol, PA 19007.

³ Product Development Mgr., Tinius Olsen Testing Company, Inc., Easton Road, Willow Grove, PA 19090.

machine and the drop tower. However, other test geometries and loading configurations have been used in the past. Pendulum tests are most commonly performed using either the Charpy or Izod test configuration. The focus of this paper is on the use of an instrumented striker system with pendulum impact machines for characterizing the dynamic response of a variety of plastics.

The instrumented impact test involves the attachment of strain gages to the striker so that the force applied during impact can be measured. The advantage of instrumented testing is that load-time data, in addition to absorbed energy, can be measured during the test. For plastics, additional data include the peak load, brittle fracture load, crack arrest load, and their corresponding energies. These parameters give insight into the fracture mechanisms and the temperature dependence of the fracture process. Provided accurate loads are measured, fracture toughness estimates can be calculated for many materials using the instrumented data. This paper reports results of instrumented impact tests on plastics which cover a wide range of ductilities and provides examples related to the interpretation of instrumented data as well as on the limitations of the test approach.

The majority of instrumented tests performed in the past have used signal filtering, and occasionally interfacial damping material, to smooth the dynamic response of the specimen to impact loading. Modern strain gages, amplifiers, and data acquisition boards do not require signal smoothing techniques. In fact, filtering is not desirable for most applications because it results in attenuation of the load signal and in skewing of the load-time curve which results in inaccurate absorbed energy measurement. Instrumented testing without filtering is shown to be superior for accurate load and energy measurement in instrumented tests.

The paper also focuses on the comparison of the Charpy and Izod test geometries. The Izod test has a potential disadvantage in that the test piece is clamped which can result in a stress field in the vicinity of the notch prior to impact. On the other hand, the Charpy test consists of a simply supported beam which is not stressed prior to impact. Test data are presented which compare impact results obtained as a function of clamping pressure for both hard, brittle plastics and for ductile materials.

Materials

The plastic materials chosen for this study cover a wide range of properties and applications. Commercially available bisphenol-A polycarbonate (PC), Tuffak®, and poly(methyl methacrylate) (PMMA), Plexiglas G®, samples, neither of them modified with toughening agents, were used. A poly(vinyl chloride) (PVC) grade was chosen so it would meet the requirements for a standard testing formulation for so-called vinyl siding. Three types of samples, each containing a different proprietary additive were prepared from the starting PVC to produce specimens with various degrees of impact resistance. The additive in each case was loaded at the level of 5 parts per hundred parts of resin. Other suitable formulation ingredients, such as processing aids, lubricants and stabilizers were added. Poly(butylene terephthalate) (PBT), a polymer that is seeing increased use in automotive applications, was used in neat and modified version. The latter, referred to as Mod-PBT in this work, contains 20 weight % of a proprietary core/shell additive.

Specimen Preparation

Except for the two commercial-grade polymers, the other formulations were first melt-blended and shaped into specimens with adequate dimensions. The PVC formulations were milled on a two-roll mill at 170°C and pressed into 3.18 mm-thick plaques. The PBT materials were first extruded and pelletized in a twin-screw extruder using a 240°C melt temperature. These materials were further injection molded into plaques of 3.18 mm thickness and 5 cm by 7.6 cm dimensions.

Notched Izod specimens were cut and notched from the above materials using a diamond-head cutter, following the ASTM D 256 standard (0.254 mm radius, 2.0 mm notch depth). The specimens for Charpy instrumented testing were also diamond cut from the same materials, using the same type of notch. Every sample was run at an ambient temperature of 23°C with no pre-conditioning, except for letting the samples equilibrate with the humidity of the room (50% relative humidity) for at least one day prior to testing.

Test Procedure

Charpy Test

Measurements were made using a state-of-the art instrumented striker system which was installed on a Tinius Olsen Model 92 T plastics impact tester. The instrument was configured for testing in accordance with ISO 179. The test machine was equipped with an optical encoder and digital readout for independent measurement of the total absorbed energy. As shown in Figure 1, the pendulum is a bifurcated (compound) design

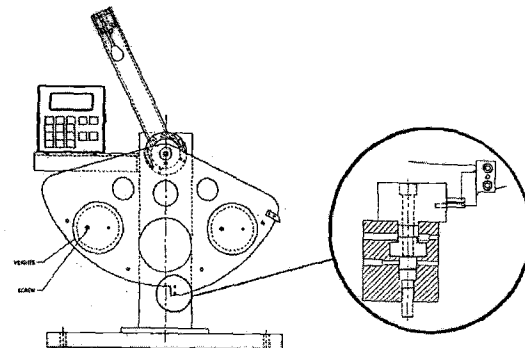


Figure 1 *Bifurcated Pendulum Geometry Used for Charpy Impact Tests*

which reduces windage and frictional losses. The test machine was leveled and securely bolted to a massive laboratory bench to prevent errors in total energy measurement. The drop height was set at 61 cm so that a 3.5 m/s impact velocity could be achieved.

The striker was fabricated in accordance with ISO 179 and contains strain gages located near the point of impact. The instrumented system is a Tinius Olsen system v2.1 which is capable of measuring any number of data points up to 19,000 per test. The time scale can be set at any range from 20 microseconds to 20 seconds, however, most impact tests have a duration ranging from about 0.5 milliseconds to 20 milliseconds. Experience in metals testing [1] has shown that at least 500 data points per millisecond are needed to accurately characterize the dynamic portions of the load-time curve. It is recommended that instrumented impact tests be conducted using 500 to 1000 data points per millisecond. The tests reported here were run with 10,000 data points acquired over 15 milliseconds.

Izod Test

Izod tests were performed in accordance with ASTM D256. The Izod tests were performed on a Tinius Olsen Model 66 equipped with an Instron Dynatup instrumented Izod striker. The test machine design is a conventional U-type hammer. The instrumented system used with the Izod tests is an older system with limited capability. First, the system has a 2048 data point limitation. Second, the system can only be set to acquire over discrete time intervals (ex., 2 milliseconds, 5 milliseconds, etc.). This approach has the disadvantage of spreading an already limited number of points over a broad time scale or forcing truncation of data. In particular, a 3 millisecond test would have to either be conducted over the 2 millisecond time range (1000 data points per millisecond) with unacceptable data loss, or it would have to be conducted over 5 milliseconds (400 data points per millisecond) with poor characterization of dynamic events. The system also uses electronic signal filtering which causes reduction of the magnitude of the measured forces and distortion of the load-time curve. The integrated energy in this system is obtained by scaling the loads so that the integrated energy matches the optical encoder energy. While this approach can produce a total absorbed energy which matches the encoder, the loads, deflections, and partitioned energies are not valid because of the effects of filtering. It is important to note that the Model 66 test machine could have been instrumented with the advanced instrumented striker system such as the one used with the Charpy test machine, however, since there are many Izod test machines with limited capability as described here the limited test machine was used to quantify the limits of such a system and to compare with the more advanced system.

Results and Discussion

Figures 2 through 4 show typical results from the instrumented Charpy tests. Figure 2 is a plot of the raw voltage-time data. Figure 3 shows the steps involved in the integration of the instrumented data to determine the total absorbed energy. First, the voltage-time signal is converted to a force-time curve using the static calibration data. Next, the force-time curve is integrated to yield the velocity-time curve. Then the velocity-time curve is integrated to give the striker displacement-time curve. Finally, the force-displacement curve is integrated to give the total absorbed energy. Figure 4 shows the final step in the data analysis. The characteristic load points are determined by fitting portions of the load-displacement curve. For ductile plastics, the important parameter is the peak load which is determined by fitting the data near the peak to give the average of the peak data. In many materials, the formation of the crack at the root of the notch along the notch front occurs just prior to or at peak load. Therefore, it is a reasonable approximation to define the energy to peak load as the "crack formation energy". Similarly, the post-peak load energy can be defined as the "crack propagation resistance" energy. These data are shown in the table given in Figure 4.

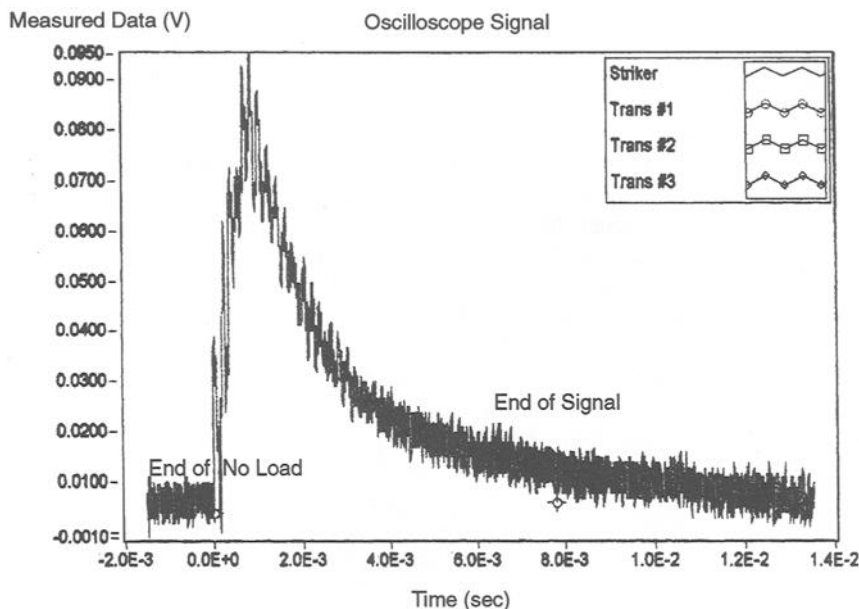


Figure 2 *Instrumented Charpy V-Notch Voltage-Time Curve for Toughened PVC*

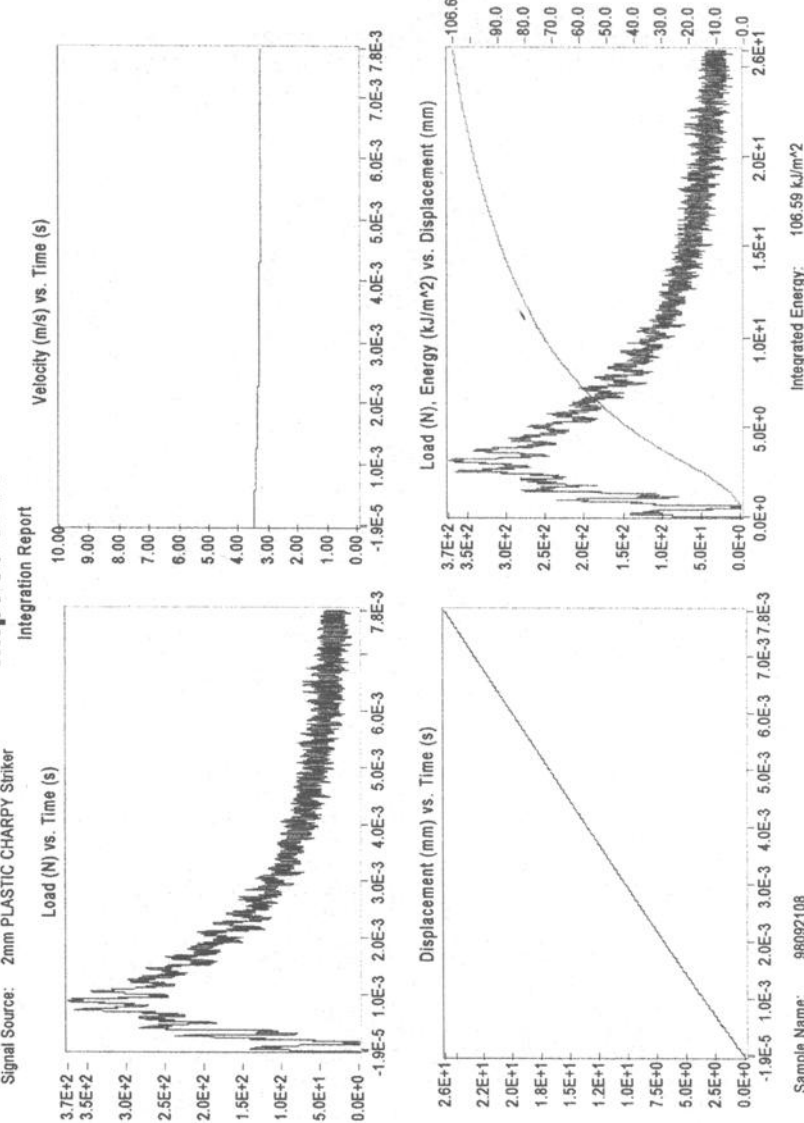
Impact V2.1

Figure 3

Integration Steps to Obtain Total Absorbed Energy a) upper left - force-time curve from striker calibration b) upper right - velocity-time curve obtained by integration of force-time curve c) lower left - striker displacement-time curve from integration of velocity-time curve d) lower right - force-displacement curve and integration to yield total absorbed energy

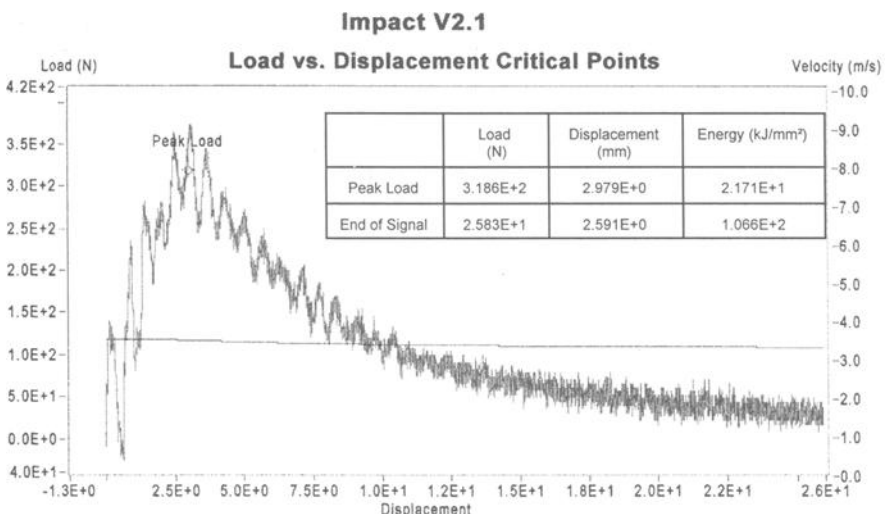


Figure 4 *Load-Displacement Critical Points for Toughened PVC. The Integrated Energy is Partitioned into Pre-Maximum Load Energy and Post-Maximum Load Energy*

Figure 5 shows the voltage-time curve with the data points indicated. This plot is used to check the settings on the time interval and number of acquired points. Also note that the time scale has been set long enough to ensure that the signal is not truncated until the fracture process is completed. Plastic tests often involve low load levels. As shown

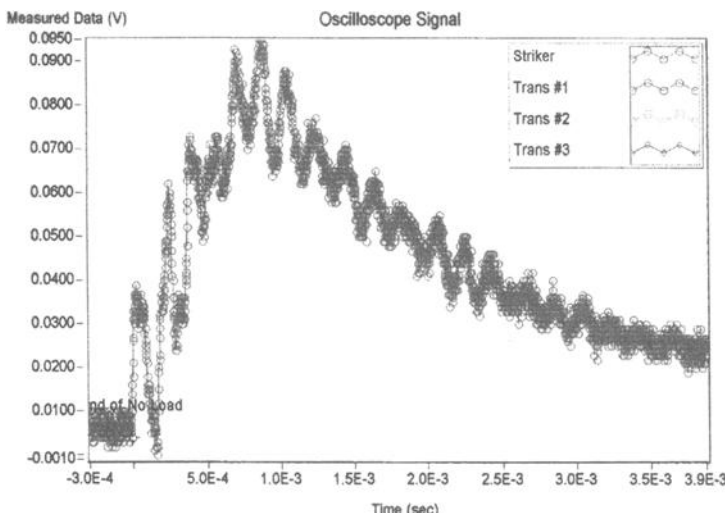


Figure 5 *Amplified View of Voltage-Time Curve Showing Individual Data Points for Test Performed on Toughened PVC*

in Figures 2 and 5, the baseline signal has ~ 15 mV of electronic noise. However, this noise is not significant, even in low applied force tests such as with plastics, because there are sufficient data acquired to fully characterize each peak and to thus obtain a robust average baseline signal. Figure 5 also shows the dynamic load oscillations which occur during load rise. There are more than enough data points to fully characterize these oscillations. Figure 6 shows a typical Dynatup load-deflection curve. It is important to note that the setup used for the instrumented notched Izod tests filters the electronic signal. The instrument also cuts off the tail of the signal and the final portion of the fracture process cannot always be properly accounted for, particularly in ductile samples. Even though it appears to contain a higher degree of noise, the instrumented Charpy signal registers substantially more data points (up to 19,000 points can be acquired) to obtain the true average signal and follows the energy absorption path from beginning to end, without any cut-offs.

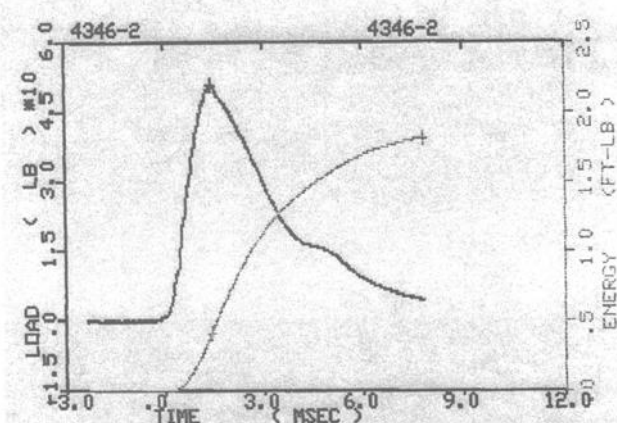


Figure 6 *Typical Dynatup Filtered Izod Load-Time Curve. As a Result of Limited Data Points the Curve is Cut Off Prior to Completion of the Test*

Table 1 provides a summary of the results obtained with the instrumented Charpy tester along with notched Izod test results. In one case (PBT and modified PBT), data were also obtained on an instrumented Izod-type setup. The mean, standard deviation and number of samples used to make the measurements are reported in the table. A signal to noise ratio (S/N), calculated as the mean divided by the standard deviation, is also reported for each material. Figure 7 compares the S/N ratios graphically. The instrumented Charpy has an S/N ratio which is about constant at all energy levels. The Dynatup system has a poor S/N for the low energy tests and a better S/N for high energy measurements. This is believed to be a result of load-time distortion due to filtering and to limited data points which has a more significant effect on low energy measurements. Overall, the Charpy and Izod tests show comparable S/N ratios for intermediate and high energy tests.

Figure 8 shows that the energy measured according to the instrumented Charpy test has a high degree of correlation with the fracture energy as measured by the 3.17 mm notched Izod, which validates the use of the more informative instrumented Charpy test.

Table 1 Comparison of Charpy and Izod Data

Sample ID	Material	Instrumented Charpy V-Notch				Notched Izod (3.17 mm)				Instrumented Izod (3.17 mm)			
		Mean (S) (kJ/m ²)	Std. Dev. (N) (kJ/m ²)	# Tests	S/N Ratio	Mean (S) (J/cm)	Std. Dev. (N) (J/cm)	# Tests	S/N Ratio	Mean (S) (J/cm)	Std. Dev. (N) (J/cm)	# Tests	S/N Ratio
Plexiglas G	PMMA	1.31	0.039	10	33.8	0.19	0.032	5	12.0	-	-	-	-
Tuffak	PC	84.38	3.01	10	28.0	9.75	0.21	5	46.3	-	-	-	-
1937-C1	Toughened PVC	106.28	5.83	5	18.2	12.07	0.23	5	53.3	-	-	-	-
1937-C2	Toughened PVC	16.51	1.87	5	8.8	1.34	0.07	5	19.2	-	-	-	-
1937-B5	Toughened PVC	1.48	0.05	5	27.8	0.15	0.02	5	7.0	-	-	-	-
PBT	PBT	4.55	0.22	9	21.0	0.51	0.04	5	11.9	0.14	0.01	10	10.0
Modified PBT	Toughened PBT	82.12	2.46	10	33.4	8.52	0.65	5	13.1	2.54	0.04	10	62.0

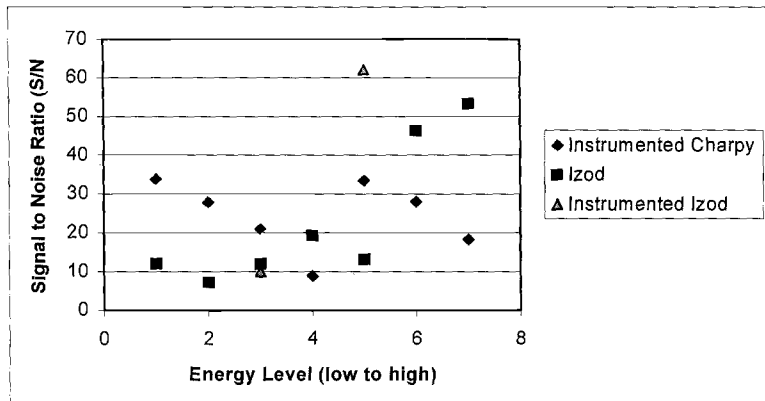


Figure 7 Comparison of Signal to Noise Ratio for Charpy and Izod Tests

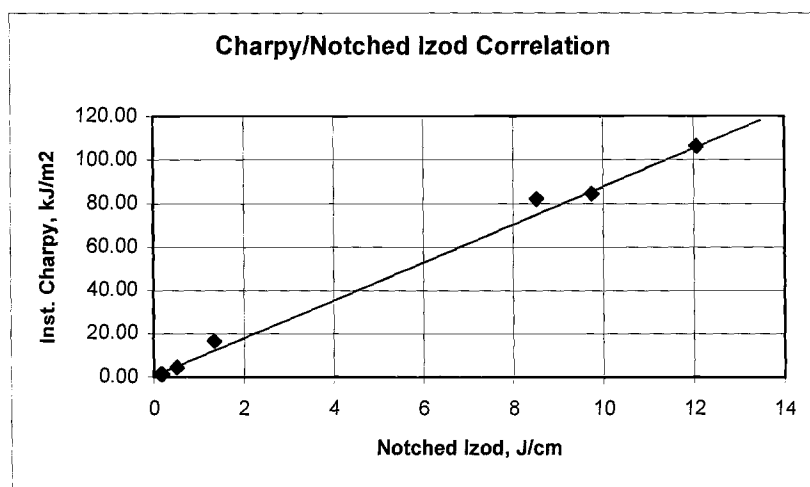


Figure 8 Correlation Between 3.17 mm Notched Izod and Instrumented Charpy Data

The amount of detail and number of data points gathered provide far more information than the single energy value from the Izod. Table 2 illustrates additional information which can be obtained. For materials which initiate a crack near peak load, the "Energy to Peak Load" represents the material resistance to crack formation. The "Post-Peak Load Energy" represents the material resistance to crack extension for ductile materials. For example, Tuffak and modified PBT both have about the same total energy, but Tuffak has a higher crack formation energy and higher peak load. The 1937-C1, with a significantly higher total energy, has a lower crack formation energy than Tuffak. Thus, total energy alone is not a good parameter for assessing the suitability of a particular material for a given application.

Table 2 *Summary of Instrumented Charpy Test Parameters*

MATERIAL	TOTAL ENERGY (kJ/m ²)	PEAK LOAD (N)	ENERGY TO PEAK LOAD (kJ/m ²)	POST-PEAK LOAD ENERGY (kJ/m ²)	TOTAL STRIKER DISPLACEMENT (mm)
Plexiglass G	1.31	109.89	0.44	0.88	0.42
Tuffak	79.46	291.92	34.95	44.52	13.13
1937-C1	106.28	326.52	24.46	81.82	26.53
1937-C2	16.51	305.12	15.80	0.71	2.70
1937-B5	1.48	117.96	0.58	0.90	0.51
PBT	4.55	191.8	1.66	2.89	1.19
Mod PBT	82.12	220.20	24.47	57.64	20.97

Izod Clamping Pressure

Another test limitation examined was the role of the clamping pressure on the outcome of the notched Izod test. Table 3 shows the results obtained when Izod specimens were clamped using a pneumatic system. The clamping pressures on the table indicate the air pressure used to clamp in the samples. The data in the table shows that clamping pressure can have an effect (perhaps ~ 5%) on ductile materials. The effect on brittle (hard) materials such as Plexiglas G is not statistically significant. The clamping pressure effect is believed to be caused by deformation in the vicinity of the notch prior to impact.

Table 3 *Effect of Clamping Pressure on Izod Test Specimens*

Clamping Pressure (psig)	Tuffak		Plexiglas G	
	Mean (J/cm)	Std. Dev. (J/cm)	Mean (J/cm)	Std. Dev. (J/cm)
18	9.75	0.21	0.19	0.02
36	9.25	0.27	0.21	0.01
54	9.43	0.13	0.20	0.01

Summary and Conclusions

It has been demonstrated that the Charpy and Izod fracture energies correlate well. There does not appear to be any practical limit to the energy level which can be measured using instrumented strikers because the strain gages can be calibrated over a wide energy range. However, it has been observed that instrumented tests should be performed without filtering because electronic filtering causes attenuation of the measured loads and time distortion of the signal. The net effect is that the load-time response cannot be accurately measured when filtering is done. Filtering is not advised because it leads to inaccurate test results which negates the many benefits of instrumented testing.

Instrumented test systems should provide continuous control over the time range for data acquisition and the total number of data points acquired over that range. Older instrumented test systems which are limited to 2000 data points are considered to not fulfill the needs of accurate instrumented testing. A minimum of 500 test points per millisecond is recommended for accurate results. Also, the instrumented data acquisition must be run long enough to ensure that the load-time signal is not truncated prior to complete unloading. This is a problem which can occur in older test systems which do not provide continuous control over the acquisition time range and number of data points.

Finally, the Izod test has been shown to be affected by clamping pressure, and this effect will be larger for more ductile materials. Additional work should be conducted in the future to address this through revision to existing standards. The reader is referred to ASTM D256 for further guidance on clamping pressure. Our overall conclusion is that the Charpy test is a superior test geometry for plastics and should replace the Izod test.

Reference

- [1] Proposed ASTM Standard Method for Instrumented Impact Tests of Metallic Materials, Draft 7, December, 1998, Prepared by ASTM Sub-Committee E28.07.08 on Miniaturized Charpy/Instrumented Testing

Andrea Pavan¹ and J. Gordon Williams^{2,3}

Development of a Standard for Determining K_{IC} and G_{IC} for Plastics at High Loading Rates: the ESIS Protocol for 1 m/s Testing

Reference: Pavan, A. and Williams, J. G., "Development of a Standard for Determining K_{IC} and G_{IC} for Plastics at High Loading Rates: the ESIS Protocol for 1 m/s Testing," *Limitations of Test Methods for Plastics, ASTM STP 1369*, J. S. Peraro, Ed., American Society for Testing and Materials, West Conshohocken, PA, 2000.

Abstract: This paper describes research work undertaken by the Technical Committee on Polymers and Composites (TC4) of the European Structural Integrity Society (ESIS) to develop a standardized testing procedure for conducting K_{IC} and G_{IC} tests on plastics at a moderately high rate of loading, namely a load-point displacement rate of 1 m/s. One of the authors (A. P.) has acted as the task group leader for this activity within the Committee, with responsibility for the preparation of the testing protocol, the coordination of interlaboratory round-robin and the analysis of data generated thereby. The proposed testing procedure stems from the linear elastic fracture mechanics scheme covered in a protocol for "quasi-static" (low loading rate) determination of K_{IC} and G_{IC} which was developed within the same ESIS group previously.

In this paper the background for the extension of the scope of the preceding protocol to higher rates is illustrated, the problems encountered are highlighted and the solutions found and proposed in the final draft of the protocol are reviewed. A summary of the test results obtained in a series of round-robin exercises - which involved some thirty laboratories across Europe on a five-year span - is reported and the significance of interlaboratory consistency of the collected data is commented upon with the view of

¹Professor of Polymer Engineering, Dipartimento di Chimica Industriale e Ingegneria Chimica, Politecnico di Milano, piazza L. da Vinci 32, I-20133 Milano, Italy.

²Professor and Head of the Mechanical Engineering Department, Imperial College of Science, Technology and Medicine, Exhibition Road, London SW7 2BX, UK.

³The authors have been acting as joint chairmen of the Technical Committee on Polymers and Composites (TC4) of the European Structural Integrity Society (ESIS) for the last few years.

validating the protocol. In conclusion, it is pointed out that an agreed standardized procedure can be finalized to form the basis of national and international standards.

Keywords: polymer fracture, toughness, fracture energy, impact testing, fracture testing standards

There already exists a range of standard tests for characterizing the fracture resistance of polymers under impact loading conditions, e.g. Izod, Charpy and tensile impact among the pendulum type tests, Gardner and Falling Dart among the falling weight type tests, etc. Some are very popular and the user-industry has established a database around them. The popularity of these tests rests on their simplicity; they are easy and quick to perform, do not call for theoretical background and do not require elaborate data handling.

The limitations of these tests cannot be overestimated, however. All of them provide the value of a single, all-inclusive parameter (e.g., the total energy subtracted from the pendulum) which might be only partly related to test specimen fracture. Fracture type is generally not assessed if there is no separate inspection of the fracture surface after the test has been carried out. Evolution of the fracture phenomenon during the test (differentiating fracture initiation, continuous or discontinuous crack propagation, final full break or fracture arrest) is simply neglected. But, above all, all these traditional tests suffer from the drawback that the quantity they measure is not a true material property but depends upon the shape and dimensions of the test specimen used. This makes these tests difficult to relate to the behavior of the material in end-use situations which do not bear an obvious geometrical similarity to the testing arrangement. Their results cannot therefore be applied to predict material behaviour in service, as required for the dimensioning of structures.

The problem is particularly acute in polymers because energy absorption on fracture is a combination of several terms whose relative contribution is altered if the test type and conditions are varied.

It has been suggested that in the absence of an interpretation of these tests in terms of accepted strength or toughness parameters, the main role they may have is the important, although limited one, of comparative quality control. Yet, because of the geometrical differences involved (meaning different types of stress and strain fields), it is not uncommon to find that different tests rank the same set of materials in different order.

A scheme which seeks to rectify this situation is the application of fracture mechanics and this is now quite well developed [e.g. 1]. The data which are so produced are intrinsic material properties and, as such, are useful both for proper material qualification and for use in engineering design. However, fracture mechanics testing methods are not simple to perform.

Instrumented Impact Testing

In an attempt to improve the utility of traditional impact testers instrumented versions are manufactured and are now commercially available, and their adoption is spreading rapidly. Use of instrumented impact testers in some cases allows one to overcome some of the deficiencies of the traditional impact tests mentioned above, thus improving the utility of the test. However, the interpretation of load-time records is far from straightforward and reliable results will not be obtained generally as long as the impact test is expected to furnish an all-inclusive index of fracture resistance. The problem of geometry dependence is still present and the difficulty of correlating impact test results with service performance remains.

However, instrumented testers, being capable of recording the entire load-vs-time curve, are well suited to provide data which can be interpreted in a fashion independent of geometry through the formalism of fracture mechanics.

The lack of standardized procedures for characterizing the fracture resistance of polymers based on sound scientific grounds, such as fracture mechanics principles, was perceived as a significant barrier to applications and international trade. The ESIS Technical Committee on Polymers and Composites has therefore undertaken the task of coordinating the required pre-normative research to develop the enabling science and establish standard testing procedures for determining the fracture resistance of polymeric materials using fracture mechanics methods.

The first protocol completed was the test method for determining the critical stress intensity factor, K_{IC} , and fracture energy, G_{IC} , in plastics under conditions of slow ('quasi-static') loading [2]. This test method has been found to be reasonably successful and it has been adopted as a standard by ASTM (Test Methods for Plane-Strain Fracture Toughness and Strain Energy Release Rate of Plastic Materials, D 5045-93) and is currently under consideration by ISO [3].

The properties K_{IC} and G_{IC} in plane strain are believed to represent a lower limiting (i.e. conservative) value of fracture resistance, and this value may be used to estimate the relation between failure stress and defect size, irrespective of geometry, thus providing transferability of the test data from the laboratory to field conditions, which is a necessary pre-requisite for their use in engineering design.

Since this first ESIS protocol served as a parent for the 1 m/s version which was derived from it, its main features will first be described briefly. This will serve as a background for the subsequent discussion of the 1 m/s extension.

The Parent K_C - G_C Testing Protocol [2]

These tests are designed to characterize the toughness of polymers in terms of the

critical stress intensity factor, K_{IC} , and the energy per unit area of crack, G_{IC} , at fracture initiation.

The procedure was based on the ASTM Standard Test Method for Plane-Strain Fracture Toughness of Metallic Materials (E 399), but takes account of the major difficulties imposed by polymers. Although polymeric materials are not strictly elastic, for many cases of practical significance linear elastic fracture mechanics (LEFM) conditions pertain, and the protocol sets out the same validity criteria as for metals.

One special problem in polymer specimen preparation is notching. As for metals, the ideal case is when a natural crack is introduced and then re-initiated in the test, but fatigue is not recommended for plastics because of difficulties in controlling crack growth and avoiding hysteretic heating. Instead, it is possible to produce sufficiently sharp initial cracks by using a razor blade and the protocol suggests two methods, tapping and sliding, depending on the material.

Since polymers are viscoelastic materials it is necessary to specify both the temperature and the time scale under which the result was obtained. This protocol is meant for low speed ('quasi-static') displacement control mode of loading and as a basic test condition, it is recommended that 23°C and a load-point displacement rate of 10 mm/min be used, but other conditions are possible. In all cases, the time-to-fracture should be quoted and all related determinations (yield stress and indentation correction, see below) should be obtained at comparable loading times as for the fracture test.

The protocol considers the determination of fracture toughness at fracture initiation, and the initiation point is to be determined from the load record. The definition of initiation is as problematic here as in metals and the same rules as in E 399 ('pop-in', maximum load and load at 5% offset) are adopted.

From the value of load at fracture initiation, P_Q , a conditional value of the initiation stress intensity factor, denoted K_Q , is calculated and its validity as an intrinsic measure of plane-strain fracture toughness, K_{IC} , is to be confirmed by checking that some size criteria are met.

This protocol also covers the determination of the energy per unit area of crack, G_{IC} (while E 399 does not). G_{IC} is of particular importance, and often preferred to K_{IC} , for polymers because it is widely used in composites and, it can be argued, is a better indication of toughness. G_{IC} can, in principle, be obtained from K_{IC} via the modulus through the LEFM relationship:

$$G_{IC} = K_{IC}^2/E' \quad (1)$$

(where $E' = E/(1-v^2)$ for plane strain, in which E is the tensile modulus and v is Poisson's ratio) but E is not usually known at the test rate so it is considered preferable to determine G_{IC} directly from the energy derived from integrating the load versus load-point displacement diagram. The procedure to be followed is to test for validity via K_Q and then to determine the energy, U_Q , up to the same load point as has been used for K_{IC} .

Thus, in addition to a load measuring (and recording) facility the test requires a means

of measuring (and recording) the load-point displacement. Care must then be taken to correct for total system compliance and test specimen indentation. This can be performed by a simple calibration of the testing system: identically prepared, but unnotched specimens, are tested using a test configuration which restrains the specimen from fracturing and bending.

ESIS Protocol for 1 m/s Testing [4]

Motivation and Scope

The testing methods covered by the preceding protocol applies to testing speeds up to 0.1 m/s, where dynamic effects are absent. Assuming that fracture mechanics principles govern fracture even under higher loading rate conditions and supposing that the problems arising from the dynamic effects which are then encountered, once recognized, can be taken into proper account, it was deemed desirable to extend the scope of the preceding protocol somewhat into the impact test range, e.g. testing speed of the order of 1 m/s. Many polymers show significant toughness decreases at these higher speeds so that characterization of fracture resistance under these conditions is important.

Developments in instrumentation in recent years, on the other hand, nowadays offer the possibility of visualizing the high speed loading processes precisely and suggest the possibility of applying the same basic fracture mechanics methodology to impact testing. Moreover, instrumented impact testers (either swinging pendulums or falling weights) and high-speed hydraulic testing machines are becoming generally available, which justifies the attempt of working out a testing method which can be adopted as a standard usable for routine testing in ordinary laboratories.

In order to take the dynamic effects occurring at high loading rates into proper account and define the scope of applicability of the testing protocol precisely, it is necessary to understand the nature of those effects. The dynamic phenomena observed when a test specimen is loaded rapidly have two possible origins. One is the finite, though great, speed of the stress wave propagation in the material under test, which prevents stresses from attaining equilibrium during the short period of the impact event, and is inherent in fast loading. The second is the high acceleration imparted to the specimen initially, which excites inertial forces and complex motions in both specimen and impactor and is mainly instrumental, depending largely on the characteristics of the latter. The relative importance of the two varies with the rate of loading.

At very high loading rates the time-scale of the fracture event is comparable with the time taken by the stress waves to travel across the test specimen, and stress wave reflections and interference with the crack may give some effect.

At moderately high loading rates (load-point displacement rates of the order of 1 m/s, loading times of the order of 1 ms) it is the dynamic effects related to the specimen motion which predominate. The inertial forces caused by the acceleration imparted to the specimen produce vibrations in the test system, oscillations in the recorded signal, and forces on the test specimen which are different from the forces sensed by the test fixture. Also possible loss (and regaining) of contact between the specimen and the tip of the moving arm of the testing machine and also between the specimen and the shoulders of the mounting vice occur.

At lower loading rates these effects become negligible and the fracture mechanics methods used for quasi-static test conditions [2] can be applied as they stand.

It is evident from the examples shown in Figure 1 that at high rates the amplitude of the oscillations may represent a high proportion of the total load, and the interpretation of the test record becomes difficult.

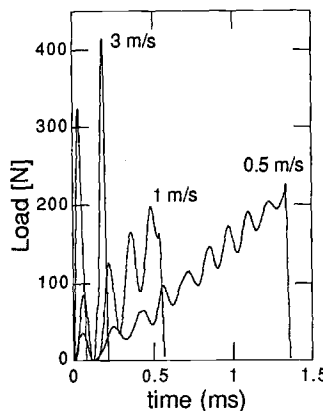


Figure 1 - Typical force/time curves recorded from impact tests at different speeds.

Material: nylon-6.⁴ Tester: Fractovis falling weight by CEAST, Turin, Italy.

Test configuration: single edge notch three-point bending (SE(B)).

Considerable work has been published, dealing with the assessment, analysis, modelling and control of the dynamic effects manifested by fluctuations of the measured force signal such as shown in Figure 1. As a result, we are in the position now to answer the question of if and how the characteristic responses of the test specimen and the force measuring system can be separated. In fact, since a part of these effects is instrumental in origin, there is room for controlling these effects by improving machine design and

⁴Radilon S-D4/100, manufactured and kindly supplied by Radici Novacips, Villa D'Ogna (Bergamo), Italy.

adopting suitable test conditions. One such expedient is to damp the load point and this is illustrated below.

The method applies to testing rates in the intermediate range defined above: speeds around 1 m/s and loading times of the order of 1 ms. For testing speeds greater than 1 m/s, control of the dynamic effects by means of mechanical damping may not be successful and the load route must be abandoned and other approaches must be sought.⁵

Although the dynamic effects related to specimen motion are largely dependent on test equipment, test geometry and material properties, no restriction is placed *a priori* on these variables in the protocol: the guidelines given for dealing with such dynamic effects are believed to be generally valid irrespective of type of test equipment, test geometry and material tested.

Control of Dynamic Effects

One of the problems arising in the presence of dynamic effects is the identification of the point of fracture initiation. In the low rate tests that point can be detected from the record of the force, but in the high rate case the oscillations in the force signal may obscure that point. Other techniques are possible, but most of them require sophisticated instrumentation and complex calibration procedures, especially so in the case of high-rate testing. However a major concern in developing scientifically based testing protocols is to maintain their practicability within the reach of laboratories having medium-level expertise and standard equipment. For this, it is desirable that the point of fracture initiation can be deduced from the load record. Two experimental approaches are possible; either to reduce the oscillations of the recorded signal artificially, *a posteriori*, by electronic filtering or to reduce them by containing the dynamic effects by some expedient. The latter option is to be preferred as electronic filtering may wipe out real effects in the specimen response and it would not help when the period of the oscillations is comparable with the duration of the test.

Previous studies have shown that the force oscillations recorded by force transducers mounted in the moving arm of the test instrument are considerably greater than the ones actually experienced by the specimen at its crack tip (see for example [5]) and depend largely on the 'contact stiffness' of the tup-specimen interface (see for example [6, 7]). Some reduction of these effects by proper control of the 'contact stiffness' can thus be envisaged as possible. With impact testers the impact may be cushioned by means of a soft pad, placed where the tup strikes the specimen. With servo-hydraulic testing machines, initial acceleration of the specimen can be controlled by means of a damper applied in the motion transmission unit.

⁵Developments in this direction are underway within ESIS TC4. A method based on measuring time to fracture is being tested and a testing protocol developed.

Ample evidence of the effectiveness of this expedient has been gathered within ESIS TC4. As the examples in Figure 2 show, signal oscillations can be practically suppressed and thus the point of fracture initiation can be easily identified and the critical load easily determined.

If damping is contained no adverse effects are observed. The value of the load at fracture is not affected and the load-point displacement rate (in a displacement control mode of testing) can be kept constant during the test, provided the testing machine is of sufficient capacity. Time to fracture is somewhat increased due to damping, so the testing speed needs to be adjusted to maintain the load-point displacement rate or the time-to-fracture fixed. Both alternatives are considered in the protocol since it is still debated whether it is the current rate of loading, dK/dt , which is important (see e.g. [8]) or the total failure time [9].

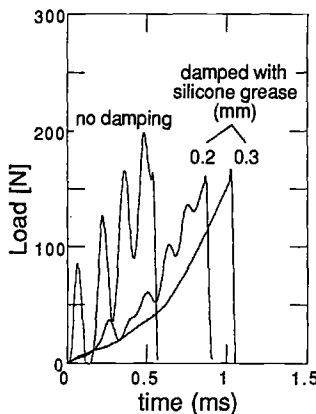


Figure 2 - *Effect of placing a layer of silicone grease of varying thickness on a SE(B) specimen of nylon-6⁴ struck at 1 m/s.*

Overdamping may induce some initial non-linearity in the load trace. That effect must be balanced against the effect on load oscillations: to this end the protocol requires that damping is contained to a minimum sufficient to confine load oscillations within the allowed limits of $\pm 5\%$ of the load at fracture initiation, P_Q , with reference to the current value of the fitting force curve, $\bar{P}(t)$ (see below). This condition must be verified in the portion of the force/time record where the force exceeds 1/2 of its value at fracture initiation, as shown in Figure 3b. Occurrence of force peaks and major fluctuations in the initial part of the load/time record is tolerated.

In view of the energy measurements, the degree of mechanical damping must be strictly controlled. Preparation of the damping device requires some skill to give reproducibility.

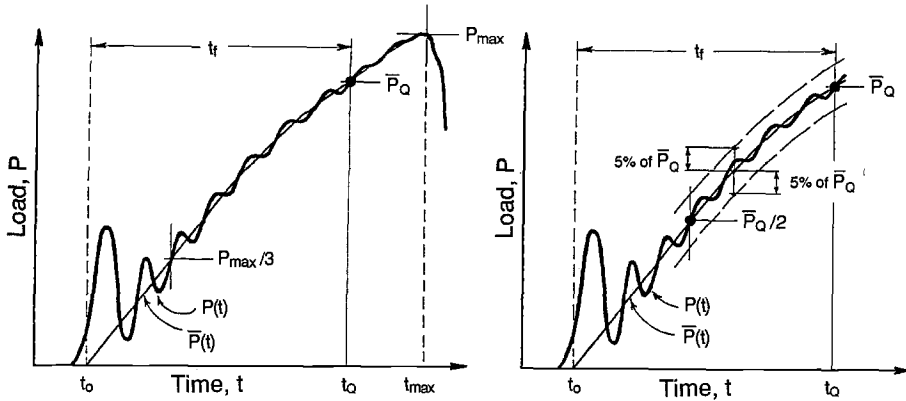


Figure 3 - a (left): curve fitting and determination of load at fracture initiation \bar{P}_Q (not shown) and time to fracture t_f (schematic). b (right): limits of allowable force fluctuations in the fracture test (schematic).

Determination of K_{IC} (via P_Q)

The same rules as those set out in E 399 and incorporated in the ESIS parent protocol [2] for the low rate case, are used to determine the load at fracture initiation, P_Q . As in the low rate case, a limited degree of ductility is allowed and the same method is used to determine fracture initiation when the load curve is moderately non-linear: the 5% offset load, $P_{5\%}$, is taken and the validity of the results is determined via the degree of linearity according to the $P_{max}/P_{5\%} < 1.1$ criterion.

However, in the presence of some, albeit contained, fluctuations in the load signal, application of the 5% offset construction is less straightforward. It is therefore suggested to "smooth" the recorded load trace further. This is to be obtained by curve fitting the experimental curve, $P(t)$, to the following empirical equation:

$$\bar{P}(t) = a(t-t_0) - b(t-t_0)^n \quad (2)$$

where t is time, t_0 , a , b and n are positive fitting parameters and an over-dashed letter is used to indicate fitted values of force. To avoid the major disturbances occurring in the initial part of the load/time record, the regression analysis should be confined to the portion of the experimental curve comprised in the time interval defined by $P_{max}/3$ and P_{max} (see Figure 3a). This curve, $\bar{P}(t)$, should then be used to determine $P_{5\%}$. On Figure 3a back extrapolation of $\bar{P}(t)$ is also shown to illustrate the definition of initial time, t_0 ,

and hence the determination of the time-to-fracture $t_f = t_Q - t_0$.

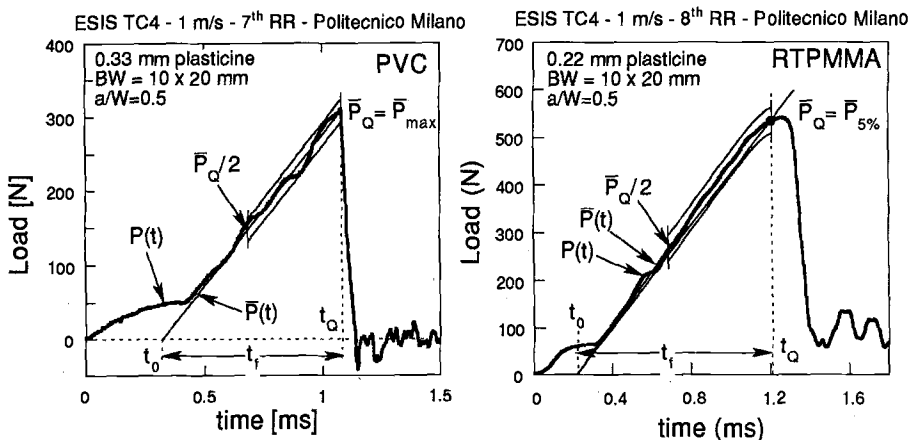


Figure 4 - Examples of application of curve fitting and check on force fluctuations.
Damping obtained by a layer of plasticine (thickness shown) on SE(B) specimens.
Material: a (left) PVC,⁶ b (right) RTPMMA.⁷ BW=area of test specimen cross-section,
 a/W =relative crack length.

This procedure was tested on both linear (brittle) and moderately non-linear (semiductile) fractures, such as exemplified by polyvinylchloride (PVC) (Figure 4a) and rubber-toughened polymethylmethacrylate (RTPMMA) (Figure 4b), respectively, and it was found to be effective.

Determination of G_{IC}

As with the low-rate method [2] both load and displacement are to be measured in the fracture test in order to derive energy from integrating the load versus load-point displacement diagram and the method must include careful measurements and corrections for machine compliance and specimen indentation (unless an external displacement measuring device is used, e.g. optical, but at high speeds this would be impractical).

At impact speeds and with a mechanical damping device in place, the area under the

⁶Sicodex 528809, manufactured and kindly supplied by EVC International SA/NV, Brussels, Belgium.

⁷Altuglas EI50, manufactured and kindly supplied by Atohaas Italia s.r.l., Rho (Milano), Italy.

measured load/displacement curve, U_Q , contains additional spurious contributions which need to be removed before G_{IC} can be calculated. As in P the low-rate case, a portion of the correction can be estimated from a separate test, to be performed on an unnotched specimen [4]. Damping rather complicates the energy analysis since the damper absorbs a large fraction of the energy applied. But even more problematic is the evaluation of the kinetic energy of the moving test specimen and of the energy associated with the inertial loads.

Since inertial loads are essentially independent of crack length as has been demonstrated in [10] and the same is true for the kinetic energy term, it is suggested in

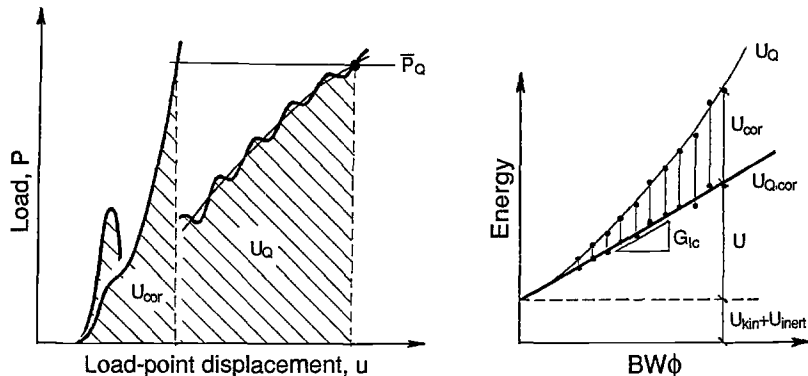


Figure 5 - a (left): Evaluation of energy U_Q (from a fracture test) and correction energy U_{cor} (from the correction test). b (right): Determination of G_{IC} from corrected energy values, $U_{Q,cor} = (U_Q - U_{cor})$. U_{kin} , U_{inert} =kinetic and inertial energy terms, respectively. U =true fracture energy.

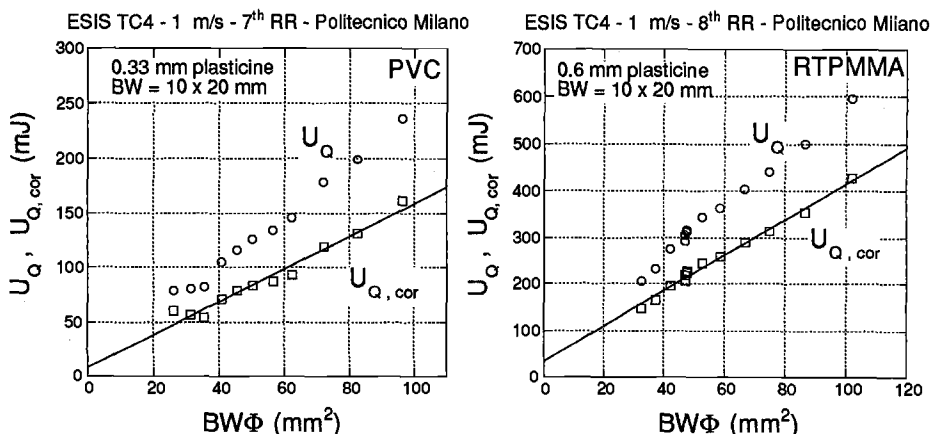


Figure 6 - Examples of G_{IC} determination. Material: a (left) PVC,⁶ b (right) RTPMMA.⁷

[6] to follow an alternative, multispecimen procedure which circumvents the need of evaluating those two terms at all. G_{IC} can be determined from the slope of a plot of fracture energy, U , versus the crack-length dependent calibration factor, ϕ [1], to be obtained by testing a series of specimens with equal dimensions but varying crack length. Since the two parasitic energy terms mentioned above are essentially independent of crack length, the slope will be unaffected and no correction is necessary. The method is schematically illustrated in Figure 5.

Examples of its application are shown in Figure 6.

Collated Results from ESIS Round Robins

The development of the testing protocol briefly illustrated above is the collective effort of some thirty laboratories across Europe (see Acknowledgments) over a five-year span. Eight round robins were conducted within ESIS TC4 with an average participation of fifteen groups. Seven materials were tested, varying in stiffness, toughness and ductility. For each material, all the samples were prepared (normally in the form of plane sheets) at one source, but the individual specimens were generally machined and notched at the laboratories which tested them, though the use of specimens prepared from the same workshop was also tried to assess reproducibility. Use of different test equipment, test geometries, damping materials and, of course, operators of varying expertise from the different laboratories was included in the philosophy of round robin exercises.

The following (Figures 7 to 10) are results obtained in the last two round robins conducted within ESIS TC4 to validate the final draft of the 1 m/s testing protocol [4].

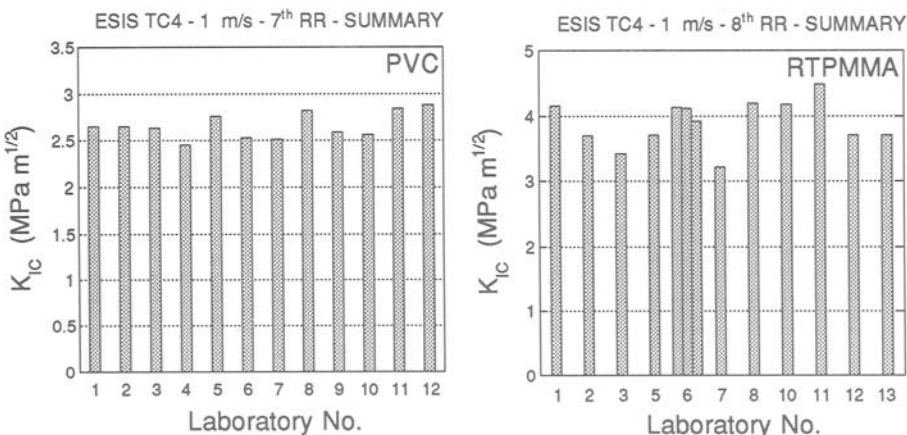


Figure 7 - K_{IC} results (average values) from the 7th (left) and 8th (right) ESIS TC4 round robins on PVC⁶ and RTPMMA⁷ respectively.

The 7th round robin used a sample of polyvinylchloride (PVC) producing fairly linear loading curves up to the maximum load, followed by unstable (brittle) fracture, as illustrated in Figure 4. To assess the applicability of the protocol to moderately non-linear fractures, a sample of rubber-toughened polymethylmethacrylate (RTPMMA) showing some ductility and limited stable crack propagation before the load drop, as seen in Figure 5, was used.

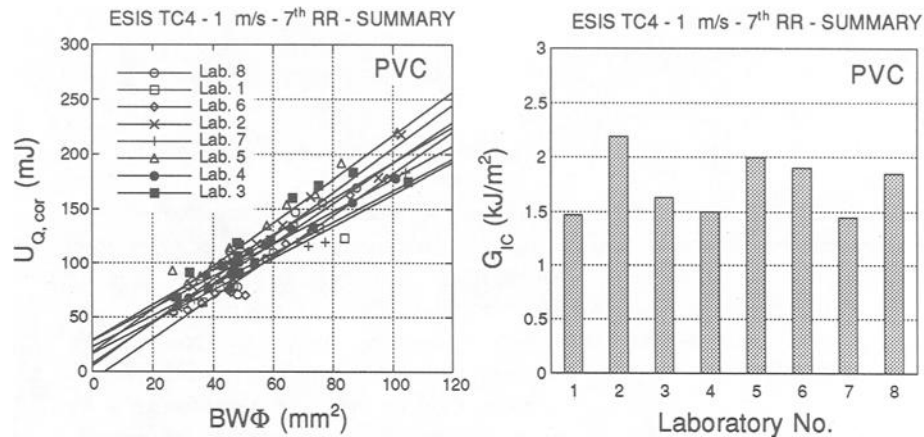


Figure 8 - G_{IC} results from the 7th ESIS TC4 round robin on PVC⁶. Values shown on the right-hand bar plot are slopes of the linear fits shown in the left-hand diagram.

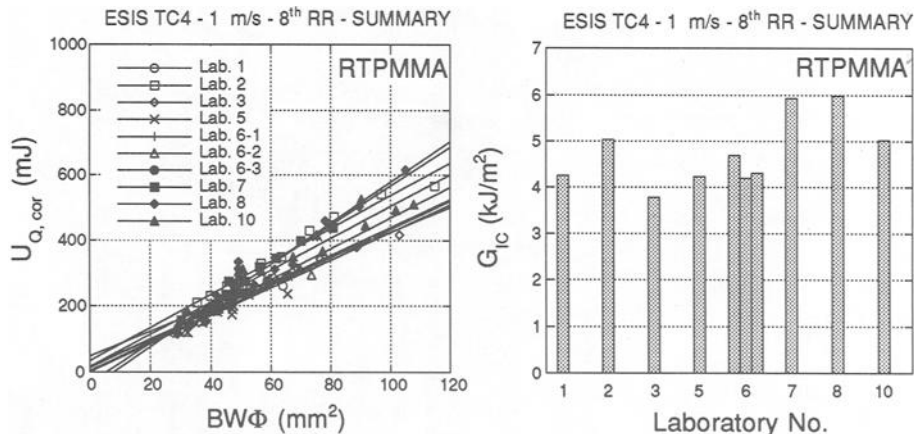


Figure 9 - G_{IC} results from the 8th ESIS TC4 round robin on RTPMMA.⁷ Caption as per Figure 8.

It should be recalled, from [4], that each test result was the average of five individual determinations for K_{IC} and fifteen separate measurements (on specimens of varying crack length) for G_{IC} . Only the results obtained by sticking rigorously to the protocol are reported here.

The significance of interlaboratory consistency of the collected data can be appreciated by comparison of the results obtained here (Figures 7 to 10) with data reported in [2] and ASTM D 5045-93 for interlaboratory measurements of K_{IC} and G_{IC} at quasi-static testing rates. Precision of K_{IC} determinations is similar at low testing rates [2 and D 5045-93] and at 1 m/s (Figure 7) and, rather unexpectedly, also the reproducibility of the determinations of G_{IC} at 1 m/s (Figure 8 and 9) compares well with that obtained at lower rates [2 and D 5045-93] in spite of the more elaborate procedure adopted and the larger corrections involved in the high rate testing determinations as compared to the low rate case.

Variability in K_{IC}^2/G_{IC} (Figure 10) is of course the combined effect of the variabilities of K_{IC} and G_{IC} . It is worth observing, however, that the average value obtained for this

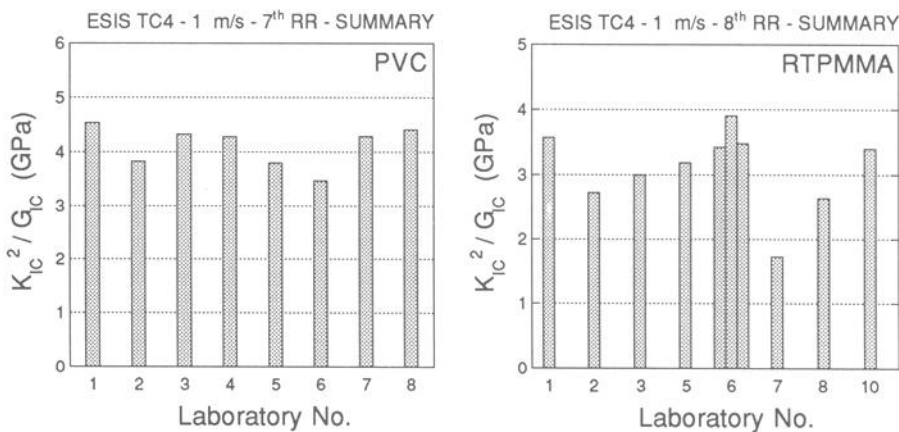


Figure 10 - *Plane strain modulus as determined from fracture test results from the 7th (left) and 8th (right) ESIS TC4 round robins.*

parameter agrees well with direct measurements of modulus E, confirming the good quality of the fracture test results. For example, for the PVC sample used in the 7th round robin a value of 3.7 was reported⁸ for the tensile modulus measured at 800 Hz, which corresponds to a value of 4.15 for the plane-strain modulus if a value of 0.33 is assumed

⁸F. Ramsteiner, private communication.

for Poisson's ratio. No direct evaluation of the modulus of the RTPMMA material used for the 8th round robin is available.

Conclusions

Application of fracture mechanics to characterize toughness at high loading rates deserves special attention because of dynamic effects inherent in the test. With polymers at speeds around 1 m/s these effects can be contained or circumvented, and K_{IC} and G_{IC} can be determined with sufficient accuracy. The protocol developed within ESIS TC4 has been validated by a large amount of experimental data and thus has now been submitted to ISO for consideration as an international standard [11].

Acknowledgments

The following organizations and experts took part in several of the eight round-robbins carried out within ESIS Technical Committee 4, to establish the 1 m/s testing protocol presented in this paper (number in parentheses is the testing laboratory identification number used in Figures 7 to 10): Delft University of Technology, NL (A. Bakker, J. Dekker); EPFL, Lausanne, CH (Ph. Béguelin) (13); Universidad de Oviedo, Gijón, E (J. Belzunce); IWM, Freiburg, D (W. Böhme); BP Chemicals, Grangemouth, UK (M. J. Cawood, Q. Clutton, A. Gray, A. J. Hemingway) (5); Du Pont, Wilmington, DE, USA (R. G. Bender, B. A. Crouch); Ciba-Geigy, Marly, CH (M. Fischer); Solvay, Brussels, BE (A. Goldberg); Martin-Luther University, Merseburg, D (H. W. Grellmann, S. Seidler); The Welding Institute, Abington, UK (G. E. Hale); University of Kaiserlautern, D (J. Karger-Kocsis); Montan University, Leoben, A (Z. Major) (2); Pipeline Developments, Manchester, UK (P. Marshall, P. Harry, K. Morley); ICI, Wilton, UK (R. Moore, R. Prediger) (7); Eastman Kodak, Kingsport, Tenn., USA (E. J. Moskala); Rhône-Poulenc, Aubervilliers, F (G. Orange); LMPL-ENSMA, Futuroscope, F (J. Parisot); Cranfield University, Bedford, UK (D. Ayre, A. Karpodinis, I. Partridge) (9); Technical University, Budapest, HU (B. Pukánszky); BASF, Ludwigshafen, D (F. Ramsteiner) (3, 4); University of Twente, NL (P. E. Reed, L. Warnet) (1); INSA Lyon, Villeurbanne, F (H. Sautereau) (12); EAHP-ICS, Strasbourg, F (Ch. Fond, Ch. Goett, R. Schirrer); VTT, Espoo, FI (A. Sivola) (8); DSM, Geleen, NL (H. Bos, P. Habets, G. Struyk); Elf-Atochem, Serquigny, F (N. Chedozeau, F. Fernagut, L. Tézé) (11); Imperial College, London, UK (L. Braga, M. Chong, H. MacGillivray, J. G. Williams) (10); Politecnico di Milano, I (A. Pavan) (6).

References

- [1] Williams, J. G., "Fracture Mechanics of Polymers", Ellis Horwood, Chichester, UK, 1984.
- [2] "A Linear Elastic Fracture Mechanics (LEFM) Standard for Determining K_C and G_C for Plastics", Testing Protocol prepared for ESIS TC4 by J. G. Williams, 1990.
- [3] "Plastics. Determination of Fracture Toughness (G_C and K_C) - Linear Elastic Fracture Mechanics (LEFM) Approach", ISO/DIS 13586.
- [4] "A Linear Elastic Fracture Mechanics (LEFM) Standard for Determining K_{IC} and G_{IC} for Plastics at High Loading Rates", Testing Protocol prepared for ESIS TC4 by A. Pavan (final draft: Sept. 1997).
- [5] Venzi, S., Priest, H. A., May, M. J., "Influence of Inertial Load in Instrumented Impact Tests", *Impact Testing of Metals, ASTM STP 466*, American Society for Testing and Materials, 1970, pp. 165-180.
- [6] Williams, J. G., *International Journal of Fracture*, Vol. 33, 1987, pp. 47-59.
- [7] Williams, J. G., and Adams, G. C., *International Journal of Fracture*, Vol. 33, 1987, pp. 209-222.
- [8] Béguelin, P., and Kausch, H. H., *Journal of Material Science*, Vol. 29, 1994, pp. 91-98.
- [9] Frassine, R., Rink, M., and Pavan, A., "On the Viscoelastic Time-Dependence of Fracture Toughness at High Loading Rates in Polymers", *Impact and Dynamic Fracture of Polymers and Composites*, ESIS 19, J. G. Williams and A. Pavan, Eds., MEP, London, UK, 1995, pp. 103-111.
- [10] Zanichelli, C., Rink, M., Riccò, T., and Pavan, A., *Polymer Engineering and Science*, Vol. 30, 1990, pp. 1117-1124.
- [11] "Plastics. Determination of Fracture Toughness (K_{IC} and G_{IC}) at High Loading Rates", ISO/CD 17281.

Norman Brown,¹ Xici Lu¹

PENT-Universal Test for Slow Crack Growth in Plastics

Reference: Brown, N. and Lu, X., "PENT-Universal Test for Slow Crack Growth in Plastics," *Limitations of Test Methods for Plastics, ASTM STP 1369*, J. S. Peraro, Ed., American Society for Testing and Materials, West Conshohocken, PA, 2000.

Abstract: Slow crack growth (SCG) under plane strain conditions as measured by the PENT test is governed by the stress intensity, K. The PENT test, ASTM specification F 1473, which was originally designed to measure the resistance to SCG in pipes, fittings, and resins for conveying gas, can be used to measure the resistance to SCG in all polyethylene products. The resistance to SCG as measured by the PENT test in hours has been directly correlated with the lifetime of large scale gas pipe systems and is expected to be correlated with the lifetime of all polyethylene piping systems. The PENT resistance to SCG has been measured on various polyethylene products. It is now possible to specify a resistance to SCG of a PE resin as measured by the PENT test which will satisfy the commercially desired lifetime of the product. For example, a gas pipe system that contains a polyethylene resin with a PENT value of 100 h will exhibit practically no SCG failures during its first 100 years of service. It is recommended that the PENT test replace the ESCR test, ASTM D 1693, in all the ASTM specifications and that it should be used in place of the ISO specification in ISO 138/SC4, known as the British Gas Notch Test.

It is shown how the PENT test can be applied to all polymers that exhibit SCG.

Keywords: slow crack growth, polyethylene, PENT test

¹Professor Emeritus and Research Associate Department of Materials Science and Engineering, University of Pennsylvania, LRSM, Philadelphia, PA 19104.

Introduction

Slow crack growth (SCG) is a phenomenon that occurs in most plastics. It is characterized by (1) crack growth under constant stress, (2) crack initiation at a point of stress concentration, (3) the remaining specimen being essentially undeformed, (4) a craze which precedes the crack, and (5) the global stress being well below the macroscopic yield point. The rate of SCG depends upon the environment. A fatigue crack has the same characteristics except that the stress is oscillatory. Sometimes SCG is called static fatigue. In this paper, SCG will be considered in the absence of an environmental factor except for air and a constant applied stress.

The ASTM Test Method to Measure the Resistance to SCG of Polyethylene (PE) Pipes and Resins (F1473) is generally known as the PENT test, initially focused on gas pipes. It is applicable to all PE products and to other plastics in which SCG occurs. Over 90 research papers on SCG in PE have demonstrated the relevance of the PENT test to engineering design and its applicability to product material behavior for end use applications [1, 2, 3]. This research shows how the methodology of the PENT test on PE can be extended to other polymers.

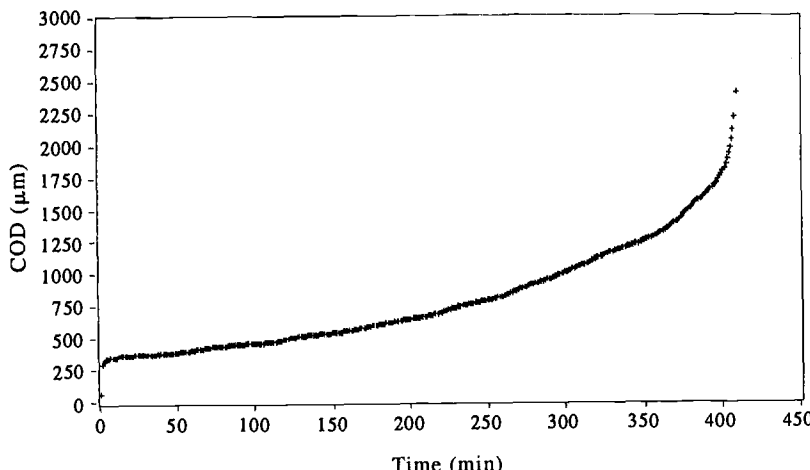


Figure 1- COD versus Time for Ethylene-Hexene Copolymer Manufactured 1980.

SCG in PE

When a notched specimen of PE is under a constant stress (load over unnotched area) and under plane strain conditions, the typical curve of crack opening displacement (COD) versus time is shown in Figure 1. The initial COD on loading is associated with a craze that forms at the root of a notch as in Figure 2. The COD grows slowly as the fibrils of the craze extend until the crack initiates when the fibrils at the base of the craze fracture. Then the COD accelerates as the crack propagates behind a craze until complete failure occurs. The time for crack initiation is a significant fraction of the total time to failure (t_f) and is related to it because both crack initiation and propagation are related to the time for a fibril to break. Extensive microscopic examinations show that the fractured surface which is produced in the laboratory is identical to those observed in gas pipes that failed after long times in service.

The stress intensity (K) is the primary driving force for SCG. The J integral is slightly better [4], but the simplicity of K makes it preferable for practical applications. Tensile and bending tests in which notch depth, stress and specimen dimensions were varied justified the use of K . The failure time is governed by the following equation [5]:

$$t_f = A K^n \exp[Q/RT] \quad (1)$$

$n = 2.6-4.8$ depending on the PE

$Q \approx 100 \text{ kJ/mol}$ for all PE

A is a material property that can vary by a factor of 10^6 .

$$K=Y S a^{1/2}$$

(2)

Y depends on geometry of specimen and on the loading method.

S=stress based on unnotched area

a= notch depth

Equations 1 and 2 can be used to predict SCG failure in any PE product if Y can be determined and SCG occurs under plain strain conditions. The limitations are (1) the global stress should be less than about half the yield point at the test temperature to avoid a significant amount of macroscopic creep in the specimen, (2) the test temperature should be less than 80°C to avoid the effects of oxidation or changes in the morphology, (3) the notched area should be less than about 40 % of the cross section area, and (4) the thickness should be such that the fracture is predominately plain strain.

Primarily, the differences in the resistance to SCG among polyethylenes is distinguished by A, which depends on the molecular and morphological structure of the material. The morphology depends on the thermal history and processing of the resin into a product.

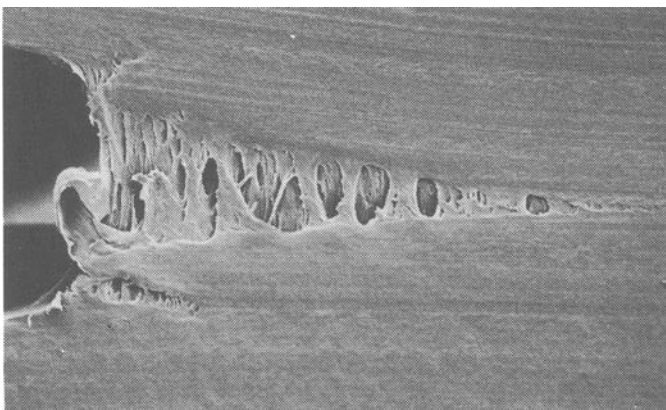


Figure 2- Craze in Polyethylene.

The PENT Test

ASTM F1473 describes test specimens from pipe and from the resin. This presentation will be focused on PENT testing of the resin from compression molded plaques. PENT is a single edge notch tensile test. A representative specimen is shown in Figure 3. Other dimensions are given in the specification. In the specification a standard value of $K = 0.468 \text{ MPa m}^{1/2}$ has been established. This value was chosen to insure that all PE would fail by the mechanism of SCG at 80°C. If K is too high, the failure could occur by a complex combination of shear deformation and fracture which is not the long time mode of failure that occurs under field conditions. The thickness of the compression

molded plaque can be varied from 4 to 20 mm, and there is a table in ASTM F1473 with corresponding notch depths that produce the standard value of K. The morphology of the resin is set in a standard state by specifying the molding conditions. The plaques are very slowly cooled because this is a readily reproduced condition and because the failure times are minimized for resins with a high resistance to SCG. The standard PENT test conditions for evaluating the resistance to SCG of a PE resin are as follows:

$$T = 80^\circ \text{ C} \quad S = 2.4 \text{ MPa} \quad a = 3.50 \text{ mm} \quad \text{specimen thickness} = 10 \text{ mm.}$$

The notch is made by pressing a razor blade into the specimen slower than 0.25 mm per min. The temperature should be controlled within $\pm 0.5^\circ \text{C}$ since a 1°C change near 80°C changes t_f by 12%.

Twenty carefully controlled tests on a single resin whose average PENT lifetime was 47.8 hours had a scatter of 7.6%. For most purposes, 2 tests are used to measure t_f , and the scatter is usually less than 15% of the average value. 6 round robins have been run at 5-10 industrial laboratories. The average reproducibility within a laboratory was 15% and the precision of the average values among the laboratories was 25%. Part of the difference between laboratories may be caused by a difference in the testing rigs from different manufacturers.

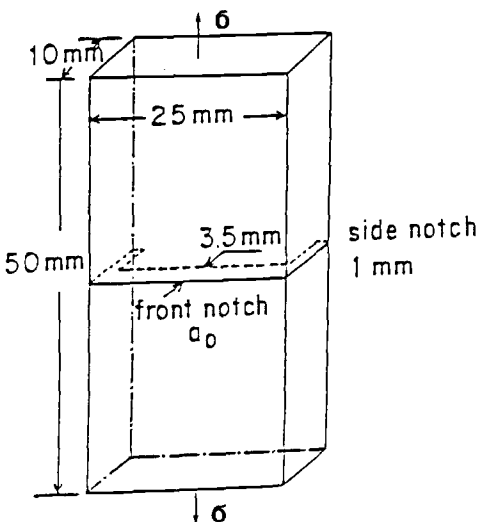


Figure 3-Specimen Geometry.

Applications of the PENT TEST

The most critical use of polyethylene is conveying gas. The resistance to SCG of practically all the gas pipe which has been used in the world since 1967 has been measured by PENT. A partial list of these resins is shown in Table 1, which shows the range in quality of the gas pipes with respect to their resistance to SCG. There has been a general improvement in quality since 1967. Currently about 20 gas grade resins are being produced in the world. It is important to note that the lot-to-lot quality may vary by a

factor of 3. Thus quality control testing of each lot is recommended. Many of the low quality resins are still in the ground, and these pipe lines should receive special surveillance.

Table 1 - *PENT Lifetime of PE Gas Pipe Resins Produced from 1965 to 1998*

Off the Market	On the Market
PENT(hr)	PENT(hr)
0.3#	85
0.7+	159
1.4	170-409*
2.2	308-1130*
9	497
14	500-16,667*
34	1320
28-50*	3733
48	7517
75	45,000

*lot to lot variation

#replaced completely

+ being replaced

The frequency of SCG failures is related to the PENT life time of the resin. Table 2 shows the relationship between the frequency of failures in large scale gas pipe systems and the PENT lifetime.

Table 2 - *Relation of PENT Lifetime to SCG Field Failures [3]*

Resin	PENT Life(hr)	SCG Field Failures
3306	0.3	Immediate replacement after 25 yr.
NIPAK	0.8	Replacing 800 mi after 25 yr. of service
Aldyl A	1.4	0.25 failures/mi after 9-21yr. of service
TR418	14	0.011 failures/mi after 10-15 yr. of service
	>14	No report of failures

The Aldyl resin with tf of 1.4 hr was the first widely used resin that was initially installed in 1966, and many thousands of miles are still in service; it has suffered a sufficiently low frequency of SCG failures that only selective replacement of the pipe has been necessary. The TR 418 resin with a tf of 14 hr was introduced about 1972. Many thousands of miles are in use, and an extremely low SCG failure rate has been reported. However, the entire pipe line with the tf of 0.3 hr has been replaced completely after about 25 years of service, and the one with a tf of 0.8 hr is being replaced. These pipelines were designed before the SCG type of failure was recognized. No failures have been reported for resins with PENT lifetimes greater than 14 hr because they have not been in service long enough and their frequency of failures is inversely related to their PENT lifetime. Based on these data and the experience of many gas companies it has been recommended by industry that the minimum PENT lifetime of a gas pipe resin be 100 hr. The 100 hr minimum for the PENT lifetime is being balloted in ASTM Committee F17.60 for inclusion in ASTM D2513.

The question is often asked as to the relationship between the lifetime of the compression molded resin and that of the pipe or fitting. The lifetime of the product is proportional to the PENT value of the resin as shown in Figure 4. The proportionality factor depends on how the product is fabricated. Since the fabrication process usually

orients the molecules, the orientation of the notch relative to the orientation direction is important. In pipes, the molecules are oriented in the extrusion direction. Table 3 shows that cracks grow faster parallel to the orientation direction than transverse to it. In the case of gas pipe lines the service failures occur most frequently at the thin fusion joint between pipes and fitting, and a small number are initiated in the pipe by rock impingement or by damage produced by squeeze-off. Thus the PENT lifetime of the resin is more relevant to the frequency of failures than is the PENT lifetime of the pipe itself.

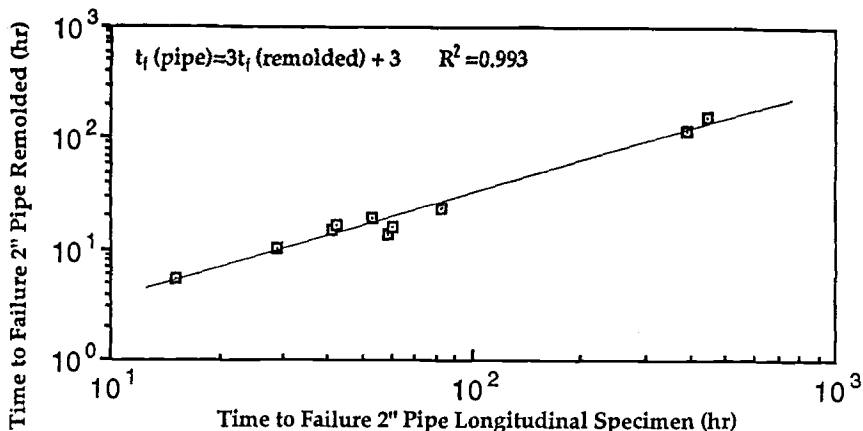


Figure 4- Failure Times TR418 2" Pipes Manufactured 1973-1985 by Same Extruder

Table 3 - Effect of Notch Direction on Time to Failure by Slow Crack Growth
80°C, 2.4 MPa

Notch Depth 3.5 mm for 110 Pipe, 2.0 mm for 60 mm Pipe
Time to Failure (min.)

Pipe	Notch Parallel to Pipe Axis	Notch Perpendicular to Pipe Axis	Ratio	$\frac{tf()}{tf(\perp)}$
A	92	96	0.96	
B	939	1116	0.84	
C	3167	6766	0.47	
D	161	329	0.50	
E	1113	6493	0.17	

A = 110 mm MDPE - mfr 1967

B = 110 mm MDPE - mfr 1985

C = 110 mm MDPE - mfr 1972

D = 110 mm HDPE - ISO (Round Robin 2)

E = 60 mm HDPE - ASTM A

The life expectancy of a PE products is related to its resistance to SCG. Table 4 shows the PENT lifetime of the resin currently used in various PE products.

Table 4 - PENT Lifetime of PE Products

Product	PENT (hr)
Milk Bottle	0.01
Drainage Pipe	0.1-1
Bleach Bottle, Household utensils	0.12
Gas Pipe-1965 vintage	1.4
Large Storage Tanks, Drums	5
Gas Pipes-1972 vintage	14
Sleeve for Under Water Cable	167
Gas Pipes from current USA Resins	100-10,000
Water Pipes	100-10,000
Geomembranes	≈1000

Now the producer of a PE product can specify the desired quality in terms of a PENT lifetime. If the current frequency of SCG failures of the product is not satisfactory, a new PENT life time can be specified with respect to the current lifetime. The frequency of SCG failures in a product is proportional to the PENT lifetime of the resin. Generally the price of the resin increases with the PENT lifetime because more comonomer and or a higher molecular weight are required.

PENT in ASTM and ISO Specifications

There are various ASTM committees and specifications that are concerned with the resistance to SCG of PE resins (Table 5). The common desire of these committees and the fundamental purpose of these specifications is to have a test that precisely measures the resistance to SCG of the PE resin and is related to the performance of the product.

Table 5 - ASTM Committees and Specifications Involved with SCG of PE.

Committee	Specification
F17.26--Water Pipe	D2104--Water Pipe
F17.60--Gas Pipe	D2513-- Gas Pipe
F17.62--Sewer Pipe	Balloting New Sewer Pipe Specification
F17.63--Drain and Waste Pipe	F 810 Drain and Waste Pipe Specification
F17.65--Land Drainage	Balloting New Land Drainage Specification
D35.02--Endurance of Geosynthetics	D 5397--Geomembranes
	D1998--Storage Tanks
	D 3350--Pipes and Fittings
	D 4976--Extruded Products
	D 1248--Jackets for Wire and Cable

Environmental Stress Cracking Resistance (ESCR) of PE (D 1693) is the oldest and most common test method for SCG. Compared to the PENT test, (1) it has poor precision with respect to inter-laboratory reproducibility being about 60%, (2) it takes longer to get a result and uses an Igpal environment that can contaminate the laboratory, (3) it involves different test conditions depending on the grade of the PE, (4) its stress intensity cannot be defined. It is recommended that all ASTM committees in Table 5 that are concerned with the resistance to SCG of their PE product remove their ESCR requirement and insert the PENT test. Each committee can then more precisely specify the desired quality of their resin with the assurance that the PENT lifetime will be related to the performance of their

product. ASTM Specifications D 3350 and D 4976 which now contain the PENT test provide a range of cell classifications for choosing the quality of the PE.

The standard test in ISO for measuring the resistance to SCG is the so called "British Gas Notch Test" that originated in ISO 138/SC4 gas committee. This test is done on a pressurized pipe with a notch depth that is 20% of the pipe thickness. Test temperature is 80°C and hoop stress is 4.6 or 4.2 MPa for PE 100 or PE80 respectively. The minimum required failure time is 165 hr. The basic purpose of the test is to assess the resistance to SCG of the resin. This test is inferior to the PENT test for the following reasons:

1. The pipe size and SDR are not specified therefore the results depend on how the pipe is processed.
2. The stress intensity is a variable because it depends the absolute value of the notch depth and not simply on the ratio of notch depth over thickness.
3. The pipeline consists of pipes of various size, fittings and the important fusion zones between fittings and pipe where most failures occur. Therefore a test on a pipe may not be the best indicator of the performance of the pipe line.
4. The ISO test requires a pipe whereas the PENT test is done on the resin.
5. ISO has a minimum requirement of 165 hr. The PENT test requires a minimum of 100 hr. to show that the resin will give excellent performance in the field.
6. The ISO test requires more expensive equipment and space than the PENT test.

Applying PENT to Other Polymers

The PENT test specimen can be used to measure SCG in all polymers that exhibit SCG failure as described in the introduction. Based on Fracture Mechanics, the geometry of the PENT specimen assures that the driving force for SCG under plain strain conditions is governed by the stress intensity. For resins with a higher yield point than PE the width of the specimen could be somewhat less. A major purpose of any test is to accelerate SCG in the laboratory in order to obtain useful results as soon as possible. Thus the highest possible stress and temperature should be used. The maximum test temperature that can be used must not produce significant molecular or morphological changes in the resin; otherwise the test results will not relate to the performance in service at lower temperature. If oxidation is not a factor that influences SCG at the service temperature, then it must not be a factor at the test temperature. A detailed understanding of the affect of temperature on the polymer must be obtained before the highest possible test temperature can be specified.

The highest stress that can be used is generally related to the yield point at the test temperature. In the case of PE it was found that, if the global stress is less than about one-half the yield at the test temperature, then the microscopic appearance of the fracture at the test temperature was the same as that at room temperature. A similar microscopic investigation must be done with any polymer under a range of stress to determine the highest stress that will produce the same failure mode in the test as that under service conditions.

If the service failure in a polymer is associated with a particular environmental agent, then it is most important to determine whether the test in air is relevant to the failure in service. The ranking of a polymer in an air environment may or may not give the same ranking as in the service environment, but only detail testing can answer this question.

There are polymers that do not craze and that do not exhibit SCG. It was found that PE with a critical amount of cross-linking did not fail by SCG. Nylon 11 did not exhibit SCG. These polymers formed a shear deformation zone at the root of the notch. Before conducting extensive tests on a new polymer, it is suggested that the damage zone at the root of the notch be examined microscopically after the specimen is initially loaded. If crazing is observed, the polymer is probably susceptible to SCG failure.

Conclusions

1. The Stress intensity is the driving force for SCG in plastics.
2. The frequency of SCG failures in a PE product in service is directly related to the lifetime of the resin as measured by the PENT test, ASTM F1473.
3. The ESCR test, ASTM D 1693, should be eliminated from all ASTM specifications and be replaced by the PENT test.
4. The PENT test is superior to the British Gas notched pipe test (ISO 138/SC4) for measuring the resistance to SCG.
5. The PENT test methodology can be used to measure the resistance to SCG in other polymers that craze besides PE.

Acknowledgment

This research was sponsored by the Gas Research Institute.

References

- [1] Lu, X. and Brown, N., "A Test for Slow Crack Growth Failure in Polyethylene Under Constant Stress," *Polymer Testing*, vol 11, 1992, pp 309-312.
- [2] Brown, N., Lu , X., Huang Y., and Ishikawa,N., "The Fundamental Material Parameters that Govern Slow Crack Growth in Linear Polyethylenes," Cambridge Conference on Deformation and Fracture of Polymers, April 1991 Plastic, *Journal Composites Rubber Processing and Applications* 17 (4) 1992 255-258.
- [3] Brown, N. and Lu X. "PENT Quality Control Test for PE Gas Pipes and Resins", *Twelfth Plastic Fuel Gas Pipe Symposium*, publisher American Gas Association., Sept. 24, 1991, p. 128.
- [4] Brown, N., Bassani, J. and Lu, X. "The J-Integral as a Criterion for the Initiation Rate of Slow Crack Growth in Linear Polyethylene," *International Journal of Fracture*, vol. 38, 1998, pp 43-59.
- [5] Brown,N.and Lu, X."The Fracture Mechanics of Slow Crack Growth in Polyethylene", *International Journal of Fracture* vol. 69, 1995, pp 371-377.

Chemical/Rheological

Mark Kelsey¹ and Jonathon Foreman¹

Temperature Measurements in TGA

Reference: Kelsey, M. and Foreman, J., "Temperature Measurements in TGA," *Limitations of Test Methods for Plastics, ASTM STP 1369*, J. S. Peraro, Ed., American Society for Testing and Materials, West Conshohocken, PA, 2000.

Abstract: The temperature of the specimen in thermogravimetric analysis (TGA) is affected by several factors, including specimen mass and heat capacity, transitions in the material, crucible mass and material of construction, and furnace response. Because many thermogravimetric analyzers have a thermal sensor that is separated from the specimen, differences in specimen conditions have no effect on the observed temperature. In this situation, the temperature sensor is calibrated by synchronization to an observed material transition. By using a TGA with a direct contact thermal sensor this study shows that the above effects have significant temperature implications. Furthermore, only by using a TGA with direct-contact temperature sensing can one observe the true sample temperature during a specimen mass change or other transition.

Keywords: temperature, TGA, calibration, furnace response, material effects

Introduction

In thermogravimetric analysis (TGA), heat flows from the walls of the furnace to the specimen mostly by convection. Ideally, the furnace creates a uniform temperature region large enough to expose the specimen, the specimen container and the thermal sensor to the same conditions. Even under ideal conditions, however, the true specimen temperature may be quite different from that of the temperature sensor because the heat absorption rates are different for the thermal sensor and the specimen in its container.

The ASTM Practice for Calibration of Temperature Scale for Thermogravimetry (E 1582) describes methods to calibrate classically designed thermogravimetric analyzers. The ASTM method warns that different instruments similarly calibrated can give results that vary by as much as 20°C. Temperature errors of this magnitude can negatively impact the precision and bias of the results generated using other ASTM methods such as Test Method for Rapid Thermal Degradation of Solid Electrical Insulating Materials By Thermogravimetric Method (TGA) (D 3850). Some factors given for this variation are the location of the temperature sensor, scan speed, nature of the specimen, crucible composition and furnace geometry. TGA instruments with direct contact temperature measurements provide the means to understand better the sources and the magnitude of these errors.

¹ Mettler-Toledo, Inc. Columbus, OH 43240 e-mail:jon.foreman@mt.com

The design for a classical TGA is illustrated below (Figure 1). A balance above the crucible suspends it into a furnace. This configuration prevents direct contact of a temperature sensor with the crucible because contact would disrupt the weight signal. The temperature, therefore, is "in the vicinity" ("itv") of the crucible. Since the specimen and "itv" sensor are two independent bodies of different mass, location, heat capacity, and color, their temperature responses are different. The calibration procedures in ASTM E1582 attempt to synchronize the responses of the "itv" sensor and the specimen.

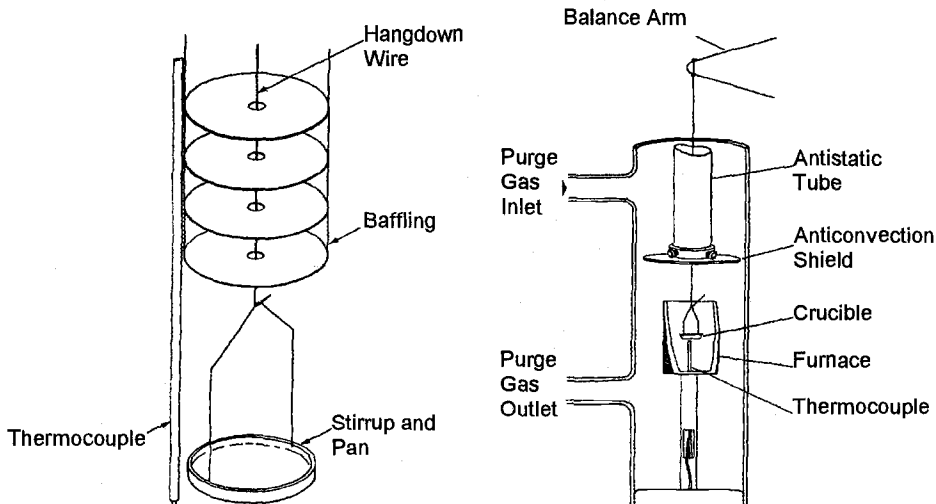


Figure 1 – Traditional TGA Instruments with Non-contact Temperature Sensors

One group of TGA instruments with direct contact thermal sensors is the Mettler-Toledo, Inc. TGA851^e series of thermogravimetric analyzers (Figure 2). These instruments incorporate two temperature sensors, one for temperature control and the other in direct contact with the bottom of the crucible. Direct contact with the crucible provides direct sample temperature measurement and allows the investigation of the sample temperature as functions of furnace response, specimen mass, crucible material, heating rate and transitions.

Theory

Possible modes of heat transfer from a furnace to a specimen are by conduction, radiation and convection. In reality, however, heat transfer occurs only by convection and radiation. Heat transfer does not occur by conduction since the specimen does not directly contact furnace walls. For convection and radiation heat transfer, the heat flow is a function of the difference in temperature of the furnace and the sample as described in Equation 1.

$$\frac{dH_T}{dt} = -\frac{T_f - T_s}{R_t} \quad (1)$$

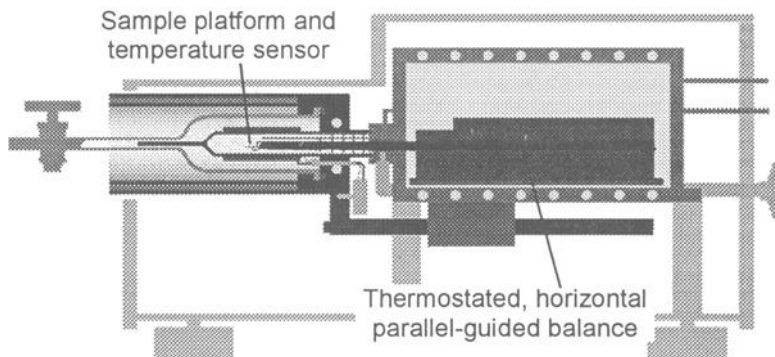


Figure 2 - Schematic of TGA851^e with Direct Contact Temperature Sensor

where

dH_T/dT = heat flow to the system

T_f = furnace temperature

T_s = system or sample temperature

R_t = resistance to heat flow from the furnace to the specimen.

The subscript "T" in equation 1 refers to the heat flow (and later heat capacity) of the total system (crucible, support and specimen). In thermal analysis, the convention is to use the "s" subscript for sample temperature, which is identical to system temperature when all items are in direct contact. A similar equation can be developed for a "reference."

$$\frac{dH_r}{dt} = -\frac{T_f - T_r}{R_t} \quad (2)$$

In Equation 2, the subscript "r" refers to the "reference" conditions. In TGA, the "reference" is all items being heated except the specimen. The net heat flow from the furnace to the specimen is calculated by subtracting the reference heat flow from the furnace heat flow as described in equations 3 and 4.

$$\frac{dH_T}{dt} - \frac{dH_r}{dt} = -\frac{T_f - T_s}{R_t} + \frac{T_f - T_r}{R_t} \quad (3)$$

$$\frac{dH_s}{dt} = \frac{T_s - T_r}{R_t} \quad (4)$$

The heat that flows into the system raises its temperature. The heat flow into the system is a function of the heat capacity of the specimen, specimen container, support, etc., as described in Equation 5. When the temperature sensor and the specimen are

separated the heat flow to these items can be quite different, since the heat capacities of the sensor and specimen will differ.

$$\frac{dH_r}{dt} = -Cp_r \frac{dT}{dt} = -(Cp_s + Cp_r) \frac{dT}{dt} \quad (5)$$

where

Cp_s = specimen heat capacity
 Cp_r = "reference" heat capacities

Unlike system temperature, the system heat capacity can be separated into the specimen and reference heat capacities.

$$\frac{dH_r}{dt} = -Cp_r \frac{dT}{dt} \quad (6)$$

$$\frac{dH_s}{dt} = \frac{dH_r}{dt} - \frac{dH_r}{dt} = -Cp_s \frac{dT}{dt} \quad (7)$$

By equating the heatflows to the specimen from Equations 4 and 7, we arrive at Equation 8. Rearranging equation 8 yields the temperature difference as a function of the system response, Equation 9.

$$-Cp_s \frac{dT}{dt} = \frac{T_s - T_r}{R_t} \quad (8)$$

$$T_s - T_r = -R_t \cdot Cp_s \frac{dT}{dt} \quad (9)$$

It should be noted that a non-contact thermal device measures the temperature of the atmosphere near the crucible. The temperature response is independent of the actual sampling system. Therefore direct contact thermal devices are needed to measure the actual sample and reference temperatures.

Experimental

All experiments are performed on a Mettler-Toledo, Inc. TGA851[°]. The SDTA^{®2} routine of the TGA851[°] measures the temperature difference as described in Equation 9. By virtue of the direct contact thermal sensor, a reference temperature is calculated from a complete set of calibrations. Alternatively, the results of an experimental reference (normally an empty crucible on the support) can be used. In this study the latter method is

² Mettler-Toledo, GmbH, Schwerzenbach, CH 8603, Switzerland.

employed. The important experimental parameters are listed in the results and discussion section for each experiment type.

Results and Discussion

From Equation 9 it can be seen that the temperature difference ($T_s - T_i$) is a function of three factors: the furnace response (R_f), the heat capacity and the heating rate. Each of these three factors are examined below along with discussions of the effects the crucibles and material transitions have on the sample temperature.

Furnace Response (R_f)

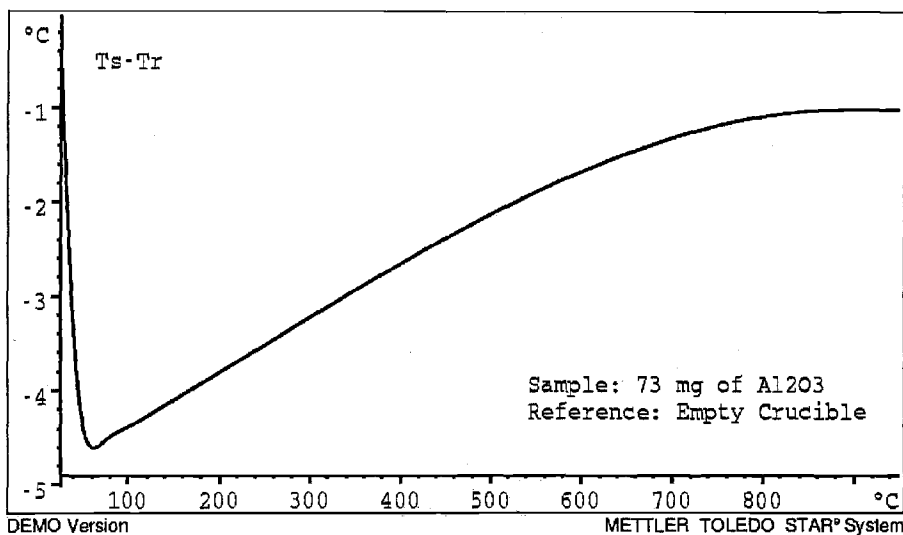
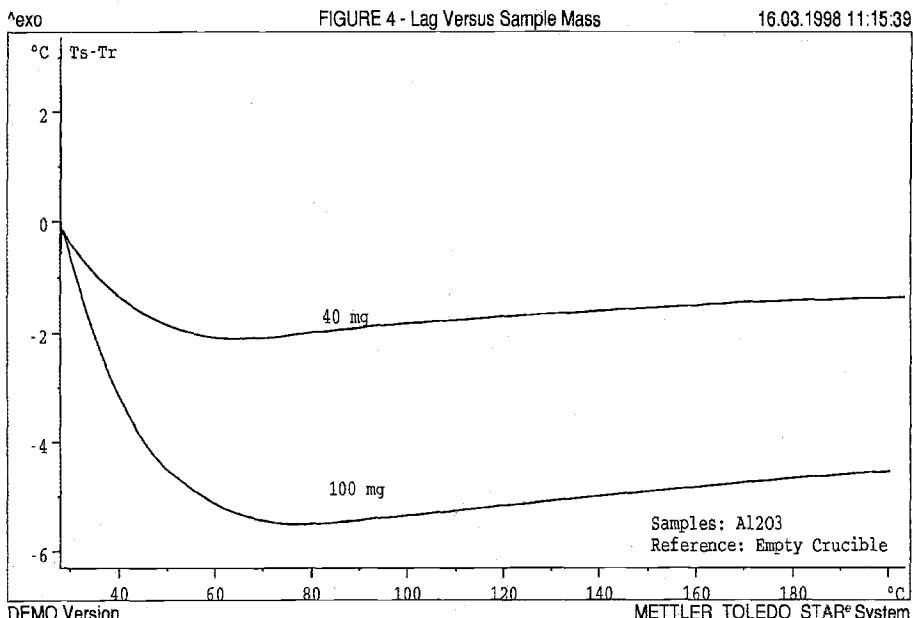
The SDTA temperature difference for a 70 mg aluminum oxide specimen heated in a platinum pan at 20° C per minute is shown below (Figure 3). It can be seen that although the Cp value for this specimen increases with temperature the observed temperature difference actually decreases. The TGA851[®] thus reveals that R_f is not constant over the entire furnace temperature range. This observation is easily explained. At low temperatures, convection and radiation heat transfer are inefficient processes making values of R_f large. As temperature increases, radiation and convection are more efficient and reduce values of R_f . That R_f values change impacts results of traditional TGA's with independent temperature sensors, requiring calibrations at several temperatures to synchronize adequately the response over the instrument operating range.

Heat Capacity

From the preceding discussions, it should be apparent that the masses of the specimen, calibration standards and specimen crucibles will affect synchronization of the temperature sensor response to the sample temperature. As mass increases, the total heat capacity increases and the sample temperature will lag even further behind the surrounding temperature as is observed for two different specimens of Al₂O₃ heated at 20° C per minute (Figure 4). That is, the 100 mg specimen lags behind the 40 mg specimen by several degrees over the entire temperature range. Thus, errors arise with traditional TGA's when the specimen mass and its heat capacity are different from the calibration material. Even more important is that traditional TGA's cannot observe or account for the reduction to total heat capacity when a specimen loses mass during an experiment.

Crucibles

Crucibles also play an important role in the temperature response of the specimen. Figure 5 shows the results of two experiments, one of the sensor without a crucible and a second with a 300 mg platinum crucible in contact with the sensor. The shift due to mass occurs at the beginning. Of course, the magnitude of this shift changes with crucible size and crucible material. Changing crucibles, therefore, requires recalibration. Calibration procedures in which the calibration material does not contact a crucible can never account for this shift and always contains a systematic temperature error by the amount of the lag for the crucible.

Figure 3 - *The Effect of Furnace Response on Temperature Lag*Figure 4 - *The Effect of Specimen Mass on Temperature Lag*

Interestingly, the crucible overcomes the lag from its mass at higher temperatures and actually becomes hotter than the sensor (temperature difference is greater than 0°C). This occurs because R_t values decrease at higher temperatures due to more efficient heat

transfer and the larger surface area of the crucible more readily absorbs convected and radiated heat than a bare sensor. As radiation becomes more efficient, the crucible color becomes an additional complicating factor. Again, with traditional "itv" sensors, the surface area and the color of the sensor do not change requiring calibration for different crucibles at short temperature increments over the full temperature range to characterize fully the heat transfer function.

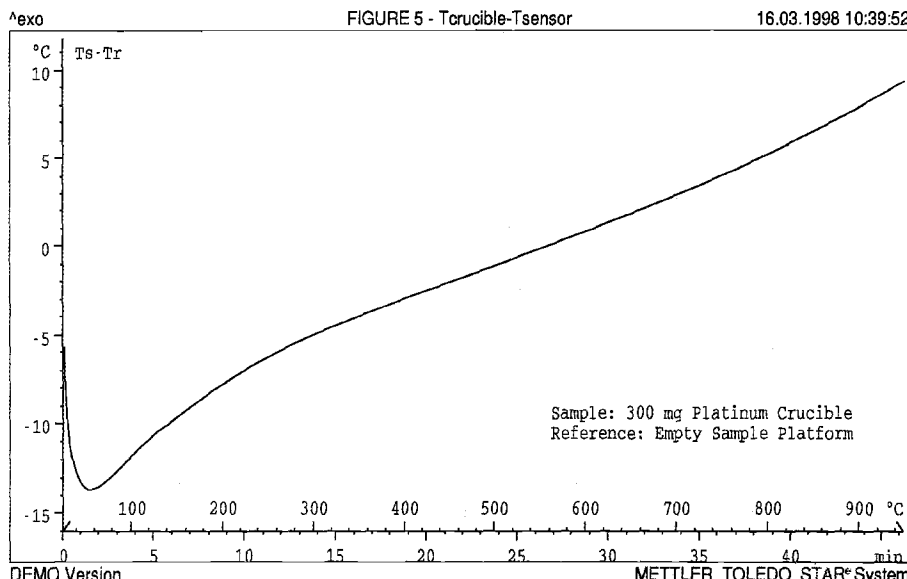


Figure 5- Shift Caused by Platinum Crucible
Heating Rate

Typical temperature gradients between the furnace and a specimen required at different heating rates for a commercial TGA instrument are shown (Table 1). Two facts emerge from these data. The first is that R_t is a function of temperature as seen previously (Figure 3). That is, the furnace advance ($T_f - T_s$) decreases with increasing temperature. The second fact is that the gradient must increase with increasing scan speeds to provide larger heat flow. As heating rates increase, the specimen lags further behind until the temperature gradient is sufficiently large to supply the required heat flow.

The melting of indium as a function of the reference temperature at various scan speeds is shown (Figure 6 and Table 2). The SDTA signal in the TGA851°, which readily detects indium melting, shows that the indium melting temperature appears to increase with increasing scan speeds. Since synchronization occurs only for a single set of conditions, the analyst is limited to a single heating rate for each calibration. Achieving accurate temperature synchronization requires recalibration at each heating rate. The third column (Table 2) shows the error caused at different heating rates for synchronization performed at 20°C/min. Experiments in which heating rates change, such as temperature ramps and holds, are subject to such error. TGA routines that automatically

lower heating rates according to specimen weight changes are especially vulnerable to synchronization errors.

Table 1 - Furnace Advance as Functions of Temperature and Scan Speed

Temperature (°C)	Furnace Advance ($T_f - T_s$) (°C) at		
	10°C/min	20°C/min	50°C/min
25	13	26	67
200	9	17	43
500	4	7	18
700	2	4	11

Table 2 - Melting Point of Indium as a Function of Scan Speed

Scan Speed (°C/min)	Melting Point (°C)	Difference from 20°C/min value (°C)
2	158.6	-8.7
5	160.0	-7.3
20	167.3	0
50	181.1	+13.8

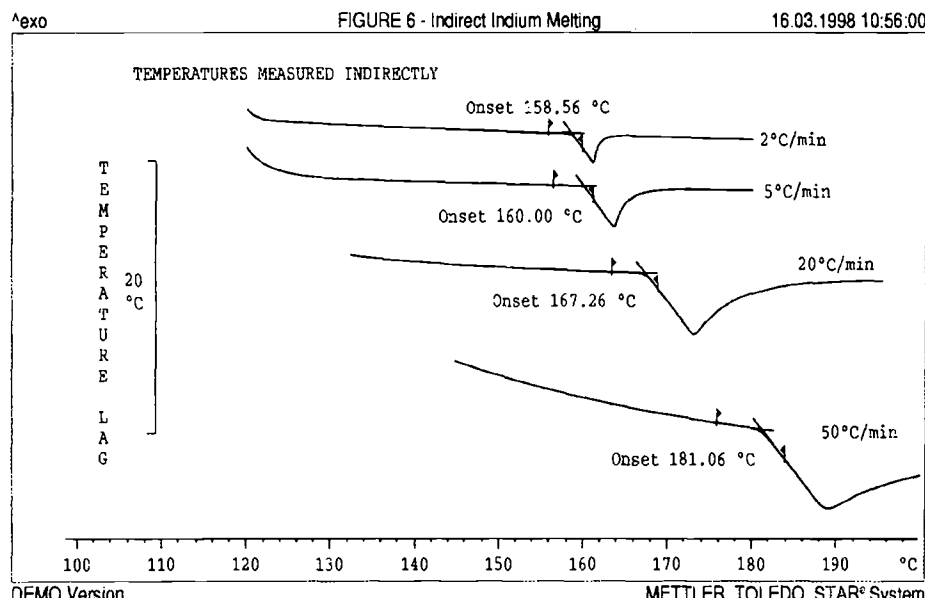


Figure 6 - Indium Melting Measured Indirectly

Figure 7 shows the same indium melting data plotted against direct contact thermal sensor temperatures. Since this sensor directly measures sample temperature, no error occurs as scan rates change. "Total" calibration, in which the lag is determined for different heating rates, reduces the variation between the sample and the control thermocouples. Advancing the furnace temperature achieves the necessary temperature gradient to prevent sample temperatures from lagging behind.

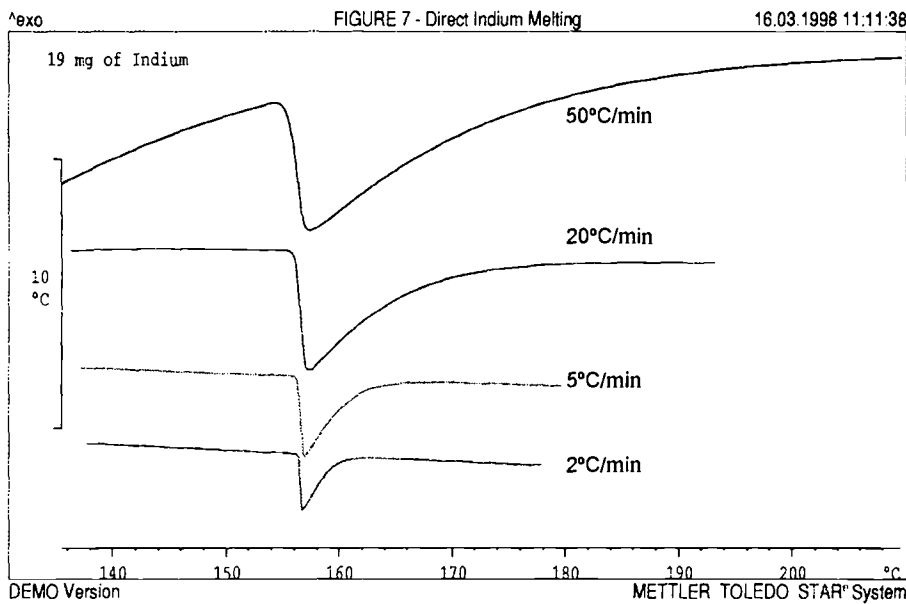


Figure 7 - Indium Melting Measured Directly

Transitions

When a specimen undergoes a thermal transition its temperature either lags behind (endothermic) or leads (exothermic) the surrounding temperature in proportion to the energy involved. For example degradation of copper sulfate pentahydrate ($\text{CuSO}_4 \cdot 5 \text{ H}_2\text{O}$) causes significant temperature lags (Figure 8). The TGA851[°] reveals that sample temperature lags are on the order of tens of degrees during the transitions. This impacts profoundly on the accuracy of degradation temperatures and becomes even more important during kinetic modeling studies, e.g. ASTM Test Method for Decomposition Kinetics by Thermogravimetry (E 1641) and ASTM Practice for Calculating Thermal Endurance of Materials from Thermogravimetric Decomposition Data (E 1877), in which small temperature errors lead to large errors in lifetime predictions.

Finally, since the TGA851[°] detects transitions from their temperature lags, events without associated weight loss, such as melting (seen previously) are also detectable. This makes "true" temperature calibration possible with melting point standards. Classically designed systems with "itv" temperature measurements that do not detect this lag must use other methods described in the ASTM procedure. One such method uses a slight

change detectable by an "itv" thermocouple when energy absorbed by a specimen becomes so large that it creates a slight "disturbance" in the heat distribution. From the data generated by the TGA851^o, this "slight" disturbance is actually an error of between 10 and 40°C in the temperature measurement. Thus, even with this calibration method, the "itv" sensor still has a large degree of uncertainty with respect to the true sample temperature.

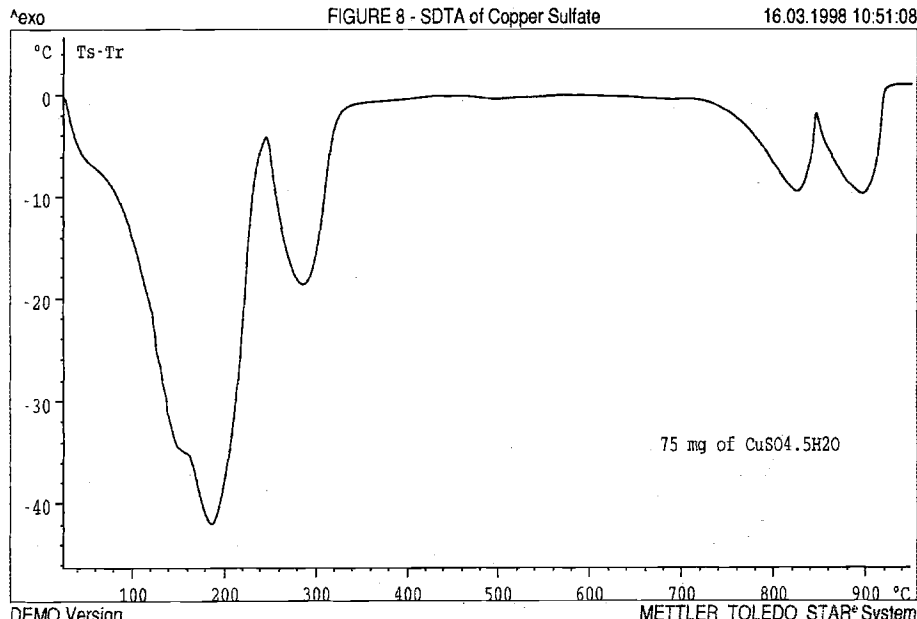


Figure 8 - Temperature Lag from Weight Losses

Conclusions

Without direct contact between a temperature sensor and the specimen crucible, the temperature displayed by classical TGA is at best an approximation. TGA temperature calibration is shown to be a function of temperature, heating rate, specimen mass, transitions, and crucible type. While some of these factors (e.g. crucible type) can be accommodated in classical TGA, factors such as specimen mass changes and transitions make synchronization between the temperature sensor and specimen behavior impossible. Direct-contact temperature devices can be calibrated for system behavior and therefore register accurate sample temperature measurements.

Peter Whittingstall

Pitfalls in Measurement of non-Newtonian Materials—“It’s a Line, Not a Point!”

Reference: Whittingstall, P., “**Pitfalls in Measurement of non-Newtonian Materials—‘It’s a Line Not a Point!’**” *Limitations of Test Methods for Plastics, ASTM STP 1369*, J. S. Peraro, Ed., American Society for Testing and Materials, West Conshohocken, PA, 2000.

Abstract: Isaac Newton in his “Principia” defined viscosity for simple liquids such as water and oils, which have a constant viscosity at a given temperature. As a result such liquids are labeled as “Newtonian” in his honor. Most materials of interest to the laboratory however are non-Newtonian, in that they do not have a single value for their viscosity at a given temperature. In fact, their viscosity is a function of applied shear stress or shear rate. The science of rheology examines the behavior of real, viscoelastic materials as they deform or flow under applied shear or extension, and an understanding of its concepts is necessary if complex fluids are to be successfully measured. This article highlights some of the anomalies that can be encountered when trying to measure the subtleties of such materials.

Keywords: rheology, non-Newtonian, artifacts

Introduction

Modern materials are increasingly more complex than ever before and the challenges of successfully measuring their physical properties grow steadily. Paradoxically, many of the techniques required to measure the viscosity of complex fluids or semisolids are poorly understood or implemented in the workplace. The simple tools for deriving point measurements [e.g. Ford cup, rising bubble tube etc.] are not only inappropriate for complex fluids but can give misleading results when used to predict the relative ease with which a sample can be processed or applied to its end use. For reasons described below, point measurements are inappropriate and can give “wrong” answers when used as guidelines for quality control.

In general terms simple liquids are described as Newtonian, in that they follow Newton’s Postulate in the Principia [1687] in that their viscosity [resistance to flow] is a constant value at a given temperature and pressure. Although other types of viscosity can be defined, it is most common to use shear viscosity, where the force is applied in the same direction as flow occurs and layers of fluid slide past one another like playing cards in a deck. Newtonian fluid viscosity [η] can therefore be described as a point value, and only the temperature of measurement need be stated. Materials that obey this rule are simple low molecular weight liquids such as water, organic solvents, glycerol, sucrose

and most oils. All other fluid materials are therefore non-Newtonian. This means that η is a function of measurement conditions i.e. shear stress [force /area] and shear rate [velocity gradient]. A single point value therefore is meaningless without stating the values for either stress or shear rate as well as temperature. Furthermore the value of the shear parameters is critical when testing these materials. End use properties may depend on fluid response at low or high shear, processing is typically a high shear situation [e.g. mixing or pumping] and stability during storage is normally a very low shear scenario, since the material is essentially at rest.

This behavior - non-Newtonianism- is complicated by the fact that it can take several forms. Some materials [the minority] shear - thicken, i.e. their viscosity increases with increasing stress or shear rate, an example is corn starch in solution which is harder to stir at high shear than at low. Most materials shear - thin, such that their viscosity diminishes with increasing shear. This behavior can be modeled mathematically, but as much data as can be reasonably gathered should be used to optimize the results. This means taking multiple data points. Other complicating factors include the coexistence of elastic behavior [solid like] with viscous behavior [liquid like]. Such viscoelasticity can lead to a variety of interesting fluid dynamic situations. One example is the Weissenberg effect, caused by normal stress differences arising in proportion to the applied shear stress. The dramatic results are that the fluid under shear [say in a mixer] will not draw down a vortex like water, but will rise up the mixer shaft apparently defying gravity! This phenomenon can be seen with certain cake batters in the home, as they are elastic materials themselves.

Finally samples can be time dependent, also known as thixotropic. This type of behavior manifests as a slow increase or decrease [antithixotropy] of viscosity with time as long as the fluid is allowed to rest up to a maximum or minimum steady state value. This constant change in viscosity makes routine measurement very difficult and complicates the use of viscosity as a quality control parameter. Modern viscometers and especially rheometers [viscoelastometers] give the investigator tools to accurately measure viscosity and elasticity in fluids with a high degree of success. When these devices are used correctly they provide a wealth of information and can be used to rank samples in order of “processability” or usefulness in their application. As a final caveat however, they can also mislead if care is not taken in making measurements, as flow artifacts can arise during testing [e.g. slippage]. The following article serves as a brief and by no means exhaustive guide to these issues.

Non- Newtonian materials – How to define them:

In the figure below a series of terms is defined in order to help describe and define viscosity and viscoelasticity. The diagram represents a simple three - dimensional volume of fluid [or solid] and shear stress strain and shear rate are described as well as the parameters for viscosity and elasticity [shear modulus]. The origin of normal forces is also shown, but this is not common to all fluids and is likely to occur in certain cases where polymers are exhibiting entanglement coupling or filled systems are colliding with each other.

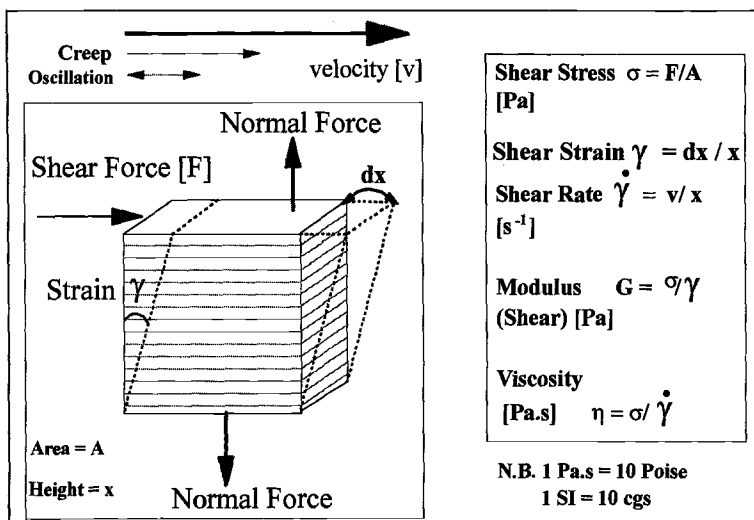


Figure 1-Dynamics of Shear

From the above figure it should be noted that an ideal solid [Hookean] is described by means of its modulus or elasticity, while an ideal fluid [Newtonian] is described by its coefficient of viscosity. For samples that are non-Newtonian, their viscosity is a function of shear stress or shear rate. Typical data for shear thinning samples that exhibit normal forces [2 latex paints] is shown in the next figure. It is clear that their viscosity changes in relation to each other depending upon where in their flow curve you sample data. If you try to compare such materials to predict their ranking the answers will be equivocal if a single point determination is used. Many data points are needed, as seen in the figure.

The importance of making multiple point measurements is clearly demonstrated below, which implies that measurements need to be more time consuming. However, once a material has been properly described as in the graph below, a single point measurement could be chosen at an appropriate stress that reflects the type of information desired [processing or shelf stability?].

How are such viscosity measurements made? The use of capillary and rotational viscometers is the most common way of obtaining such data. A capillary device contains the fluid in a cylindrical tube and flow down this tube is set up by means of a pressure difference. The driving pressure and volumetric flow rate are used to calculate viscosity.

This type of device suffers from the drawback that it does not give a uniform velocity profile across the tube cross section. At the center, the velocity is a maximum, while at the edge it is a minimum. This in turn means that the shear rate [velocity /distance to wall] is not constant either. For this reason, rotational rheometers and viscometers will be considered in isolation from now on. These devices use torque to drive a spindle to which is attached a cone, a plate or a cylinder. The fluid is contained between the spindle and either a plate in the first two cases or a cylindrical cup in the

third case. Such a system generates a defined shear field that can give steady simple shear or torsional flow in the case of the parallel plate geometry. [See Figure 3].

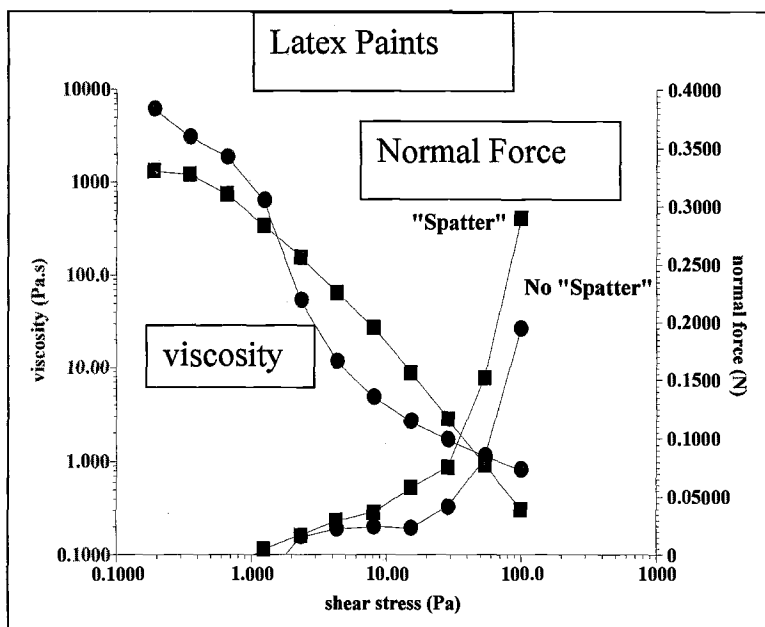


Figure 2-Paint Flow Curves

Artifacts arising from Normal Forces

In the above data [Figure 2], normal force values are seen that increase with shear stress. This can cause flow anomalies at high shear rates that are exactly what a latex paint can experience in use. Other materials such as polymer melts give much stronger values of normal force and are difficult to measure in rotational viscometers or rheometers because they escape from the edges of the geometry. This type of information is critical to the manufacturer, because these flow behavior patterns can ruin the final product. Examples of this are the phenomenon of spatter in the latex paint, caused by too high a value for normal force, reflecting a high degree of elasticity in the product. For polymer melts that are extruded to make products with a defined shape, such as tubing, normal forces can cause "die swell" that makes the extrudate expand in an unpredictable manner. In extreme cases a surface irregularity known as "sharkskin" can appear and spoil the finish of the plastic product. Figure 4 shows this effect in a schematic fashion.

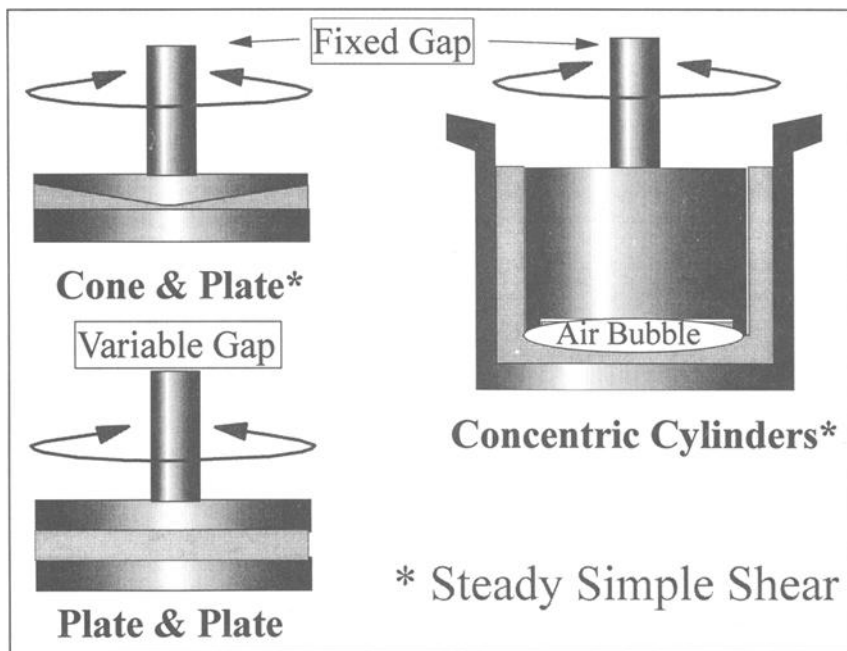


Figure 3-*Geometry of Shear Flow*

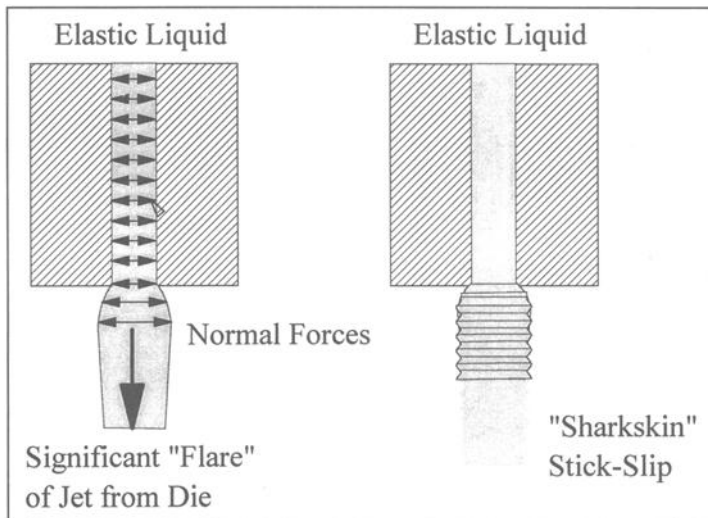


Figure 4-*Die Swell and Melt Instability*

Normal forces arise from two components of the three-dimensional stress tensor that describes an elastic fluid. These are called the first and second normal stress differences. The first normal stress difference is large and positive [pushes the plates apart], the second is much smaller in value and negative. Although it is reasonable to suppose that the first normal stress difference is more important, certain artifacts are ascribed to changes in the second normal force difference. Often, a sample will appear to crack at the edges at moderate to high shear rates and this crack will spread to break the sample film completely. This effect is represented in the figure below, and is called "edge fracture"

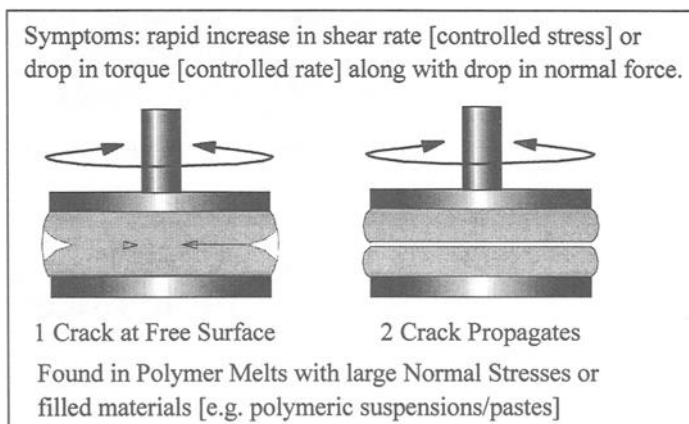


Figure 5 – Edge Fracture

The above problem is difficult to avoid when it occurs in filled systems [pastes] because a certain minimum gap is needed to avoid artifacts due to the size of the particles. In general, the gap should be a minimum of $10 \times$ particle size, and the remedy for this problem is to reduce the gap to improve the stabilizing effect of surface tension. However, it is also possible to change the geometry type to a concentric cylinder, with a sufficiently large radius ratio to accommodate the particles. Since the free edge is at the top, and the cause is due to the second normal stress difference in a direction perpendicular to the rotation axis, this effect is almost non-existent.

Slip at the Rotor or Stator

Certain samples are particularly prone to slippage at the shear zone of the rotor or stator. This may be due to a syneresis where a slip film develops as the sample phase separates, or because the sample itself is not capable of wetting the confining walls. The sharksin phenomenon is also thought to be related to a stick-slip behavior. The most straightforward way to diagnose slip is by repeating the tests using different gap settings. If slip is occurring then the response of the sample will be strongly dependent upon the gap and the data plots will not superimpose well. Slip may sometimes be detected in stiff systems using a visual technique. This involves cutting a slot from top to bottom and observing if the orientation of the slot changes as shear occurs. The slot should change

from the vertical to some angle without a discontinuity. Any discontinuity will indicate that layers of sample are slipping relative to one another [recall the deck of cards analogy]. Figure 6 shows the problem as a schematic.

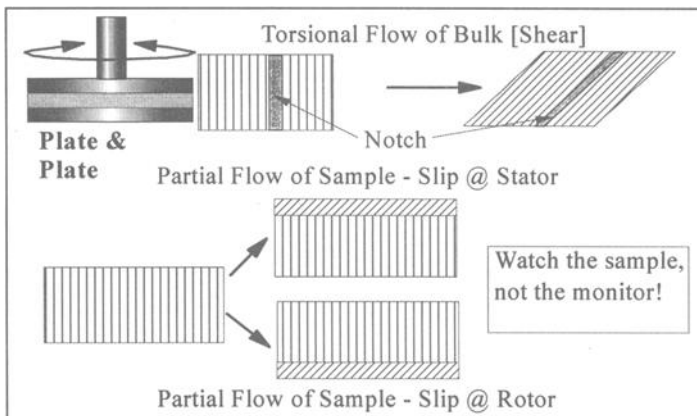


Figure 6-Slip in Parallel Plates

There is often no clue to be seen in standard viscosity versus shear rate plots that slip is occurring, but by replotted as a function of stress, the problem reveals itself as steps or plateaux in the data. When slip is seen to be occurring the options are again to reduce the gap, or to use special geometries that have a roughened surface. This can be achieved by machining serrations or grooves or by sanding the surface, or lastly by gluing sandpaper to the surface of the plates.

Shear Fracture

This is an extreme example of slip, where the structure actually breaks down in the sample in a very narrow zone at the interface of shear and the rotor breaks free of the surface. This can happen at high shear where the sample has slumped down from viscosity break down or from fast step changes in position [stress relaxation tests]. The latter is the same principle that allows an "Oreo" cookie to be split by a rapid twisting of the top cookie relative to the filling. When shear fracture occurs in a sample, it is usually accompanied by a dramatic fall in torque or an increase in shear rate.

Inertial Effects

Inertia is the tendency of an object to resist changes in acceleration or deceleration or direction. In a rotational system, this can be a problem, as the sample does not naturally want to turn in a circle. Furthermore if the inertia of the drive system and geometry is high compared to the inertia of the sample [due to its lower density and low viscosity], then the signals seen by a rheometer will be dominated by the motor/geometry combination and the response of the sample itself may be masked. At high shear rates the inertial effects are particularly acute, and may cause certain artifacts in the data. Most

common of these is an apparent shear thickening [increase in viscosity] in low viscosity liquids that are otherwise Newtonian. [e.g. water]. The reason for this can be diagnosed if the normal force response is monitored at the same time. A dramatic drop in normal force accompanied by an increase in viscosity is almost certainly an inertial artifact. The figure below shows this in effect.

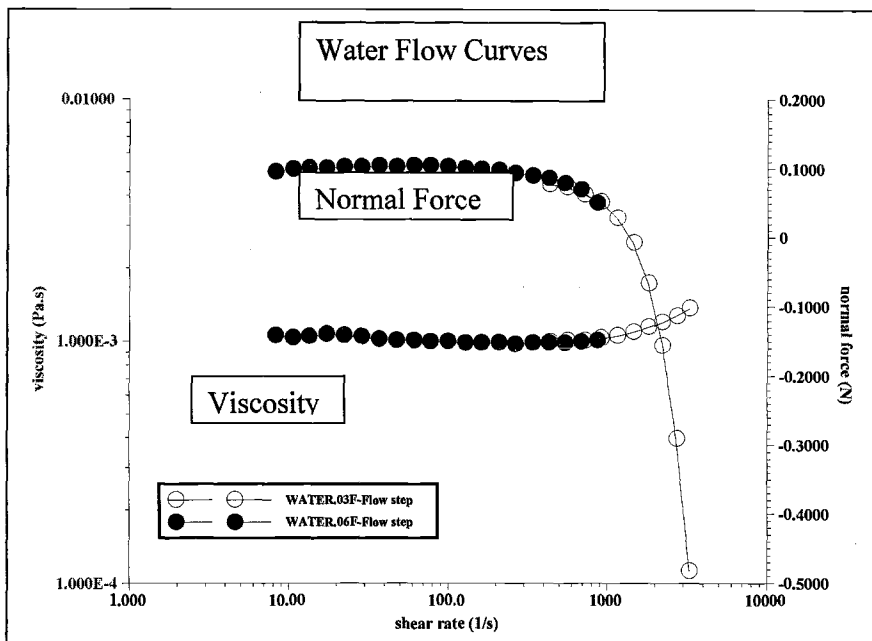


Figure 7-Shear Thickening Artifact for Water

In the figure the normal force is seen to drop sharply at high shear rates, which equate to high rotational speeds. The sample is thus thrown to the edge of the geometry by centrifugal effects, and held in place only by surface tension. The surface tension for water is especially high, and thus the water is at a different pressure in the center than at the edge. This low pressure at the center causes the drop in normal force, the uneven distribution of the water causes the apparent increase in viscosity. The next figure shows the effect in the geometry.

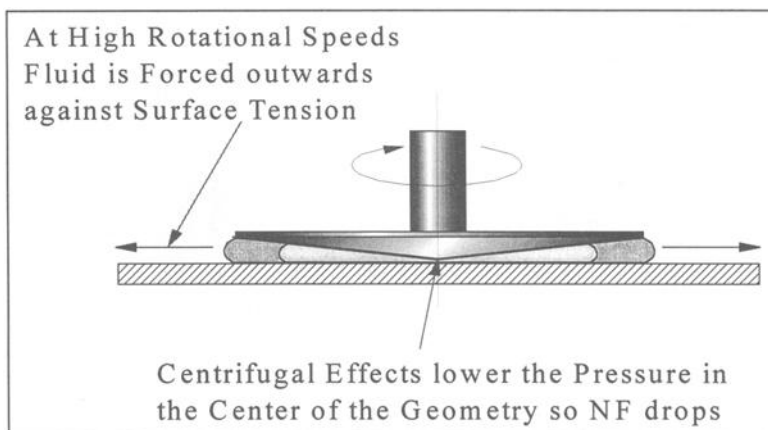


Figure 8-Negative normal force at high speed

Turbulence and Viscous Heating

Viscosity is defined as resistance to flow, and like electrical resistance it is associated with a heating of the bulk medium itself. Viscosity arises as a friction between infinitesimally small lamellae of fluid, rubbing past each other as flow streamlines. One of the boundary conditions for defining viscosity is that the flow must be laminar – i.e. the flow streamlines are stable with respect to each other - and the only energy dissipation arises from viscous forces. If the flow is in the transition or turbulent region these streamlines are no longer stable and interfere with each other causing excess energy dissipation, not associated with fluid viscosity.

The onset of turbulence happens at different flow conditions for each material considered; the Reynold's Number has to exceed a critical value. This is a dimensionless group that relates the inertial forces to the viscous forces, and so if inertial forces overwhelm the viscous forces, the flow is destabilized leading to turbulence. Viscosity will appear to increase as energy dissipation increases. It is relatively rare for this to happen, except at extremely high shear rates.

Viscous heating is more common, and results from the localized increase in temperature of the bulk fluid as it is sheared, causing the viscosity to drop sharply and the fluid to shear thin. This phenomenon occurs when another dimensionless group – the Nahme-Griffith number- increases above a critical value. The effect can be enough to cause damage to the sample in the form of degradation of the polymer, or cross - linking can sometimes occur.

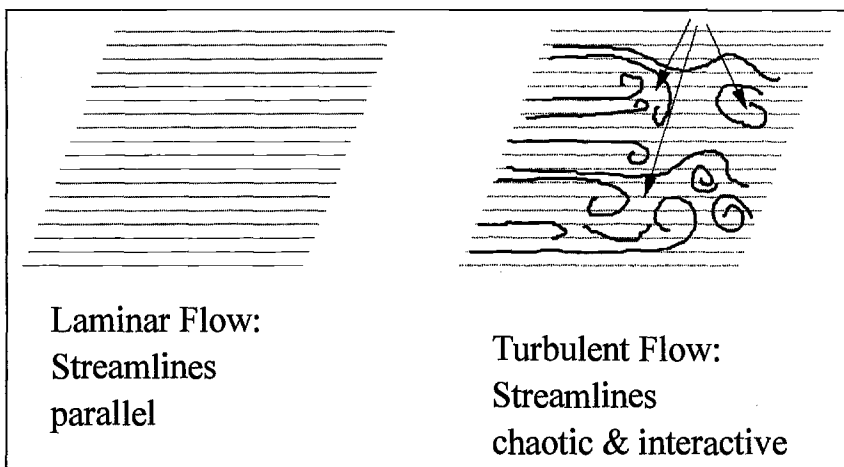


Figure 9-Laminar and Turbulent Flow

If the sample is a solution, the heating can cause the solvent to be driven off by evaporation. In the figure below, an example of viscous heating is shown involving a polymer solution called a Boger Fluid. This type of material is designed as an elastic fluid which does not shear thin [is approximately Newtonian], and this is achieved by using a high viscosity solvent and a low concentration of a high molecular weight polymer. As can be seen in the data, the sample shear thins abruptly and the normal force declines. Repetition of the flow curve causes the same trend in the viscosity, but the normal force never recovers, possibly indicating shear degradation?

Trying to avoid this problem requires an overall increase in temperature of the bulk fluid, so as to minimize the effects of the localized heating on the sample by reducing its viscosity. The gap can also be reduced so as to improve heat transfer.

Thixotropy or time-dependent behavior.

Many modern materials are time dependent, also referred to as thixotropic materials. These samples will slowly build in viscosity at rest, but under shear will break down at a rate that is appreciably faster than the rebuild rate. This will result in a hysteresis effect if a flow curve where the stress or shear rate is increased is followed by a flow curve where the same parameter is decreased. Highly filled materials with a viscous suspending phase are prone to this effect, as are latices and plastisols. Sometimes this effect is deliberately encouraged in a formulation to improve its properties in use. An example of this would be "non-drip" paint, where the recovery of viscosity prevents the paint from dripping from the substrate or running off the brush or roller.

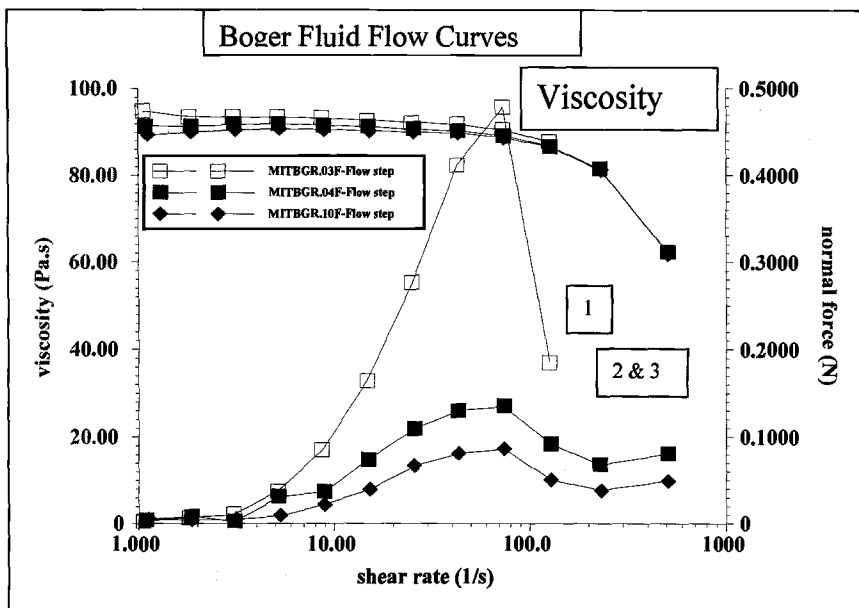
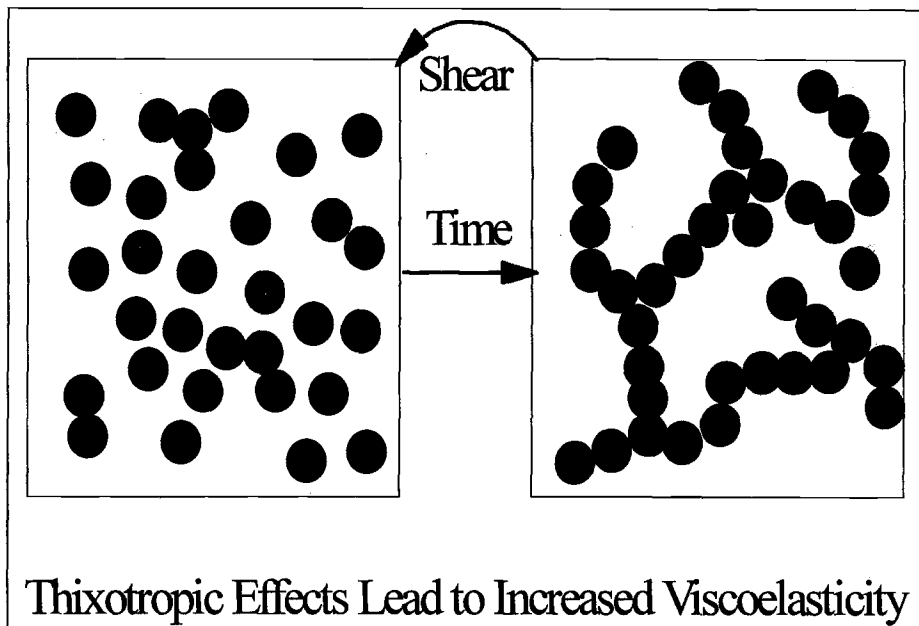


Figure 10-*Effect of Viscous Heating*

For measurement purposes, however it makes the quantification of viscosity quite difficult, due to the sample's sensitivity to its shear history. Differences in handling of the fluid will lead to different responses and thus operator variability can be unacceptably high for QC/QA purposes. The sample rebuilds structure normally by means of a slow recovery to a randomized orientation of anisotropic particles or molecules, that increase the viscosity in start up of flow. A three-dimensional structure of particles or aggregates or even crystals [e.g. greases] can develop over time [see figure below]. It should be noted that sample drying from solvent loss can often be mistaken for thixotropy, so take precautions to prevent evaporation! Such precautions include use of a cover or trap or covering the free edge with a light silicone oil.

In the above figure, the particles are able to interact to form chains and a network in three dimensions, that builds a rigidity in the fluid. Flow breaks this down rapidly, and this structure rebuilds slowly if the fluid is at rest. Since the rebuild process is a kinetic phenomenon, the measurement of viscosity at a given stress or shear rate must be done under steady state conditions. The use of ramped tests to measure flow is therefore unsuitable. A recovery period after loading, and precautions to minimize disruption of the sample during loading, help to speed up the time required to reach steady state. Certain materials such as greases may require more than 20 hours at rest to allow full recovery of the equilibrium structure!



Thixotropic Effects Lead to Increased Viscoelasticity

Figure 11-Structure in Thixotropic Fluids

A technique known as equilibrium flow (steady state flow) is useful in determining viscosity in an unequivocal fashion. At each stress or shear rate the output signal is monitored until a steady state response is achieved, and only at that point is data calculated to give a viscosity value. In this way a series of accurate data points can be generated for viscosity as shown in the figure overleaf.

As can be seen above, the equilibrium technique, gives a single line of data points in contrast to the hysteresis loops from traditional ramping techniques. While equilibrium flow may take a long time, it is certainly better to get the data in a usable form than to repeat ramp tests and try to estimate the steady state data.

Conclusions

The measurement of viscosity for non-Newtonian materials is a matter fraught with potential problems for the investigator. Some of the issues that can be encountered have been described here in an effort to aid the viscometer or rheometer user that is interested in optimizing their data and avoiding potential artifacts. Some problems may not lend themselves to an easy solution, and testing in other systems such as capillary devices might help generate the required data.

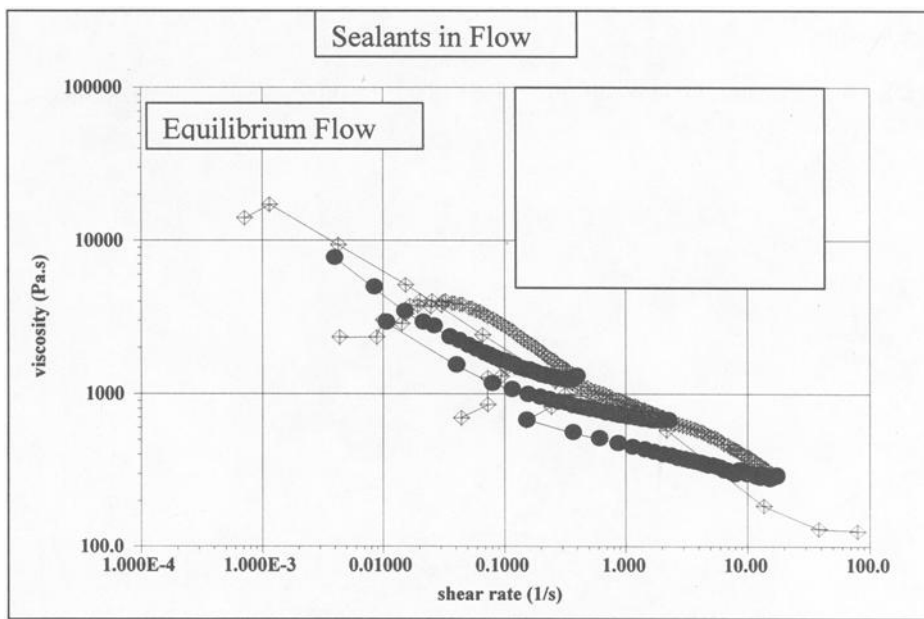


Figure 12-*Equilibrium flow eliminates hysteresis in time dependant fluids*

Acknowledgements

The author would like to thank Professor Gareth McKinley of M.I.T. for his generous help in the preparation of this paper. As a reference of flow artifacts his knowledge is encyclopedic!

Bibliography:

The following general text books will help the interested reader:

Rheometry – Ken Walters F.R.S. published by Chapman & Hall 1975 reprinted for TA Instruments 1987

Dynamics of Polymeric Liquids Vol. 1 – R.B. Bird, R.C. Armstrong & O. Hassager Wiley Interscience 1987

Also these papers are relevant:

Arigo & McKinley, J. Rheol submitted 1998 "Thermal Blowup in Oligomeric solvents and Boger Fluids."

180 LIMITS OF TEST METHODS FOR PLASTICS

Lee, Tripp & Magda, *Rheol. Acta* 31 [1992] 306-398 "Does N1 or N2 control the onset of edge fracture?"

Archer, Larson & Chen *J. Fluid Mech.* 301 [1995] 133-151 "Direct measurements of Slip in sheared polymer solutions."

Jonathon Foreman,¹ Mark Kelsey,¹ and Georg Widmann²

Factors Affecting the Accuracy of TMA Measurements

Reference: Foreman, J., Kelsey, M. and Widmann, G., "Factors Affecting the Accuracy of TMA Measurements," *Limitations of Test Methods for Plastics, ASTM STP 1369*, J. S. Peraro, Ed., American Society for Testing and Materials, West Conshohocken, PA, 2000.

Abstract: This study investigates factors that cause differences between reported temperatures in thermomechanical analysis (TMA) instruments and actual sample temperatures. Observations of the melting of indium are made under several sets of conditions. These include varying the indium specimen size, altering the position of the thermal sensor, changing the heating rate, and placing pieces of indium atop and below glass and copper specimens of varying thickness. A TMA instrument with direct-contact thermal sensor and single differential thermal analysis capability yields better sample temperature measurements and allows direct examination of the effects of heat capacity. In a second set of experiments, the glass transition of polycarbonate film is measured in the tension mode using different forces and specimen lengths. The results of this study show that low material thermal conductivity and high specimen heat capacity cause the sample temperature to be lower than that of the surrounding atmosphere. Temperature gradients along the length of the furnace can intensify the temperature difference. Furthermore, stress applied to specimens in tension can lead to erroneous Tg values. Specimen and calibration procedural changes are recommended.

Keywords: TMA, temperature, calibration, SDTA, glass, copper, film, indium, heat capacity, thermal conductivity, force, stress

Introduction

Thermomechanical Analysis (TMA) measures unidirectional dimensional changes in materials as functions of time, temperature and applied force. The TMA measurements are coefficient of linear thermal expansion (CLTE), glass transition temperatures (Tg) and softening points (Ts). Newer applications of TMA include elasticity, melt viscosity, and heat deflection temperature. In addition to traditional TMA instruments, many modern dynamic mechanical thermal analysis (DMTA) instruments can operate in a TMA (static force) mode. The main differences between the two types of instruments are the size of the specimens and the materials used to fabricate the measurement fixtures (stage, probe, clamps, etc.). Most TMA instruments use quartz, while DMTA instruments use larger steel components. The specimens used in these experiments are

¹ Mettler-Toledo, Inc. Columbus, OH 43240 e-mail:jon.foreman@mt.com

² Mettler-Toledo GmbH, CH-8603 Schwerzenbach, Switzerland.

usually rather large and are shaped according to the mode of operation (e.g. tension, compression or bending) and the instrument used. The size and variety of possible TMA specimens leads to an equal variety of possible calibration and measurement procedures. For example, for large specimens there is the debate between calibrating the temperature response of the instrument versus attempting to mimic the internal temperature of the specimen itself. The ASTM Test Method for Temperature Calibration of Thermomechanical Analyzers (E 1363) takes the former approach. Unfortunately only one ASTM test method actually refers to this method. All other methods tell the user to calibrate temperature according to manufacturer's procedures. Variations among manufacturers can make comparisons among different instruments quite challenging. Most ASTM test methods caution the user to ensure that the temperature sensor does not change position between calibration and actual experimentation, which is quite critical for temperature reproducibility.

Several papers examine the effects of conditions on the reported temperatures in TMA and DMTA [1-5]. The factors cited include heating rate, temperature range, position of the thermal sensor, purge gas and rate, applied force, specimen size and specimen preconditioning. The precision and bias statements of E 1363 and Test Method for Assignment of the Glass Transition Temperature by Thermomechanical Analysis (E 1545) report that interlaboratory variation (standard deviation) can be as large as $\pm 1.7^{\circ}\text{C}$ for simple melting and $\pm 4.0^{\circ}\text{C}$ for the glass transition.

A major source of temperature error is nonlinear temperature response, as was observed by both Seyler and Earnest [1] and Matsumori et al. [2]. That is, a straight line cannot describe the differences between the literature melting points of known materials and the temperature reported by the TMA over large temperature intervals. This phenomenon limits the linear temperature corrections of E 1363 to a smaller temperature range. To achieve accurate temperatures over wider ranges, it is critical to calibrate the TMA instrument at relatively small intervals over the range of interest.

Temperature errors also affect CLTE measurements. For example, Matsumori et al. [2] estimate that in certain circumstances the temperature error arising from nonlinearity can contribute about 2% error to the observed CLTE value. The Test Method for Linear Thermal Expansion of Solid Materials by Thermomechanical Analysis (E 831) states that precision of CLTE values will depend upon the specimen's size, thermal conductivity, and CLTE along with heating rate. Even with proper calibration, uncertainty can range from $\pm 2\%$ for high CLTE materials to $\pm 15\%$ for low CLTE materials. Since large specimens are needed for low CLTE materials, furnace temperature gradients become important. The more widely accepted Test Method for Linear Expansion of Solid Materials With a Vitreous Silica Dilatometer (E228) recognizes these factors and requires larger specimens (25 mm) using isothermal temperature holds or slow heating rates ($<3^{\circ}\text{C}/\text{min}$) with very small furnace gradients ($<0.5^{\circ}\text{C}/\text{cm}$). The precision of this method is much better at 0.8% standard deviation over a broad range of CLTE values.

The use of TMA (and DMTA) to measure the properties of thin films and fibers is growing. TMA can be used, for example, to observe the effects of processing on specimen dimensions (e.g. shrinkage and anisotropy) and transition temperatures. As these properties are often measured with long specimens in a tensile arrangement, a new type of temperature calibration may be required. Although no ASTM test method exists for such a purpose, Moscato [3] used indium and lead foils as melting point standards at a

variety of heating rates. Unfortunately, the Test Method for Assignment of a Glass Transition Temperature Using Thermomechanical Analysis Under Tension (E 1824) only suggests following manufacturer's procedure and cautions against moving the thermal sensor. As one can imagine, furnace temperature gradients will have a profound effect on the results. Most studies avoid this latter complication by using a single specimen length.

Measurement of temperature gradients within the TMA furnace is no simple task. While in most instruments the thermal sensor can readily be repositioned, this action can modify the thermal surroundings of the sensor. Another approach is to adjust the height of the calibration standard using a variety of materials such as metals and glasses. Jankowsky et al. [5] took a similar approach, imbedding a thermocouple within DMTA specimens in order to compare the temperatures within the specimens to those displayed by her instruments. They found the specimen temperature lagged behind the instrument temperature. The lag increased with temperature and heating rate, with temperature differences exceeding 40°C in some cases.

The stage, probe and temperature sensor arrangement of the Mettler-Toledo, Inc. TMA840 (Figure 1) allows a different approach to measuring furnace gradient. In this instrument, the center of travel of the probe is fixed while the stage moves to accommodate different specimen sizes. The thermal sensor is embedded in the stage with only a very thin coating of quartz separating the sensor from the specimen. Thus the observed temperature readily reflects the temperature at the bottom of the specimen. This arrangement ensures the thermocouple position is not altered; the sensor always sees the same environment. The stage can be moved to the extremes of the probe travel in order to observe the furnace gradient under nearly constant conditions.

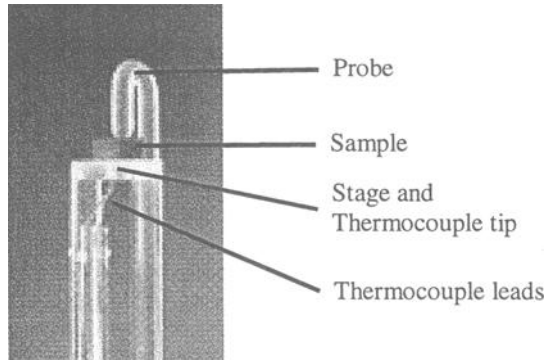


Figure 1 - TMA840 Stage and Probe Arrangement

This study has three phases. Since temperature nonlinearity is well characterized, this paper will not focus on broad temperature ranges. Rather, this paper observes the properties measured by TMA instruments around 150°C, which is near the melting point of indium and the glass transition in polycarbonate. In the first section, the temperature calibrations and gradients within the furnace are explored. Second is an examination of the effects of specimen heat capacity and heating rate on observed temperatures. Third is a discussion of experimental conditions on the measured properties of films, including preliminary results of interlaboratory testing for E 1824 (Test Method for Assignment of a Glass Transition Temperature Using Thermomechanical Analysis Under Tension).

Theory

Heat is transferred from the furnace to the specimen by convection and, at higher temperatures, radiation. One can define a "reference" condition as the heat flows from the furnace to the specimen platform, probe, temperature sensor, etc. When the specimen is added, the heat capacity of the system is changed, and thus the temperature of the system (specimen plus "reference") will respond differently to the same furnace temperature program. The temperature difference is affected not only by the specimen response (C_p and transitions) but also by the furnace response (R_t) and the heating rate, as can be seen in Equation 1 which was derived elsewhere [6].

$$T_s - T_r = -R_t \cdot C_{p_s} \frac{dT}{dt} \quad (1)$$

where:

T_s = system or sample temperature

T_r = "reference" temperature

R_t = resistance to heat flow from the furnace to the specimen.

C_{p_s} = specimen heat capacity = mass * specific heat

dT/dt = heating rate

As discussed previously, R_t is usually nonlinear with respect to temperatures, so that linear corrections may not adequately describe specimen response (T_s). The furnace gradient makes R_t a function of height, $R_t(y, T)$, where y is the position within the furnace. It is generally held that $R_t(y, T)$ varies with purge gas and purge rate.

Until recently it has been very difficult, if not impossible, to measure $T_s - T_r$ in TMA instruments. With most instruments the thermal sensor is an independent body separated from the length measuring system; it measures the temperature of the atmosphere near the specimen. By embedding the thermal sensor in the sample stage, a more accurate assessment of the true "system" temperature can be achieved. The sensor is essentially part of the system "reference." The reference temperature can, therefore, be measured and stored for comparison to specimen runs. An alternate approach used in the SDTA^{®3} routine of the TMA840 models the reference response against the furnace sensor. A special calibration routine, which uses indium and zinc melting temperatures, measures the reference response as functions of temperature and heating rate as part of this model. With a well-behaved furnace, i.e. reproducible $R_t(y, T)$ and minimal furnace gradient, temperature differences ($T_s - T_r$) can be attributed to the specimen and the heating rate.

Experimental

Experiments were performed to characterize the temperature responses of TMA furnaces as functions of position within the furnace, specimen length, specimen heat capacity and heating rate. Two instruments were used in this study, the TMA840 from Mettler-Toledo, Inc., (heretofore referred to as TMA1) and another commercially-available TMA (heretofore referred to as TMA2). The latter instrument is representative

³ Mettler-Toledo GmbH, CH-8603 Schwerzenbach, Switzerland.

of traditional TMA instruments and uses a fixed position stage and a thermal sensor which is independent of the stage and specimen. The stage and thermocouple arrangement for TMA1 differ from the traditional arrangement and allow additional measurements as were described previously. Experiments for TMA1 were performed on a single instrument by two different operators. Experiments were performed on two separate TMA2 instruments by two different operators.

TMA1 was calibrated according to the manufacturer's procedure using indium and zinc in the total calibration routine. This routine measured the melting temperatures of the materials using the SDTA response at a variety of heating rates to calibrate R_t , the temperature scale, and the specimen holder response. The temperature scale was recalibrated against the melting of indium at 5°C/min using the TMA dimension change response according to E 1363. TMA2 was calibrated using indium melting at 5°C/min according to E 1363. Unless otherwise noted, the thermocouple of TMA2 was positioned on the stage, but the tip was not touching the surface of the stage. The thermocouple of TMA1 is permanently mounted in the stage and therefore could not be moved.

Two substances were used as temperature indicators, indium metal (>99.99% pure from Mettler-Toledo, Inc.) and 0.05 mm thick polycarbonate film. Indium specimens were cut from indium pills which had been pressed to 20-250 µm thick. The indium specimens were sandwiched between two pieces of aluminum foil to protect the fixtures.

In TMA2 both the 1 and 3 mm diameter probes were used. With TMA1, a thin disk of quartz was placed between the top aluminum foil and the probe according to the manufacturers recommendation. The results of this study indicate negligible influence on the observed temperatures from the additional quartz disk. In all indium experiments a force of 50 mN (0.05 N) was applied to the specimens.

A static air environment was utilized in all calibrations and experiments. Results may be affected by using different gas environments. However since Nitrogen, the most common purge gas used in TMA, has properties similar to air, the differences are small. On the other hand, the use of helium would probably alter the results significantly.

Most experiments were performed by heating from 120 to 175°C at the rate of 5°C/min. To study the effects of heating rate, three further conditions were used: 140 to 165°C at 2°C/min; 100 to 200°C at 10°C/min; and 50 to 250°C at 20°C/min.

The furnace gradient was investigated in several sets of experiments which all used the melting of indium as the temperature indicator. For the first set of experiments the position of the thermal sensor was altered. In TMA1 this was accomplished by varying the position of the stage from the bottom of the probe sensing range to the top. In TMA2, the thermocouple was moved from the stage to several positions above the stage. Unfortunately, this series of experiments on TMA2 was not completed due to time constraints. While the two TMA2 instruments showed similar results for the small number of experiments performed and the results followed the trends seen in other experiments, the data reported here should be considered anecdotal.

Additional series of experiments were performed on both instruments to measure furnace gradients. In these experiments indium was placed atop and sometimes atop and underneath borosilicate glass or copper supports. A variety of support lengths were employed using supports cut from samples of NIST SRM⁴ 731 and 736.

⁴ Standard reference materials from National Institute of Standards and Technology, Gaithersburg, MD.

The experiments on the polycarbonate film were performed in the tension mode of TMA1 only. The stage and probe of TMA1 were replaced with their tensile counterparts and temperature was recalibrated using indium wire (0.5 mm >99.99% pure from Alfa-Aesar) mounted in the tensile clamps. The ends of the wire were wrapped in aluminum foil to protect the clamps.

To fashion specimens of the polycarbonate film, strips 3 mm wide were cut from a larger sample. The specimens were mounted into inconel clamps. Specimen lengths and applied forces are described in the results and discussion section. All specimens were heated from 80 to 180°C at 5°C/min in a static air atmosphere.

Results

Effect of Specimen Size and Probe/Pressure on Calibrations

Before beginning the experiments, it was important to ensure that both instruments were calibrated in a similar manner. E 1363 recommends that 10-20 mg of indium be used to calibrate the instrument. The indium used in this study is received in the form of pills approximately 6 mg in weight and 0.5 mm thick. While the specimens fall below the recommended weight, it is the thickness of this specimen that can lead to misleading observations of the melting temperature.

E 1363 requires that tangents be drawn to the baseline and to the steepest part of the TMA softening curve. This analysis is shown in Figure 1 for a 0.25 mm thick specimen. It can be seen that the onset of indium melting reported in this manner is approximately 0.5°C higher than that observed for thinner specimens. The best (most reproducible) results are achieved with much smaller specimens, about 20-100 µm thick. The value of 156.2°C was used to calibrate the instrument in this particular instance.

Also seen in Figure 1 are comparisons of measurements performed with a 0.9 mm probe only and with a quartz disk between the probe and the specimen. It appears that the quartz disk has minimal influence on the observed melting temperature, and may actually improve the results for thicker indium specimens.

Measurement of Furnace Temperature Gradient

The first set of experiments endeavor to investigate the temperature gradient along the height of the TMA furnaces by altering the position of the temperature sensor. With TMA1, the melting of indium is observed as the stage in the middle of the probe range and at the two extremes of the probe range, approximately ± 5 mm from the center. The results of these experiments are quite remarkable, with indium melting at 156.6°C $\pm 0.1^\circ\text{C}$. Because the temperature sensor is in direct contact with the sample stage, it was suspected that the stage temperature was 156.6 °C while the atmospheric temperature was somewhat different. In this instrument, the reference temperature is modeled from the furnace temperature and therefore is not influenced by the position of the sample stage. The reference temperature shows the same level of uncertainty thus supporting the data from the sample temperature sensor.

In TMA2 the thermocouple is moved from the stage to several positions above the stage. The results of the limited data generated here indicate a much greater temperature

gradient, on the order of about 1-2°C per millimeter above the stage. While these results are limited, the data of the next section appear to confirm these findings.

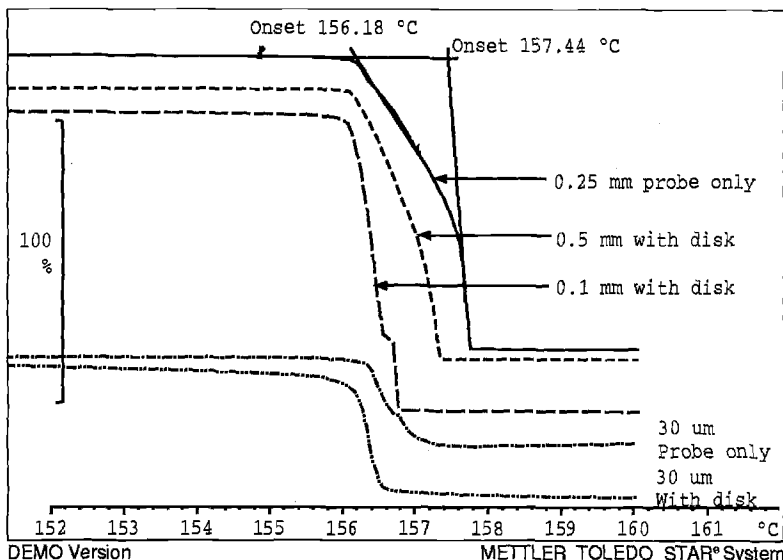


Figure 2 - Melting of Indium as a Function of Specimen Thickness and Probe Dimension Observed in TMA1 Using the 0.9 mm Diameter Flat Probe With and Without Quartz Disk

Measurements of Furnace Gradient Using Glass and Copper Supports

The indium melting temperatures (T_m) as functions of the thicknesses of glass and copper supports are shown below. At first the results are somewhat confusing and apparently contradictory. For the glass supports (Figure 3) T_m decreases with increasing thickness, indicating that the temperature at the top of the support (the location of the indium specimen) is hotter than the thermal sensor which is located near the bottom of the support. TMA1 shows a small dependence of T_m on the thickness, on the order of 0.2°C per millimeter of thickness. TMA2 shows a larger dependence, on the order of 1°C/mm. The temperature uncertainties were on the order of $\pm 0.1^\circ\text{C}$ for TMA1, and $\pm 0.6^\circ\text{C}$ for TMA2 (up to 10 mm support thickness).

Interestingly, when the thermocouple of TMA2 was moved to halfway up the support height for two different supports, indium melted at $156.9^\circ\text{C} \pm 0.7^\circ\text{C}$. This is reasonable considering the two previous observations. The thermocouple sitting above the stage reports temperatures that are about 2°C/mm higher than expected for indium melting. The apparent T_m values for indium on the glass supports are 1°C/mm higher than expected. Since 1/2 of 2°C/mm equals 1°C/mm, a thermocouple sitting halfway up a glass support should report the same temperature the indium is encountering at the top of the support.

With the copper supports, on the other hand, T_m increases with support thickness (Figure 4). This appears to indicate that the top of the support is cooler than the thermal sensor. Furthermore, TMA1 shows a rather large increase in observed T_m with respect to copper support height (0.4°C/mm) while TMA2 shows lesser influence (0.16°C/mm).

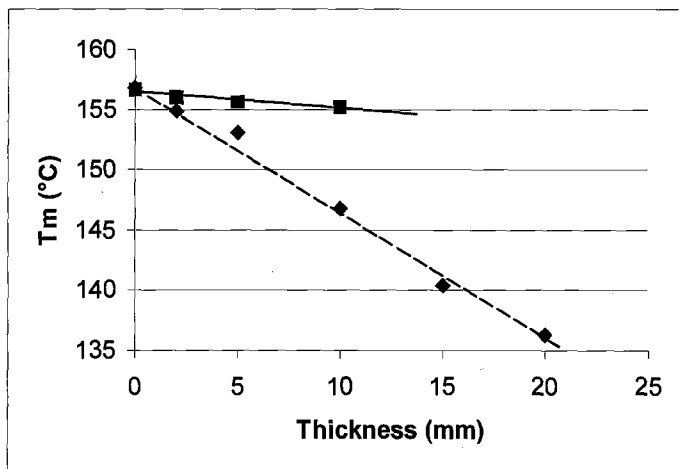


Figure 3 - *Melting Temperature (T_m) of Indium as a Function of Glass Support Thickness
TMA1 (■), TMA2 (◆)*

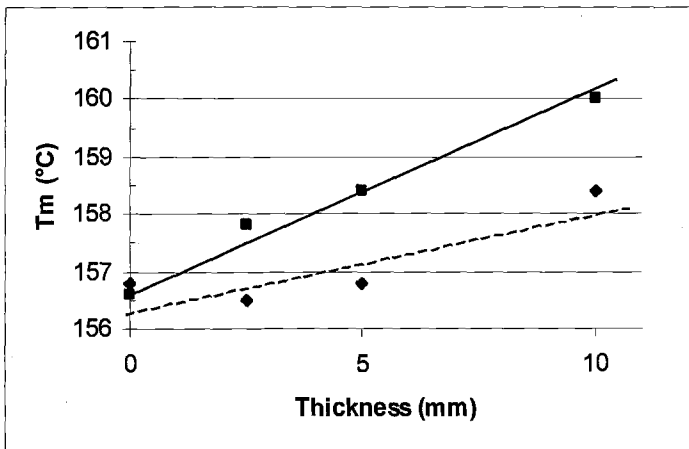


Figure 4 - *Melting Temperature (T_m) of Indium as a Function of Copper Support Thickness TMA1 (■), TMA2 (◆)*

In order to investigate these apparently contradictory results, further measurements are performed with indium placed both atop the supports and below. A typical result, from the 5 mm glass support in TMA1, is shown below (Figure 5). Two melting transitions are observed. It can be reasoned that the lower temperature T_m should correspond to the top of the support, and the higher temperature to the bottom. The SDTA response (T_s-T_r) of TMA1, which measures heat flow at the stage, clearly confirms the bottom indium specimen, which is in contact with the stage, melts second.

All glass supports show a clear distinction between the temperatures at the tops and bottoms of the supports. The results for TMA1 are shown in Figure 6 and Table 1. In

TMA1 both the temperatures at the bottom of the supports and the differences between the temperatures at the two ends of the supports increased with increasing thickness. The former result is similar to the T_m behavior observed with copper supports, though at a decreased magnitude.

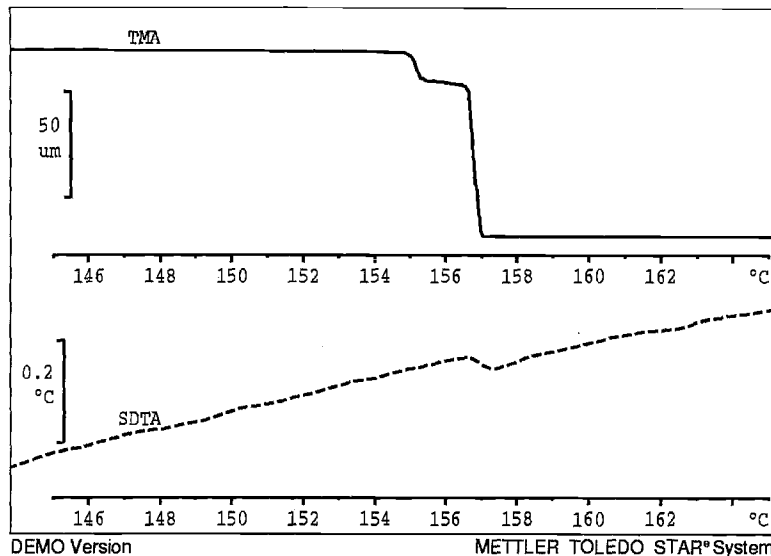


Figure 5 - Dimension Change (Solid Line) and SDTA (Dashed Line) Signals for Indium Specimens Atop and Below 5 mm Glass Support

Table 1 - Indium Melting at 5°C/min from Top and Bottom of Glass and Copper Supports as Observed by Specimen (T_s) and Reference (T_r) Temperatures in TMA1

Support	T_s , Top °C	T_r , Top °C	T_s , Bottom °C	T_r , Bottom °C	T_s-T_r °C	C_p _s J/°C
Glass 2 mm	156.0	156.5	156.8	157.7	-0.9	0.13
Glass 5 mm	155.6	156.7	157.0	158.2	-1.2	0.29
Glass 10 mm	155.2	156.8	157.2	158.9	-1.7	0.59
Copper 2.5 mm			157.8	159.5	-1.7	0.28
Copper 5 mm			158.4	161.4	-3.0	0.57
Copper 10 mm			160.0	165.4	-5.4	1.18

Also shown in Table 1 are the reference temperatures (T_r) at the melting temperatures (reported as T_s). Interestingly, at the tops of the glass supports, T_r is nearly constant at $156.7 \pm 0.1^\circ\text{C}$. Furthermore, T_s-T_r is rather uniform between the tops of and the bottoms of the supports.

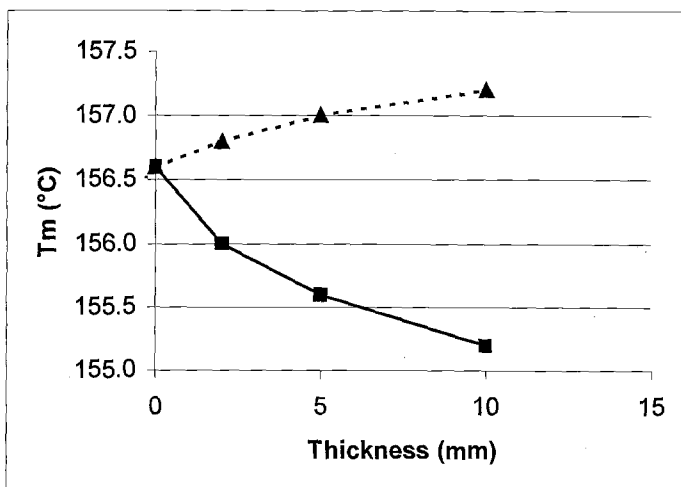


Figure 6 - Indium Melting (T_m) at Top (■) and Bottom (▲) of Glass Supports

Though a complete series of similar experiments was not run for TMA2, results from a series of experiments on the 10 mm glass specimen (at various heating rates) show the indium at the top of the specimen melting 11°C lower than the indium at the bottom of the specimen. This corroborates the results observed previously for TMA2 (Figure 3).

For all experiments using copper supports (see Table 1), only one T_m is observed. As was observed for the glass supports, T_s-T_r increases with increasing support thickness. The magnitude of the increase is much larger than is observed for the glass supports.

A number of conclusions can be drawn from these observations. First, thermal conductivity plays a key role in temperature distribution within the specimen. Copper is nearly 400 times more conductive than the glass and should have a nearly uniform temperature distribution along its thickness. Thus only one T_m can be observed.

Second, T_m values at the top of the glass supports are somewhat indicative of the temperature at the various positions within the furnace, but they are influenced by the heat capacity of the support. The similar T_r values observed in TMA1 for melting at the top of all the supports indicate uniformity of the atmosphere temperature over the furnace length in this instrument. But since the glass is not thermally conductive, the temperature at the core of the glass lags behind the temperature at the surface. At the top surface heat flows only into the support and the top gets warmer from poor heat transfer to the core of the specimen. On the other hand, the bottom surface of the support conducts heat to and from the stage in addition to the heat transfer into the core. Because of the relatively uniform temperature profile in TMA1, a slightly elevated stage temperature is needed to provide sufficient heat flow to overcome the heat capacity of the support and melt the indium. It is difficult to measure actual stage temperatures in most instruments and thus the contributions of the stage temperature to the specimen are difficult to measure.

The situation will become more complicated as more DMA instruments are being used for TMA measurements. The main concern is the differences between the thermal quantities (heat capacity and thermal conductivity) of quartz (used for the stages and probes in most TMA's) and those of the metal fixtures used in most DMA instruments.

Third, heat capacity has a significant impact on the true sample temperature in a manner that can only be measured by direct-contact thermal sensors. As discussed previously (Equation 1), the difference between reference temperature and sample temperature is directly proportional to the heat capacity of the specimens. By plotting $T_s - T_r$ versus heat capacity (mass*specific heat), straight lines are obtained for both the glass series and the copper series (Figure 7). It is not surprising that the two lines do not overlap, since the internal temperatures of the glass specimens are not uniform, being somewhat lower on average than the reported temperatures (thus $T_s - T_r$ would be larger).

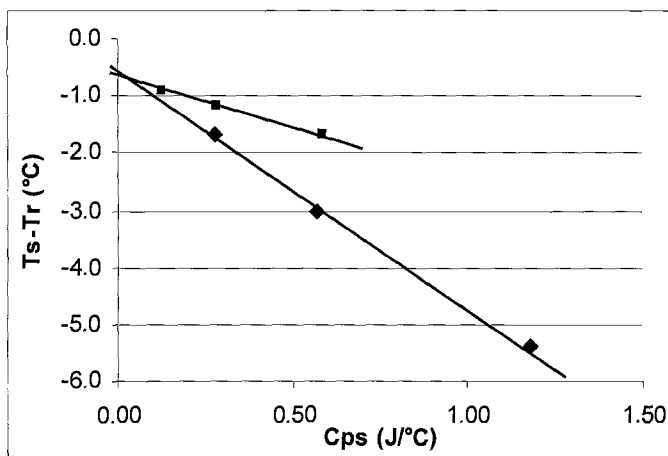


Figure 7 - Temperature Difference Versus Heat Capacity Measured at the Indium T_m at the Bottom of the Glass (■) and Copper (◆) Supports in TMA1 at 5°C/min

Influence of Heating Rate on the Observed Melting Temperatures

The melting temperature of pure materials such as the indium used in this study does not change with heating rate. However in most thermal analysis instruments the observed temperature rises with increasing heating rate. This behavior can be seen for T_m of indium measured on the stage (no support) using TMA2 (Figure 8).

TMA1, on the other hand, can be calibrated for sensor and furnace time constants (τ lags) to achieve a heating-rate independent melting temperature of indium in both the sample and reference temperature axes (via the FlexCal routine). That TMA1 shows a decrease in T_m with increasing heating rate indicates the instrument is not properly calibrated. The data generated here can be used to recalibrate the instrument by calculating the slope of the T_m versus heating rate curve. For example, for the reference temperature curve, the slope is -0.15 minutes {°C/(°C/min)} indicating a reduction in time constant of about 9 seconds will bring the instrument into calibration, and remove the heating rate dependence of T_m .

To determine the influence of heating rate on furnace gradient, the melting of indium pieces both atop and below the 10 mm thick glass support was examined at the same

heating rates as above. For TMA2, two important trends are seen, though the results are not conclusive. First, T_m values for the indium at the bottom of the support follow a trend similar to that seen in Figure 8. Additionally, T_m values at the top of the specimen lag behind the T_m at the bottom by approximately 11°C, which is similar to and helps corroborate the previous findings (Figure 3).

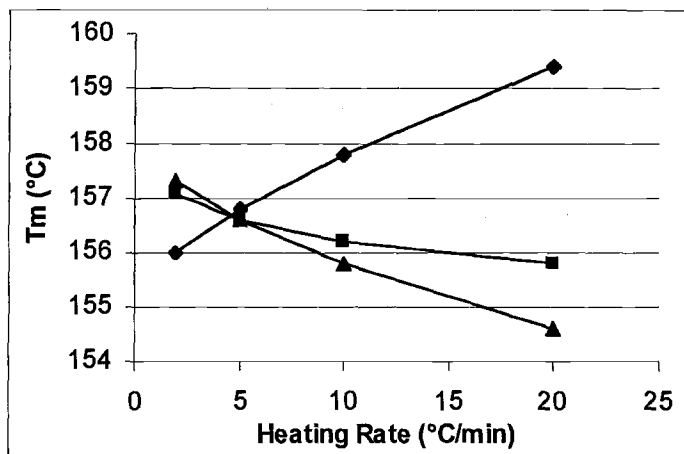


Figure 8 - Melting Temperature (T_m) of Indium Without Support versus Heating Rate Measured at the Stage by T_s in TMA1 (■), T_r in TMA1 (▲), and TMA2 (◆)

For TMA1 the melting temperatures were corrected for heating rate according to the previous results (Table 2). All melting temperatures increase with increasing heating rate. It is important to note that this occurs even at the bottom of the support, where the indium is closely coupled to the thermal sensor. This can be expected from lags caused by the heat capacity of the glass. An interesting observation is that the temperature at the top of the support is more greatly influenced by heating rate than at the bottom, to the extent that only one T_m could be observed at 20°C/min. This latter observation may result from the thermal conductivity of the support, or it could indicate a variation in the furnace gradient. More work needs to be done to analyze this data more fully.

Table 2 - Indium Melting at various heating rates from Top and Bottom of 10 mm Glass Support as Observed by Sample (T_s) and Reference (T_r) Temperatures in TMA1

Heating Rate °C/min	T_s at Top °C	T_r at Top °C	T_s at Bottom °C	T_r at Bottom °C	T_s-T_r at Top °C	T_s-T_r at Bottom °C
2	153.9	154.2	156.4	156.7	-0.3	-0.3
5	155.2	156.8	157.2	158.9	-1.6	-1.7
10	156.7	160.4	158.2	161.9	-3.7	-3.7
20			159.3	166.9		-7.6

An interesting outcome of this portion of the study is that this data can be used to confirm the heating rate (dT/dt) effect on T_s-T_r (see Equation 1). By plotting T_s-T_r , which is independent of specimen height, versus heating rate (Figure 9) a straight line and near zero intercept are achieved, thus confirming the theory. The implication is that calibrations of a thermal device that only measures T_r for different heating rates can be very misleading when considering specimens of different heat capacities.

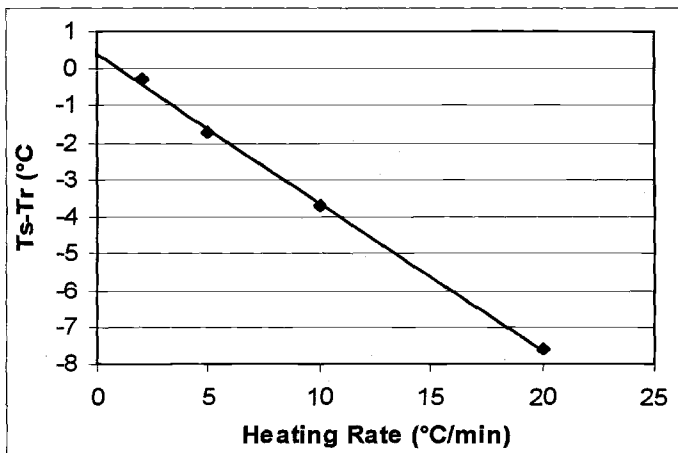


Figure 9 – Temperature Difference versus Heating Rate at Indium T_m Measured at the Bottom of 10 mm Glass Support in TMA1

Film Experiments

Specimen conditions and furnace gradients will have profound effects on measurements of films in tension. An interlaboratory test is currently being conducted to determine the precision and bias for E 1824. In this test method two sets of force conditions are described to determine the glass transition temperature (T_g) of films based upon expansion or upon contraction (for highly oriented materials). In Figure 10, experiments are performed on 10 mm long specimens of polycarbonate films using forces which should cause the film to elongate according to E 1824 (0.03 and 0.05 N). Calculating T_g according to the method of E 1824 yield anomalously high values that are dependent on the applied force. Upon closer examination the polycarbonate film is shown to contract at around 145°C (T_g) then grow as the material plastically deforms. This can be seen in the magnified view of these curves (Figure 11). On this finer scale, the T_g (by contraction) is independent of force. Under an increased force (0.5 N) the specimen elongates at T_g . Unfortunately, force is not an adequate quantity to uniformly measure materials in tension. Rather, stress (force per cross sectional area) should be used, as was observed earlier [3, 4]. More work is needed to investigate the stress levels to be used in this test method and a revised method will be available in the near future.

The results of TMA measurements for various lengths of polycarbonate films measured at the 0.5 N force level are shown below (Figure 12). Though there appears to be great differences among the specimens in the non-normalized Y-axis (5 mm scale), the

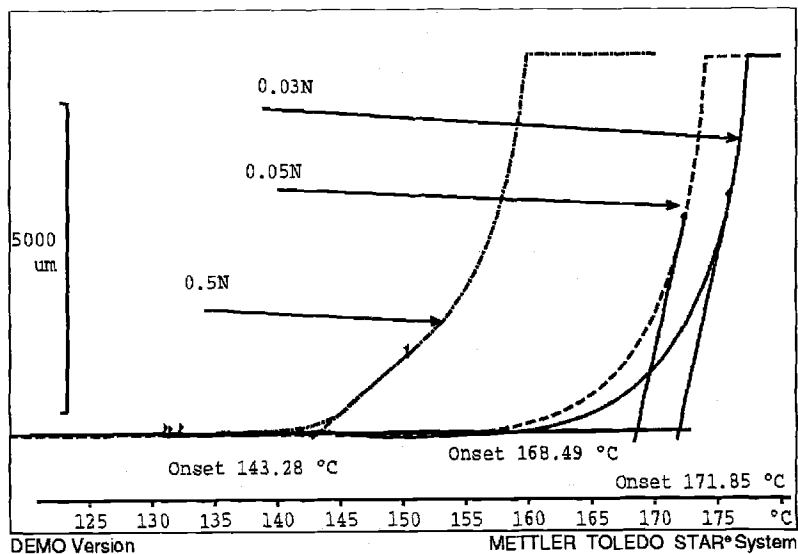


Figure 10 - T_g of 10 mm Long Specimens Polycarbonate Film According to Test Method E1824 for 0.03 N (solid line), 0.05 N (dashed line) and 0.5N (dash-dot line)

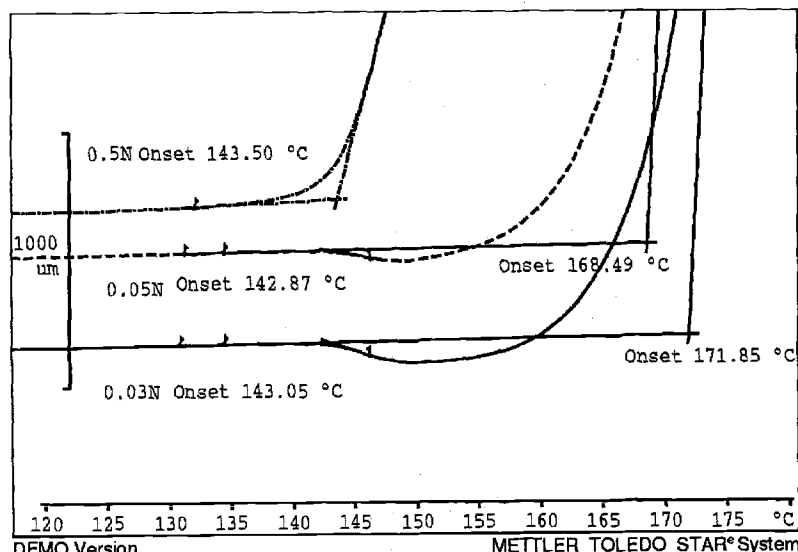


Figure 11 - Magnified View of Figure 10 Showing Force-Independent T_g Measurement

normalized (100%) Y-axis view shows all specimens behaving in a similar manner through T_g . Not surprisingly, the T_g values are little influenced by length. There are small differences in the plastic deformation which are likely to be caused by uncertainty in the clamping force and alignment.

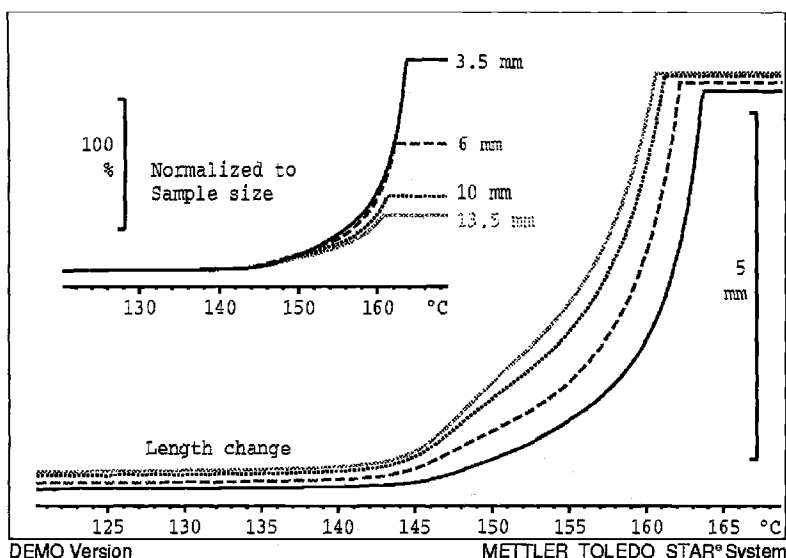


Figure 12 - *Length Change of Polycarbonate Films Versus Specimen Length. Inset Shows All Specimens Behave Similarly Over Most of Temperature Range.*

Conclusions

This study shows that thermal conductivity, heat capacity and specimen size will affect TMA measurements in a compression mode. Materials of low thermal conductivity will have significant gradients from the surface to the interior, while materials of high heat capacity will lag behind the atmosphere temperature to a larger extent. In addition applied stress (force) affects specimens in the tension mode. Furthermore, due to differences in furnace temperature gradients (which can be approximated using glass or other low thermal conductivity specimens of varying thickness) among TMA instruments, these factors will affect each instrument to a different extent. Caution therefore must be used when testing materials against current test methods for TMA instruments, including E 1363, E 831, E 1545 and E 1824, and several recommendations are made here:

- Smaller temperature calibration specimens (about 100 µm thick) should be used.
- It is critical that the thermal sensor not be moved during experimentation or temperatures could vary by several degrees. Frequent temperature checks should be performed to ensure the quality of the temperature data.
- Temperature calibrations must be made at each heating rate.
- For instruments that only report reference (or program) temperatures, there will be significant temperature errors for high heat capacity specimens.
- Small specimens should be used for Tg and Tm measurements to minimize thermal gradients within the specimens. This may require softening points (penetration) to be used to measure Tg instead of expansion for materials with low CLTE values.

- Per the recommendations of E 831, calibrations for CLTE measurements should be performed using reference specimens that are the same size and thermal conductivity as the test specimen to duplicate thermal gradients within the specimens.
- When measuring the Tg of film and fiber specimens by TMA in tension, the curves should be examined on a magnified scale to determine if shrinkage is occurring. If shrinkage does occur, then Tg should be analyzed using shrinkage method instead of the expansion method as described in E 1824.
- Film and fiber specimens should all be measured under the same stress (force divided by cross sectional area) level in order to make proper comparisons. Furthermore, specimen length should be held constant in order to avoid inconsistencies arising from furnace gradients and clamping.

References

- [1] Seyler, R. J. and Earnest, C. M., "Temperature Calibration of Thermomechanical Analyzers: Part II – An Interlaboratory Test of the Calibration Procedure," *Materials Characterization by Thermomechanical Analysis, ASTM STP 1136*, A. T. Riga and C. M Neag, Eds., American Society for Testing and Materials, West Conshohocken, PA 1991, pp. 22-31.
- [2] Matsumori, N., Penn, J., Nakamura, N. and Teramoto, Y., "Evaluating the Accuracy of Thermomechanical Analysis Expansion Coefficient Measurements in a Wide Temperature Range," *Materials Characterization by Thermomechanical Analysis, ASTM STP 1136*, A. T. Riga and C. M Neag, Eds., American Society for Testing and Materials, West Conshohocken, PA 1991, pp. 32-48.
- [3] Moscato M. J., "The Use of Thermomechanical Analysis as a Viable Alternative for the Determination of the Tensile Heat Distortion Temperature of Polymer Films," *Materials Characterization by Thermomechanical Analysis, ASTM STP 1136*, A. T. Riga and C. M Neag, Eds., American Society for Testing and Materials, West Conshohocken, PA 1991, pp. 100-107.
- [4] Moscato, M. J., and Seyler, R. J., "Assigning the Glass Transition Temperature in Oriented Poly(ethylene terephthalate)," *Assignment of the Glass Transition Temperature, ASTM STP 1249*, R. J. Seyler, Ed., American Society for Testing and Materials, West Conshohocken, PA 1994, pp. 239-252.
- [5] Jankowski, J. L., Wong, D. G., DiBerardino, M. F., and Cochran, R. C., "Evaluation of Upper Use Temperature of Toughened Epoxy Composites," *Assignment of the Glass Transition Temperature, ASTM STP 1249*, R. J. Seyler, Ed., American Society for Testing and Materials, West Conshohocken, PA 1994, pp. 277-292.
- [6] Kelsey, M. and Foreman, J., "Temperature Measurements in TGA," *Limitations of Test Methods for Plastics, ASTM STP 1369*, J. S. Peraro, Ed., American Society for Testing and Materials, West Conshohocken, PA, 1999.

John F. Houle¹

Acetone Immersion Testing per ASTM Test Method D2152

Reference: Houle, J. F., "Acetone Immersion Testing per ASTM Test Method D2152," *Limitations of Test Methods for Plastics, ASTM STP 1369*, J. S. Peraro, Ed., American Society for Testing and Materials, West Conshohocken, PA, 2000.

Abstract: In the late 1950s and early 1960s, inadequate fusion of PVC materials was a relatively frequent occurrence for North American PVC pipe manufacturers. As a result, an acetone-immersion test method was developed and published in 1963 as ASTM D2152 "Standard Test Method for Adequacy of Fusion of Extruded Poly(Vinyl Chloride) (PVC) Pipe and Molded Fittings by Acetone Immersion."

Over the years, PVC pipe extrusion machinery and materials became more sophisticated. As a result, inadequate fusion occurred infrequently and failure rates of acetone tests dropped to near zero. Manufacturers also realized that other quality tests (such as impact and flattening tests) were identifying the occasional fusion problem that did occur.

Another complication arose in the 1980s: acetone, once considered a relatively harmless chemical, was determined to be a health and safety hazard and a toxic waste. Strict government regulations were imposed on the storage, use, and disposal of acetone.

This paper will show that the acetone-immersion test is severely limited in its usefulness due to its application and to the properties of the substance itself.

Keywords: acetone, fusion, hazardous substance, health and safety risk, PVC pipe, quality-control testing, toxic waste

¹Market Development Engineer, PW Pipe, PO Box 10049, Eugene, OR 97440

Acetone

Acetone is an organic solvent that is classified as a ketone. It is a colorless, flammable liquid with a distinct aromatic odor. Acetone is used primarily as a solvent for paint, varnish, lacquers, inks, and adhesives. It is also used as a chemical intermediate in the production of pharmaceuticals, plastics, and resins. Acetone's chemical formula is C₃H₆O, or more specifically, (CH₃)₂CO.

History of Acetone Testing

In the late 1950s and early 1960s, inadequate fusion of PVC materials was a relatively frequent occurrence for North American PVC pipe manufacturers. As a result, an acetone-immersion test method was developed and published in 1963 as ASTM D2152 "Standard Test Method for Adequacy of Fusion of Extruded Polyvinyl Chloride (PVC) Pipe and Molded Fittings by Acetone Immersion."

Requirements for acetone testing were later included in seventeen ASTM PVC piping standards. D2152 testing was also included in PVC pipe standards published by organizations such as the American Water Works Association (AWWA) [1], Underwriters Laboratories (UL) [2], and the American Society of Agricultural Engineers (ASAE) [3].

Evolution of D2152*Scope and Significance Statements -- 1967*

The 1967 edition of ASTM D2152 contained the following statements on the applicability of the test method:

1. Scope

1.1 This method covers the determination of the quality of extruded rigid poly(vinyl chloride) (PVC) plastic pipe as indicated by reaction to immersion in anhydrous acetone.

1.2 This method may be used also to determine the quality of molded PVC fittings.

2. Significance

2.1 This method is applicable only for distinguishing between unfused and properly fused PVC. The difference between thermally degraded and properly fused PVC cannot be determined by this method.

2.2 There are insufficient data at this time to provide direct correlation between the results of this test and other physical and chemical properties of the pipe. For this reason, acetone immersion is not recommended as a substitute for burst and impact tests on pipe or fittings.

2.3 This method is not intended for use in purchasing specifications because the conditions of processing plastic compounds vary widely, and the degree of correlation of data obtained by this method with chemical and physical properties has not been completely determined. However, despite this limitation, this method does yield data of value in establishing such correlations and in judging the quality of extruded PVC pipe.

Scope limitations -- From these paragraphs it is clear that at its inception in the 1960s, the acetone-immersion test had a limited scope. The first sentence of Paragraph 2.1 mentions the intended usage (distinguishing between properly fused and improperly fused PVC). The remainder of Section 2 is devoted to placing limits on the test:

- The second sentence of 2.1 states that the test cannot be used to distinguish between properly fused and thermally degraded pipe.
- Paragraph 2.2 points out that there is no correlation between results of the acetone test and the pipe's properties.
- Paragraph 2.3 reiterates that the correlation has not been determined, but states that the acetone test does provide data that is of value in determining such correlation.

Scope and Significance Statements -- 1995

The most recent revision to D2152 was published in 1995. Section 2 from the earlier edition was changed to Section 3, and more limitations were added. (The new Section 2, titled "Reference Document," is not relevant for this paper.) The new Sections 1 and 3 read as follows:

1. Scope

1.1 This test method covers the determination of the adequacy of fusion of extruded rigid poly(vinyl chloride) (PVC) pipe and molded fittings as indicated by reaction to immersion in anhydrous acetone.

1.2 The values stated in inch-pound units are to be regarded as the standard except where instruments are calibrated in SI units.

1.3 This standard does not purport to address all of the safety concerns, if any, associated with its use. It is the responsibility of the user of this standard to establish appropriate safety and health practices and determine the applicability of regulatory limitations prior to use. Specific hazards statements are given in Annex 1.

3. Significance and Use

3.1 This test method is applicable only for distinguishing between inadequately fused and adequately fused PVC. The difference between thermally degraded and adequately fused PVC cannot be detected by this test method. Acetone immersion is not a substitute for burst, impact, or other physical or chemical tests on PVC pipe or fittings and it, therefore, shall not be used as the only test specification for purchasing of PVC pipe or fittings.

3.2 This test method is useful in determining whether inadequate fusion contributed to failure of PVC pipe or fittings in other physical or chemical tests, or in service.

3.3 This test method is useful in evaluating the adequacy of PVC fusion obtained in process or materials trials.

3.4 This test method determines adequacy of fusion on a single, relatively small specimen. This test method requires the use of a hazardous reagent which must be properly handled and disposed. Therefore, this test method may not be cost-effective to employ as a routine quality control test.

Paragraph 1.3 references Annex A1 for specific hazards statements. The Annex, which is mandatory information, reads as follows:

A1. RECOMMENDED SAFETY PRECAUTIONS TO BE USED WITH ACETONE**A1.1 Safety Requirements:**

A1.1.1 No source of ignition is to be permitted where acetone is used.

A1.1.2 Dispense acetone only from approved safety containers.

A1.1.3 Dispose of used acetone, or acetone-impregnated cloths only in an approved safety waste receptacle.

A1.1.4 Avoid prolonged breathing of acetone. Use acetone only in a well ventilated area.

A1.1.5 Use proper eye protection such as chemical-workers' goggles or a face shield when handling acetone.

A1.1.6 Avoid prolonged exposure to the skin. If prolonged exposure to the skin cannot be avoided, use protective clothing.

A1.2 Health Hazards:

A1.2.1 Acetone is a mild irritant to eyes, nose and throat but only minor residual injury will occur if no medical treatment is given.

A1.2.2 Prolonged or continuous exposure of acetone to the skin may cause acute or chronic dermatitis. Exposed skin areas should be washed and dried. Consult a physician if a rash develops.

A1.3 Fire Hazard:

A1.3.1 Acetone is a very flammable liquid having a flash point of -18°C (0°F). Use dry chemical, alcohol foam, or carbon dioxide to fight a fire. Use water to keep fire-exposed containers cool or to wash away or dilute spills which have not ignited.

Changes in D2152 Scope and Significance

The portion of the standard that deals with scope and significance almost tripled between 1967 and 1995. The result was to add further limitations to those that existed in the earlier document. Additional information on applications includes:

- Use in forensic analysis (Paragraph 3.2)
- Use in production trials (Paragraph 3.3)
- Qualifier on use as a routine quality-control test (Paragraph 3.4)

The net result of these three items was to remove acetone testing from everyday pipe-quality applications. The addition of forensic and experimental applications provides reasons for continued use of the test, but on a severely limited basis.

The major addition was not to the test's applications, however, but to safety issues. Annex A1 was included because of the dangers caused by acetone's flammability, explosiveness, and toxicity.

D2152 Procedural Limitation

In Section 5, Note 3 states: "The presence of water in the acetone reduces its sensitivity to differences in the degree of fusion of rigid poly(vinyl chloride) (PVC). It is important to dry the acetone properly and conduct the test in a sealed container, because acetone rapidly absorbs moisture from the atmosphere."

Limitations in UL Standard 651

D2152 is not the only standard that places limitations on acetone testing. Underwriters Laboratories Standard UL651 "Standard for Safety: Schedule 40 and 80 Rigid PVC Conduit" states in Paragraph 8.2:

8.2 Acetone [dimethyl ketone ($\text{CH}_3)_2\text{CO}$] is an extremely volatile liquid whose vapors form explosive mixtures with air. Open flames, glowing cigarettes, and other sources of ignition must be kept away. Acetone and acetone-PVC products are toxic, damag-

ing to clothing, and rapidly absorb moisture from air, the skin, and other sources. They should not touch the skin, nor should the vapors of these substances be inhaled. Because acetone with moisture in it is not effective in this test, the test is to be conducted with each specimen in its own covered container. Acetone can be dehydrated by filtering it through anhydrous calcium sulfate (CaSO_4).

Health and Safety Issues

Acetone was once considered a relatively harmless chemical. However, as more has become known about acetone in recent years, regulations on its use have been tightened. Special training and equipment are now required for personnel who use acetone. Both the Occupational Safety and Health Administration (OSHA) and the National Institute for Occupational Safety and Health (NIOSH) have established workplace limits for acetone exposure.

Health Effects

Acetone is known to have the following health effects:

- Eyes: Acetone liquid is severely irritating to the eyes; high vapor concentrations are also irritating. Pre-existing conditions may be aggravated by exposure.
- Skin: Acetone liquid is mildly irritating to the skin. Prolonged or repeated contact can cause drying and dermatitis. Pre-existing conditions may be aggravated by exposure.
- Central nervous system: Inhalation of high vapor concentrations or ingestion of acetone liquid may produce central nervous system depression. Moderate depression is evidenced by nausea, headaches, and dizziness; extreme depression is evidenced by unconsciousness and death.

To reduce exposure to acetone, workplace controls such as local exhaust ventilation, respirators, and protective clothing are recommended.

Safety Properties

In addition to direct health effects, acetone has the following safety properties:

- Flammability: Acetone is extremely flammable. The NFPA hazard rating is 3 (serious). In addition, poisonous gases are produced in fire.
- Explosiveness: Acetone is an explosion hazard.

Summary

Acetone is a health and safety risk for workers at PVC pipe extrusion plants.

Environmental and Regulatory Issues

In recent years acetone has fallen under increased scrutiny by the Environmental Protection Agency and other federal and state regulatory agencies. Listed below are several of the federal laws that regulate acetone:

- Environmental release -- Acetone had been listed by the National Response Center under the Comprehensive Environmental Response, Compensation, and Liability Act (CERCLA). (This law is also called the Superfund Act.) The Superfund Act requires that releases of acetone to air, land, or water which exceed the reportable quantity must be reported to the National Response Center. However, acetone was removed from the list of toxic chemicals in 1995.
- Hazardous waste -- Acetone is listed under the Resource Conservation and Recovery Act (RCRA) with an RCRA code of U002 (toxic waste). This act requires that if acetone becomes a waste material, it is banned from land disposal. All disposal of acetone must be in accordance with applicable EPA and state regulations for hazardous waste.
- Toxic material -- Acetone is listed as toxic under the Emergency Planning and Community Right-to-Know Act (EPCRA).

In summary, acetone is a hazardous and toxic substance. Releases of acetone to the environment or entry of acetone into the waste stream are heavily regulated because of the danger the chemical poses.

The dangers posed by acetone mean that it is not appropriate for general use in a manufacturing facility. Special training in storage, use, and disposal is required. Only personnel who have been trained are allowed to handle acetone and to perform the immersion test.

Applications Limitations

Sensitivity to Moisture

Since the presence of water in acetone reduces its ability to determine the adequacy of fusion and since acetone rapidly absorbs moisture from the atmosphere, it is necessary to take special care to prepare and to conduct the test. Carelessness in safeguarding the material causes meaningless tests.

Quality-Control Testing

The 1995 edition of D2152 points out that acetone testing might not be cost-effective as a routine quality-control test. However, there are more problems with acetone testing than cost-effectiveness.

Purpose of Quality-Control Testing -- The purpose of quality-control testing is to inform the manufacturer that a problem exists. Once the problem is known, steps can be taken to correct the underlying causes.

A meaningful quality test should have the following properties:

- The test accurately identifies a significant problem.
- The test identifies a problem that would not be discovered by other typical quality tests.
- Testing can be performed on line, as near to the time of manufacture as practical.
- Tests can be done quickly, simply, and safely.

Does acetone immersion meet the requirements for a meaningful quality test? Each of the four properties listed in the preceding paragraph will be discussed below in relation to acetone immersion.

Property #1: Accurate Identification of a Significant Problem -- The sole purpose of the acetone immersion test is to identify inadequately fused PVC. However, inadequate fusion is not a significant problem in the 1990s. As proof of this contention, data were collected from two large manufacturers of PVC pressure pipe:

- Manufacturer A -- Acetone tests were performed during a continuous time period in 1993 at several pipe-extrusion plants. A total of 5717 tests were done, with 5710 "pass" results. The pass rate was 99.9%. Four of the failed tests occurred on the same extruder in a short time period due to mechanical problems; the pipe that failed the acetone tests had already been identified as inadequately fused as a result of other quality tests.
- Manufacturer B -- Acetone tests were performed during a continuous time period in 1993 at several pipe-extrusion plants. There were 2171 tests with all tests achieving "pass" results. The pass rate was 100%.

The total number of tests was 7888, with the pass rate at 99.9%.

From this data it is clear that the acetone test does not meet the first criterion: it does not "accurately identify a significant problem."

Property #2: Problem Identified by Test not Found by Other Tests -- Acetone immersion is designed to identify inadequate fusion of PVC. However, when inadequate fusion occurs, the physical properties of the pipe are substandard. Other tests discover the substandard pipe.

There are three ASTM pipe standards that do not include acetone testing (D2665, F480, and F1760). None of these standards appear to have suffered as a result of this omission.

Thus, acetone immersion does not meet the second criterion: it is not a test that uniquely identifies a problem that other tests would overlook.

Property #3: Testing Performed on Line at Time of Manufacture -- On-line testing is valuable because problems can be identified (and corrected) immediately. This keeps product quality high and reduces product fall-down to a minimum.

Acetone immersion testing is not performed on line. Because only specially trained personnel are allowed to perform the test, tests must be performed in a laboratory.

Once again, acetone testing does not meet the criterion.

Property #4: Testing Performed Quickly, Simply, and Safely -- Acetone immersion testing is quick and simple. However, as discussed above, the safety of plant personnel is at risk due to the toxic and hazardous material used.

Summary -- The acetone-immersion test fails to meet even one of the criteria for a meaningful quality test.

Conclusion

The acetone-immersion test is beset with difficulties. First and foremost, the purpose for which it is intended is no longer meaningful: inadequate fusion of PVC pipe is a rare occurrence in present-day manufacturing. Furthermore, the test does not meet any of the criteria for quality-control testing. Added to this are health and safety problems combined with environmental and regulatory issues. It seems appropriate that this test be relegated solely to forensic and experimental use.

References

- [1] American Water Works Association, 6666 W. Quincy Ave., Denver, CO 80235
- [2] Underwriters Laboratories, 333 Pfingsten Road, Northbrook, IL 60062
- [3] American Society of Agricultural Engineers, St. Joseph's, MI 49085

Giorgio Zaffaroni,¹ Claudio Cappelletti,¹ Stefania Guerra,¹ and Sandro Risetti¹

Reinforced Epoxy Resin Cure Assessment in Composite Materials: Measure and Effects

Reference: Zaffaroni, G., Cappelletti, C., Guerra, S. and Risetti, S., "Reinforced Epoxy Resin Cure Assessment in Composite Materials: Measure and Effects," *Limitations of Test Methods for Plastics, ASTM STP 1369*, J. S. Peraro, Ed., American Society for Testing and Materials, West Conshohocken, PA, 2000.

Abstract: The effects of three degrees of cure (low, standard and postcured) on two carbon reinforced epoxy resins are examined. The polymerization degree is tentatively assessed by thermal analysis techniques, namely by Differential Scanning Calorimetry (DSC) and Dynamic Mechanical Analysis (DMA). The effects on both static mechanical and fracture toughness properties have been checked. It has been found that the glass transition temperature measured by DMA is the parameter, among those studied (both thermal and mechanical), that is more sensitive to the cure degrees.

Keywords: epoxy resin, cure degree, thermal analysis

Introduction

Carbon fiber reinforced epoxies are widely used in aeronautical structures. With some kinds of resin formulations a residual reactivity can be found even after curing [1]. This behavior has been found also after subjecting the prepeg to the standard cure cycle recommended by the supplier. It is likely that the under-cure of a thermosetting polymer gives rise to anomalous properties [1]. Moreover minor differences in the cure degree can be produced by unintentional dissimilarities in the polymerization cycle. For example they can be generated by different positions and air flow situations in the autoclave. Therefore it is important to have a method to check the level of cure. The usual way to do that is to submit small samples taken from the composite under examination to Differential Scanning Calorimetry (DSC). In fact it is expected that incomplete polymerization generates a residual heat of cure in the DSC signal. Moreover it is known that the glass transition temperature (T_g) is dependent on the degree of cure (see e.g. [2]) and it is customary to measure the T_g by Dynamic Mechanical Analysis (DMA). On the other hand it is important to verify the real importance of a slight under-curing level from a performance standpoint.

¹ AGUSTA - a Finmeccanica Company - via G.Agusta,520 - 21017 C.COSTA DI SAMARATE (VA) - ITALY

This present paper deals with two kinds of connected problems:

- What is the more suitable thermal analysis technique for assessing the cure status?
- Do small differences in the production cycle (which give polymers which are hardly distinguishable by thermal analysis techniques) really affect the mechanical performance? In other words, are the thermal analysis techniques more sensitive than mechanical tests in identifying the cure level?

Experimental

Two kinds of commercial unidirectional reinforced carbon epoxy resins, namely A and B, are examined here. The resin content of prepreg A was 42% (by weight) and 35% for prepreg B. The matrices materials used the prepgs were:

matrix A: a standard commercial epoxy (DiGlycidyl Ether of Bisphenol-A/TetraGlycidyl Diamino Diphenyl Methane/Novolac, curing agent: Diamino Diphenyl Sulphone) ;

matrix B: a standard epoxy (TriGlycidyl ParaAmino Phenol / TetraGlycidyl Diamino Diphenyl Methane, curing agent: Diamino Diphenyl Sulphone) mixed with 18% of PolyEtherSulphone (toughener).

The specified plies of prepreg were laid up using the appropriate fiber orientations and cured using three different cure cycles:

- LOW: heat up from R.T. to 170°C @ 2°C/min, then dwell @ 170°C for 2 hours;
- STANDARD (suggested by the suppliers and abbreviated in the text by STD): heat up from R.T. to 180°C @ 2°C/min, then dwell @ 180°C for 2 hours;
- HIGH: the same schedule of the standard cure cycle was followed by the postcure @ 200°C for 2 hours.

The specimens to be tested were machined from the cured laminates.

Some specimens (3 samples for each cycle condition and for each material) were aged @ 70°C/84%R.H. to determine the moisture diffusion coefficient (D) and the relative saturation weight gain (M_∞). After moisture saturation the samples were analyzed by DMA to determine the Tg.

The lay up's of the laminates considered and the tests carried out on them are shown in Table 1.

On $[\pm 45^\circ]_{14}$ samples, after the first DMA scan, an additional run was carried out on the same specimen.

The static mechanical and fracture toughness tests have been selected to highlight the resin dependent properties.

The experimental apparatus were:

DSC: Rheometric Scientific DSC PLUS.

DMA: Rheometric Scientific DMTA Mk III.

Mechanical Testing Machine: Instron mod. 1175.

Table 1- *Test plane*

Lay up	Test	Test Method	Test Condition	Property measured
[0°] ₂₄ ^(*)	DCB	ASTM D5528 ^a	dry	G _{IC}
	ENF		dry	G _{IIC}
	SBS	ASTM D2344 ^b	dry	I.L.S.S.
	DSC	ASTM E537 ^c & E967 ^d	dry	Spec. Heat vs. Temp.
[±45°] ₁₄	Tension	ASTM D3518 ^e	dry	G ₁₂ , τ _R
	DMA: (two runs)	ASTM D5023 ^f & E1640 ^g	dry	E', E'', tanδ vs. Temp.
	DSC		dry	Spec. Heat vs. Temp.
[0°] ₇	Tension	ASTM D3039 ^h	Dry	E ₁₁ , σ _R
	DMA	ASTM D5023 ^f & E1640 ^g	Dry & Wet	E', E'', tanδ vs. Temp.
	Moisture Absorption	ASTM D5229 ⁱ	Wet	D, M _∞ , (Tg "WET")

(*) with a Teflon® insert

- ^a Standard Test Method for Mode I Interlaminar Fracture Toughness of Unidirectional Fiber-reinforced Polymer Matrix Composites
- ^b Standard Test Method for Apparent Shear Strength of Parallel Fiber Composites by Short-Beam Method
- ^c Standard Test Method for Assessing the Thermal Stability of Chemicals by Method of Differential Thermal analysis. (Specimens weight varies from 20 to 30 mg. The reference was an empty pan. The Heat Rate used was 10 °C/min)
- ^d Standard Test Method for Temperature Calibration of Differential scanning Calorimeters and Differential Thermal Analyzers
- ^e Standard Test Method for Practice for In-Plane Shear Response of Unidirectional Reinforced Plastic
- ^f Standard Test Method for Measuring the Dynamic Mechanical Properties of Plastic Using Three Point Bending (The relevant experimental conditions were: Frequency 1Hz, Heat Up Rate 2°C/min)
- ^g Standard Test Method for Assignment of the Glass transition Temperature by Dynamic Mechanical Analysis
- ^h Standard Test Method for Tensile Properties of Fiber-Resin Composites
- ⁱ Standard Test Method for Moisture Absorption Properties and Equilibrium Conditioning of Polymer Matrix Composite Materials

Experimental Results and Discussion

Thermal Analysis Techniques

DSC analysis is the most common method used to assess the degree of cure [3] of thermosets. In fact Quality Control Procedures usually require that no exothermal peak associated with the cure process is present.

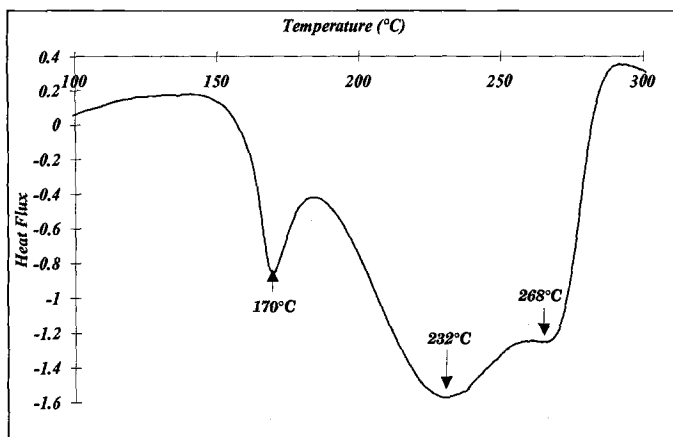


Figure 1 - Typical DSC plot for MATERIAL A

The typical DSC's of the prepgs are shown in Figure 1 and Figure 2. In the above figures the characteristic temperatures of the reaction peaks are displayed. The calorimetric analysis carried out on the samples previously submitted to the various cure cycles are reported in Figure 3 for material A and Figure 4 for material B. Each heat flux curve is normalized with respect to the sample's weight and the curves are vertically shifted by an arbitrary amount.

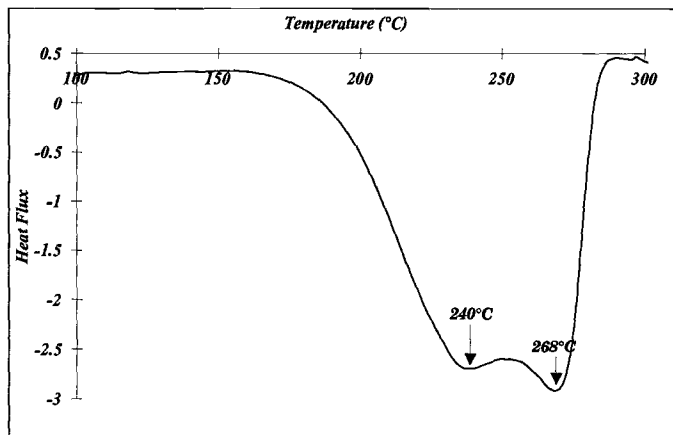


Figure 2 - Typical DSC plot for MATERIAL B

The DSC analysis of both the materials when submitted to the LOW cycle show a lack of cure that can be seen in the figures as an endothermic (residual heat) peak. While STANDARD cured samples of Material B clearly show a residual heat of cure, such evidence is not so clear for DSC traces of material A-STANDARD cured. In fact the presence of an incomplete cure could be seen in the A-STANDARD case only by comparison of its DSC trace with the A-HIGH DSC plot. The HIGH cycle

DSC traces of the MATERIAL A shows a complete cure.

The integration of the peaks should provide the residual heat of cure: ΔH_{res} . It is to be highlighted that the result of integration, with the kind of signals considered here, can give only a roughly estimated value. In fact it is well known that ΔH_{res} depends on the local resin content which is not easy to measure in a sample as small as is used in DSC analysis. Moreover with broad peaks like the ones shown here, it is very difficult to select a good baseline for the integration. To fully understand this it is enough to look at the signal of the STANDARD sample in Figure 3: some doubts could arise on the presence of a residual reactivity signal. Nevertheless in Table 2 an estimate of the residual heats (ΔH_{res}) are compared with the typical total heat of cure ΔH_{TOT} .

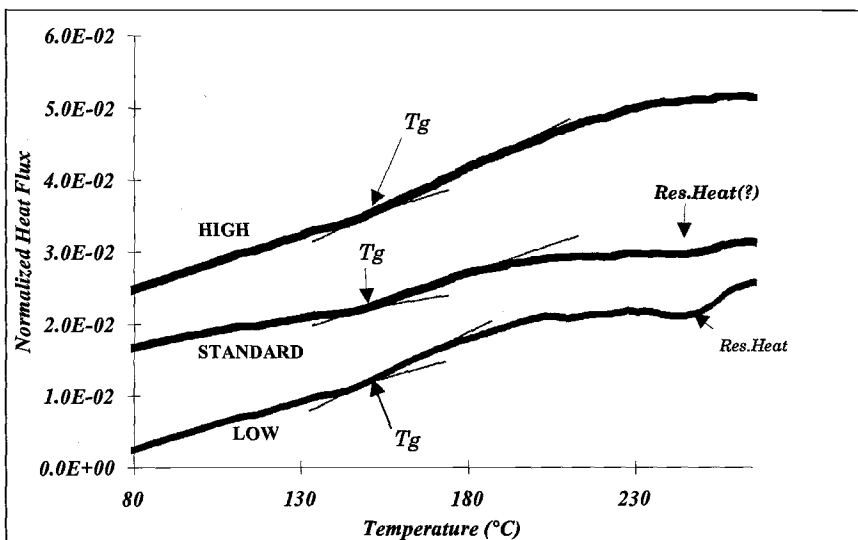


Figure 3 - DSC plots for MATERIAL A after the cure cycles (the traces are shifted by an arbitrary amount)

Table 2 - Heat of Cure by DSC analysis

	LOW (J/g)	STD (J/g)	HIGH (J/g)	Typical (J/g)
ΔH_{res} material A	2.3	(0.5?)	NONE	
ΔH_{TOT} material A				209± 8%
ΔH_{res} material B	8.0	1.0	NONE	
ΔH_{TOT} material B				189±10%

From Figure 3 and Figure 4 it is likewise possible to see that near 150°C there is the glass transition of the polymer. In the above mentioned figures the interpolation of the heat flux lines below T_g and in the transition zone (thin lines) whose

intersection can be taken as the glass transition point (i.e. T_g onset) are displayed. The values found are reported in Table 3.

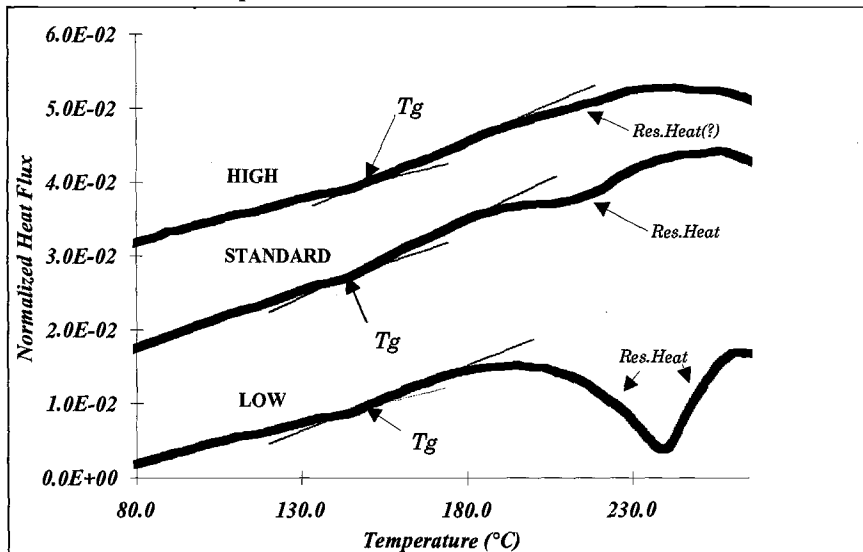


Figure 4 - DSC plots for MATERIAL B after the cure cycles (the traces are shifted by an arbitrary amount)

It is not easy to discriminate among the different cases. In fact all T_g's are spread in the range 143-146°C. Moreover the values of T_g's found are highly dependent on the way in which one draws the interpolation of the heat flux lines (i.e. the range considered for the regression).

Table 3 - T_g Values by DSC Analysis

	LOW	STD	HIGH
T _g composite A (°C)	145	145	146
T _g composite B (°C)	143	144	145

A further DSC run on the previously scanned specimens gave approximately the same T_g as those shown in Table 3 (the values are not reported here). Probably the real value is hidden by the signal noise.

The curves representing the temperature dependence of the real part of the complex modulus: E' curves measured by DMA are summarized in Figure 5 and Figure 6 for composite A and B respectively. In the above mentioned figures the reported curves are relative to both [0°]₇ and [±45°]₁₄ lay up's. The tanδ and E'' curves are not shown in the figures. The [±45°]₁₄ specimens were submitted to successive DMA scans in order to check whether the T_g has changed after the heavy thermal treatment experienced by the sample in the first run (the maximum temperature reached was 250°C).

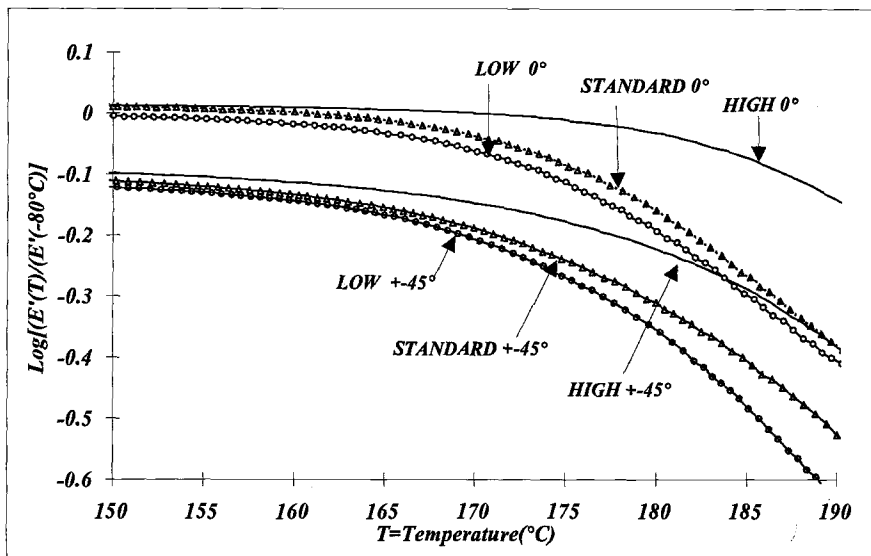


Figure 5 - DMA traces (Log E') for MATERIAL A after the cure cycles indicated (both the lay up considered are shown here)

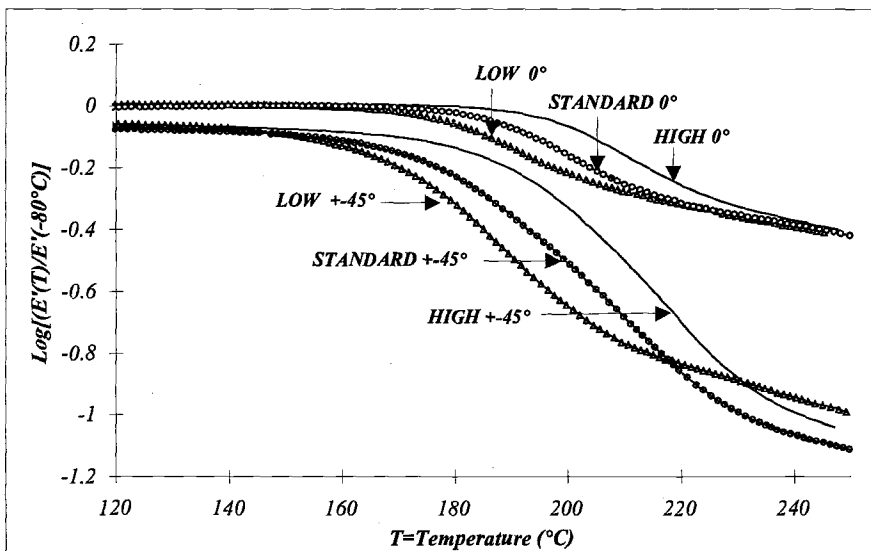


Figure 6 - DMA traces (Log E') for MATERIAL B after the cure cycles indicated (both the lay up's considered are shown here)

The Tg's taken as the maximum of the $\tan\delta$ curve and as the onset (i.e. the intersection of interpolated lines) of the E' drop are compared in Table 4 for test carried out on unidirectional specimens and in Table 5 for test carried out on $[\pm 45^\circ]_{14}$ specimens.

Table 4 - *Tg of material A and B: [0°]7 specimens*

	LOW	STD	HIGH
MATERIAL A (max tanδ)	186	187	198
% dev. from final Tg (*)	6.1	5.5	---
MATERIAL A (onset E')	172	173	184
% dev. from final Tg (*)	6.5	6.0	---
MATERIAL B (max tanδ)	201	204	215
% dev. from final Tg (*)	6.5	5.1	---
MATERIAL B (onset E')	175	185	194
% dev. from final Tg (*)	9.8	4.6	---

(*) % dev. From final Tg = $100 \cdot (Tg(\text{High}) - Tg)/Tg(\text{High})$

Table 5 - *Tg of material A and B: [\pm 45°]14 specimens*

	LOW		STD		HIGH	
	1 st Run	2 nd Run	1 st Run	2 nd Run	1 st Run	2 nd Run
MATERIAL A (max tanδ)	200	205	203	203	207	207
% dev. from final Tg (*)	3.4		1.9		---	
MATERIAL A (onset E')	176	187	177	188	184	191
% dev. from final Tg (*)	4.3		3.8		---	
MATERIAL B (max tanδ)	200	216	212	216	220	219
% dev. from final Tg (*)	9.1		3.6		---	
MATERIAL B (onset E')	166	193	177	188	189	191
% dev. from final Tg (*)	12.2		6.3		---	

(*) % dev. From final Tg = $100 \cdot (Tg(\text{High}) - Tg)/Tg(\text{High})$

The similarity of all the 2nd-Run-Tg's suggests that the polymer structures are strictly comparable in all the cases considered here when the same level of cure is reached and the thermal history is removed. In addition because 2nd-Run-Tg's for all the polymerization cycles are approximately equal to 1st-Run-Tg's for HIGH cycle for both materials it is manifest that the postcure originates the maximum degree of cure.

As expected the Glass Transition temperatures determined by taking the onset of E' modulus curve and as the maximum of tangent δ curve follow a similar trend.

In Table 6 the cure assessment results by means of different thermal analysis techniques are qualitatively summarized: as it can be seen, the situations obtained after the different cure cycles are not as clear as one wishes even in a qualitative way. In fact an uncertainty on Material A cure degree could arise because the different ways (by DMA-tan δ, by DMA-Log E', by DSC-Tg or by DSC-ΔH_{res}) of evaluating the polymerization degree seem to show a different trend. Probably in that case the

cure degrees, especially after the Low and the Standard cycles, are not different enough in order to be discriminated by both thermal analysis techniques. No problems arise when one considers Material B by using Calorimetric or Dynamic Mechanical tests.

From a QUANTITATIVE point of view it seems that DMA is more reliable than DSC to establish the cure degree of a composite because the Tg shift is more easy-to-quantify than the residual heat.

Table 6 - *Cure Assessment Results by Thermal Analysis*

Material	Technique	Specimen	Tg taken as	
A	DSC (ΔH_{res})			LOW < STD $\leq (?)$ HIGH
	DMA	$[\pm 45^\circ]_{14}$	max tan δ onset E'	LOW < STD \approx HIGH = 2 ND RUN
	DMA	$[0^\circ]_7$	max tan δ	LOW \approx STD < HIGH < (?) 2 ND RUN
	DMA	$[0^\circ]_7$	onset E'	LOW \approx STD < HIGH
B	DSC (ΔH_{res})			LOW < STD < HIGH
	DMA	$[\pm 45^\circ]_{14}$	max tan δ onset E'	LOW < STD < HIGH \approx 2 ND RUN
	DMA	$[0^\circ]_7$	max tan δ	LOW < STD < HIGH \approx 2 ND RUN
	DMA	$[0^\circ]_7$	onset E'	LOW < STD < HIGH

The next point is to establish whether the differences among different cure cycles that DSC and DMA (hardly) distinguish are really meaningful when one evaluates the performance.

Performance Tests

Moisture Absorption @70°C/84%R.H

From the weight gain plots the apparent diffusion coefficients and the saturation weight gains reported in Table 7 were found.

Table 7 - *Summary of Moisture Absorption Tests @ 70°C/84%R.H.*

	MATERIAL A			MATERIAL B		
	LOW	STD.	HIGH	LOW	STD.	HIGH
Resin Cont. (% weight)	33	33	34	24	25	23
D ($10^7 \cdot \text{mm}^2/\text{s}$)	3.5590	3.5054	3.6759	2.4349	2.9475	2.7901
M_∞ (% weight)	1.05	1.00	1.09	0.95	0.98	1.03

From Table 7 it is clear that in the cure range examined here no measurable influence on the diffusion coefficients can be found. On the other hand it seems that a definite trend could be present on the moisture saturation level of the material B. However, the increase in the saturation level observed in the last case is smaller than

the usual precision of this test (the typical standard deviation found in a single batch of material B when standard cured is 10%) and therefore, the result has to be taken with great care.

The glass transition temperatures are depressed by the absorbed moisture as expected.

The DMA plots for both the materials show an additional peak (e.g. see Figure 7) at a higher temperature. The nature of that peak is not easy to establish and an explanation is outside the scope of the present work. On the other hand it has to be highlighted that the test method E1640 (Assignment of the Glass Transition Temperatures by Dynamic Mechanical Analysis) does not provide any indication on how to determine the position of the less accentuated transition.

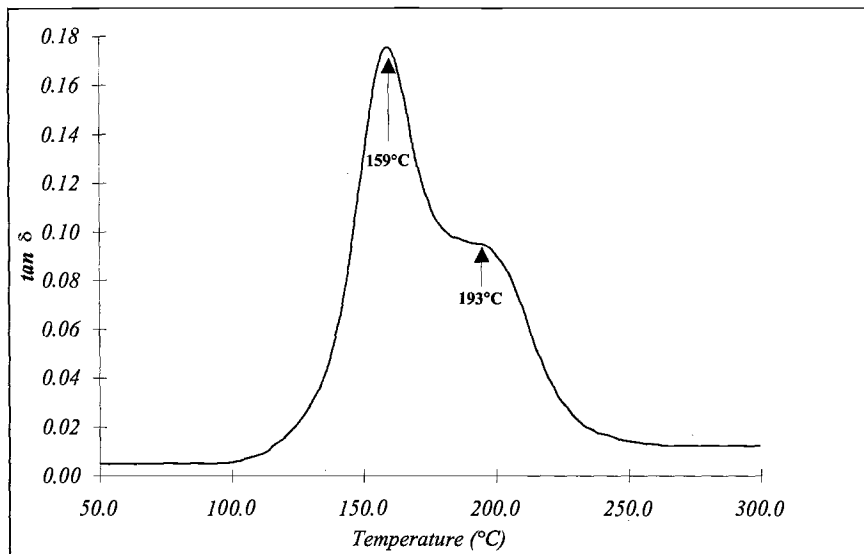


Figure 7 - DMA plot (max $\tan \delta$) of moisture saturated MATERIAL A [0°]7 specimen after the LOW cure cycle.

Table 8 - T_g of [0°]7 Specimens (max $\tan \delta$) before ("Dry") and after ("Wet") moisture saturation

	MATERIAL A			MATERIAL B		
	LOW	STD.	HIGH	LOW	STD.	HIGH
Tg "Dry"	186	187	198	201	204	215
Tg "Wet": first peak	159	161	166	183	182	192
Tg "Wet": second peak	193	196	200	215	224	232

Taking into account the results reported in Table 8 it has to be highlighted that from the T_g standpoint the LOW and the STD cure cycle have very similar effects on

the prepreg A. In addition it seems that the Tg depression (i.e. Tg("Dry,,)-Tg("Wet")) generated by the absorbed moisture does not depend on the cure cycle.

Mechanical Properties: Static Tests

In Table 9 are summarized the parameters obtained from static tension test carried out on $[\pm 45^\circ]_{14}$ specimens.

Table 9 - *Summary of Tension Test Results on $[\pm 45^\circ]_{14}$ Specimens*

	MATERIAL A			MATERIAL B		
	LOW	STD.	HIGH	LOW	STD.	HIGH
fiber volume %	53	57	52	60	59	58
G ₁₂ (GPa)	3.66	3.76	3.61	4.76	4.94	4.96
standard deviation %	1.1	1.8	3.0	6.8	5.5	3.7
τ _R (MPa)	90.3	105.8	91.5	133.6	131.7	104.9
standard deviation %	4.0	4.1	3.1	0.7	0.6	1.0

The anomalous in-plane-shear strength (τ_R) found for Material A submitted to standard cure cycle can be understood by taking into account the very high fiber content of the specimens. Accordingly to that results Dynamic Mechanical Analysis has found Low ≈ Std < High. For material B the decrease of 20% of τ_R obtained going from Low to High could be trusted. In fact 20% has to be compared with the typical test standard deviation for composite B of 4%. Correspondingly for material B, DMA technique has found the Tg trend: Low < Std < High.

Table 10 summarizes the Inter Laminar Shear Strength obtained from Short Beam Shear tests on $[0^\circ]_{24}$ specimens and in Table 11 the moduli E₁₁ and the strengths σ_R found from tension tests on $[0^\circ]_7$ specimens are shown.

Table 10 - *Short Beam Shear Test Results: Inter Laminar Shear Strengths*

	MATERIAL A			MATERIAL B		
	LOW	STD.	HIGH	LOW	STD.	HIGH
fiber volume %	53	54	53	60	65	61
I.L.S.S. (Mpa)	101.8	103.5	99.0	115.6	115.8	111.1
standard deviation %	3.1	3.6	3.5	1.6	1.2	1.3

Table 11 - *Tension Test on [0°]7 Specimens*

	MATERIAL A			MATERIAL B		
	LOW	STD.	HIGH	LOW	STD.	HIGH
fiber volume %	59	59	59	66	66	67
E ₁₁ (Gpa)	122.7	120.5	123.5	134.3	132.7	133.3
standard deviation %	1.2	0.6	2.1	0.9	1.8	4.0
σ _R (Mpa)	1867	1895	2045	2084	1950	(*)
standard deviation %	4.7	3.0	1.5	5.0	7.4	

(*) anomalous failures

Any difference in the behavior of the composite which could depend on such cure cycles cannot be seen by I.L.S.S. or by tension tests on [0°]₇ specimens.

Mechanical Properties: Fracture Mechanics Tests

Results obtained from D.C.B. and E.N.F. tests are reported in Table 12. The G_{IC} values are found taking into account the beam corrected approach.

Table 12 - *Fracture Mechanics Test Results*

	MATERIAL A			MATERIAL B		
	LOW	STD.	HIGH	LOW	STD.	HIGH
fiber volume %	53	54	53	60	65	61
G _{IC} (J/m ²)	168	163	148	301	312	270
standard deviation %	4.5	3.5	11.0	3.4	4.6	30.1
G _{IIC} (J/m ²)	650	591	606	836	840	500
standard deviation %	11.9	6.6	11.4	12.0	4.8	13.3

No well displayed trend on interlaminar fracture toughness G_{IC} is present as expected [1]. It appears that for material B there is a meaningful reduction of G_{IIC} in the High cycle.

Summary of Results and Conclusions

Results obtained in thermal analysis tests as yet stated are summarized as follows: if a QUANTITATIVE determination is requested it seems that DMA is more reliable than DSC, but when one deals with very high polymerization degrees both techniques give ambiguous results. As expected the T_g's determined by taking the onset of E' curve follow the same trend as that determined by the maximum of the tan delta peak.

The different cure cycles examined here have minor effects on the mechanical properties.

In general the characteristic, among those considered (both mechanical and

thermal), most sensitive to the cure degree is the glass transition temperature (as measured by DMA). Therefore a very useful quality parameter to be checked could be: $\Delta T_g = T_g(2^{nd} \text{ Run}) - T_g(1^{st} \text{ Run})$ with the Tg's determined by DMA. In fact for epoxy resin like the ones here considered it is expected that if $\Delta T_g < 10^\circ\text{C}$ only minor modifications of the composite behavior should occur.

Acknowledgment

The authors wish to thank Dr. C. Bozzi (Staz.Sper. Carta e Cellulosa) and Dr. C. Zanotti for their precious help.

References

- [1] Yuan J and Berglund L., "The Effect of Postcure on Transverse Cracking Strain in Toughened Carbon Fiber/Epoxy Cross Ply Laminates" in *Proceedings of Fourth European Conference on Composite Materials*, J. Füller et al. Ed. (Stuttgart 1990), pp. 919-924.
- [2] Stutz H., Illers H., and Mertes J., "A Generalized Theory for The Glass Transition Temperature of Crosslinked and Uncrosslinked Polymers", *Journal of Polymer Science: Part B: Polymer Physic*, Vol. 28 (1990) , pp. 1483-1498.
- [3] Prime R.B., "Thermosets" in *Thermal Characterization of Polymeric Materials* E.A.Turi Ed., Academic press (1981).

Author Index

A

Albrecht, M., 72
Albrecht, P., 72

B

Blaese, D., 22
Bradley, S. W., 10
Bradley, W. L., 10
Brown, N., 146

C

Cappelletti, C., 206
Cruz, C. A., Jr., 118

D

Douglas, M., 109
Driscoll, S. B., 3

E

Eley, K., 72

F

Foreman, J., 157, 181
Friday, M. J., 35

G

Guerra, S., 206

H

Houle, J. F., 197

J

Jia, N., 54

K

Kagan, V. A., 54
Kelsey, M., 157, 181

L

Leevers, P. S., 109
Lu, X., 146

M

Manahan, M. P., Sr., 118

P

Paschal, J. R., 93
Pavan, A., 130
Puckett, P. M., 10

R

Risetti, S., 206

S

Schmachtenberg, E., 22
Sepe, M. P., 44
Shaffer, C. M., 3

W

Whittingstall, P., 167
Widmann, G., 181
Williams, J. G., 130

Y

Yohn, H. E., 118
You, J., 72

Z

Zaffaroni, G., 206

Subject Index

A

Acetone immersion test
D 2152, 197
Acrylonitrile-butadiene-styrene
(ABS), 35
Adhesive specimens, thin, bulk,
72
Aging, 22
Applied shear stress, 167
Arrhenius statement, 22
ASTM standards
D 638, 35
D 648, 44
D 882, 72
D 1693, 146
D 2152, 197
D 3850, 157
E 1582, 157
F 1473, 146
tensile properties tests, 54

B

Bond strength testing, 93
British gas notch test, 146
Bulk adhesive specimens, tension
testing, 72

C

Calibration, 157
CAMPUS template, 3
Carbon reinforced epoxy resins,
206
Charpy test, 109, 118
Clamping pressure, 118
Compliance measurements, 10
Composite materials, 206
Technical Committee on
Polymers and
Composites, 130
Compression creep compliance,
10
Conductivity, thermal, 181
Copper, 181

Crack growth, 109
slow, 146

Cracking, stress
D 1693, 146
Creep compliance, 10
Cure degree, 206

D

Data sheet, 3
Deflection data, 118
Deflection temperature
ASTM D 648, 44
Design considerations, 3
Differential scanning
calorimetry, 206
Diffusion, 93
Distortion temperature under
load, 3
Dynamic fracture, 109
Dynamic loading, 118
Dynamic mechanical analysis,
44, 206

E

Elongation, 35
Epoxy resin, 206
ESCR test, 146
Ethylene plastics, stress cracking
D 1693, 146
European Structural Integrity
Society, 130

F

Film, 181
Flexural creep compliance, 10
Flexural load, 44
Flow behavior, 3
Fluid measurement, complex, 167
Fracture, 109
Fracture resistance, 118
Furnace response, 157
Fusion, polyvinylchloride
materials, 197

222 LIMITATIONS OF TEST METHODS FOR PLASTICS

G

G_{IC} , 130
Glass specimens, 181
Glass transition, 181, 206

H

Heat capacity, 157, 181
Heat deflection, 44

I

Impact behavior, 3
Impact fracture, 109
Impact testing, 109, 118
Indium, 181
Instrumented pendulum impact testing, 118
International Organization for Standardization (ISO)
ISO 75, 44
ISO 138, 146/SC4, 146
ISO 527, 35
ISO 10350, 3
ISO 11403, 3
tensile properties tests, 54
Izod test, 109, 118

J

Joint, fitting, pipe, 93

K

K_{IC} , 130

L

Lap-shear method, 93
Lifetime estimation, 22
Linear elastic fracture mechanics, 130
Load-deflection curve, 118
Loading rates, 130
Load-point displacement rate, 130

M

Mass, specimen, effect on temperature, 157

Modulus measurements, 54
Modulus of elasticity, 35
Modulus, temperature dependence, 44

N

Non-Newtonian materials, 167
Notched impact testing, 109

P

Pendulum impact testing, 118
PENT test, 146
Pipe and fittings
D 2152, 197
joint testing, 93
polyvinylchloride, 197
slow crack growth resistance, 146
Point measurements, 167
Polyamide, 54
Polycarbonate, 35
film, 181
Polyethylene, 146
Polyethyleneterephthalate (PET), 54
Polystyrene, 35
Polyvinylchloride, 93
pipe, 197
Property data sheet, 3

R

Resin, epoxy, 206
Rheology, 167

S

Sensors
direct contact thermal sensor, 181
temperature, calibration, 157
Shear, 93
Shear rate, 167
Sheeting, thin plastic, 72
Solvent-cement, 93
Stiffness, 10
Strain gages, 118
Strain rate, 72

Stress, 181
Stress-strain curves, 72
Structural adhesive, 72

T

Tangential compliance, 10
Temperature dependence of modulus, 44
Temperature measurements, 157
Tensile creep compliance, 10
Tensile properties, 54, 72
D 638, 35
D 882, 72
Tensile strain, 54
Tensile stress, 35
Tensiometer, 72
Thermal analysis, 206
Thermal conductivity, 181

Thermal degradation, 157
Thermogravimetric analysis D 3850, 157
Thermomechanical analysis, 181
Time-lapsing lifetime test, 22
Time-temperature-shifting principle, 22
Toxic waste, 197

V

Vinylesters, 10
Viscosity, 167

Y

Yield strain, 72
Yield stress, 72
Young's modulus, 54